This is to certify that the

dissertation entitled

Excited State Raman Spectroscopy of Organic
Transition Metal Complexes

presented by

Young C. Chung

has been accepted towards fulfillment
of the requirements for

_____Ph. D.____ degree in __Chemistry__

Major professor

Date___8/26/85_____

0-12771

RAMAN SPECTROSCOPY OF GROUND AND EXCITED ELECTRONIC

STATES OF ORGANIC COMPLEXES OF d⁸ TRANSITION METALS

By

Young C. Chung

A DISSERTATION

Submitted to

Michigan State University
in partial fulfillment of the requirements
for the degree of

DOCTOR OF PHILOSOPHY

Department of Chemistry

1985

ABSTRACT

RAMAN SPECTROSCOPY OF GROUND AND EXCITED ELECTRONIC STATES OF ORGANIC COMPLEXES OF d⁶ TRANSITION METALS

by

Young C. Chung

Resonance Raman spectroscopy has been utilized to study the ground and excited state properties of three classes of transition metal (poly)-pyridyl complexes: $Ru(II)(NH_3)_5(PY-X)$ (where PY = pyridine, X = para substituent), $Ru(II)(L)_m(L')_{3-m}$ (L,L' = bidentate ligand, m = 0~3) and $[Ru(II)(L)_2]bpym[M(II)(L')_2]$ where M = Ru, Os). In the first class, excited state resonance Raman spectra could be observed for complexes which have metal-to-ligand charge transfer (MLCT) as the lowest excited state; complexes with ligand field (LF) lowest excited states show resonance Raman spectra very similar to their ground state Raman scattering. The Raman results are consistent with photochemical studies in other laboratories whereby the classification of these complexes as "reactive" or "unreactive" based on photosolvation quantum yields was interpreted according to the excited state ordering. In the second class of complexes it was found that the nature of the lowest excited state is very sensitive to the structure of the bidentate ligand. Excited state (MLCT) Raman spectra could be readily observed when L = 2,2'-bipyridine or 2,2'-bipyrimidine. Excited state spectra could not be observed from the ligand L = 1,10-phenanthroline whereas with L = 4,5-

diazafluorene reversal of energy levels was observed, with LF now being the lowest excited state. The third class was comprised of organic ligand-bridged bimetallic species with either the same or different metal centers which have absorption spectra which better match solar emission and thus are potential sensitizers for photochemical energy conversion. In these complexes the Raman data show that the excited state lifetimes are sensitive to both the nature of the metal and the external ligand.

Raman scattering resonant to the S_1 and S_2 excited states was utilized to study vibronic coupling in pyridine. Unlike the more symmetric pyrazine analog, the Raman spectrum resonant to the S_2 (π-π^*) state of pyridine displays the ν_{10a} C-H out-of-plane wagging mode. The general features of the pyridine S_2 resonance scattering are more similar to those observed in the Raman spectrum of benzene preresonant to the (π-π^*) state. This analogy suggests that the ν_{10a} mode enhancement in pyridine resonant to the S_2 state may be due to vibronic coupling between the S_2 and $B_1(\sigma$-π^*) states.

Two-photon induced fluorescence excitation experiments were initiated on perylene. Consistent with the two-photon parity selection rule, two strong and three weak peaks were observed in a region where there is minimal one-photon absorption. In order to extend the laser tuning range for this kind of experiment, a near-IR tunable dye laser was constructed which operates efficiently in the 780~910 nm region.

ACKNOWLEDGMENTS

TABLE OF CONTENTS

LIST OF TABLES

LIST OF FIGURES

CHAPTER 1

INTRODUCTION

A. Solar Energy Conversion

Inorganic photochemistry has been an active field of research in recent years. The intense interest and enthusiasm is due to the potential applications in such areas as solar energy conversion[1], lasers and catalysis. Crucial to the elucidation of the photochemistry and spectroscopy of inorganic complexes as well as to the rational design of useful systems, is a knowledge of the energy levels and degradation pathways.

The use of solar energy as an alternative to fossil fuels is an attractive option due to its abundance, low costs, and environmental considerations. Because solar radiation is diffuse and is not constantly available, some method of storage is required so that solar energy can be stored when it is plentiful for use at times when demand exceeds supply. Nature stores energy by the process of photosynthesis in green plants.

Through a complex series of steps, carbon dioxide and water are converted photochemically to oxygen and combustible carbohydrate. The challenge, then, is to devise an artificial cycle which will produce storable fuel from readily available and inexpensive raw materials. Several criteria have been mentioned in devising a practical photochemical energy storage cycle.[2]

1

1. The photochemical reaction should be endergonic ($\Delta G > 0$).

2. The photochemical reaction should operate over a significant portion of the solar spectrum.

3. The photochemical quantum yield should be high.

4. Energy stored per unit weight or volume of photoproduct(s) should be large.

5. Energy-releasing back reactions should be negligibly slow at ambient temperature, but should proceed rapidly and controllably upon addition of a catalyst.

6. Side reactions leading to depletion of reactants, products, photosensitizers or catalyst must be minimal.

7. Reagents of the system should be readily available, non-toxic and easy to handle.

Most energy-storing photoreactions can be divided into three general categories: photodissociation, photoisomerization, and photoredox. Only the photoredox process will be discussed.

The photochemical cleavage of H_2O into its elements has been intensely investigated.

$$H_2O(l) \xrightarrow{\text{sensitizer}} H_2(g) + 1/2O_2(g) \quad \Delta G_{298}^\circ = 57 \text{ kcal/mole}$$

Since H_2O does not absorb light above 200 nm, however, this reaction requires sensitizers. The basic approach to sensitization makes use of excited state redox properties of transition metal complexes for reduction and oxidation of H_2O, i.e.,

$$2e^- + 2H_2O = 2OH^- + H_2 \qquad -0.41V \text{ at pH 7}$$

$$2H_2O = 4H^+ + O_2 + 4e^- \qquad +0.82V \text{ 1 atm.}$$

The water splitting process based on photoredox chemistry is shown in Figure A-1.[3] Light initiates a bimolecular electron transfer reaction between D and A resulting in D^+A^-. The reducing power of A^- then is coupled to the reduction of H_2O (or H^+) by a suitable catalyst while oxidation of H_2O to O_2 is accomplished by D^+. The light −

absorbing species D or A plays the role of the photosensitizer. This
species should have the following properties.

1.   Appreciable light absorption within the solar energy wave length
      region.

2.   Sufficiently long-lived excited state lifetime so that bimolecular
      chemical reactions can compete with other deactivation processes.

3.   Must be able to undergo excited state electron transfer reactions
      with suitable quenchers.

4.   Long term photochemical stability.

excited state

*DA or DA* electron transfer

$D^+ + A^-$

H_2O

O_2

H_2O

H_2

D+A
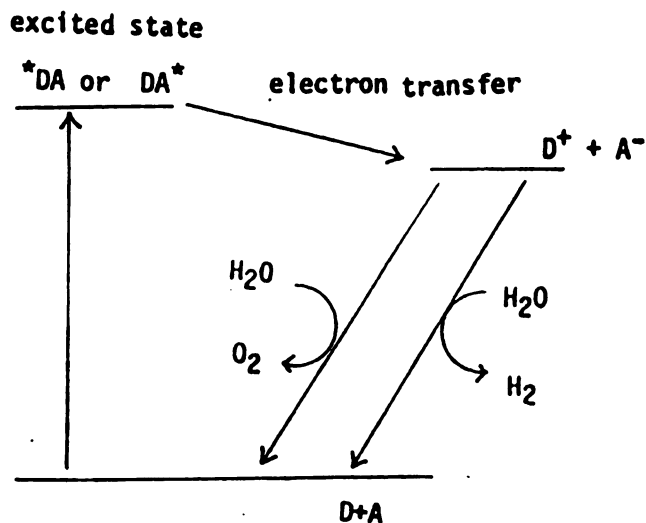
A-1   Water Splitting Process Based on
       Photoredox Chemistry

    The most widely used sensitizer for photoredox reactions is
Ru(II)(bpy)$_3$ (where bpy = 2,2'-bipyridine)(Figure A-2). This complex
displays an intense metal-to-ligand charge transfer absorption at 450
nm. The singlet-like state initially populated relaxes to the lowest
excited triplet state on a subpicosecond time scale. This lowest excited
state has a lifetime of 0.6ms at 25°C in aqueous solution. Both reductive

and oxidative quenching has been observed. The complex is also relatively inert to decomposition.

$$Ru^*(bpy)_3^{2+}$$

-0.84v   +0.84v

$h\nu$ | 2.1 ev

$Ru(bpy)_3^{3+}$ ⟶ $Ru(bpy)_3^{2+}$ ⟶ $Ru(bpy)_3^{+}$

1.26 ev   -1.28 ev
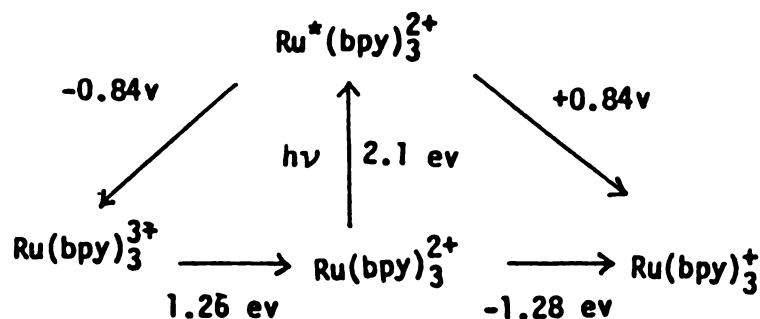
A-2   Redox Properties of Ru(II)(bpy)₃

Formation of $Ru^*(bpy)_3^{2+}$ by light absorption creates a separated electron-hole pair within the complex. Consequently it is both a stronger reductant and a stronger oxidant than the ground state by 2.1eV.

A prototype H₂-evolving system is outlined in Figure A-3.[3] Here, $Ru^*(bpy)_3^{2+}$ undergoes oxidative quenching by methylviologen MV^{+2}. The oxidized sensitizer is reduced back by the sacrificial reagent TEOA (triethanol amine). In the presence of colloidal platinum the other photoproduct MV^+ reduces H₂O to H₂ and is oxidized to the original dication. Production of O₂ is shown in Figure A-3. Here $Ru^*(bpy)_3^{2+}$ is oxidatively quenched by $Co(NH_3)_5Cl^{2+}$, generating $Ru(bpy)_3^{3+}$ and $Co(NH_3)_5Cl^+$. The latter complex decomposes irreversibly. The $Ru(bpy)_3^{3+}$ ion is sufficiently strong oxidant to oxidize H₂O to O₂ in the presence of a RuO₂ suspension.

While $Ru(bpy)_3^{2+}$ remains the most popular photosensitizer, many other transition metal complexes have in recent years, been tested for

this role, particularly since species having a broader visible absorption range would be desirable.

Ru(II)(bpy)₃ Sensitized Decomposition of H₂O

$$MV^{2+} = \text{—} N \text{⟨pyridine⟩⟨pyridine⟩} N \text{—}$$

$$TEOA = N(CH_2CH_2OH)_3$$
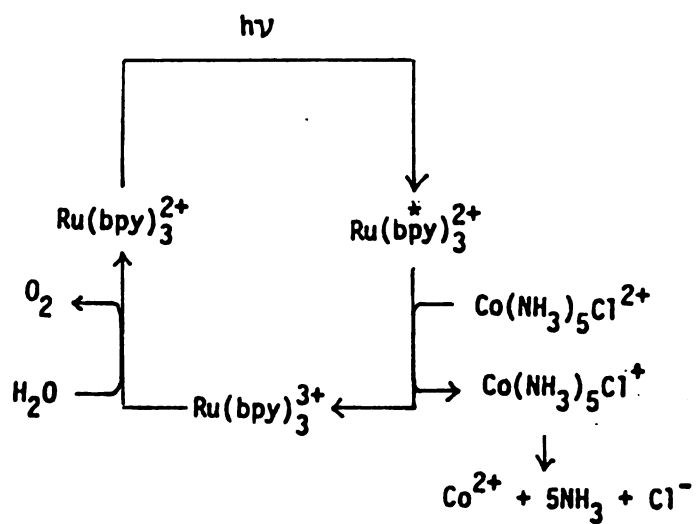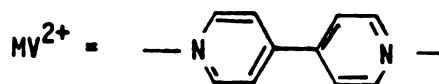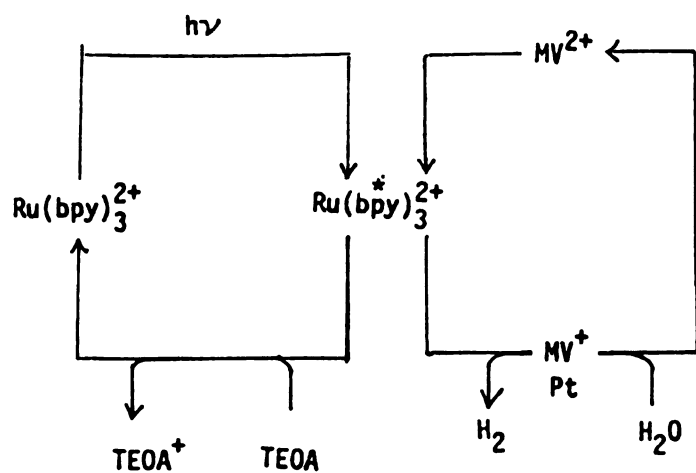
Fig A-3

REFERENCES

1. (a) Kalyanasundaram. K., Coord. Chem. Rev. **46**, 159 (1982). (b) Solar Power and Fuels, Bolton, J. R. (Editor), Academic Press, New York (1977). (c) Photochemical Conversion and Storage of Solar Energy, Connolly, J. S. (Editor), Academic Press, New York (1981).

2. (a) V. Balzani, L. Moggi, M. F. Manfrin, F. Balletta, M. Gleria, Science, **189**, 852 (1975). (b) J. Bolton, Science **202**, 705 (1978).

3. (a) N. Sutin, C. Cruetz, Pure Appl. Chem., **52** 2717 (1980). (b) M. Gratzel, Acct. Chem. Res., **14**, 376 (1981).

B. Structure and Bonding of Coordination Complexes.

Progress in the study of the photochemistry and photophysics of transition metal coordination complexes depends, to a large degree, on a clear conceptual, theoretical scheme which allows a coherent organization of available experimental facts and provides a qualitative model for predicting future experiments.

There are three basic approaches to describing bonding in coordination complexes: Valence Bond Theory, Crystal Field Theory (or Ligand Field Theory) and Molecular Orbital Theory. Molecular orbital theory probably offers the best current interpretation of the properties of coordination complexes. With increasingly accurate wave-functions and the increased availability of high-powered computers, molecular orbital theory is assuming a dominant position in the theoretical interpretation of metal complexes. The derivations of the three methods are widely available (see any standard textbook on inorganic chemistry), so they will not be repeated here.

Of intense photochemical and spectroscopic interest are the complexes of Rh(III), Co(III), Ru(II), Os(II), and other d^6 transition metal systems. This interest is due to the wide variety of these complexes that can be designed to have quite different types of lowest excited electronic states accessible with visible and near UV light. Typical structures and geometries of these complexes are shown in Figure B-1 with their abbreviations, which will be used throughout this thesis.

In considering the relative energy levels of these d^6 transition metal complexes it is assumed in all cases that the central metal is in an octahedral environment, in the strong field case $(t_{2g})^6$; although the ligand distribution provides a lower symmetry, this approximation holds
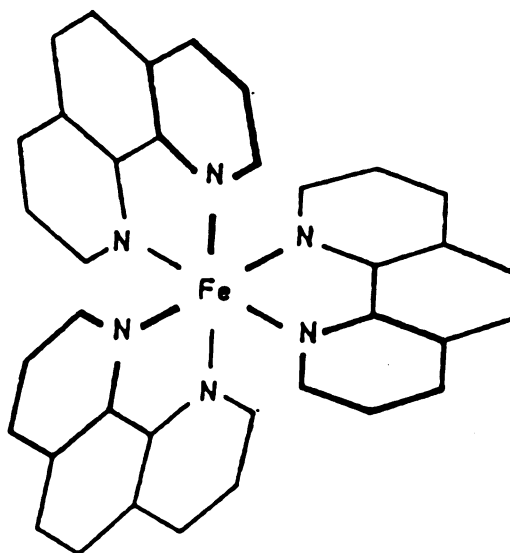
D_3
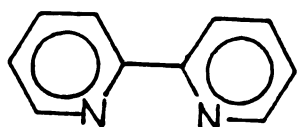
bpy = 2,2'- bipyridine
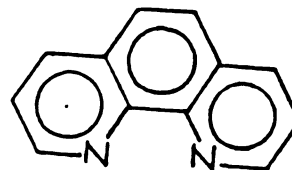
phen = 1,10 - phenanthroline
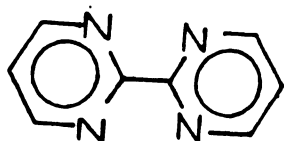
bpym = 2,2'-bipyrimidine
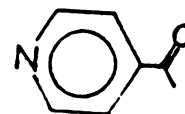
4-acpy= 4 acetylpyridine
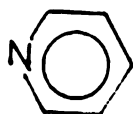
py = pyridine
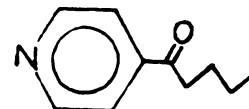
4-vp = 4-valeryl pyridine

Structures of Organic Ligands

Fig B-1

rather well for all complexes investigated in this work. Conceptually, one combines the metal orbital diagram with that of the ligands to arrive at a composite molecular orbital model for the entire system. The relative positions of the two sets of orbitals can vary and several different possibilities of orbital arrangement are possible as shown in Figure B-2:
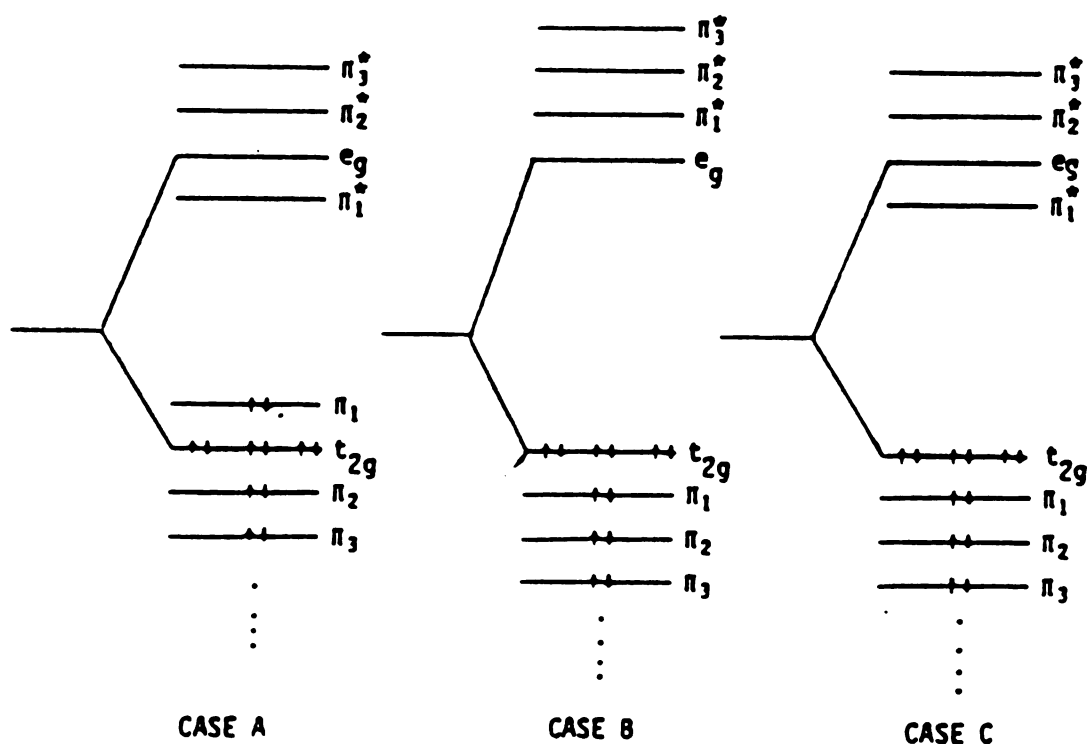
Orbital Energy Levels in Organic Complexes of d^6 Transition Metal

Figure B-2

Spectrocopic studies on Rh(III)(bpy)₃ and Rh(III)(phen)₃ and other analogous complexes show that a $\pi \to \pi^*$ transition is the lowest absorption possible.[2] This ligand localized or internal ligand (IL) transition means that the metal plays a secondary role. This is the situation in case (A) above. Spectroscopic studies on such complexes as the [Co(CN)₆]³⁻ ion leads one to conclude that the lowest excited state involves promotion of one of the metal d-electrons: $(t_{2g})^6 \to (t_{2g})^5(e_g)^1$. That is, the transition is basically a metal-localized or ligand field transition (LF). Case (B) describes this situation.

The third case reveals an entirely new set of transitions that are neither metal centered nor ligand localized. From extensive spectroscopic studies, it has been determined to be charge transfer in nature.[3] Absorption of a photon promotes an electron from the t_{2g} orbital on the metal center to an antibonding π^* orbital in the ligand system. This case (C) is of intense interest because the internal redox like "reaction" creates a completely new species which is capable of acting either as a strong oxidant or reductant. The study of the reactive channels of these complexes has direct application to solar energy conversion schemes described earlier in this chapter.

A qualitative MO scheme for a typical octahedral complex such as Ru(II)(CO)₆ is shown in Figure B-3.[4] In all of the complexes studied here, the ligands possess π orbitals and the d-π^* interaction becomes crucial in interpreting the optical spectra. In the simplest example, each ligand has a pair of mutually perpendicular π orbitals making twelve altogether. From a standard group theory treatment, these may be combined into four triply degenerate sets of classes t_{1g}, t_{2g}, t_{1u}, t_{2u}, with t_{1g}, and t_{2u} non-bonding. The t_{1u} orbitals of the metal
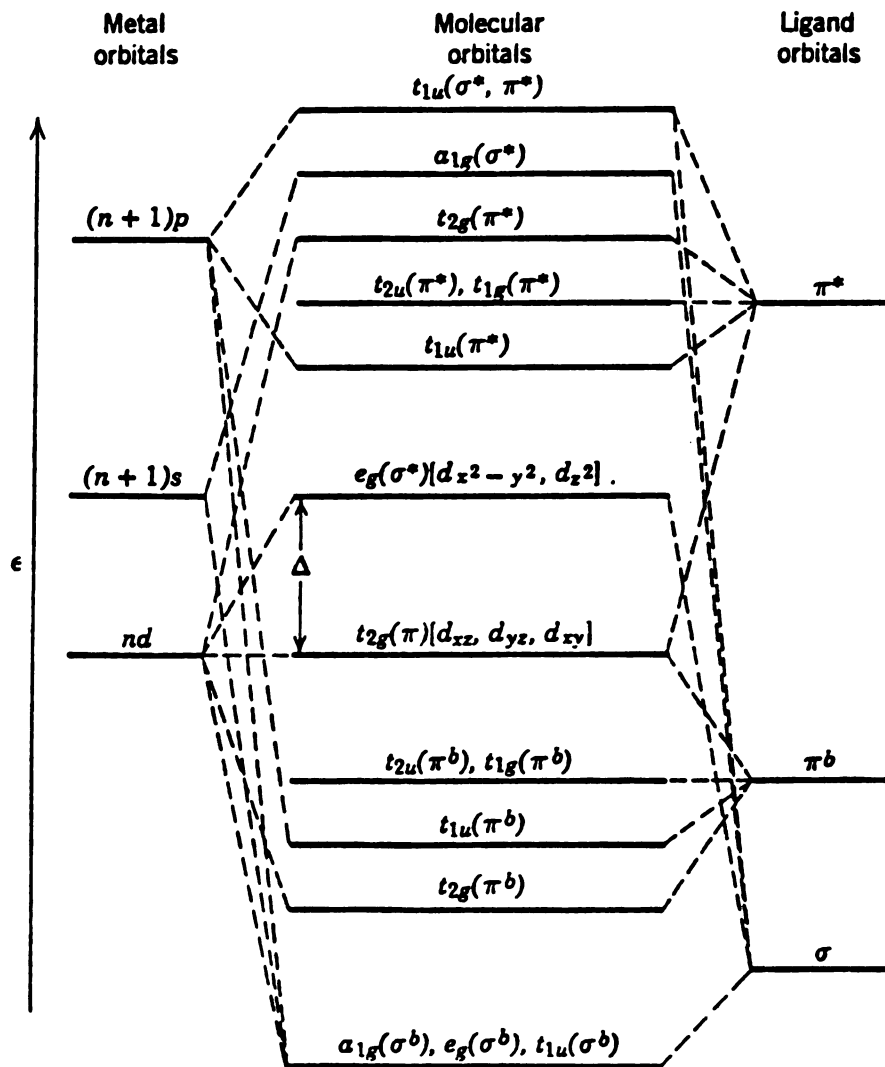
MO Diagram of Typical ML₆ Complex.

Fig B-3

participate in σ bonding which leaves the t_{2g} set to interact with the ligands by $d\pi^*$ interaction. The effect of this π bonding by molecular orbitals of the t_{2g} type on the energy of the complex is as follows. If the ligands have empty low-lying π^* orbitals, but higher in energy than t_{2g} metal orbitals, the net result is that the π interaction stabilizes the t_{2g} orbitals relative to the metal e_g^* orbitals. The metal t_{2g} orbitals also acquire some ligand orbital character. In effect, the π interaction causes the Δ value (ligand field splitting parameter) for the complex to be greater than it would be if only σ interaction took place. The second possibility is that the ligands possess only filled π orbitals of lower energy than the metal t_{2g} level. The interaction then destabilizes the t_{2g} orbitals relative to the e_g^* level, thus diminishing the effective Δ

Due to the importance of $Ru(bpy)_3^{2+}$ in solar energy conversion schemes, this complex has come under intense scrutiny from both experimental and theoretical points of view. Assignments of the orbital spin labels for the various absorption bands and of luminescence have been controversial. The absorption spectrum of $Ru(bpy)_3^{2+}$ is shown in Figure B-4. Absorption at 208 and 285 nm are assigned to ligand centered $\pi-\pi^*$ transitions.[4,5a,b] Weak shoulders at 323 nm and 345 nm are assigned as ligand field (d-d*) transitions. The intense absorption band in the visible with maximum at 452 nm is the metal to ligand charge transfer (MLCT). A qualitative MO scheme for $Ru(bpy)_3^{2+}$ is shown in Figure B-5:

The MO diagram presented is in O_h symmetry. Of course, the symmetry of $Ru(bpy)_3^{2+}$ in the ground state is D_3 and strictly the
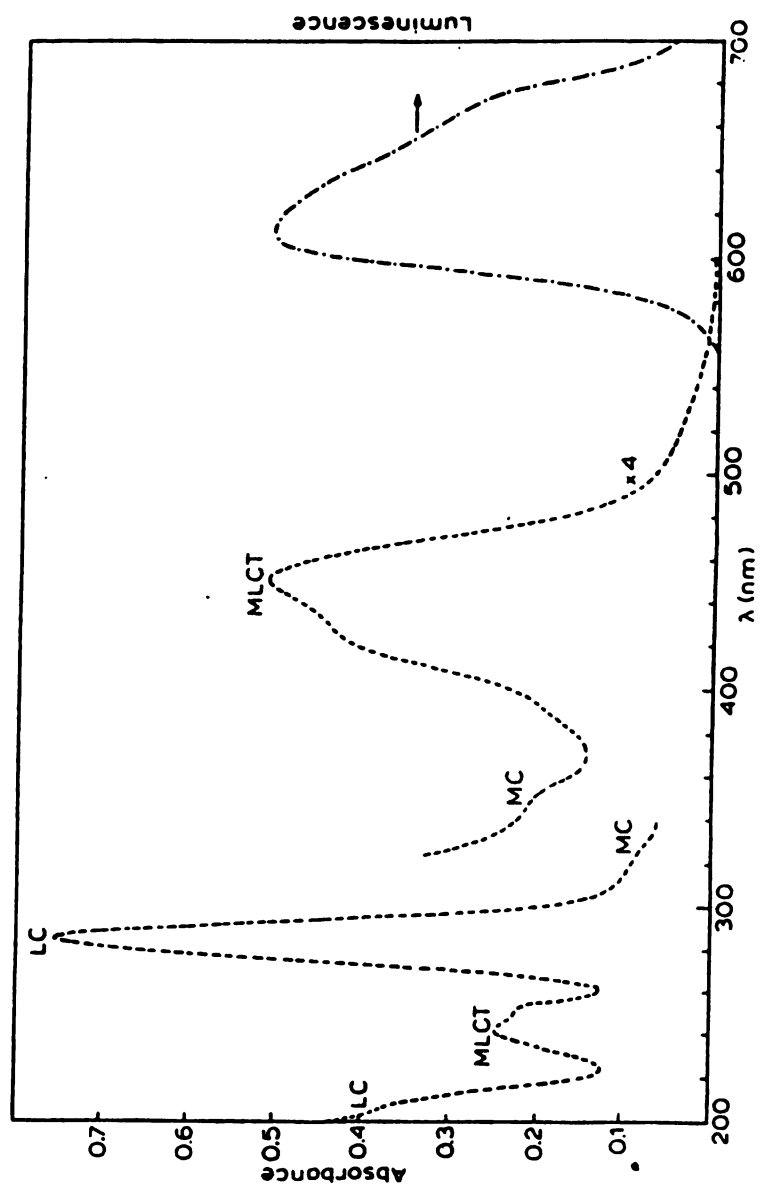
Fig B-4

Electronic Absorption Spectrum of Ru(II)(bpy)₃

MO Diagram of Ru(II)(bpy)₃
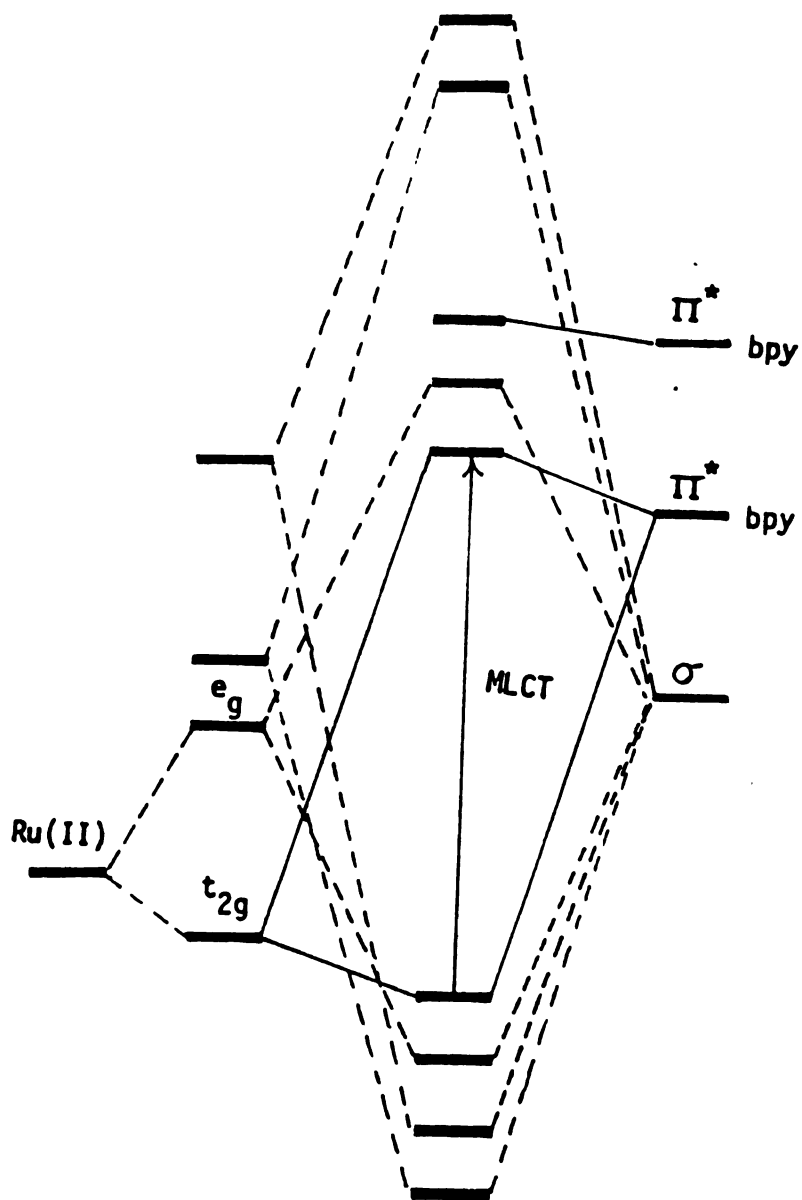
Fig 8-5

orbitals should be considered in this symmetry group. The t_{2g} and e_g orbitals of the metal transform as a_1,e and e symmetry in D_3.[6]

O_h	D_3	Symmetry
$d_{x^2-y^2}$	$d_{x^2-y^2}$	e
d_{z^2}	d_{z^2}	
d_{xy}	$(d_{xy} + d_{xz} + d_{yz})$	a_1
d_{xz}	$(d_{xz}-d_{yz})$	e
d_{yz}	$(2d_{xy}-d_{xz}-d_{yz})$	

That is, the t_{2g} orbitals in O_h become a_1 and e in D_3

The lowest MO's of bipyridine have a_2 and e symmetry[6] and transitions to states of A_1, A_2, E symmetry are possible. However, only the $^1A_1 \rightarrow {}^1E$ transition is seen at 452 nm.

For each class of complex a qualitative MO scheme will be presented to explain the optical and Raman data. Since the splitting of the octahedral symmetry levels in the non O_h environments of the complexes of interest is small, and there results no qualitative change in the description of the optical transitions in these transition metal complexes for clarity and simplicity the octahedral pattern for the metal orbitals will be retained in these diagrams.

REFERENCES

1. F. A. Cotton, G. Wilkinson, Adv. Inorg. Chem. 4th ed. J. Wiley and Sons (1980).

2. D. H. Cartens, G. A. Crosby J. Mol. Spec., 34, 113 (1970).

3. D. M. Klassen, G. A. Crosby, J. Chem. Phys., 48, 1853 (1968).

5. (a) G. A. Crosby, Acc. Chem. Res., 8, 231 (1975).   (b) F. E. Lytle, D. M. Hercules, J. Am. Chem. Soc. 91, 253 (1969).

6. E. Kober, T. J. Meyer, Inorg. Chem. 22, 1614 (1983).

C. Resonance Raman Spectroscopy

The theory of the Raman effect is well documented and numerous review articles exist.[1-22] Therefore, only a very brief presentation of the pertinent equations will be presented here.

The Raman effect is a molecular light scattering phenomenon in which light scattered by a sample shows a change in frequency with respect to the incident light. The frequency difference corresponds to a difference in quantum levels of the sample. Resonance Raman scattering is a form of high resolution vibronic spectroscopy in which the intensity of vibrational light scattering is studied as the excitation source is tuned in the proximity of an electronic absorption band of the sample. Much information can be obtained about the potential surfaces of both ground and excited states. Because of the resonance-enhanced selectivity, it may be used to probe a local chromophore in a complex mixture. This allows, for example, the study of porphyrin chromophore in a protein system without interference from the polypeptide chain.

It is crucial for the Raman process that the electric field of the electromagnetic radiation induces a dipole moment π in the molecule which is roughly proportinal to the field strength E. Thus, $\pi = \alpha E$, where α is called the electric polarizability of the molecule. In general, the vector π has a different direction from that of the vector E and thus α is not a solar quantity. In fact α is a second order tensor. Thus,

$$\pi_x = \alpha_{xx} E_x + \alpha_{xy} E_y + \alpha_{xz} E_z$$

$$\pi_y = \alpha_{yx} E_x + \alpha_{yy} E_y + \alpha_{yz} E_z$$

$$\pi_z = \alpha_{zx} E_x + \alpha_{zy} E_y + \alpha_{zz} E_z$$

This polarizability tensor can be evaluated by a second order perturbation approach developed by Kramers and Heisenberg in analogy to classical dispersion theory.

$$(\alpha_{\rho\sigma})_{gf} = 1/h \sum_e \frac{\langle f|\mu_\rho|e\rangle\langle e|\mu_\sigma|g\rangle}{\nu_{eg} - \nu_0 + i\Gamma_e} + \frac{\langle f|\mu_\sigma|e\rangle\langle e|\mu_\rho|g\rangle}{\nu_{ef} + \nu_0 + i\Gamma_e}$$

--μ_ρ and μ_σ are dipole moment operators

--$|g\rangle$, $|f\rangle$ are initial and final state wavefunctions

--$|e\rangle$ is the wave function of an excited state, e of half bandwidth Γ_e

--ν_{eg}, ν_{ef} are frequencies of transitions, and ν_0 is the frequency of the illuminating electromagnetic radiation

Notice that when $\nu_0 \ll \nu_{eg}$ both terms contribute and polarizability is nearly independent of the incident frequency. As ν_0, the excited frequency approaches ν_e, however, the first term becomes dominant and we have resonance enhancement. For a Raman transition between states g and f, the scattering intensity is

$$I_s = \frac{8\pi\nu_s^4}{9c^4} I_0 \sum_{\rho\sigma} |(\alpha_{\rho\sigma})_{gf}|^2$$

where I_0 is the incident intensity at frequency ν_0, ν_s is the scattered frequency, c is velocity of light, α is polarizability tensor as defined above, and ρ and δ are the incident and scattered polarization. Albrechts vibronic coupling model[16-18] then invokes the Born-Oppenheimer approximation to separate the wave function into electronic and vibrational parts, which gives $\langle\phi|\mu|e\rangle=\langle j|M_e|v\rangle$ and $\langle e|\mu|g\rangle=\langle v|M_e|i\rangle$ where $|i\rangle$ and $|j\rangle$ are initial and final vibrational wavefunctions of the ground electronic state and $|v\rangle$ is a vibrational wave function of the excited electronic state e. M_e is the pure electronic transition moment between g and e. This is a weakly varying

function of the nuclear coordinates and is Taylor expanded about the equilibrium geometry o; i.e., Me = Me° + $(\partial M/\partial Q)°Q$; where Q is given normal mode of the molecule. The expansion of the α expression now gives: $\alpha = A + B + C$ where

$$A = (Me°)^2 \; 1/h \; \sum_v \; \frac{\langle j|v\rangle\langle v|i\rangle}{w_1 - v_0 + i\Gamma v}$$

and

$$B = Me°(\partial M/\partial Q)° \; 1/h \; \sum_v \; \frac{\langle j|Q|v\rangle\langle v|i\rangle + \langle j|v\rangle\langle v|Q|i\rangle}{w_1 - v_0 + i\Gamma v}$$

The C-term results from coupling of the excited state to the ground state and can be neglected in most cases.

The A-term scattering or Franck-Condon scattering is ordinarily the main contributor to the resonance Raman intensity. Only totally symmetric modes can contribute by this term, however, because only these modes will displace the equilibrium nuclear position giving non-zero Franck-Condon overlaps. Among the normal modes available to a complex molecule, the ones that experience the strongest resonance enhancement via the A-term scattering are those whose coordinates most closely correspond to the distortions experienced by the molecule in the excited state.[19] Therefore, molecular π-π^* transitions cause large enhancements for modes involving stretching of π-bonds, but little enhancement is seen for C-H stretches, for example, since they are not significantly affected in the excitation. Metal-ligand charge transfer transitions enhance ligand-metal stretching modes which are weakened in the excited state and/or some internal ligand modes which are affected by the excitation.[20]

Nontotally symmetric modes can gain intensity by Albrechts B-term due to the Q-dependent vibrational integral. The derivative can be evaluated directly[23] if the potential surfaces are known. The Herzberg-Teller[3] approach is to expand the excited state wave function in terms of the normal modes and this results in the following expression.

$$B = \frac{(Me^0)(Ms^0)hes}{(\nu_s - \nu_e)} \quad \Sigma_v \quad \frac{\langle j|Q|v\rangle\langle v|i\rangle + \langle j|v\rangle\langle v|Q|i\rangle}{(\nu_i - \nu_0 + i\Gamma v)}$$

where S is a higher-lying excited state and $h_{es} = \langle s|\partial H/\partial Q|e\rangle$. For this integral to be non vanishing, the symmetry of the vibration must be contained in the direct product of the two electronic symmetries. Albrecht's B-term scattering may become important when the excitation is in resonance with a weakly-allowed transition that is vibronically coupled to a nearby strongly-allowed transition. The nontotally symmetric modes which mixes two transitions will be especially strong. The first clear experimental example of B-term scattering was observed in pyrazine.[24-26] For N-heterocyclic aromatic molecules the lowest electronic transition is $n-\pi^*$ in character, which is orbitally forbidden. This state, however, mixes with a nearby $\pi-\pi^*$ state via the out-of-plane C-H bending mode ($\sim$900 cm^{-1}). The B-term can also be expected to be responsible for resonance effects associated with symmetry-forbidden transitions such as ligand field (d-d*) bands of transition metal complexes.[27,28]

A plot of the Raman scattering intensity vs excitation laser wavelength is called an excitation profile. It is similar to a fluorescence excitation spectrum except that individual Raman bands are monitored

separately. For a mode which Raman scatters via the A-term, the excitation profile is expected to show a peak at the 0-0 origin of the resonant electronic transition and subsequent peaks at successive excited state vibrational levels, the amplitudes depending on the successive Franck-Condon factors. It is also possible for the excitation profile to show peaks at positions which correspond to the excited state level of a different normal mode than the one under consideration.[29] Another source of vibrational enhancement arises when the normal mode vectors change their composition upon electronic excitation, the so called Dushinski effect.[30] Excitation profiles can be a powerful tool in resolving unstructured absorption profiles. The profile of a mode due to B-term scattering is expected to show maxima at the 0-0 and 0-1 positions for each mixing mode. This was demonstrated for vibronic modes of a porphyrin macrocycle which showed a common 0-0 maximum, so called α absorption, and second maxima which were individually shifted from the α-band frequency by the vibrational frequency of that mode.[31] Since the Raman tensor can have contributions from several resonant states, the shape of the excitation profile will be influenced by interference effects.[32] In centrosymmetric transition metal complexes a resonant de-enhancement of modes has been observed. The resonance scattering amplitude from vibronically induced ligand field states was comparable to the pre-resonance amplitude from higher energy charge transfer states.[33]

The polarization properties of the scattered Raman signal give information on the polarizability tensor. The tensor contains nine elements which in principle, can be measured in an oriented system.

For random orientation the tensor has three invariants which are defined as follows:

$$\alpha^2 = 1/9 \left(\sum_\rho \alpha_{\rho\rho} \right)^2$$

isotropic part

$$\gamma_s^2 = 1/2 \sum_{\rho\sigma} (\alpha_{\rho\rho} - \alpha_{\sigma\sigma})^2 + 3/4 \sum_{\rho\sigma} (\alpha_{\rho\sigma} + \alpha_{\sigma\rho})^2$$

symmetric anisotropy

$$\gamma_{as}^2 = 3/4 \sum_{\rho\sigma} (\alpha_{\rho\sigma} - \alpha_{\sigma\rho})^2$$

antisymmetric anisotropy

These are equivalent within numerical factors to the trace, quadrupole, magnetic dipole invariants as defined by Placzek.[34] If the incident beam is linearly polarized perpendicular to the scattering direction, the intensity of the scattered component that is polarized parallel to the incident polarization is given by $I_{11} = K(45\alpha^2 + 4\gamma_s^2)$, K is a constant of the experiment, while the intensity of the perpendicular component is $I = K(3\gamma_s^2 + 5\gamma_{as}^2)$. The experimentally useful definition of the depolarization ratio is

$$\rho = I_L/I_{11} = (3\gamma_s^2 + 5\gamma_{as}^2)/(45\alpha^2 + 4\gamma_s^2)$$

If, as is generally the case the tensor is symmetric, i.e., $\alpha_{\rho\sigma} = \alpha_{\sigma\rho}$ then, $\gamma_{as}^2 = 0$ and $\rho \leq 3/4$. However, ρ can exceed 3/4 in what is called anomalous polarization. The expected value of ρ for each symmetry point group has been worked out by McClain and others.[36]

The Raman spectrum of $Ru(bpy)_3^{+2}$ has been intensely investigated by many groups.[37-44] Upon excitation into the intense near-UV metal to ligand charge transfer absorption band, the ring stretching modes of the ligand are resonantly enhanced, consistent with populating an antibonding orbital. Only totally symmetric modes are enhanced and the excitation profile shows that there are two excited states of degenerate symmetry separated by less than a typical high frequency vibrational mode. The excited state Raman spectrum obtained with pulsed 355 radiation shows that the optical electron is localized on one bpy ligand rather than delocalized over all three at least on the time scale of the Raman experiment.

REFERENCES

1. T. G. Spiro, T. M. Loehr, Adv. in Infrared and Raman Spec., edited. R. H. H. Clark and R. E. Hester, Vol. 1, London: Heyden (1975).

2. T. G. Spiro, B. P. Gaber, Ann. Rev. Bioch. 46, 553 (1977).

3. J. Behringer, Raman Spectroscopy, H. A. Szymanski, edited, 168, (1967), New York: Plenum Press.

4. J. Tang, A. Albrecht, Raman Spectroscopy, H. A. Szymanski, edited, 2, 33, (1967), New York, Plenum Press.

5. W. L. Peticolas, L. Nafie, P. Stein, B. Francori, J. Chem. Phys. 52, (1576), 1970.

6. J. M. Friedman, R. M. Hochstrasser, Chem. Phys. 1, 457, 1973.

7. M. Mingardi, W. Siebrand, J. Chem. Phys. 62, 1074 (1975).

8. M. Garazzo, F. Galluzzi, J. Chem. Phys. 64, 1720 (1976).

9. L. D. Barron, Mol. Phys. 31, 129 (1976).

10. B. Johnson, L. A. Nafie, W. L. Peticolas, Chem. Phys. 19, 303 (1977).

11. B. Johnson, W. L. Peticolas, Ann. Rev. Phy. Chem. 27, 465 (1976).

12. J. M. Friedman, R. M. Hochstrasser, Chem. Phys. 6, 155 (1974).

13. J. Berg, C. Langhoff, G. W. Robinson, Chem. Phys. Lett. 29, 305, (1970).

14. R. C. Hilborn, Chem. Phys. Lett. 32, 76 (1975).

15. S. Mukamel, J. Jortner, J. Chem. Phys. 62, 3609 (1975).

16. A. C. Albrecht, J. Chem. Phys. 34, 1476 (1961).

17. A. C. Albrecht, M. C. Huntley, J. Chem. Phys. 55, 4438 (1971).

18. A. C. Albrecht, J. Chem. Phys. 33, 156 (1960).

19. A. Hirakawa, M. Tsuboi, Science 188, 359 (1975).

20. B. P. Gaber, V. Miskowski, T. Spiro, J. Am. Chem. Soc. 96, 6868, (1974).

21. J. Behringer, Chem. Soc. Specialist report on mol. spec. 2, 100. R. F. Barrow, D. A. Long, D. J. Millen, editors, London (1974).

22. S. Porto, D. Wood., J. Opt. Soc. Am. 52, 251 (1962).

23. A. Warshel, Ann. Rev. Biophys. Bioeng. 6, 273 (1977).

24. M. Ito, I. Suzuka, Y. Udagawa, K. Kaya, N. Mikami, Chem. Phys. Lett. 16, 211 (1972).

25. K. kamagowa, M. Ito, J. Mol. Spec. 60, 277 (1976).

26. A. H. Kalantar, E. S. Franzosa, K. K. Innes J. Mol. Spec. 17, 335 (1972).

27. P. Stein, V. Miskowski, W. H. Woodruff, J. P. Griffin, K. G. Werner, B. P. Gaber, T. G. Spiro, J. Chem. Phys. 64, 2159 (1976).

28. G. A. Schick, D. F. Bocian, J. Raman Spec. 11, 27 (1981).

29. A. Kiefer, H. J. Bernstein, Chem. Phys. Lett. 8, 381 (1971).

30. F. Dushinski, Acta Physicochim. USSR 1, 551 (1973).

31. T. G. Spiro, T. C. Strekas, Proc. Natl. Acad. Sci., USA 69, 2622 (1972).

32. J. Friedman, R. Hochstrasser, Chem. Phys. Lett. 32, 414 (1975).

33. L. A. Nafie, R. Pastor, J. Dabrowiak, W. H. Woodruff, J. Am. Chem. Soc. 98, 8007 (1976).

34. G. Placzek, Handbuch der Radiologie, ed. E. Marx, 2, 209. Leipzig, Academisch Verlagsgesellschaft (1934).

35. W. Kiefer, H. J. Bernstein, App. Spec. 25, 500 (1971).

36. W. M. McClain, J. Chem. Phys. 55, 2789 (1971).

37. A. Basu, H. D. Gafney, T. C. Strekas, Inorg. Chem. 21, 2231 (1982).

38. T. C. Strekas, S. K. Mandal, J. Ram. Spec. 15, 109 (1984).

39. S. McClanahan, J. Kinkaid, J. Ram. Spec. 15, 173 (1984).

40. P. J. Miller, R. S. L. Chao, J. Ram. Spec. 8, 17 (1979).

41. R. F. Dallinger, W. H. Woodruff, J. Am. Chem. Soc. 101, 4391 (1979).

42. P. G. Bradley, N. Kress, B. Hornberger, R. F. Dallinger, W. H. Woodruff, J. Am. Chem. Soc. 103, 7441 (1981).

43. M. Foster, R. E. Hester, Chem. Phys. Lett. 81, 42 (1981).

44. W. K. Smothers, M. Wrighton, J. Am. Chem. Soc. 105, 1067 (1983).

D. Experimental

The complexes studies in this thesis were synthesized by established methods and they were characterized by NMR, UV-visible absorption, emission and IR spectroscopies.[1]

Typically, ~10^{-3}M aqueous solutions of the complexes were used in a standard 1 cm x 1 cm cuvette. The cw Raman spectra were obtained with a He-Cd laser (441.6 nm, 50 mW; Liconix model 4240) or Ar^{+} laser (Coherent Radiation Innova model 90-5). For excited state Raman spectra a Nd:YAG pulsed laser (2~7 mj/pulse, 10 ns fwhm, 10Hz; Quanta-Ray DCR-1A was used). This laser could also be used to pump one of an assortment of dyes in a Quanta-Ray PDL-1 dye laser. Photons within the same laser pulse pumped and probed the transient species present. Scattering the high frequency ring vibration region ($\Delta\nu$ = 1000~1700 cm^{-1}) was collected at 90° to the incident laser beam and dispersed by a Spex triplemate polychromator onto an EGG/PARC model 1420 Reticon multichannel detector coupled to an OMA-II signal processing system. Wave number calibration was achieved by using toluene, cyclohexene and fenchone. Typical operating conditions of the triplemate/OMA system were 1800 or 2400 groove/mm grating, 600 delays, 20 scans. Absorption spectra were taken for each complex both before and after the Raman experiment to monitor possible photodecomposition.

REFERENCES

1.   N. Leventis, Ph.D. Dissertation, Michigan State University (1985).

CHAPTER 2

.

Resonance Raman Spectra of Ground and Low-Lying Excited States of Ruthenium(II) Pentaammine Pyridine Derivatives

Y. C. Chung, N. Leventis, P. J. Wagner,* and G. E. Leroi*

*Department of Chemistry, Michigan State University
East Lansing, Michigan 48824*

Raman spectra of electronically excited molecules have been reported for polypyridine complexes of d^6 transition metals.[1-5] The prototypical case has been tris(2,2'-bipyrdine)ruthenium(II) [$Ru(bpy)_3^{2+}$], for which it has been demonstrated that the electron promoted by metal-to-ligand charge-transfer (MLCT) absorption is localized (on the Raman time scale) on one of the bipyridine ligands.[1-4] We describe here observations on two pentaammineruthenium(II) pyridine complexes, models of another system for which the photochemistry and photophysics have received considerable recent attention.[6-10] The results are consistent

(1) Dallinger, R. F.; Woodruff, W. H. *J. Am. Chem. Soc.* 1979, *101*, 4391.
(2) Bradley, P. G.; Kress, N.; Hornberger, B. A.; Dallinger, R. F.; Woodruff, W. H. *J. Am. Chem. Soc.* 1981, *103*, 7441.
(3) Forster, M.; Hester, R. E. *Chem. Phys. Lett.* 1981, *81*, 42.
(4) Smothers, W. K.; Wrighton, M. S. *J. Am. Chem. Soc.* 1983, *105*, 1067.
(5) McClanahan, S.; Hayes, T.; Kincaid, J. *J. Am. Chem. Soc.* 1983, *105*, 4486.
(6) Malouf and Ford (Malouf, G.; Ford, P. C. *J. Am. Chem. Soc.* 1977, *99*, 7213) provide a summary and references to 1977.
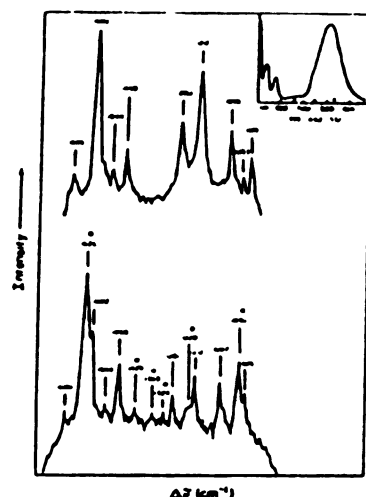
Figure 1. Resonance Raman spectra of deoxygenated 10^{-3} M aqueous solutions of $Ru^{II}(NH_3)_4(acpy)(BF_4)_2$. Top frame: under CW excitation at 441.6 nm. Bottom frame: under pulsed excitation at 354.7 nm. Wavenumber shifts are given above the peaks. Bands attributed to excited-state scattering are marked by asterisks. [Inset: absorption spectrum in the 250–650-nm region, with excitation wavelengths marked by arrows.]

with excited state ordering based on photochemical evidence and provide the first example of an excited-state Raman spectrum involving a monodentate pyridine ligand.

Resonance Raman spectra have been obtained for ~10^{-3} M aqueous solutions of $Ru^{II}(NH_3)_4(py)(BF_4)_2$ (py = pyridine) (1) and $Ru^{II}(NH_3)_4(acpy)(BF_4)_2$ (acpy = 4-acetylpyridine) (2). The complexes were synthesized and characterized by well-established methods. Raman spectra were excited by the following sources: He-Cd CW laser (441.6 nm, 50 mW; Liconix Model 4240), Nd:YAG pulsed laser (532.0 and 354.7 nm, variable power up to ~8 mJ/pulse, 10 ns fwhm, 10 Hz; Quanta-Ray DCR-1A). Excited-state spectra were observed under high-power illumination of the Nd:YAG laser. Photons from the same laser pulse served both to pump the sample and to interrogate the species present in solution following absorption. Scattering in the range $\Delta\nu$ = 1000–1700 cm^{-1} was collected at 90° to the incident laser beam and dispersed by a Spex Triplemate polychromator onto an EGG/PARC Model 1420 Reticon multichannel detector, which was coupled to an OMA-II signal processing system. Toluene, cyclohexene, o-chlorotoluene, and fenchone were utilized for wavenumber calibration. Under typical operating conditions of the Triplemate/OMA system (1800 or 2400 groove/mm grating, 600 delays, 30 scans), wavenumber accuracy of the measured peak positions is ±2 cm^{-1}.

The near-UV/visible spectrum of aqueous 2 (inset, Figure 1) displays strong MLCT absorption with λ_{max} = 524 nm. This
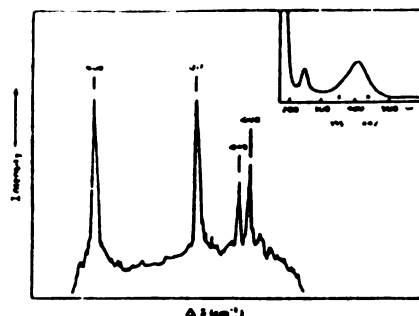
(7) Ford, P. C.; Malouf, G.; Petersen, J. D.; Durante, V. A. Adv. Chem. Ser. 1976, No. 150, 187.
(8) Matsubara, T.; Ford, P. C. Inorg. Chem. 1978, 17, 1747.
(9) Natarajan, P.; Endicott, J. F. J. Am. Chem. Soc. 1973, 94, 5910.
(10) Wagner, P. J.; Bartoszek-Loza, R. J. Am. Chem. Soc. 1981, 103, 5587.
(11) Ford, P. C.; Rudd, D. F. P.; Gaunder, R.; Taube, H. J. Am. Chem. Soc. 1968, 90, 1187.
(12) Vogt, L. H., Jr.; Katz, J. L.; Wiberley, S. E. Inorg. Chem. 1965, 4, 1157.
(13) Chaisson, D. A.; Hintze, R. E.; Stuermer, D. H.; Petersen, J. D.; McDonald, D. P.; Ford, P. C. J. Am. Chem. Soc. 1972, 94, 6665.

Figure 2. Resonance Raman spectrum of deoxygenated 10^{-3} M aqueous solution of $Ru^{II}(NH_3)_4(py)(BF_4)_2$ excited by pulsed 354.7-nm radiation. [Inset: absorption spectrum in the 250–500-nm region.]

complex exemplifies species classified as "unreactive" toward ligand photoactivation, for which MLCT absorption is thought to lie at lower energies than the dissociative ligand field (LF) transitions. The ground-state resonance Raman spectrum of 2 excited at 442 nm is displayed in the top frame of Figure 1. It is dominated by vibrations of the acpy ligand. Attempts to obtain the Raman spectrum of the MLCT excited state by excitation with intense (5–8 mJ) pulses of 532-nm radiation from the Nd:YAG laser were unsuccessful. (Only the ground-state spectrum was observed.) The lifetime of this excited state is extremely short, so only very small concentrations of the excited species, representable as $Ru^{III}(NH_3)_4(acpy^-)^{2+}$ (2*), can be generated. Moreover its Raman spectrum is not expected to be resonance enhanced at 532 nm since the lowest energy absorption of the acpy radical anion occurs at ~325 nm. Two-color experiments involving 532-nm pump and 355-nm probe wavelengths also failed, probably due to synchronization difficulties with the short-lived excited state.

However, new Raman peaks in addition to ground-state acpy scattering were generated when aqueous solutions of 2 were excited by 5–8-mJ pulses of 354.7-nm radiation; the Raman spectrum in the 1000–1700-cm^{-1} region is shown in the lower frame of Figure 1. Six peaks attributable to excited-state scattering are denoted by asterisks. Three are relatively prominent; the remainder are weak, but quite reproducible. The C=O stretching vibration (1646 cm^{-1}) is conspicuously diminished. The pattern correlates reasonably well with the ground-state resonance Raman spectrum of the free acetylpyridine radical anion. Further support for the assignment of the new peaks to 2* is provided by several acylpyridine complexes of rhenium carbonyls and tungsten carbonyls, for which there is strong evidence that the lowest excited states are MLCT. Preliminary excited-state resonance Raman spectra of these species are dominated by peaks near 1620 and 1030 cm^{-1}. Observation of MLCT excited-state scattering from 2 is thus consistent with Ford's model for photochemically "unreactive" complexes in the $Ru^{II}(NH_3)_4L$ series.

$Ru(NH_3)_4(py)^{2+}$ is an example of a photoactive complex for which the dissociative LF state is thought to lie below the MLCT

(14) Only slight frequency shifts and intensity variations are observed in relation to the Raman spectrum of uncomplexed aqueous acpy excited at 441.6 nm.
(15) Paramount flash photolysis experiments on this complex show τ(MLCT) ≤ 25 ps. Netzel, T. L., private communication.
(16) The absorption spectrum of an resonance Raman scattering from acpy were obtained from THF solution of Na$^+$acpy$^-$.
(17) Wrighton, M. S.; Abrahamson, H. B.; Morse, D. L. J. Am. Chem. Soc. 1976, 98, 4105.
(18) Lees, A. J.; Adamson, A. W. J. Am. Chem. Soc. 1982, 104, 3804.
(19) Giordano, P. J.; Fredericks, S. M.; Wrighton, M. S.; Morse, D. L. J. Am. Chem. Soc. 1978, 100, 2257.
(20) Chung, Y. C.; Leventis, N.; Wagner, P. J.; Leroi, G. E., unpublished results.

1416

levels;[a] here λ_{max} (MCLT) = 407 nm (see inset in Figure 2). The Raman spectra observed under both low-power 441.6-nm and high-power 354.7-nm (Figure 2) excitation exhibit scattering only from the complexed ground-state py ligand[21] and show only slight variation in relative peak intensities at the two excitation wavelengths. Although excitation in either case leads initially to MLCT, rapid deactivation by internal energy relaxation presumably leaves the complex in a lower lying LF excited level. It is possible that scattering from a short-lived $Ru^{III}(NH_3)_5(py^{-})^{2+}$ species might not be enhanced at 355 nm. Although the pyridine radical anion has an absorption peak near 340 nm in MTHF solution,[22] the proximity of the metal cation may blue-shift the transition sufficiently to move it off resonance. Thus failure to observe py[-] scattering in these experiments does not prove that the photoactive LF state lies below the MLCT state in 1, although it is consistent with Ford's picture.[a]

Excited-state Raman scattering from transition-metal complexes had been reported heretofore only for molecules containing the bpy ligand.[1-5] The observation of MLCT scattering from $Ru(NH_3)_5(acpy)^{2+}$ suggests that the resonance Raman technique may be utilized to charaterize low-lying excited electronic states of complexes containing multiple pyridyl ligands. We report the result of one such investigation in the following paper.[23]

(21) Clark, R. J. H.; Stead, M. J. J. Chem. Soc. Dalton Trans. 1981, 1760 See also: Dollish, F. R.. Fateley, W. G., Bentley, F. F. "Characteristic Raman Frequencies of Organic Compounds"; Wiley: New York, 1974
(22) Grimison, A., Simpson, G. A., Trujillo Sanchez, M., Jhaveri, J. J. Phys. Chem. 1969, 73, 4064
(23) Chung, Y. C., Leventis, N.; Wagner, P. J.; Leroi, G. E. J. Am. Chem. Soc. following paper in this issue

APPENDIX

The photochemistry of Ru(II)(NH$_3$)$_5$PY-X complexes has been extensively studied by Ford and others. These complexes with unsaturated organic ligands typically display intense transitions in the visible assigned as metal-to-ligand charge transfer (MLCT). Irradiation with visible light leads initially to the population of this MLCT state, however, the excited state responsible for photosolvation is thought to be ligand field in character. Ford and Malouf have categorized a large number of these complexes as "reactive" vs "unreactive" with respect to photosubstitution of the pyridyl ligand by a solvent molecule. The reactive complexes presumably have ligand field lowest excited states whereas in unreactive complexes the lowest excited state is MLCT. Furthermore, they made the empirical observation that reactive complexes have MLCT maxima at wavelengths lower than 460 nm and quantum yields for photosolvation of the pyridine (ϕ) greater than 0.02 mol/einstein at each irradiation wavelength. The unreactive complexes have lower energy MLCT maxima and much lower quantum yield of photosolvation. The identity of X, that is, the substituent on pyridine is critically important in determining the photochemical behavior of these complexes. it should be possible, then, to "tune" the energies of the MLCT state so that a sytematic variation of quantum yield is obtained.

When Ru(NH$_3$)$_5$PY is irradiated in aqueous solution, ligand substitution occurs:

```
                          ┌──── (a)    Ru(NH₃)₆H₂O  + PY
Ru(NH₃)₆PY ───────┤
                          └──── (b)    Ru(NH₃)₄PY(H₂O)  + (NH₃) cis & trans
```
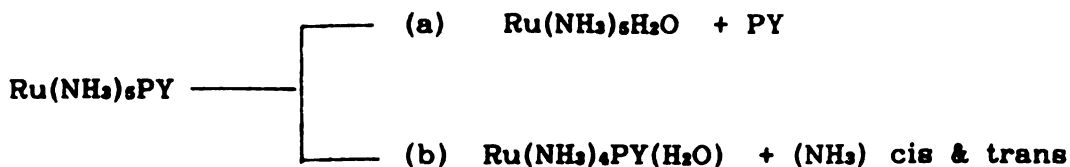
In this complex, the MLCT maximum falls at 407 nm. The MLCT state can
be conceptualized as having an oxidized Ru(III) metal coordinated to the
Pyridine anion radical. In other words, an internal redox reaction.
Ford and Malouf have demonstrated, however, that Ru(III) d^5 ammine
complexes are unreactive to ligand substitution. Thus, they concluded
that the MLCT excited state must not be responsible for the observed
photoreactivity. The wavelength-independent quantum yield for pyridine
substitution suggested a common state in which photo solvation occurs.
Upon studying numerous organic ligands of substituted pyridine ligands,
they generalized their observation as follows:
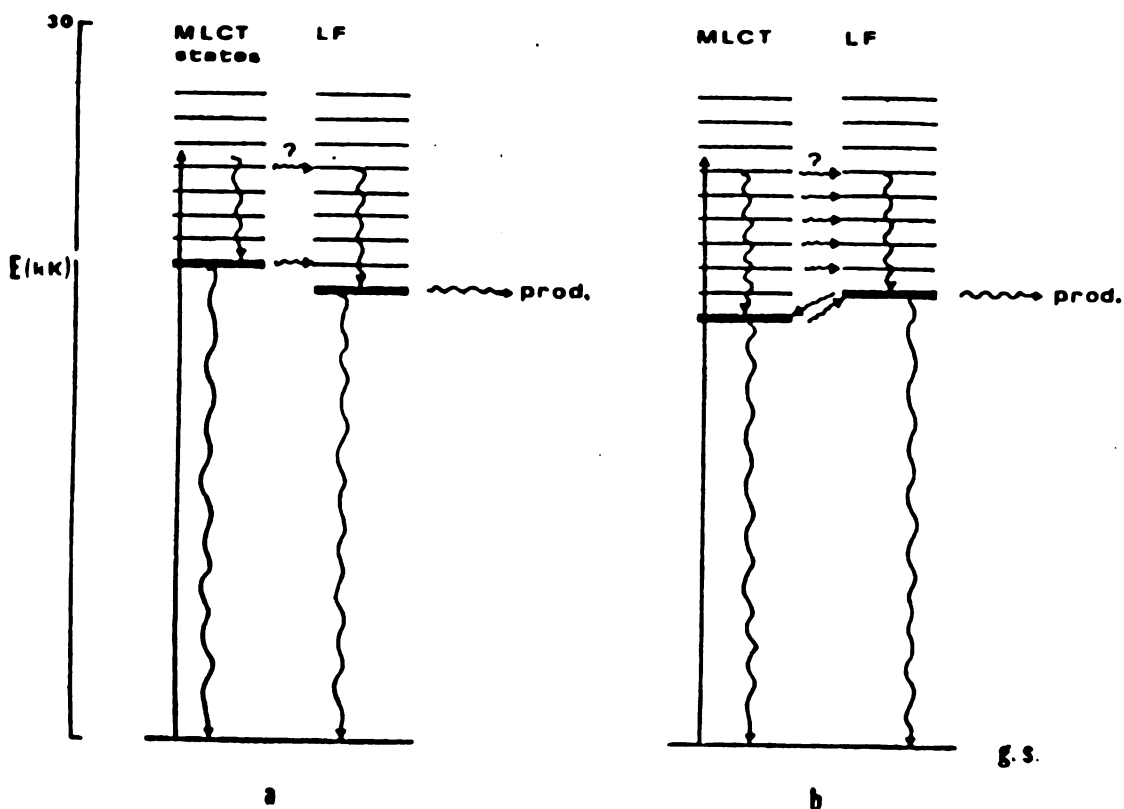
It was assumed that initial excitation into the MLCT* manifold resulted in efficient deactivation into the lowest energy LF* state from which it could either decay to the ground state or lead to photosubstitution.

Changing the solvent can introduce some perturbation to the energy levels of these complexes. One obvious possibility is solvent induced shifts of the MLCT maxima. Such behavior has been observed in similar systems.[2] It is also possible that other photophysical parameters such as non-radiative deactivation rates can be affected.[3] This offers a second potential method of "tuning" the charge transfer excited states and hence, the photochemical reactivity. This question has not been vigorously pursued by Ford or others and it is proposed that the excited state Raman spectra be studied under various solvents to detect any reversal of energy levels. There are various ligand systems which show their MLCT λ_{max} around 460 nm, and varying the solvents should result in reversal of MLCT, LF ordering. This would be very difficult to detect by measuring the small differences in photosolvation quantum yields, but it should be detactable by direct spectroscopic means.

The other experiments initiated on similar systems in this laboratory have been to utilize different metals with the same substituted pyridine ligands. This, of course, has a drastic effect on the electronic absorption spectra due to the change in ligand field splittings. The absorption spectra of Re(CO)₃(4-acpy)Br (4acpy = 4-acetyl pyridine) and W(CO)₄(4-Vp)₂ (Vp = Valeryl pyridine) are shown in Figure 2-1. The first complex has a respectable absorption at the 355 nm pump wavelength unlike the Ru(NH₃)₅(acpy) case. The pulsed Raman

spectra at 355 nm in CH$_2$Cl$_2$ solvent is shown in Figure 2-2. The strong 1620 cm^{-1} peak can be clearly seen with residual intensity at 1600 cm^{-1}. An expanded view of the high frequency region is shown in Figure 2-3. Solvent interference (see lower trace) made it necessary to repeat the experiment in other solvents such as CHCl$_3$ and CH$_3$CN. The spectrum in CHCl$_3$, Figure 2-4, shows clearly the 1620 cm^{-1} peak and other small peaks which could be correlated with the excited state peaks of Ru(NH$_3$)$_5$(4-acpy). In particular bands at 1329, 1371, 1023 cm^{-1} are observed as well as 1534 cm^{-1} which could be the 1544 cm^{-1} of Ru(NH$_3$)$_5$(4-acpy). In CH$_3$CN solvent the signal-to-noise ratio was poorer but the bands at 1624 and 1030 are present. These results for the Re(I) complexes must be interpreted with caution, however, since this complex is more susceptible to decomposition than the Ru(II) complexes. The necessary compromise between irradiation time and signal to noise ratio resulted in less than satisfying spectral quality.

The appropriate MO diagrams for Ru(II)(NH$_3$)$_5$PY-X complexes in O$_h$ microsymmetry are shown in Figure 2-6. Notice that the pyridine ligand possesses a higher lying LUMO than 4-acetylpyridine which therefore makes the ligand field transition lowest in energy in the pyridyl Ru(II) pentaamine. This situation is reversed in 4-acetylpyridine due to the substitution at the 4-position which lowers the LUMO. The ligand field splitting is probably slightly different due to different σ-donor ability but this has been ignored here. Also σ-bond formation by orbitals other than the d-orbitals has been omitted to make the diagram more tractable; this does not change the final picture.

Electronic Absorption Spectrum of
Re(I)(CO)₃(acpy)₂

Fig 2-1

- - - - fac-Re(I)(CO)₃(4-acpy)₂Br solvent CH₂Cl₂
———— W(CO)₄(4-acpy)₂ solvent CH₂Cl₂
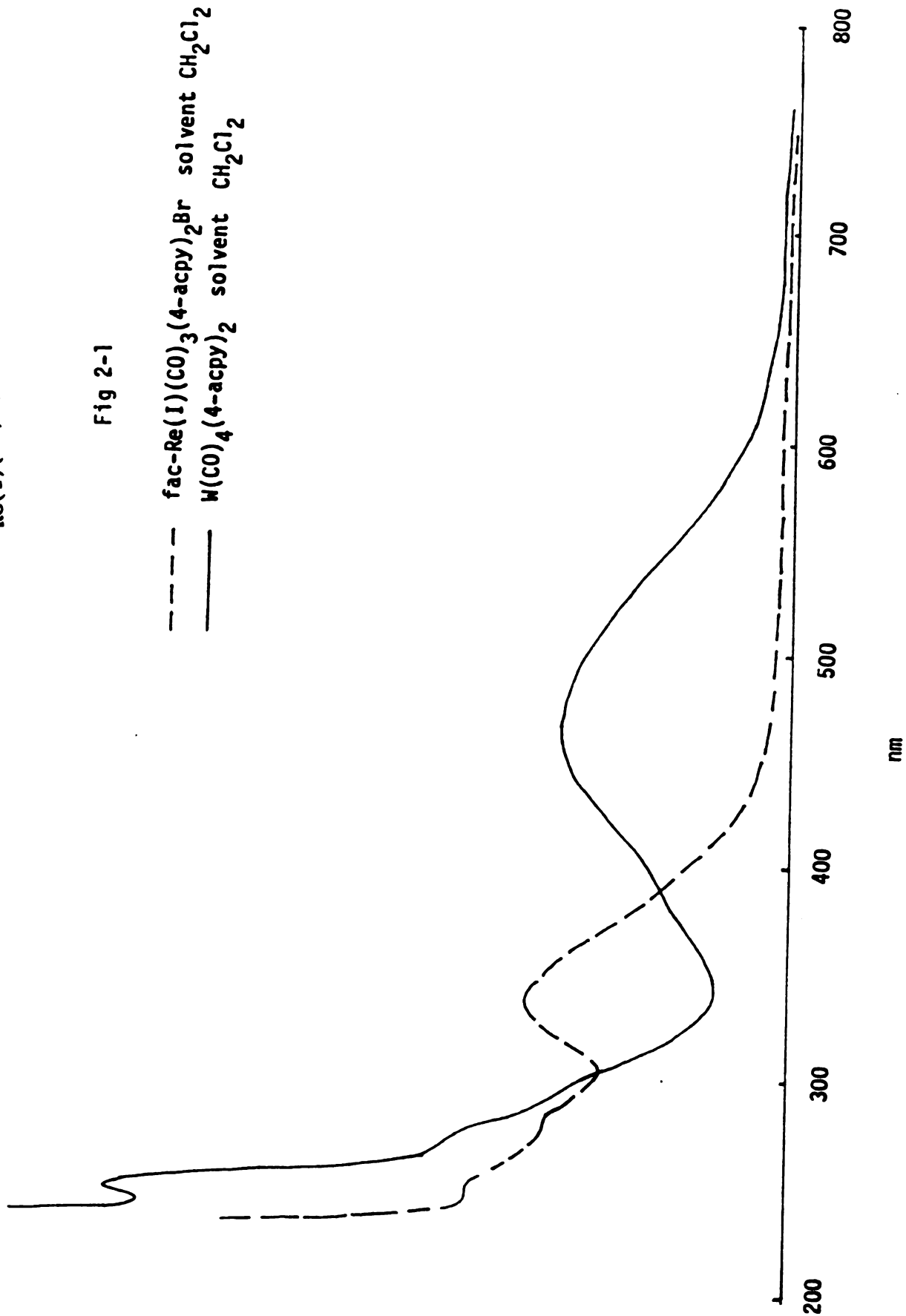
R.R. of Re(I)(CO)₃(acpy)₂, 354.7 nm.

Fig 2-2

Re(I)(CO)₃(4-acpy)₂ solvent CH₂Cl₂
354.7 nm pulsed

Fig 2-3

R.R. of Re(I)(CO)$_3$(4acpy)$_2$ solvent CH$_2$Cl$_2$

354.7 nm exc
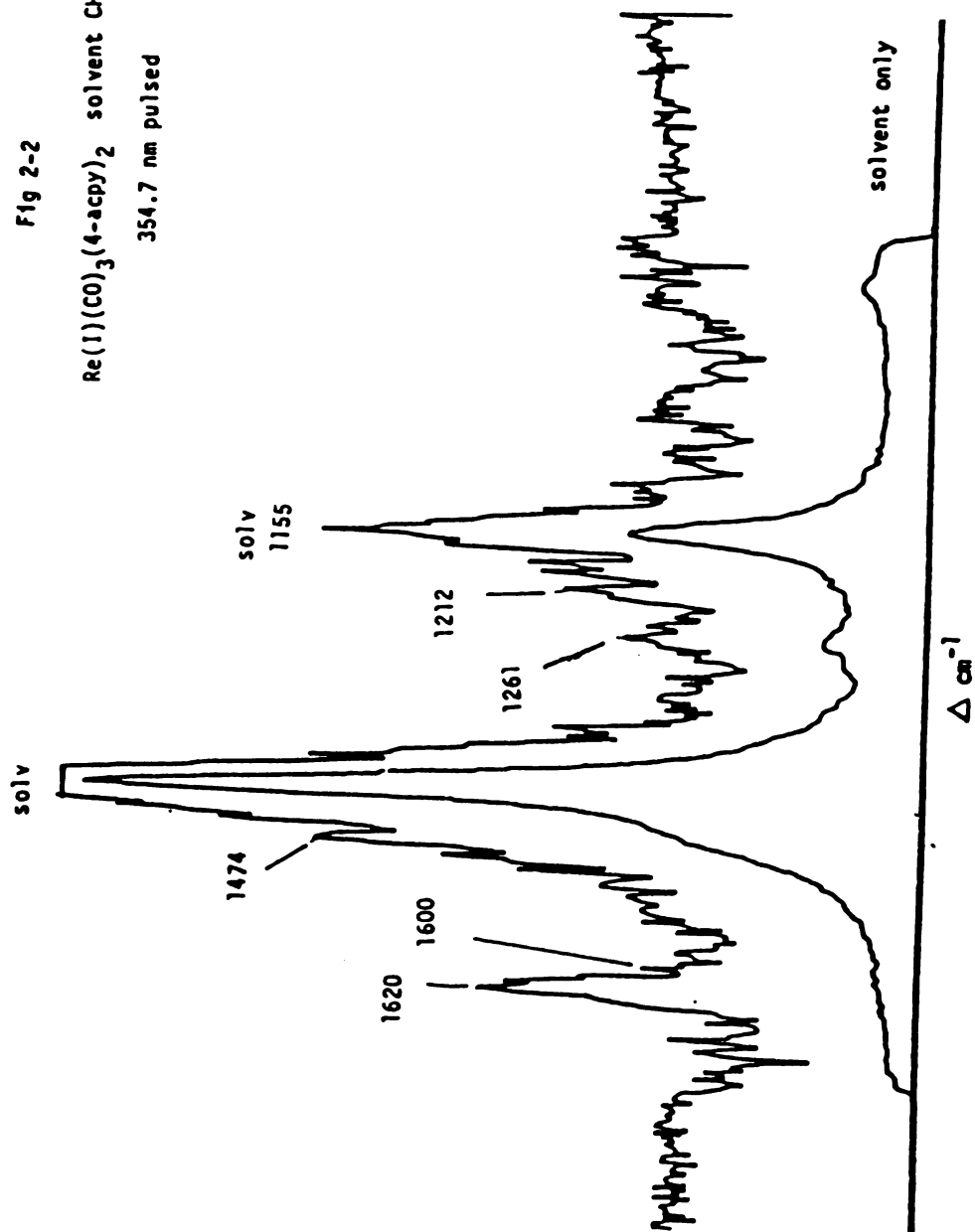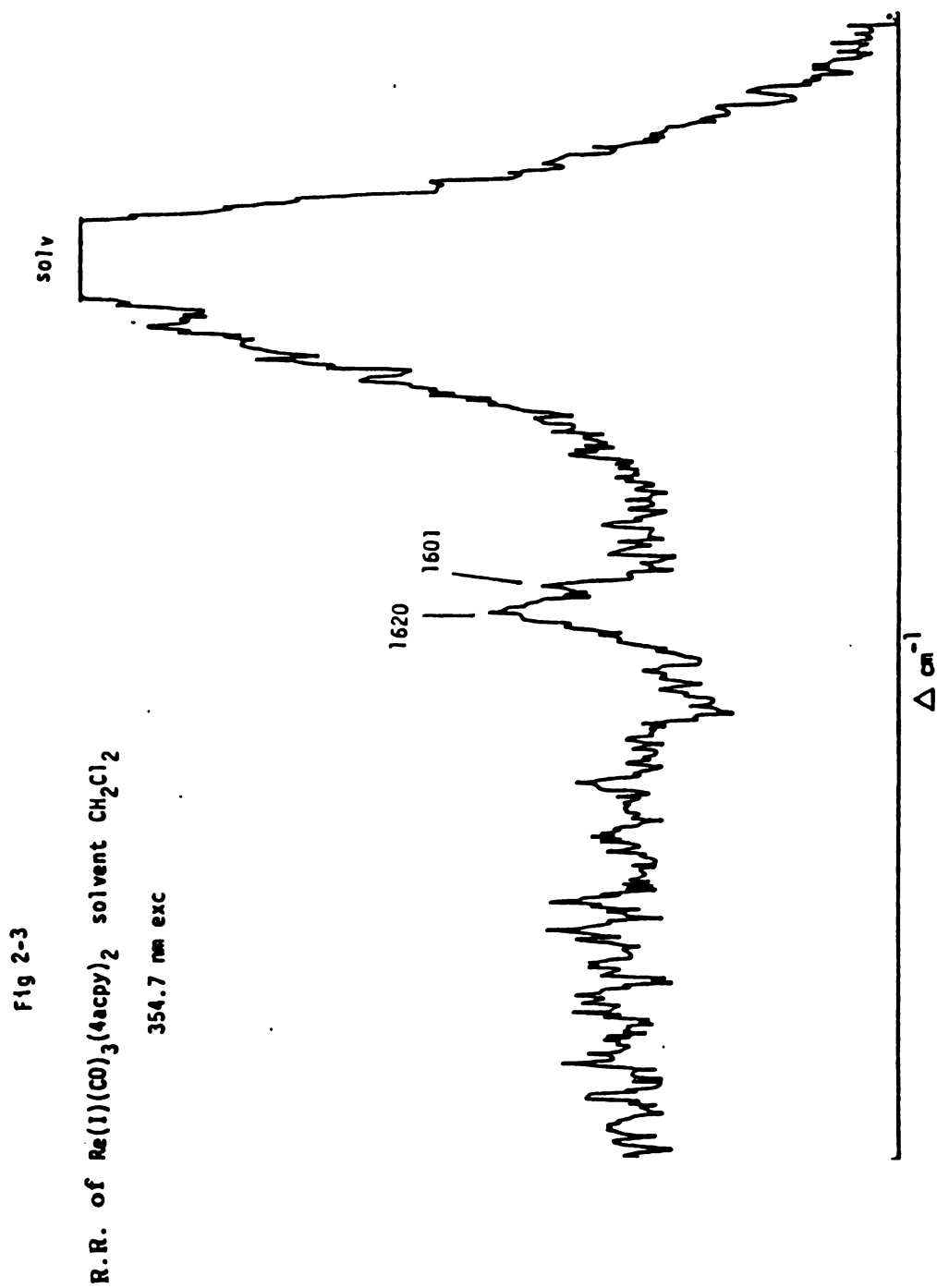
Fig 2-4

R.R. of Re(I)(CO)$_3$(4-acpy)$_2$ solvent CHCl$_3$

354.7 nm pulsed
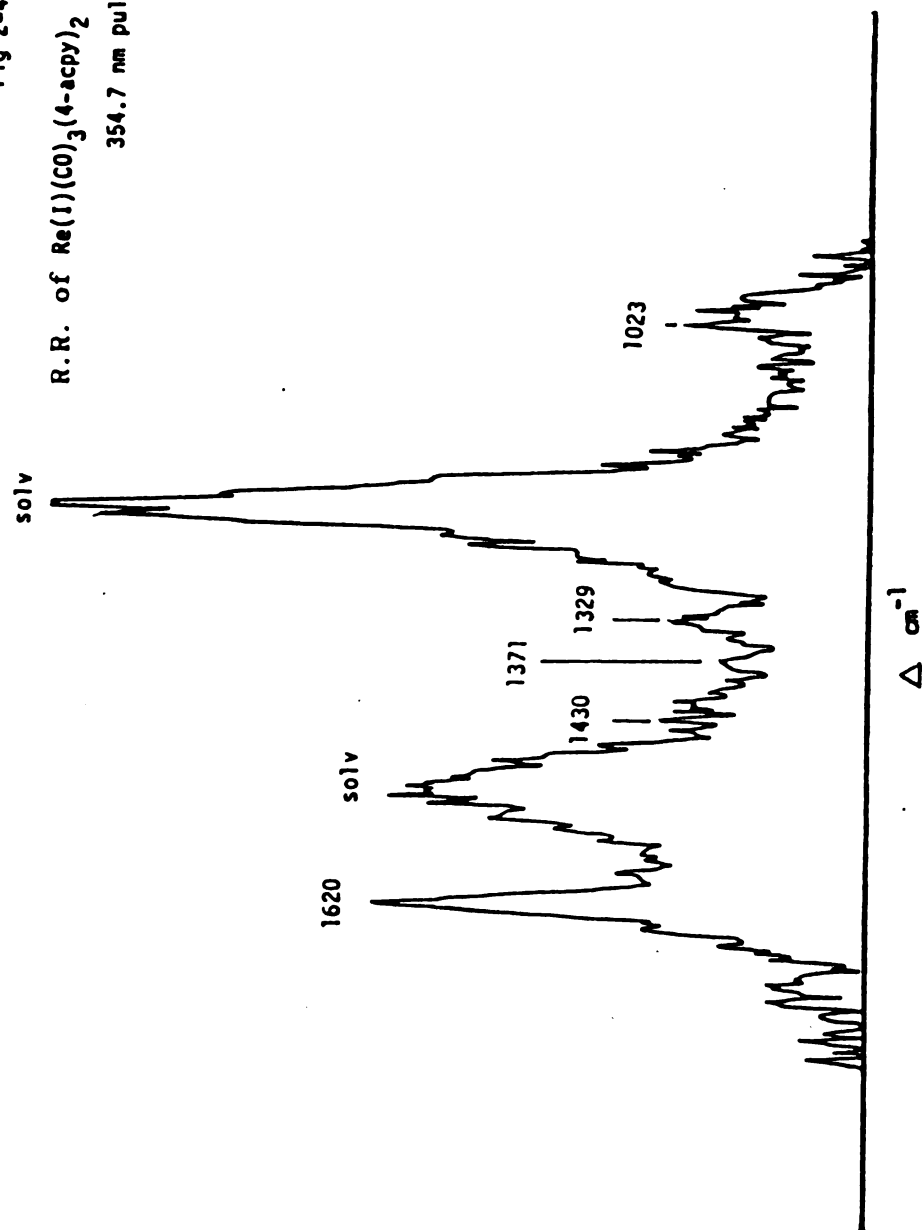
Fig 2-5

R.R. of
Re(I)(CO)$_3$(4-acpy)$_2$ solvent CH$_3$CN

354.7 nm pulsed

1030

solvent only

1624

1600

Δ cm^{-1}

Ru(II)(NH$_3$)$_5$(py)
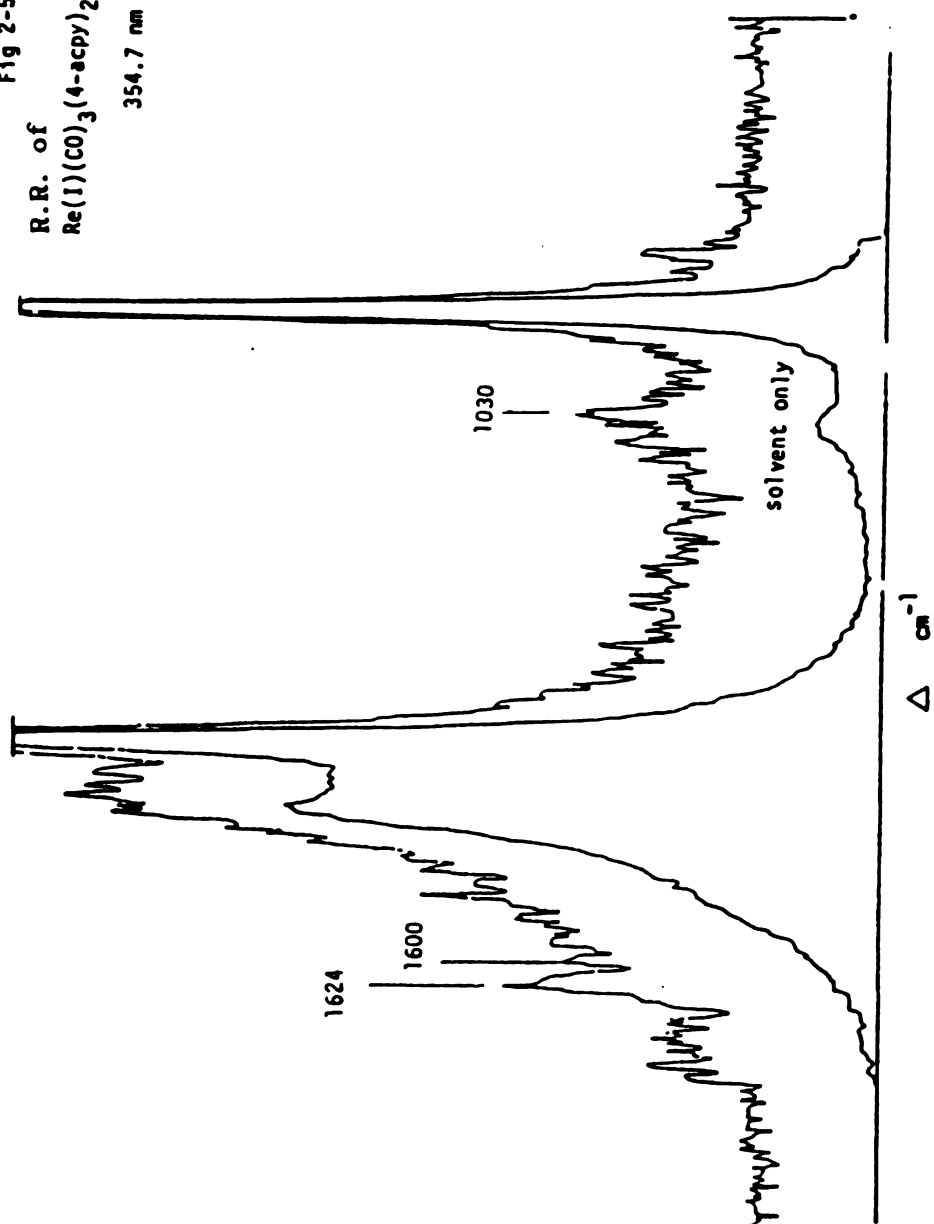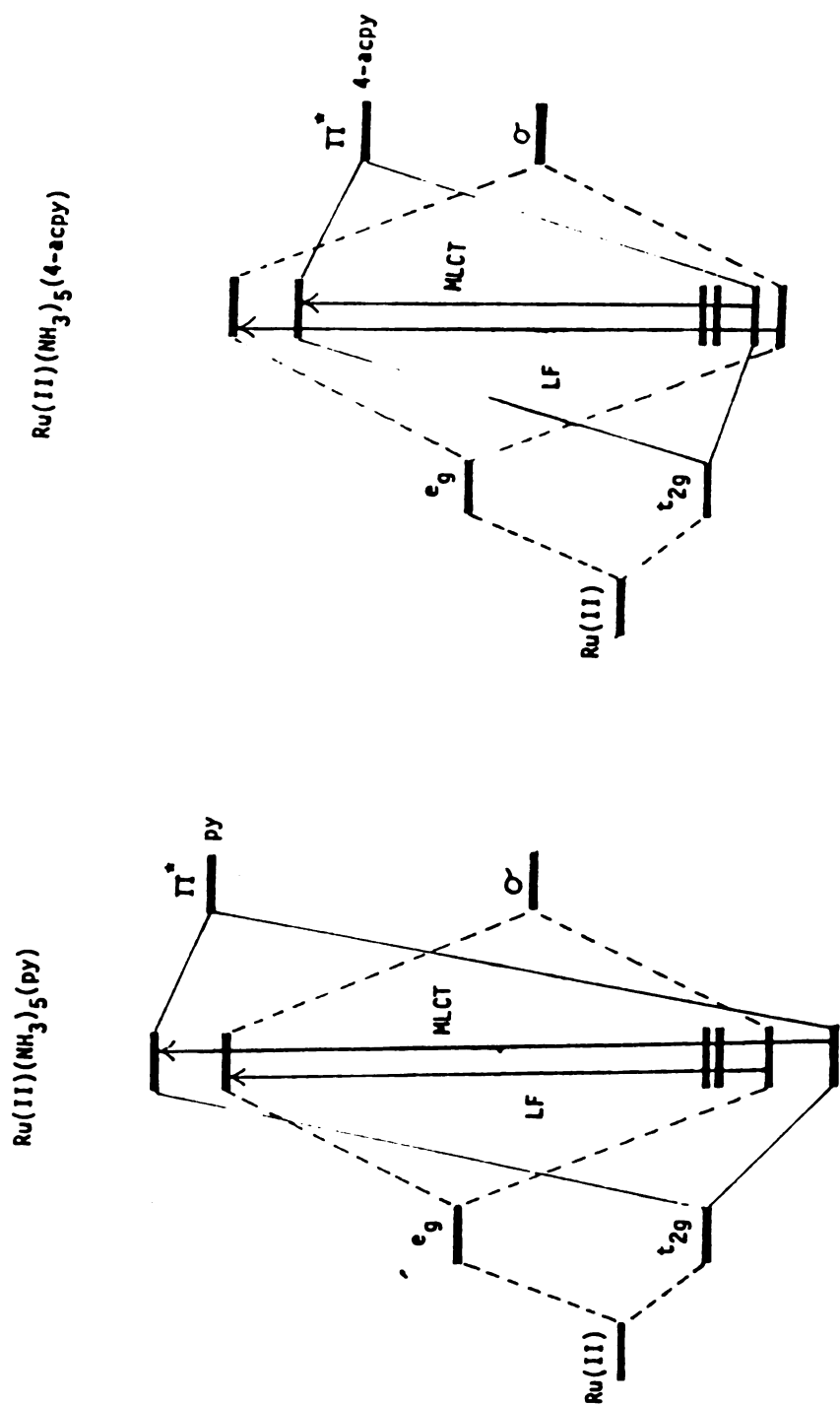
Ru(II)(NH$_3$)$_5$(4-acpy)

Fig 2-6
MO Diagram of Ru(II)(NH$_3$)$_5$(PY) and
Ru(II)(NH$_3$)$_5$(acpy)

42

REFERENCES

1. G. Malouf, P. C. Ford, J. Am. Chem. Soc. 99, 7213 (1977). T. Matsubara, P. C. Ford, Inorg. Chem. 17, 1747 (1978). R. E. Hintze, P. C. Ford, J. Am. Chem. Soc. 97, 2664 (1975).

2. H. Saito, J. Fugjita, K. Saito, Bull. Chem. Soc. JPR, 41, 863 1968. J. Burgess, J. Organometal. Chem. 19, 218 (1969).

3. K. Nakamura, A. Tazawa, M. Kanno, Bull. Chem. Soc. JPR. 48, 3486 (1975). C. K. Wong, A. D. Kirk, Can. J. Chem. 54, 3794 (1976).

Resonance Raman Spectra of Ground and Lowest Excited Electronic States of Some Ruthenium(II) Mixed-Ligand Complexes

Y. C. Chung, N. Leventis, P. J. Wagner,* and G. E. Leroi*

*Department of Chemistry, Michigan State University
East Lansing, Michigan 48824*

Received August 27, 1984

Several examples of resonance Raman (RR) scattering from excited electronic states of d^6 transition-metal complexes which contain the 2,2'-bipyridine (bpy) ligand have been published.[1-6] In the preceding paper we report the first observation of such scattering from a different ligand, 4-acetylpyridine (acpy) in $Ru(NH_3)_5(acpy)^{2+}$.[7] Here we describe RR spectra of complexes that contain both bpy and monodentate pyridyl ligands. The results suggest that the localized excitation model proposed by Woodruff and co-workers for $Ru(bpy)_3^{2+}$ (1)[1,2] and supported in subsequent work[3-6] applies as well to these more general coordination complexes. They also indicate some limitations of ns timescale measurements.

RR spectra at selected excitation wavelengths have been obtained for $\sim 10^{-4}$ M aqueous solutions of cis-$Ru^{II}(bpy)_2(L)_2(BF_4)_2$ salts, where L = acpy (2) or pyridine (py) (3). The complexes were synthesized and identified according to the literature,[8,9] and RR spectra were acquired as described in the accompanying paper.[7]

The UV–vis spectrum of 2 (Figure 1, inset) differs little from that of 1, the metal-to-ligand charge-transfer (MLCT) absorption in the blue being somewhat broadened here due to overlapping transitions to the bpy and acpy ligands. RR spectra of each group in its lowest MLCT excited state have been observed previously under pulsed 355-nm excitation.[1,2,4-7] Yet in the mixed-ligand complex 2 no excited electronic state Raman scattering is obtained under these conditions; the RR spectrum shown in Figure 1 is essentially a superposition of the ground-state scattering from bpy and acpy under UV excitation. An excitation profile obtained at several points in the composite MLCT absorption shows smooth variations in the relative intensities of the ground state bpy and acpy Raman peaks, reflecting the changing mixture of π^* levels

(1) Dallinger, R. F.; Woodruff, W. H. *J. Chem. Soc.* 1979, 101, 4391.
(2) Bradley, P. G.; Kress, N.; Hornberger, B. A.; Dallinger, R. F.; Woodruff, W. H. *J. Am. Chem. Soc.* 1981, 103, 7441.
(3) Forster, M.; Hester, R. E. *Chem. Phys. Lett.* 1981, 81, 42.
(4) Smothers, W. K.; Wrighton, M. S. *J. Am. Chem. Soc.* 1983, 105, 1067.
(5) McClanahan, S.; Hayes, T., Kincaid, J. *J. Am. Chem. Soc.* 1983, 105, 4486.
(6) Casper, J. V., Westmoreland, T. D.; Allen, G. H.; Bradley, P. G.; Meyer, T. J.; Woodruff, W. H. *J. Am. Chem. Soc.* 1984, 106, 3492.
(7) Chung, Y. C.; Leventis, N., Wagner, P. J.; Leroi, G. E. *J. Am. Chem. Soc.*, preceding paper in this issue.

Figure 1. Resonance Raman spectrum of deoxygenated 10^{-4} M aqueous solution of $Ru^{II}(bpy)_2(acpy)_2(BF_4)_2$ under pulsed excitation at 354.7 nm. Wavenumber shifts are given above the peaks. Key to band assignments: (●) bpy, (▼) acpy. (Inset: Absorption spectrum in the 250–600-nm region.)

of the two ligands across the absorption envelope.[10] The absence of detectable excited-state scattering from 2 may indicate that the lifetimes of the excited states formed by 355-nm excitation are too short for the nanosecond timescale of these Raman measurements. Even the lowest excited state may be shorter lived than that of 1, since we have been able to detect only very weak luminescence from 2, and that only at 77 K.[11]

The lowest MLCT state of $Ru(bpy)_2(py)_2^{2+}$ (3), however, has a lifetime approaching that of the tris bpy complex, 1.[12] The absorption spectrum of 3 (inset, Figure 2) is distinguished from those of 1 and 2 primarily by the presence of a peak at 338 nm (ϵ 20.4 × 10³), which we attribute to metal-to-pyridine CT. RR spectra of 3 in the 1000–1650-cm^{-1} region are shown in Figure 2. Under 442-nm CW excitation (top frame) seven peaks are observed; all have been previously identified as ring stretching modes of the bpy ligand in its ground state.[1,5,13] No py scattering

(8) Dwyer, F. P.; Goodwin, H. A.; Gyarfas, E. C. *Aust. J. Chem.* 1963, 16, 42.
(9) Bosnich, B.; Dwyer, F. P. *Aust. J. Chem.* 1966, 19, 2229.
(10) Braunstein, C. H.; Baker, A. D.; Strekas, T. C.; Gafney, H. D. *Inorg. Chem.* 1984, 23, 857.
(11) Pinnick, D. V.; Durham, B. *Inorg. Chem.* 1984, 23, 1440.
(12) Casper, J. V.; Meyer, T. J. *Inorg. Chem.* 1983, 22, 2444.
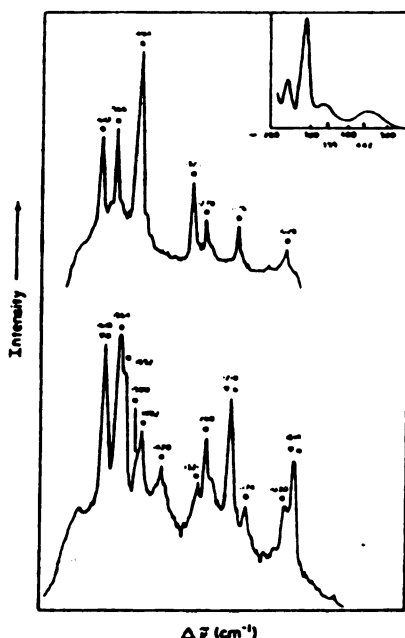
Figure 2. Resonance Raman spectra of deoxygenated 10^{-4} M aqueous solutions of $Ru^{II}(bpy)_2(py)_2(BF_4)_2$. Top frame: under CW excitation at 441.6 nm. Bottom frame: under pulsed excitation at 354.7 nm. Wavenumber shifts are given above the peaks. Key to band assignments: (●) bpy, (°) bpy⁻, (▼) py. (Inset: Absorption spectrum in the 250–600-nm region.)

is observed at this excitation wavelength, which is resonant with metal-to-bpy CT absorption. The bottom frame of Figure 2 displays the RR spectrum of 3 upon excitation with ~5-mJ pulses at 355 nm. In comparison to the top frame, the more intense, higher energy illumination produces many additional peaks and gives rise to strong variations in relative peak intensities. Although

(13) Clark, R. J. H.; Turtle, P. C.; Stromnea, D. P.; Streusand, B.; Kincaid, J.; Nakamoto, K. *Inorg. Chem.* **1977**, *16*, 84.

3 is being excited in resonance with Ru-to-py CT absorption, rapid internal energy relaxation apparently leaves a significant proportion of the complex in its lowest MLCT excited state, such that RR scattering characteristic of bpy* is observed. However, the spectrum differs from that of 1 excited under similar conditions[1,2,3] in that ground-state bpy scattering predominates for 3. (For example, the excited-state peak at 1552 cm⁻¹ is much stronger than the ground-state mode at 1564 cm⁻¹ in the RR spectrum of 1 excited by 355-nm laser pulses.) Moreover, the intensity pattern is altered by the underlying presence of ground-state py scattering.[3] The origins of the peaks are denoted directly in the figure.

The wavennumber shifts and relative intensities of the Raman peaks observed for 3 under 355-nm excitation suggest that the localized exctation model applies as well to this mixed ligand system; i.e., the species responsible for the excited state scattering can be represented as $Ru^{III}(bpy^-)(bpy)(py)_2^{2+}$ (3*). Because the excitation is resonant primarily to metal-to-py CT absorption and alternative decay channels exist (e.g., photochemistry, internal conversion), the relative population of 3* suffers in comparison to the corresponding state in the tris bpy complex. The Raman probe photons in a given laser pulse encounter a larger concentration of ground-state molecules in 3 than in 1, giving rise to a relatively large contribution to the Raman scattering from $Ru^{II}(bpy)_2(py)_2^{2+}$. Within the limitations set by the time scale of these experiments and the requirement that the pump radiation used to excite the sample molecules be in resonance with an absorption of the electronically excited species so prepared, our results indicate that the localized excitation model previously advanced for $Ru(bpy)_3^{2+}$ and its analogues applies also to transition-metal complexes having multiple ligands with different low-lying π^* levels.

APPENDIX

The Ru(II) complexes of the Ru(bpy)$_2$L$_2$ type have been intensively investigated by many groups as an extension of the Ru(bpy)$_3$ system. Since the substitution of L$_2$ (i.e., two monodentate ligands) has a strong effect on the photophysical behavior, some general properties of these complexes will be discussed here. Meyer and others have studied a series of Ru(bpy)$_2$L$_2$ complexes where L = pyridine, pyridazine, 2-(2-aminoethyl) pyridine, etc. They have found that the decay of the lowest MLCT state (i.e., Ru → bpy π*) depends on several factors such as the radiative decay pathway (kr) which is relatively insensitive to L, and non-radiative (knr) decay which was found to vary according to the predictions of the energy gap law for radiationless transition.[1] They also found the thermal activation of MLCT to low lying ligand field states to be important in determining the lifetime of the MLCT excited state.

Electrochemical studies on these complexes[2] have also been made. The reduction potential for L = pyridine have been measured and assigned to Ru(III)(bpy)(bpy-)L$_2$ consistent with our Raman data. The optical transition in absorption is largely Ru → bpy singlet in character and the emission is bpy → Ru(III) triplet in character and the electrochemical studies reveal that emission is from a common electronic origin in all of these complexes, with a variety of organic ligand L. They note, however, that the reduction potentials for the Ru(III)/Ru(II) couple is sensitive to the nature of L.

These complexes also show a temperature dependent lifetime which has been explained as a thermally activated transition from the lowest MLCT to a low lying ligand field state. The relative ordering of the LF(d-d^z) energy level as it depends on the ligand L, however, is not easy to predict or explain even though photosubstitution quantum yields show a dependence on the nature of L. One of the few Raman studies reported on such Ru(bpy)$_z$L$_z$ complexes is that of Strekas, et al.[3] on Ru(azpy)$_z$L$_z$ where azpy is 2-(phenylazo)pyridine.
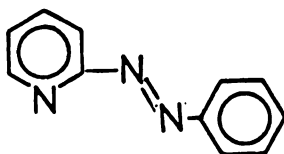
azpy = 2-(phenylazo)pyridine

On the basis of the observed resonance Raman spectra, the authors suggest that in the lowest MLCT (which is a d - π^* of acpy) the charge is localized primarily on the N=N bond and that the phenyl ring is intimately coupled. Interestingly the pyridine part of the azpy ligand is only weakly involved. This is another example of the utility of Raman spectroscopy in elucidating the nature and "picture" of excited states.

The MO diagram for Ru(II)(bpy)$_z$(PY-X) is shown in Figure 3-1. Notice that the MLCT to pyridine as well as to 4-acetylpyridine has been considerably blue shifted as compared to the Ru(II)(NH$_3$)$_5$PY-X analog. This is due to the larger ligand field splittings induced by the two bpy ligands. Notice also that the lowest charge-transfer transition possible, the Ru(II) - bpy is only slightly perturbed. The two bpy's also cause the ligand field transition to shift to higher energies. Only d-π^* interactions and d-σ bonds are shown.

Ru(II)(bpy)$_2$(4-acpy)$_2$.
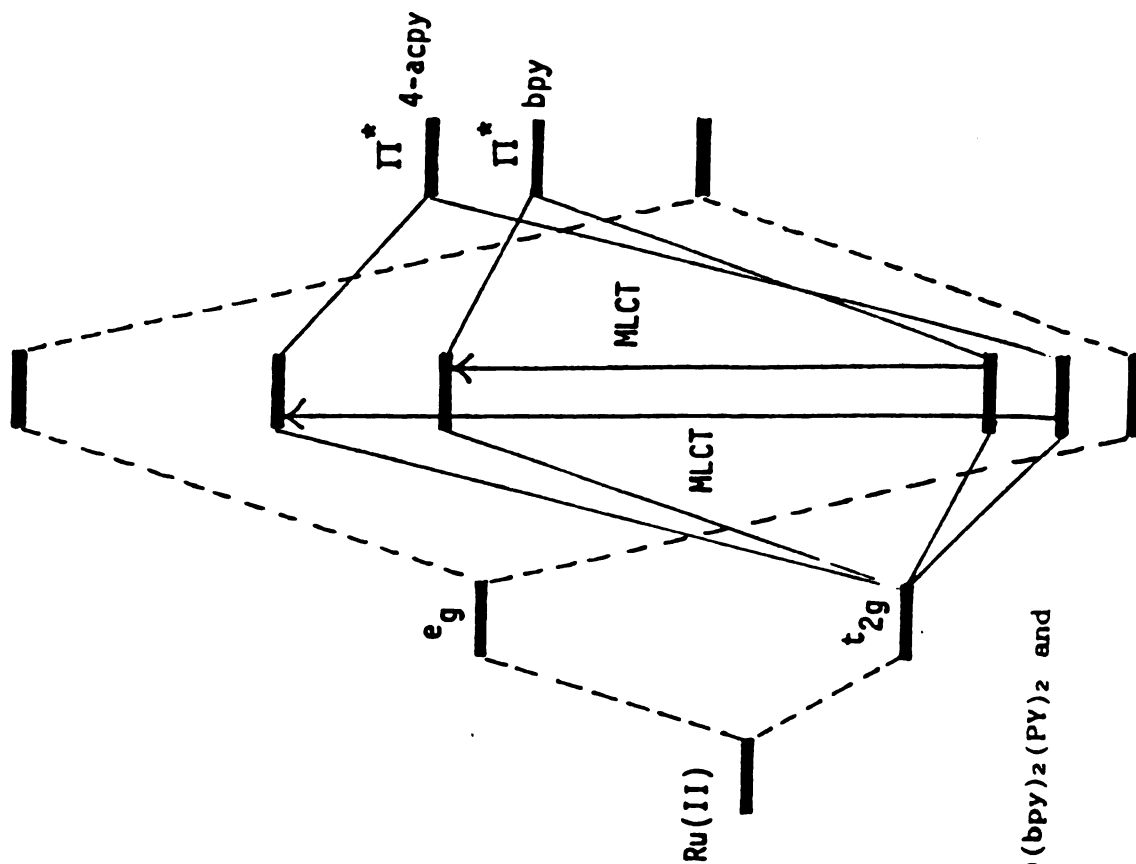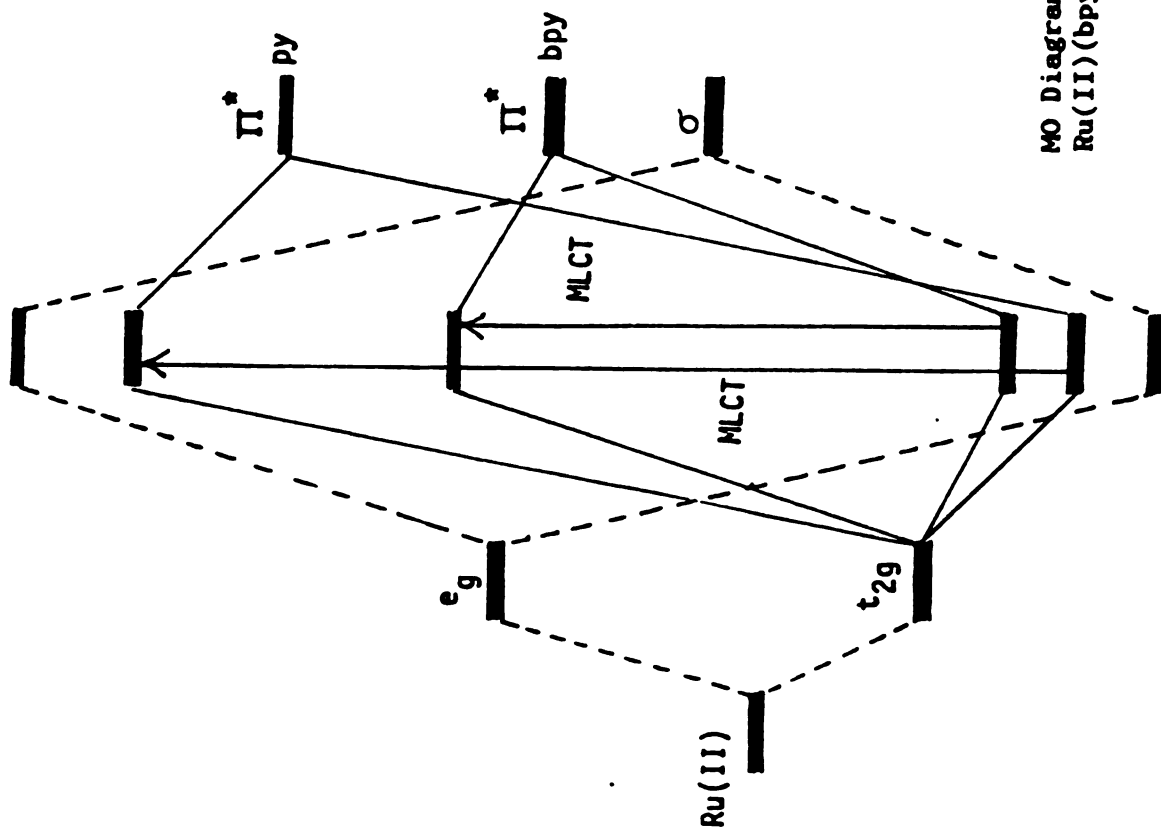
Ru(II)(bpy)$_2$(py)$_2$

MO Diagram of Ru(II)(bpy)$_2$(PY)$_2$ and
Ru(II)(bpy)$_2$(acpy)

Fig 3-1

REFERENCES

1. (a) J. V. Caspar, E. M. Kober, B. P. Sullivan, T. J. Meyer, Chem. Phys. Lett. 91, 91 (1982). (b) T. J. Meyer, Prog. In Inorg. Chem. 30, 389 (1983). (c) E. M. Kober, B. P. Sullivan, W. J. Dressick, J. V. Caspar, T. J. Meyer, J. Am. Chem. Soc. 102, 7383 (1980).

2. (a) B. Bosnich, F. P. Dwyer, Aust. J. Chem. 19, 2229 (1966). (b) F. P. Dwyer, H. A. Goodwin, E. C. Gyrfus ibid 16, 544 (1963). (c) F. P. Dwyer, H. A. Goodwin, E. C. Gyarfus, ibid 16, 42 (1963). (d) D. V. Pinnick, B. Durham, Inorg. Chem. 23, 1440 (1984). (e) B. Durham, J. L. Walsh, C. L Carter, T. J. Meyer, Inorg. Chem. 19, 860 (1980).

3. S. Wolfgang, T. C. Strekas, H. D. Gafney, R. A. Krause, K. Krause, Inorg. Chem. 23, 2650 (1984).

Characterization of Multiple Charge-Transfer Excited States of Tris(2,2'-bipyrimidine)ruthenium(II) by Resonance Raman Spectroscopy

Sir:

Resonance Raman scattering can be used effectively to characterize excited electronic states since the nature of the upper state is reflected in those ground-state vibrational modes that display intensity enhancement.[1] The technique is particularly useful for large molecules, which often show broad, featureless electronic absorption. In addition, under favorable lifetime conditions electronic and vibrational information about an excited state itself may be obtained by resonance Raman spectroscopy.[2] We report here Raman scattering in resonance with several partially resolved transitions in the complex ground-state absorption spectrum of tris(2,2'-bipyrimidine)ruthenium(II) [Ru(bpym)$_3^{2+}$]; Raman scattering from the lowest metal-to-ligand charge-transfer (MLCT) excited state—which may be represented as Ru^{III}-(bpym)$_2$(bpym$^-$)$^{2+}$—in resonance with different excited states of the complexed anion radical is also presented.

Ru(bpym)$_3$Cl$_2$ was synthesized from anhydrous RuCl$_3$ and excess 2,2'-bipyrimidine by a modification of the method reported by Hunziker and Ludi.[3] Structural confirmation of the recrystallized product was obtained by UV–visible, emission, and NMR spectroscopy. Raman spectra of ~10^{-3} M nitrogen-purged aqueous samples were obtained by dispersing the 90° scattered light through a Spex Triplemate polychromator onto an EGG/PARC Model 1420 Reticon multichannel detector that was coupled to an OMA-II signal processing system. Ground-state resonance Raman spectra were excited by CW radiation at 441.6 nm (Liconix Model 4240 He:Cd laser, 50 mW) or 363.8 nm (Coherent Model 90-5 Ar$^+$ laser, 60 mW). Excited-state Raman spectra were generated by high-power pulses of the 354.7-nm third harmonic of a Nd:YAG laser (Quanta-Ray Model DCR-1A, 10 Hz, ~10-ns fwhm, ~5 mJ/pulse) or a dye laser pumped by that source. Photons from the same pulse served both to pump the sample and to probe the excited electronic state. Toluene, o-chlorotoluene, cyclohexene, and fenchone were utilized for wavenumber calibration. Under typical operating conditions of the Triplemate/OMA system (1800 or 2400 groove/mm grating, 20 scans), wavenumber accuracy of the peak positions is ±2 cm^{-1}.

Typical d^6-transition-metal polypyridine complexes display absorption spectra showing a broad peak with a subsidiary higher energy shoulder in the 400–550-nm range—attributed to MLCT

Figure 1. Resonance Raman spectra of deoxygenated 10^{-3} M aqueous solutions of Ru^{II}(bpym)$_3$Cl$_2$: top frame, under CW excitation at 441.6 nm; bottom frame, under CW excitation at 363.8 nm. Wavenumber shifts are given above the peaks. [Inset: absorption spectrum in the 250–700-nm region, with excitation wavelengths marked by arrows.]

transitions—and stronger band systems below 300 nm—due to internal ligand excitations and higher energy MLCT transitions.[4] The absorption spectrum of Ru(bpym)$_3^{2+}$, shown in the inset of Figure 1, is more complex, suggesting the presence of several excited electronic states in the 300–500-nm range. The ground-state resonance Raman spectrum in the Δṽ = 1000–1600-cm^{-1} region excited by CW radiation at 442 nm is traced in the top frame of Figure 1. Seven distinct peaks are observed; their wavenumber shifts correlate well with ring-stretching modes of the 2,2'-bipyrimidine group.[5] The same bands are observed

(1) Tang, J.; Albrecht, A. C. In "Raman Spectroscopy"; Szymanski, H. A., Ed., Plenum Press: New York, 1970; Vol. 2.
(2) Dallinger, R. F.; Woodruff, W. H. J. Am. Chem. Soc. 1979, 101, 4391. Bradley, P. G.; Kress, N.; Hornberger, B. A.; Dallinger, R. F.; Woodruff, W. H. J. Am. Chem. Soc. 1981, 103, 7441 Forster, M.; Hester, R. E. Chem. Phys. Lett. 1981, 81, 42. Smothers, W. K.; Wrighton, M. S. J. Am. Chem. Soc. 1983, 105, 1067. Chung, Y. C.; Leventis, N.; Wagner, P. J.; Leroi, G. E. J. Am. Chem. Soc. 1985, 107, 1414, 1416.
(3) Hunziker, M.; Ludi, A. J. Am. Chem. Soc. 1977, 99, 7370.

(4) See for example the absorption spectrum of tris(2,2'-bipyridine)ruthenium(II): Bradley, P. G.; Kress, N.; Hornberger, B. A., Dallinger, R. F.; Woodruff, W. H. J. Am. Chem. Soc. 1981, 103, 7441.
(5) The vibrational spectrum is similar to, but somewhat different from, that of uncomplexed bipyrimidine. See for example: Overton, C.; Connor, J. A. Polyhedron 1982, 1, 53.
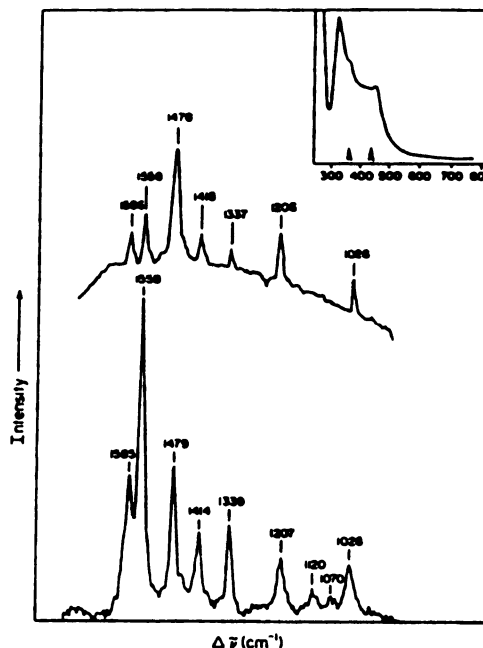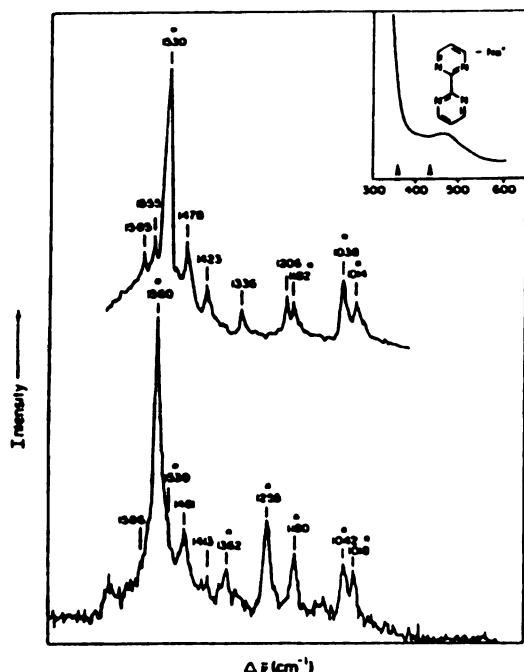
Figure 2. Resonance Raman spectra of deoxygenated 10^{-3} M aqueous solutions of $Ru^{II}(bpym)_3Cl_2$: top frame, under pulsed excitation at 440.0 nm; bottom frame, under pulsed excitation at 354.7 nm. Wavenumber shifts are given above the peaks. Bands attributed to (MLCT) excited-state scattering are marked with asterisks. (Inset: Absorption spectrum (300–600 nm) of Na^+bpym^- in THF, with $Ru(bpym)_3^{2+}$ pulsed excitation wavelengths denoted by arrows.)

under 364-nm CW excitation (Figure 1, bottom frame); however, their relative intensities are markedly different—note the three highest frequency peaks in particular—and two weak new bands are observed, at 1070 and 1120 cm^{-1}. The enhancement pattern has changed, which shows that two (or more) excited states are differently in resonance at the two excitation wavelengths.

Raman spectra of $Ru(bpym)_3^{2+}$ excited by relatively high-power pulses at approximately the same wavelengths as the CW experiments are reproduced in Figure 2. Scattering from an excited electronic state is clearly evident in both cases. Consider first the blue excitation (top frames). Ground-state peaks are still evident

in Figure 2 with the same relative intensities shown in Figure 1, but the pulse-excited spectrum is dominated by new peaks at 1014, 1038, 1182, and 1530 cm^{-1}, which are denoted by asterisks in Figure 2. These new bands are also observed under pulsed UV excitation (Figure 2, lower frame). However their relative intensities differ somewhat from those observed under 440-nm irradiation, and there are three new excited-state peaks, at 1255, 1362, and 1560 cm^{-1}. (Some ground-state scattering also contributes to the peak at 1560 cm^{-1}; see relative intensities in bottom frame of Figure 1.) We attribute the excited-state scattering to complexes having one of the bidentate ligands in the MLCT state: $Ru^{III}(bpym)_2(bpym^-)^{2+}$. This model, in which on the vibrational time scale the excitation is localized on one of the ligands, is well established for 2,2′-bipyridine (bpy) complexes of Ru and Os.[6] Our Raman data indicate that different upper electronic states are in resonance with the MLCT-excited tris(bipyrimidine)ruthenium complex at the two excitation wavelengths employed. This is consistent with the electronic absorption spectrum of Na^+bpym^- in THF (Figure 2, inset), which shows two well-separated transitions.

A complete excitation profile of the $Ru(bpym)_3^{2+}$ ground state and additional resonance Raman spectra of the MLCT-excited state, as well as resonance Raman spectra of the mixed-ligand complex $Ru(bpym)_2(bpy)^{2+}$, will be given in a subsequent publication. The photophysical and photochemical properties of such d^6-transition-metal polypyridine complexes are of great interest because of their potential photosensitization applicability;[7] we have demonstrated here that resonance Raman spectroscopy provides a powerful probe of the relevant excited states.

(6) Caspar, J. V.; Westmoreland, T. D.; Allen, G. H.; Bradley, P. G.; Meyer, T. J.; Woodruff, W. H. J. Am. Chem. Soc. 1984, 106, 3492 and references cited therein.

(7) Connolly, J., Ed. "Photochemical Conversion and Storage of Solar Energy"; Academic Press: New York, 1981. Gratzel, M., Ed. "Energy Resources through Photochemistry and Catalysis"; Academic Press: New York, 1983.

Department of Chemistry   Y. C. Chung
Michigan State University   N. Leventis
East Lansing, Michigan 48824   P. J. Wagner
     G. E. Leroi*

APPENDIX

As an extension of the tris-bidentate series, various mixed bidentate ligand systems have been investigated. One example, the Ru(bpy)(phen)$_{3-n}$ series (n = 0~3) is discussed in the Ru(phen)$_3$ appendix. Other ligand systems have been investigated by various other workers.[1] The types of ligand and its structures are shown in Figure 4-1. Vast number of mixed bidentate ligands have been studied by electrochemical and optical spectroscopy from which conclusions have been reached that dual emission was absent from these complexes. All claims of emission from two different ligand centers later proved to be erroneous; the extraneous emission was due to impurities. The conclusion has been drawn that coupling between the two different ligands is apparently strong enough to cause relaxation which occurs faster than the radiative decay of the upper excited states. Thus, the only sufficiently long-lived state to give rise to luminescence emission and therefore to be involved in bimolecular process is the lowest charge transfer excited state.

We have also studied some mixed ligand systems by Raman spectroscopy. It was initially hoped that the ligands chosen had their LUMO's sufficiently close in energy such that we could observe excited state scattering from both charge transfer states (Raman scattering is an extremely fast event). However, in every case studied the excited state scattering showed strictly localized behavior. The Ru(bpy)$_n$(phen)$_{3-n}$ case is discussed separately in the appendix for Ru(phen)$_3$.

The absorption spectrum of Ru(bpy)₂(bpym) is shown in Figure 5-1a. As compared to the parent complex Ru(bpy)₃ which has its λ_{max} at 450 nm, the maximum of the substituted complex is blue shifted to 417 nm and a distinct shoulder can be seen at 490 nm. The discussion of the Raman data is in the [Ru(bpy)]₂bpym manuscript. The point to be made here is that excited state scattering from the bpym modes only can be seen with no evidence of bpy* peaks. The Ru(phen)₂(bpym) complex absorption spectra likewise shows (Figure 4-2) a shoulder at about 500 nm with the λ_{max} at ~390 nm and a shoulder at 420 nm. The lowest MLCT is from Ru - bpym as can be seen in the Raman profile obtained with 472.7 nm excitation (Figure 4-3). Again, the excited state spectrum taken at 355 nm showed a clean bpym* profile. Clearly, regardless of which MLCT state is pumped relaxation is fast relative to luminescence from the upper excited states. This was also the case with Ru(bpy)₂(PY)₂ even though 355 nm directly pumped the complex into the Ru → PY MLCT states.

The MO diagram for Ru(II)(bpym)₃ is shown in Figure 4-4, with Ru(II)(bpy)₃ as comparison. It is well established that the LUMO's of bpym are lower in energy than bpy. However, the absorption λ_{max} for Ru(II)(bpym)₃ and Ru(II)(bpy)₃ are quite comparable, which strongly implies that the bpym ligand induces a larger ligand field splitting of the metal d-orbitals. This also drives the d-d* transition to higher energies, which predicts a higher stability of this complex than Ru(bpy)₃. Again, only d-π* interaction and dσ bonds are shown for sake of clarity.

pq = 2-(2-pyridilquinoline)

biq = 2,2'- biisoquinoline

i-biq = isobiquinoline

DMCH
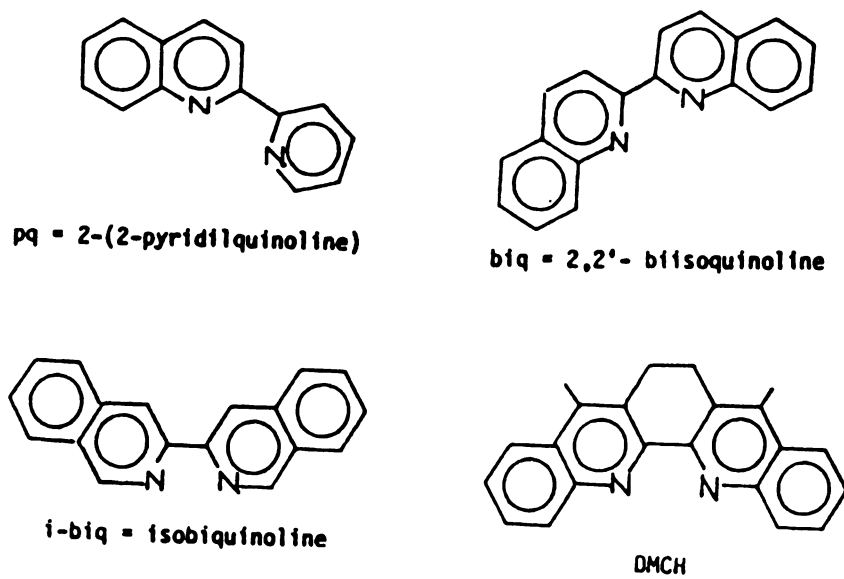
Fig 4-1

Structures of Bidentate Organic Ligands.

Fig 4-2
Electronic Absorption Spectrum of
Ru(II)(phen)$_2$(bpym)

Fig 4-3

R.R. of Ru(II)(phen)$_2$(bpym)   ext exc = 472.7 nm
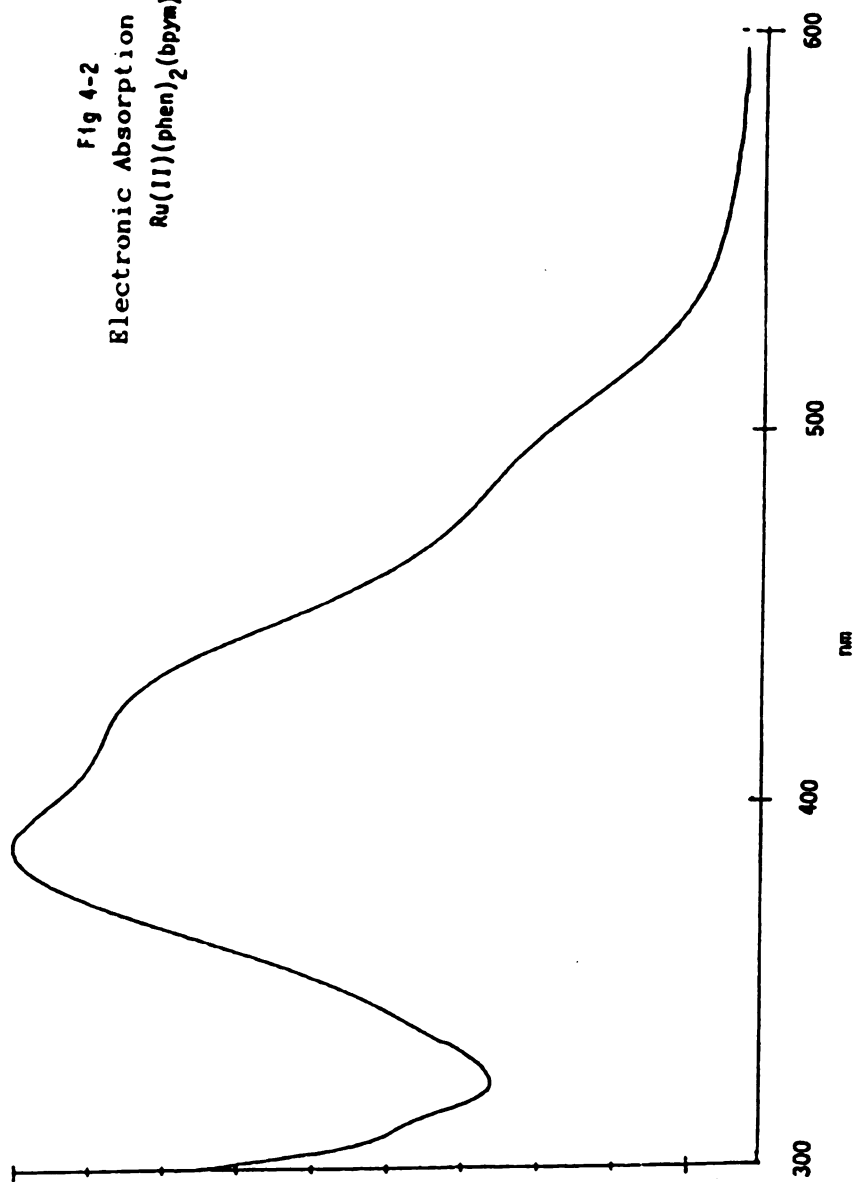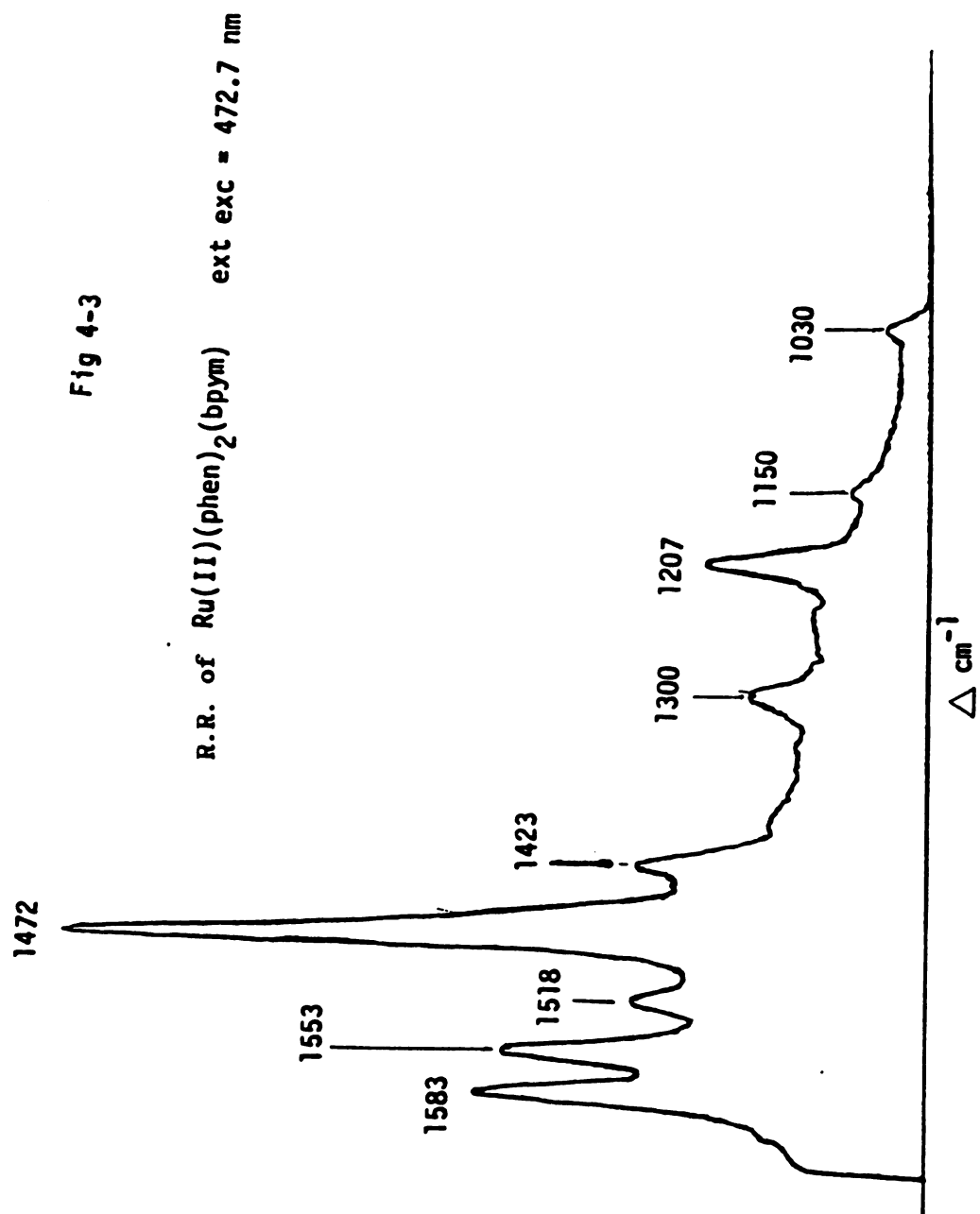
MO Diagram of Ru(II)(bpy)₃ and
Ru(II)(bpym)₃.
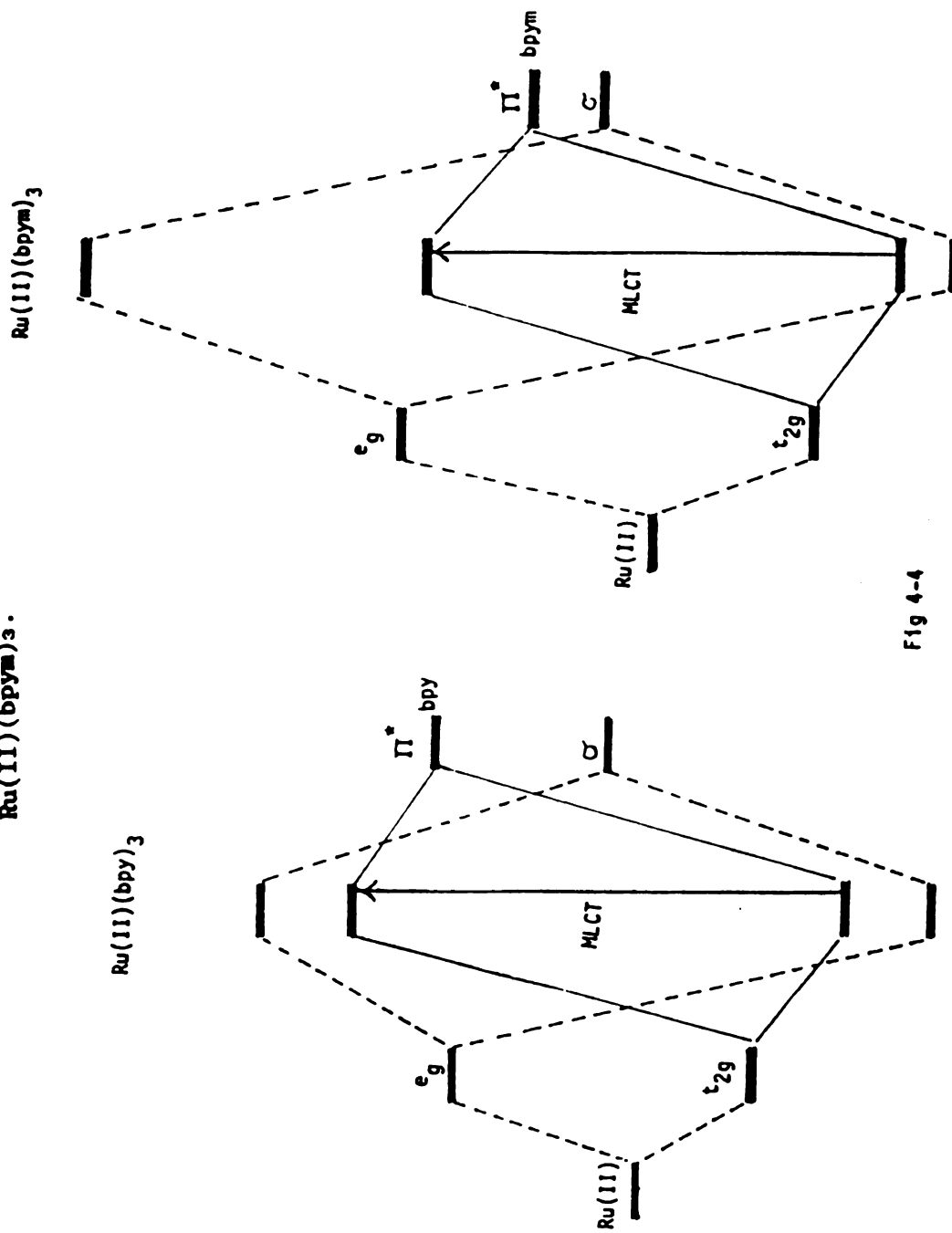
Fig 4-4

REFERENCES

1. (a) S. Anderson, K. R. Seddon, R. D. Wright, A. T. Cocks, Chem. Phys. Lett. **71**, 220 (1980). (b) D. M. Klassen, Chem. Phys. Lett. **93**, 383 (1982). (c) P. Besler, A. von Zelewskyu, A. Juris, F. Barigelletti, V. Balzani Chem. Phys. Lett. **104**, 100 (1984). (d) A. Juris, F. Barigelletti, V. Balzani, P. Belser, A. Von Zelewsky, Inorg. Chem. **24**, 202 (1985).

CHAPTER 5

Characterization of Charge Transfer
States of [Ru(II)(bpy)₂]₂bpym by Resonance Raman Spectroscopy

The photoinduced redox properties of Ru(II)(bpy)₃ has in recent
years, stimulated intense interest in transition metal complexes
containing polypyridyl organic ligands. These complexes typically have
a low-lying luminescent metal-to-ligand charge transfer (MLCT) state as
well as metal-localized ligand field states (LF). Current interest in this
field centers around the potential for utilizing the MLCT states, which
can act as powerful oxidizing or reducing agents.[1] In the same vein,
another approach has become popular. A number of bridged, dimeric
Ru(II) complexes have been prepared and their physical properties, such
as intervalence transitions and electrochemical potentials have been
studied.[2] The electronic absorption spectra of these bimetallic complexes
are red shifted in comparison with their nonmetallic counterparts,
resulting in absorbance over a wavelength range which better matches
the solar emission. In principle, then, the larger complexes are better
sensitizers for solar energy conversion applications.

Resonance Raman spectroscopy has been shown to be a useful
techniqe in studying the ground and excited states of d⁶ transition
metal polypyridine complexes.[3] Resonance enhancement of particular
Raman vibrational peaks are diagnostic of the electronic transition. The
most prominent vibrational modes in these complexes belong to the
organic ligand ring stretching vibrations in the 1300–1700 cm⁻¹ region.
Other modes are active in lower wavenumber regions, such as in C–H

58

bending, ring angle deformation modes, etc. In this chapter, the ground and excited state resonance Raman spectra of the "symmetric" bimetallic [Ru(II)(bpy)₂]₂ bpym (where bpy = 2,2'-bipyridine, bpym = 2,2'-bipyrimidine) and those of the corresponding monomer, Ru(II)(bpy)₂(bpym) are described.

The absorption spectra of the two complexes are shown in Figure 5-1a,b. The Ru(II)(bpy)₂(bpym) monometallic complex exhibits a peak at 417 nm with a distinct shoulder at 490 nm and another 390 nm. The "parent" complex, Ru(II)(bpy)₃ has λ_{max} at 450 mn with no shoulder to lower energy. (See Chapter 4 also.) The Raman spectrum excited by CW radiation at 488.0 mn (Figure 5-2) shows unambigiously that the low energy should in the mixed ligand complex can be assigned to the Ru(II) - π* of bipyrimidine (MLCT) transition. The strongest peaks at 1584, 1553, 1474, 1422, 1203 cm⁻¹ can all be attributed to bipyrimidine modes. Under CW 441.6 nm excitation (Figure 5-3) the bpy modes are considerably enhanced and now dominate the spectrum. Notice at the same time that bpym modes show essentially no change. Finally at 363.8 nm (Figure 5-4), the excitation is in resonance both to the Ru - bpy (MLCT) as well as to a different Ru → π* bpym state (second MLCT). For bpy the relative intensities of the peaks at 1610, 1566 and 1495 cm⁻¹ closely resemble the resonance enhancement of the Ru → bpy π* transition of Ru(II)(bpy)₃ taken at 450 nm. The 1566 cm⁻¹ peak is a little more intense than expected due to contributions from the 1559 cm⁻¹ band of bpym, which clearly can be seen as a shoulder. The strongly altered intensities of the 1559 and 1476 cm⁻¹ bpym peaks clearly show that at 363.8 nm the excitation is in resonance to a different, higher lying MLCT state. In summary, the CW Raman data shows that the

electronic absorption spectrum of Ru(II)(bpy)₂(bpym) can be assigned as Ru - bpym (MLCT) at 490 nm and Ru - bpy (MLCT) at 417 nm. At 380 nm a second MLCT Ru to bpym charge transfer transition can be assigned. Due to the favorable $d\pi^*$ interaction of Ru and bpym the Ru - bpy MLCT absorption appears blue shifted in comparison to Ru(II)(bpy)₃. The Raman spectrum obtained under pulsed excitation at 355 nm, Figure 5-5 clearly shows the excited state scattering of Ru - bpym MLCT state. (See Chapter 4).

The absorption spectrum of the bimetallic complex is shown in Figure 5-1b. In contrast to the monometallic partner, this complex shows absorption well into the visible. The 490 nm shoulder has been red-shifted to 610 nm and the 417 nm peak is slightly blue-shifted to 410 nm. The Raman spectrum obtained with 610 nm excitation (Figure 5-6) shows only two strong Raman modes which are due to bipyrimidine. The lowest energy absorption (610 nm) is separated from its nearest neighboring peak at ~556 nm by about 1592 cm⁻¹. From Raman spectra (not shown) obtained in the 610 nm to 530 nm excitation region, this shoulder is assigned as a vibronic peak, rahter than a new electronic transition. The Raman scattering is essentially excitation wavelength independent. Under 441.6 nm excitation (Figure 5-7) the relative intensities of bipyrimidine Raman modes are now completely different from the low energy excitation. Notice the vastly decreased intensity of 1482 cm⁻¹ and the dominance of 1330 cm⁻¹ and 1552 cm⁻¹ scattering. The 441.6 nm line is ~1745 cm⁻¹ to the red of the 410 nm peak, and some contribution from Ru - bpy (MLCT) is also observed. At 363.8 nm (Figure 5-8) the Ru - bpy (MLCT) is in full resonance. The intensities of the bipyrimidine 1552 cm⁻¹ and 1331 cm⁻¹ modes have not changed

from 441.6 nm excitation which reflects the fact that no new MLCT transitions of bipyrimidine are being accessed. In summary, the absorption spectrum of [Ru(II)(bpy)₂]bpym can be assigned as follows: 610 nm, (0-0) of Ru - bpym (MLCT), with 556 nm a vibronic peak; 410 nm Ru - bpy (MLCT) and 440~460 nm region a second Ru to bpym MLCT transition.

The pulsed Raman data is not shown, but the excited state spectrum clearly showed bpym localized scattering. Due to the shorter lifetimes of the bimetallic complexes there was also significant contribution from ground state scattering.

In conclusion, it has been demonstrated that resonance Raman spectroscopy can be effectively utilized to locate MLCT states in ligand bridged bimetallic polypyridyl complexes. Results for other complexes which involve different d⁶ transition metal centers and/or external ligands are contained in the Appendix to this Chapter.

Figs-1 a

Electronic Absorption Spectrum of
Ru(II)(bpy)2(bpym)
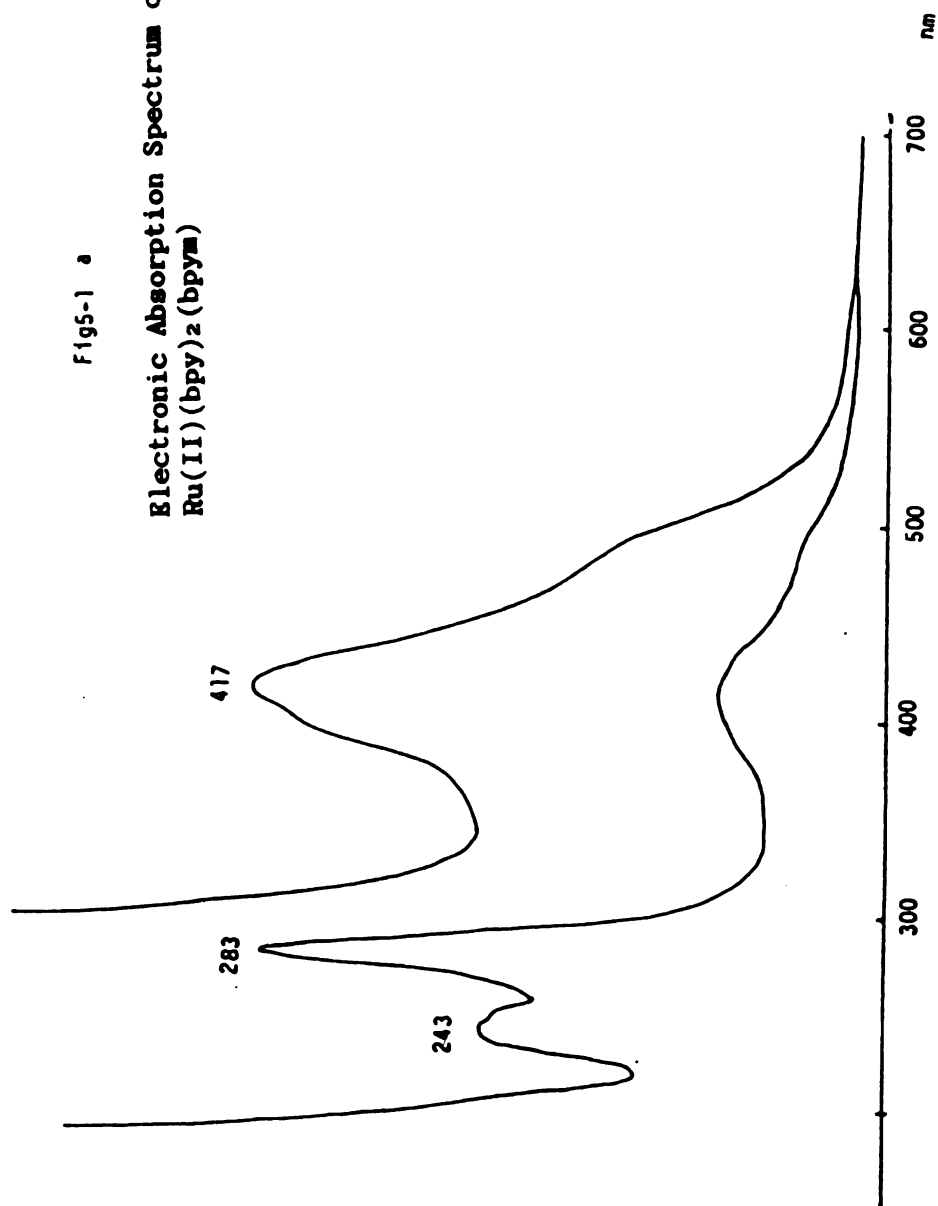
Fig 5-1b

Electronic Absorption Spectrum of
[Ru(II)(bpy)2]2(bpym)

Fig 5-2

R.R. of Ru(II)(bpy)$_2$(bpym)   488.0 nm exc

Fig 5-3

R.R. of Ru(II)(bpy)$_2$(bpym) 441.6 nm exc

Fig 5-4

R.R. of Ru(II)(bpy)$_2$(bpym)   363.8 nm exc

Fig 5-5

R.R. of Ru(II)(bpy)$_2$(bpym) 355 nm exc

1568

1496

1362

1323

1256 1181

1042 1025

1610

$\triangle$ cm^{-1}

Fig 5-6

R.R. of [Ru(II)(bpy)$_2$]$_2$ bpym   610 nm exc

1485

1552

Δ cm^{-1}

Fig 5-7

R.R. of [Ru(II)(bpy)₂]₂ bpym 441.6 nm exc

Fig 5-8

R.R. of [Ru(II)(bpy)₂]₂ bpym 363.8 nm exc
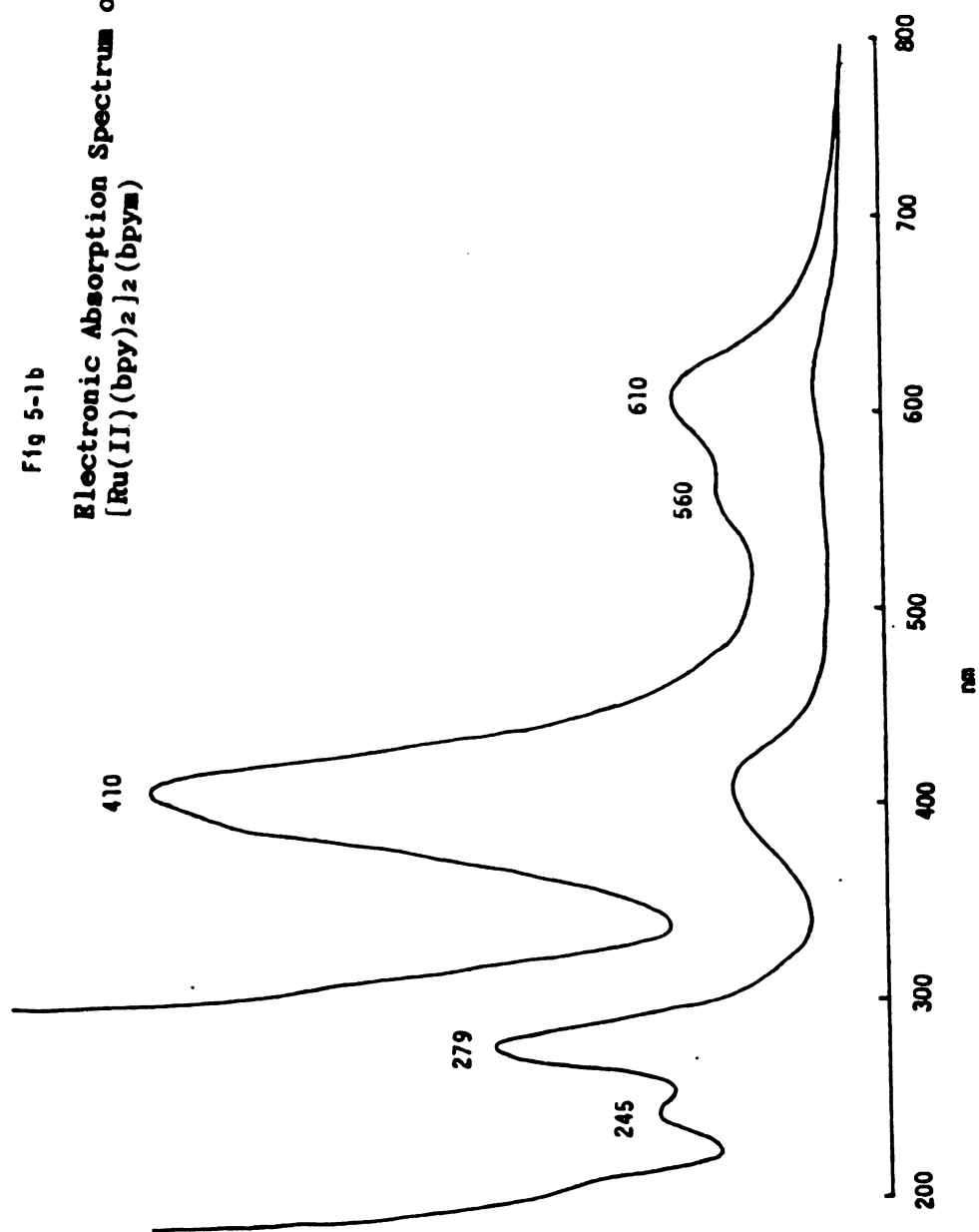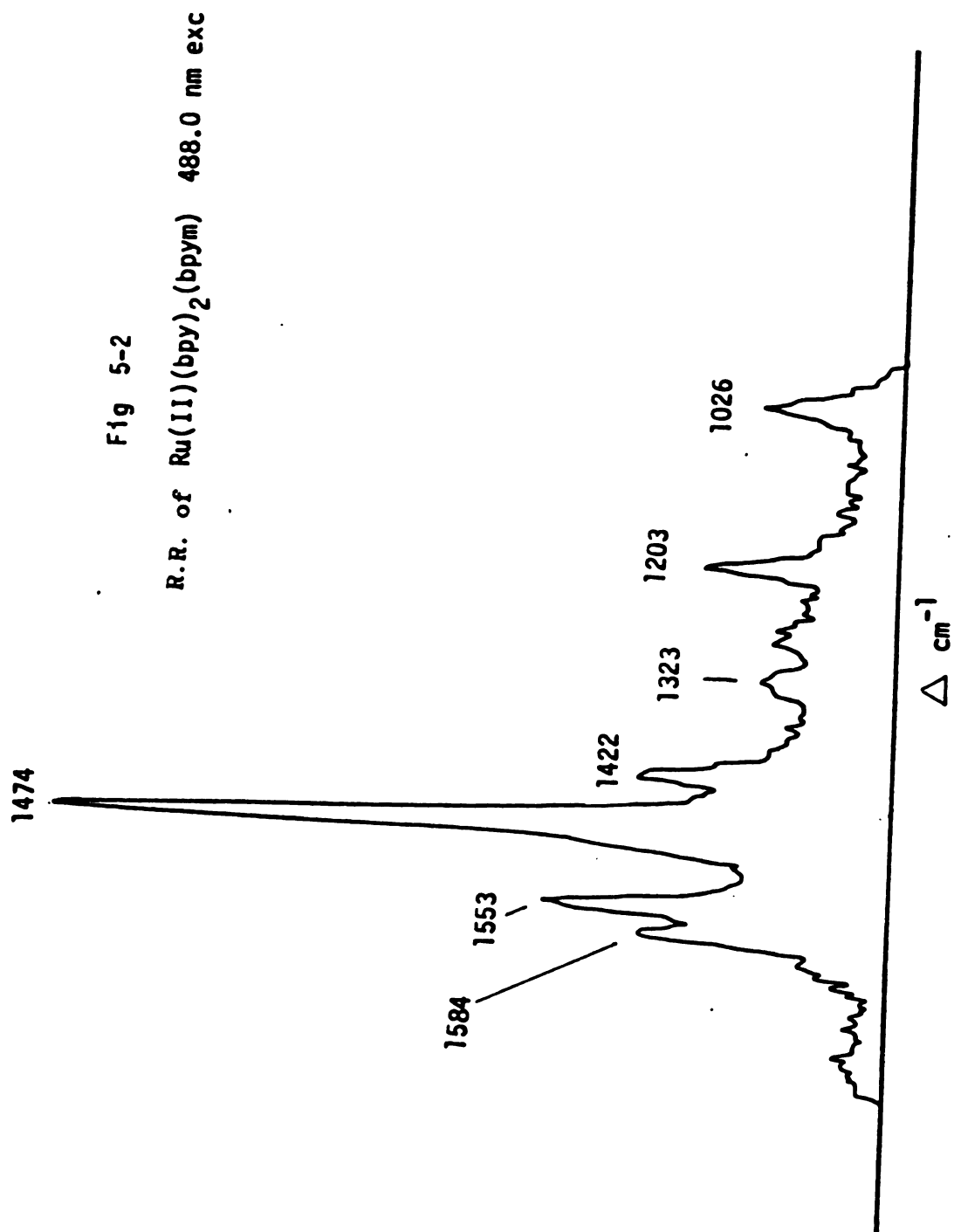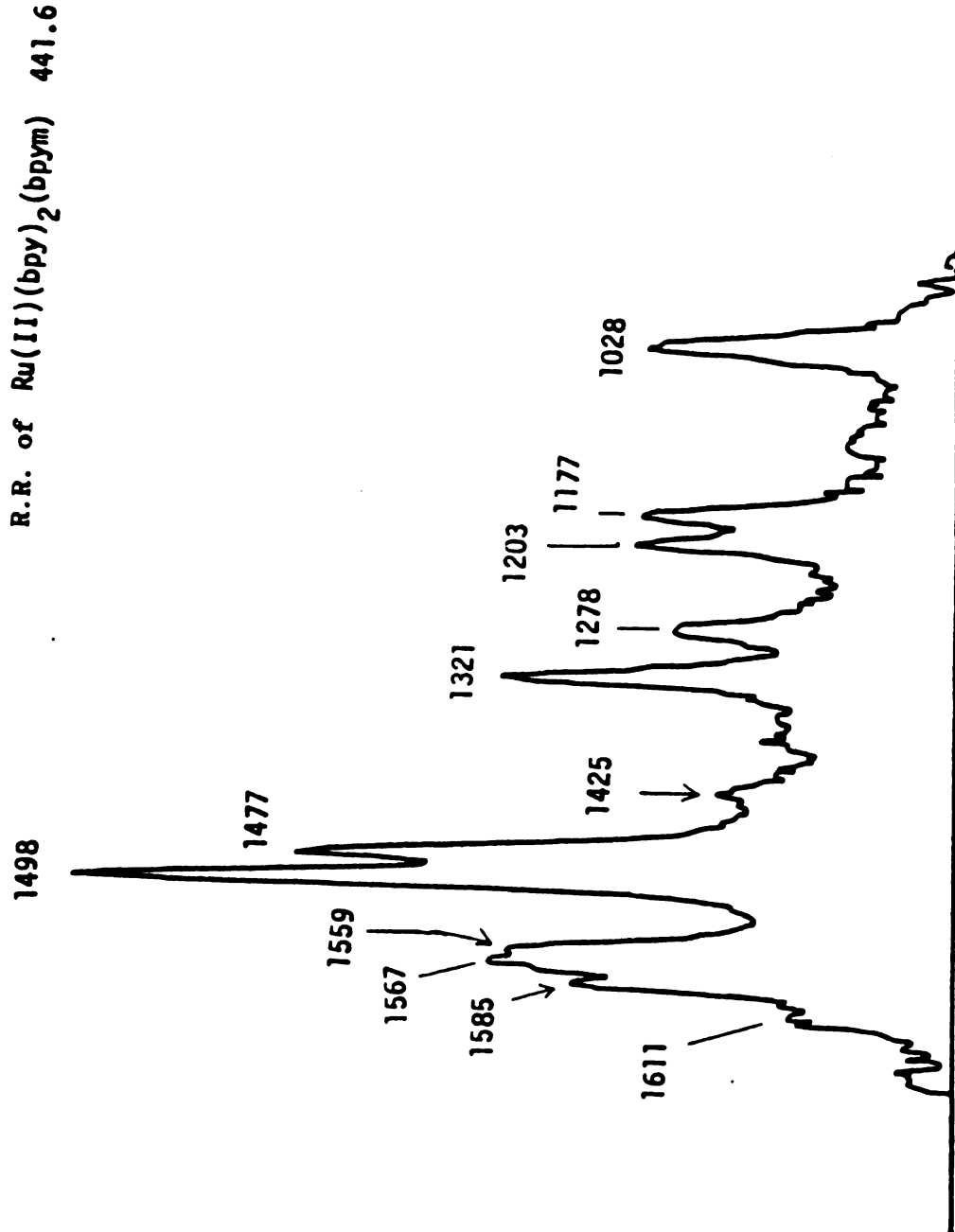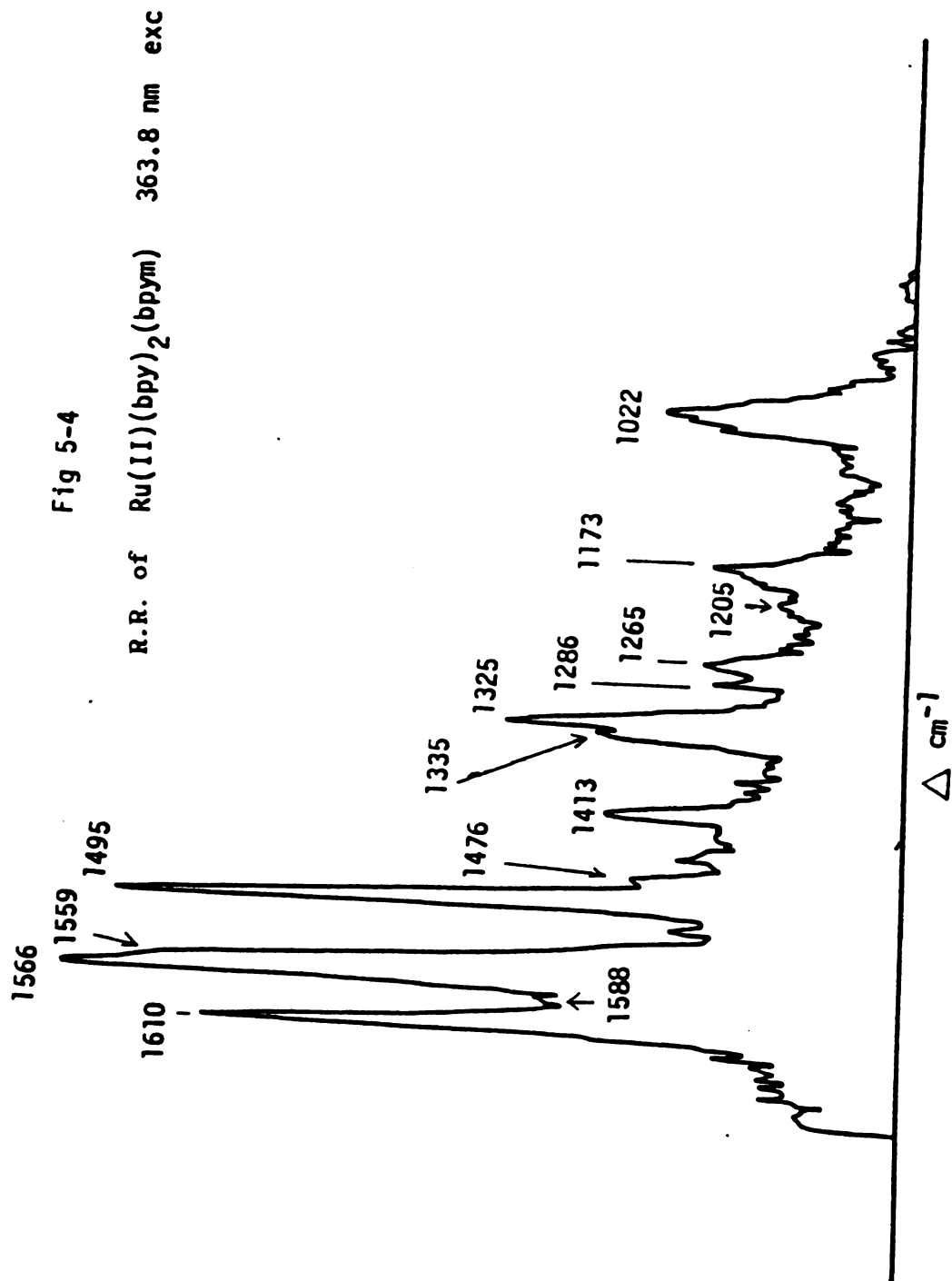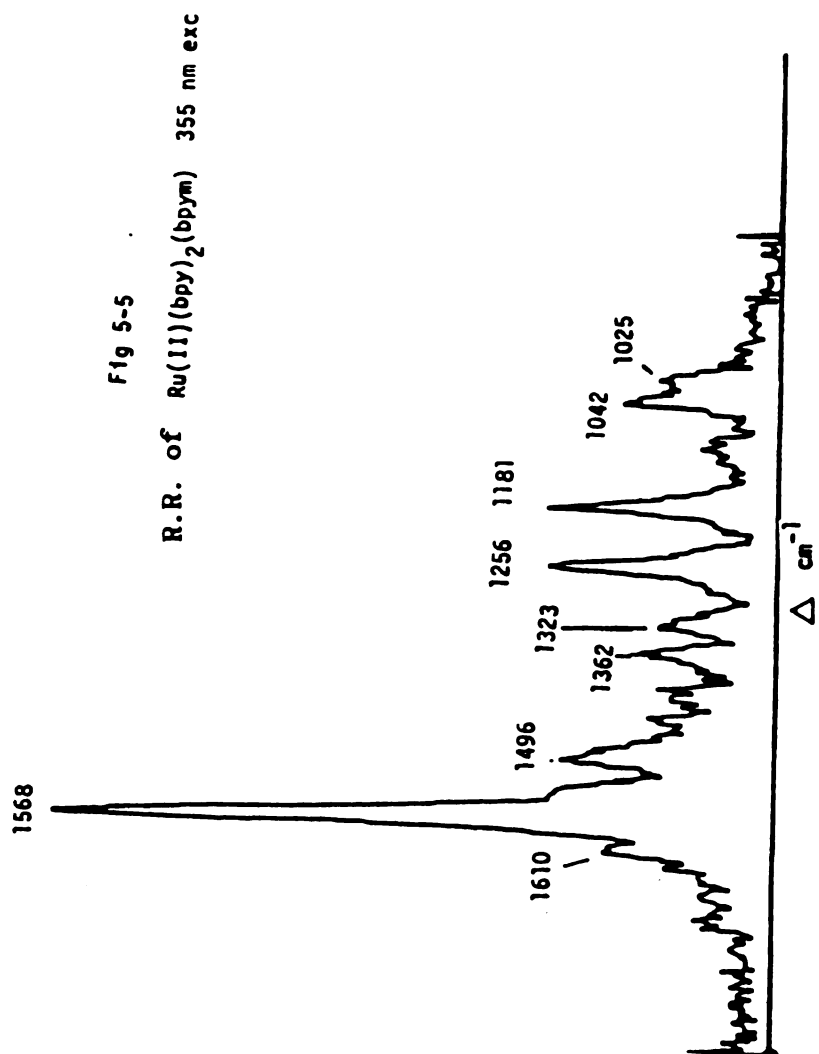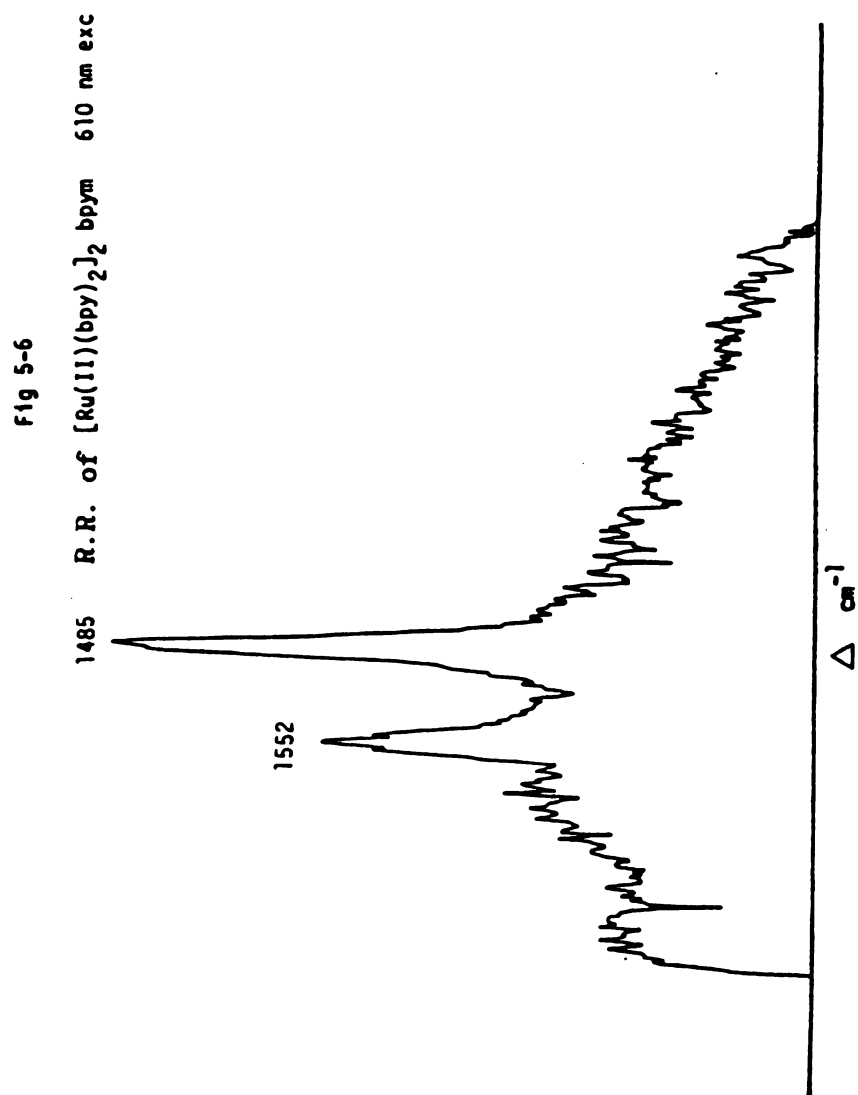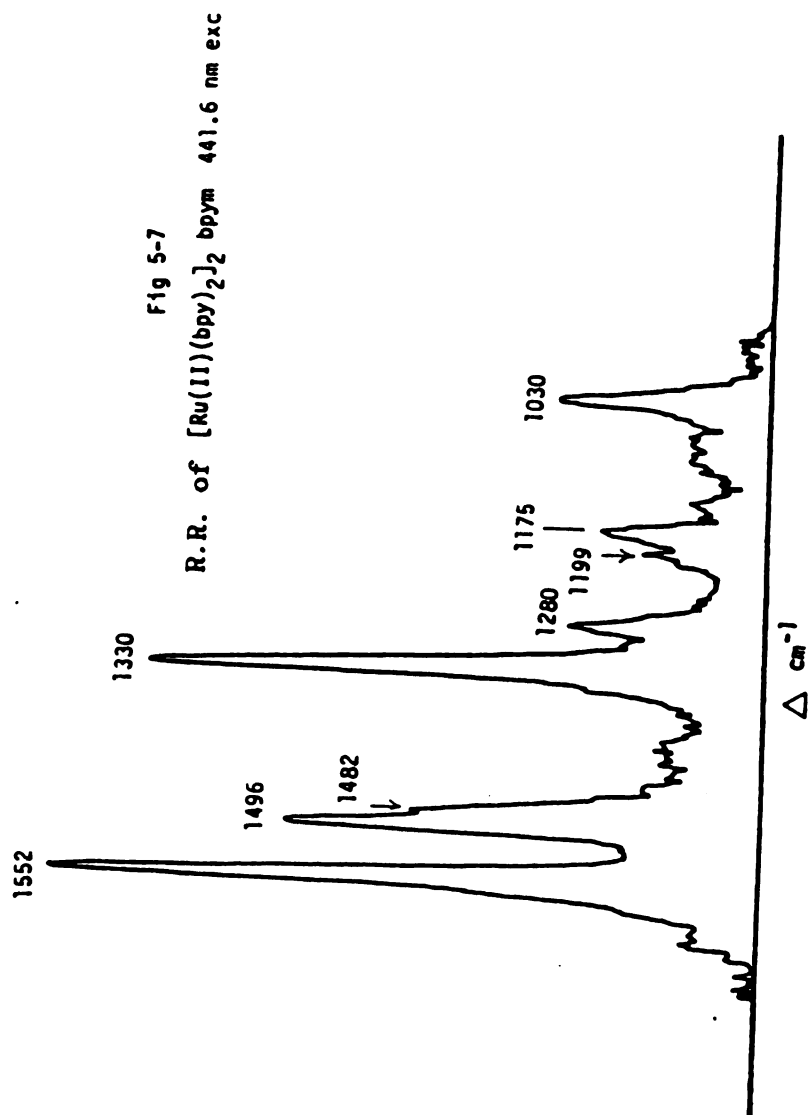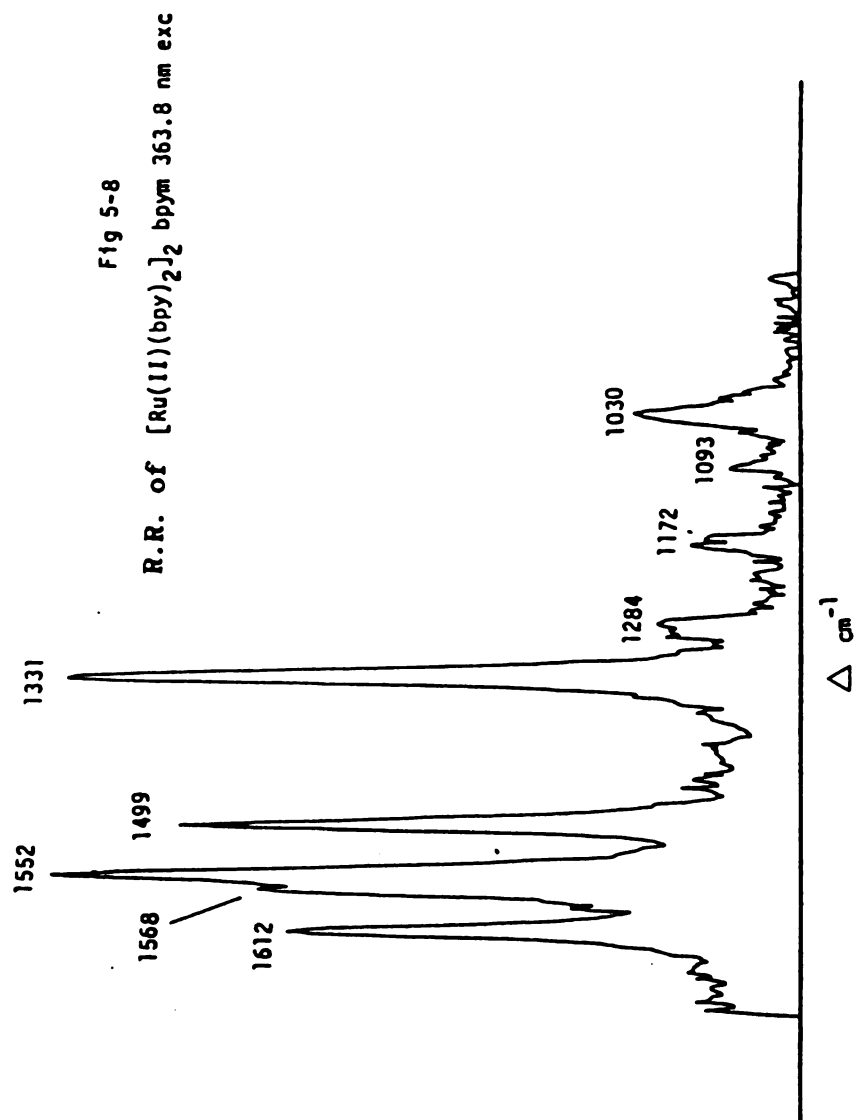
REFERENCES

1. For a recent review see: Kalyanasundaram, K. Coord. Chem. Rev. 46, 159 (1982).

2. (a) R. Dallinger, W. H. woodruff, J. Am. Chem. Soc. 101, 4391 (1979). (b) M. Forster, R. E. Hester, Chem. Phys. Lett. 81, 42 (1981). (c) Y. C. Chung, N. Leventis, P. Wagner, G. E. Leroi, J. Am. Chem. Soc. 107, 1416 (1985).

3. (a) D. P. Rillema, R. W. Callahan, K. B. Mack, Inorg. Chem. 21, 2589 (1982). (b) C. H. Braunstein, A. D. Baker, T. C. Strekas, H. D. Gafney, ibid 23, 857 (1984). (c) A. Basu, H. Gafney, T. C. Strekas, Inorg. Chem. 21, 2231 (1982). (d) E. Dose, L. J. Wilson, Inorg. Chem. 17, 2660 (1978). (e) M. Hunziker, A. Ludi, J. Am. Chem. Soc. 99, 7370 (1977).

APPENDIX

The [Ru(II)(bpy)₂]₂bpym symmetric bimetallic complex displays visible as well as near UV electronic transitions. This bimetallic system has been extended to include "non-symmetric" systems in an attempt to understand further the electronic energy levels. The electronic absorption spectra of [Ru(II)(bpy)₂]bpym[Os(II)(phen)₂] and [Ru(II)(phen₂]bpym[Os(II)(bpy)₂] are shown in Figure 5-9, 5-10. The spectra are quite similar to the symmetric analog. The [Ru(II)(phen)₂]bpym[Os(II)(bpy)₂] Raman spectra will be discussed first. The cw spectrum excited at 514.5 nm (Figure 5-11) shows two major peaks at 1549 and 1482 cm⁻¹ as well as a weak one at 1332 cm⁻¹. These three are due to bpym scattering, enhanced by Os(II) – bpym (MLCT) transition. A shoulder can be seen at 1565 cm⁻¹ which is assigned to bpy enhanced by Os(II) – bpy (MLCT) resonance; the weak 1184 cm⁻¹ peak can be similarly assigned. When the sample is excited at higher energy with 454.5 nm radiation (figure 5-12) the 1330 cm⁻¹ band is comparable in intensity to the 1478 cm⁻¹ peak. This reflects the onset of the second Os(II) – bpym resonance. There are new peaks as 1459, 1305, 1212 cm⁻¹. All three features can be assigned to phen scattering, enhanced by Ru(II) – phen MLCT resonance. The Raman spectrum excited by the 441.6 nm cw, He-Cd laser (Figure 5-13) shows clearly that the excitation is in resonance with the second MLCT of bpym. The intensity of the 1330 cm⁻¹ peak has surpassed the 1541 and 1477 cm⁻¹ peaks. Notice as well that the Ru – phen MLCT peaks are also strong;

1213, 1304, 1459, 1523 and 1584 cm^{-1} features are all due to phenanthroline. Finally at 363.8 nm (figure 5-14) bands for each polypyridyl ligands are resonance enhanced due to all three MLCT transitions. Peaks 1634, 1583, and 1454 cm^{-1} can be assigned to Ru - phen MLCT; those at 1616, 1564 and 1498 cm^{-1} can be assigned to Os(II) - bpy MLCT; the peaks at 1544, 1478, and 1330 cm^{-1} are due to the second Os(II) - bpym MLCT.

The pulsed Raman spectrum obtained at 430 nm (Figure 5-15) shows only ground state peaks. It is interesting to compare this spectrum with that observed with 454.5 nm CW excitation. It is clear that the Ru - phen MLCT state is in resonance; the peaks at 1525, 1460, 1309, 1210 and 1150 cm^{-1} are due to the phen ligand. Some bpy peaks can also be seen, although they are weaker (1566, 1497, and 1181 cm^{-1}). This confirms the earlier assignment of Ru - phen being at higher energy than Os(II) - bpy MLCT transiton. The pulse excited Raman spectrum at 355 nm (Figure 5-16) shows several peaks which can be attributed to Raman scattering from the bridging ligand in the excited state following Os - bpym charge transfer. The strongest peak at 1570 cm^{-1} can be assigned to the excited state as well as weaker ones at 1362, 1256 and 1177 cm^{-1}. The 1177 cm^{-1} peak (as well as the 1570 cm^{-1} peak) contains some contribution from bpy modes. At 355 nm, three transitions are heavily overlapped (i.e., Ru - phen, Os - bpy, Os - bpym), but fast deactivation leaves the complex in the lowest excited state, which is the Os - bpym MLCT state. This excited state is probed with the second 355 nm photon which provides the Raman scattering shown in Figure 5-16.

In summary, the absorption spectrum of [Ru(II)(phen)$_2$]bpym[Os(II)(bpy)$_2$] can be interpreted as Os - bpym, Os - bpy, Ru - phen, Os - bpym(2nd) in order of increasing energy. Of course, more quantitative 0-0 transition energies can be obtained by following Raman excitation profiles for selected bands. The 1331, 1482, 1549 cm^{-1} excitation profile would show the two MLCT states for bpym; 1309, 1460, 1525 cm^{-1} should be monitored for phenanthroline; 1566 and 1497 cm^{-1} should be monitored by bpy.

The related complex [Ru(II)(bpy)$_2$]bpym[Os(II)(phen)$_2$] was studied to see how the interchange of "external" ligands would influence the electronic energy levels. The Raman data available on this compound is limited, however, due to difficulties with emission. This emission could either be due to impurity or to some dual emission, although the latter possibility is unlikely because it is rare. The pulsed Raman spectrum obtained with 430 nm excitation, Figure 5-17, shows only two types of transitions. The 1183, 1495 cm^{-1} bands are due to bpy in resonance with the Ru - bpy MLCT transition; bpym peaks at 1540 and 1330 cm^{-1} are enhanced by Os - bpym MLCT absorption. The spectrum excited at 388 nm, Figure 5-18, clearly shows resonance to Ru - bpy MLCT. The strong peaks at 1613, 1566, 1497 cm^{-1} can all be assigned to bpy. The bands at 1540 and 1330 cm^{-1} are resonance enhanced by the second Os - bpym MLCT. As 355 nm, Figure 5-19, the Raman spectrum is quite similar to that excited at 388 nm. It is interesting that this complex does not show any excited state peaks. Apparently switching the external ligands influences the lifetime. A more extensive study involving various ligands would be needed to understand the reasons for the shorter lifetime of this complex as compared to the previous

complementary compound. Elucidation of the various factors which influence the lifetimes of these complexes will be critical to the design of superior photosensitizers.

Three additional complexes in the bimetallic series have been investigated. [Ru(bpy)₂]bpym[Os(bpy)₂] was studied to investigate the effects of breaking the symmetry of the metal d-orbital levels, i.e., in comparison to "symmetric" [Ru(bpy)₂]₂bpym. The electronic absorption spectrum is quite typical of a bimetallic species, Figure 5-20. The Raman spectrum (Figure 5-21) excited with low power pulses at 532 nm shows strong bpym peaks at 1539, 1480 and 1327 cm⁻¹. This spectrum very closely resembles that of the symmetric dimer under similar excitation conditions. The cw spectrum at 441.6 nm in Figure 5-22 shows resonance to the second MLCT transition of bpym as well as charge transfer to bpy. In comparison with the symmetric dimer, the 1480 cm⁻¹ bpym mode has almost completely died out, reflecting a lower second charge transfer energy. Also the bpy peaks at 1498 and 1565 cm⁻¹ are more prominent. When the excitation line is moved to 420 nm, Figure 5-23, the 1537 cm⁻¹ line of bpym continues to decrease. The bpy peaks at 1611, 1564, 1493, 1280, 1176, 1030 cm⁻¹ are clearly descernible. With 363.8 nm excitation, the Raman spectrum (Figure 5-24) shows one interesting difference from the symmetric complex. In the symmetric dimer the intensities were 1499>1568>1612 cm⁻¹ whereas the intensity trend is reversed in the unsymmetric case. In the symmetric complex this was explained by assuming a blue shift of the Ru - bpy MLCT transition due to the favorable dπ* interaction of Ru and bpym. This dπ* interaction in the unsymmetric case is between Os(II) and bpy and leaves the Ru(II)(bpy)₂ center relatively unperturbed. That is, the

Ru(II)(bpy)₂ fragment is relatively isolated giving rise to Ru - bpy MLCT absorption which more closely resembles the Ru(bpy)₃ case. An excited state Raman spectrum could not be obtained at 355 nm, Figure 5-25, reflecting the short lifetime of the mixed bimetallic complex. In the symmetric case an excited state spectrum albeit, a weak one, was obtainable. In the unsymmetric case the Os - bpym MLCT is the lowest excited state and Os complexes generally have shorter lifetimes than their Ru counterparts.

The complex [Ru(II)(phen)₂]bpym[Ru(II)(phen)₂] was also studied. (Figure 5-26). This species is the phen analog of the [Ru(II)(bpy)₂]bpym complex described in the earlier part of this chapter. The 363.8 nm cw spectrum (Figure 5-27) shows phen as well as bpym modes. The bpym modes at 1335 and 1552 cm⁻¹ are very intense and the Raman spectrum in general is quite similar to that of the bpy analog. In the [Ru(II)(bpy)₂]₂bpym complex the Ru - bpy MLCT was shown to be blue-shifted in energy and this was reflected in the relative intensities of the bpy high frequency modes. This blue-shifting of the "external" ligand MLCT transition can be more clearly seen in the phen bimetallic complex. The phen ligand has at least two distinct MLCT transitions in the near UV visible range. Under 363.8 nm excitation the phen Raman modes are reflective of the second MLCT state. However, compared to Ru(II)(phen)₃ (Chapter 7), this transition is blue-shifted. Note in Figure 5-26 that the 1636 cm⁻¹ peak is still weak in comparison to that at 1589 cm⁻¹. Also notice that the 1440 cm⁻¹ band is very weak where as it is very strong in Ru(phen)₃. Again, in this complex the bpym bridging ligand with its low π* orbitals, interacts favorably with the Ru d-orbitals which drives the Ru - phen MLCT transition to higher

energy. An excited state spectrum was not obtainable with high power 355 nm pulsed excitation. The Raman spectrum was obtained with poor signal to noise ratio (Figure 5-28). It shows relatively strong phen modes and weak bpym modes. This again illustrates the effect of the "external" ligand on the lifetime of the charge transfer excited state.

The complex [Ru(II)(phen)₂](bpym)[Os(II)(phen)₂] was studied (Figure 5-29) to monitor the effect of Os(II) substitution for one of the Ru(II) metal centers. The 363.8 nm cw Raman spectrum (Figure 5-30) like the symmetric [Ru(II)(phen)₂]₂bpym analog, shows bpym modes as well as phen modes. The difference is that the intensity distribution of the phen modes here is closer to that of the second MLCT resonance enhancement in Ru(phen)₃. That is the bands at 1638, 1460, and 1638 cm⁻¹ are strong in comparison to the peak at 1332 cm⁻¹. Breaking the symmetry by Os(II) substitution again seems to cause less metal-metal interaction. In other words, the Ru(phen)₂ fragment is more isolated than in the symmetric case. This is not surprising since Ru(II) and Os(II) have different d-orbital energies. The pulsed Raman spectrum excited at 355 nm (Figure 5-31) shows a very surprising difference from the other complexes in the bimetallic series. The [Ru(II)(phen)₂]bpym[Os(II)(phen)₂] complex shows a very clean excited state spectrum, reflecting a longer-lived excited state. Why this particular combination of "external" ligand and metal should give a long-lived excited state is unknown. It is clear from the spectra of various bimetallics described here that the charge transfer excited state lifetime is very sensitive to the nature of the organic ligands as well as the metal(s). It is proposed that different ligands and metals be utilized to extend the scope of this bimetallic series. For example, external ligands
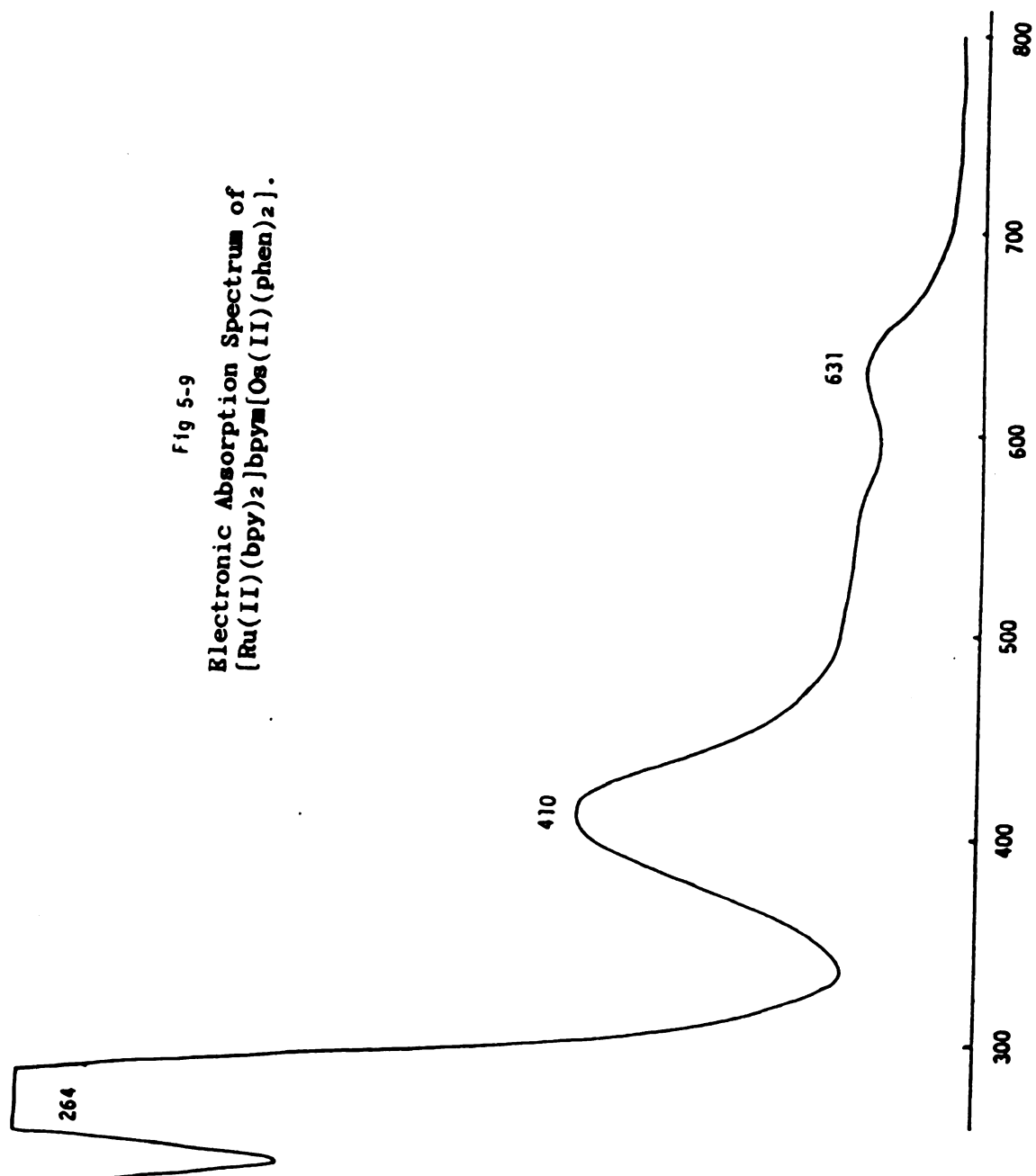
with differing electron withdrawing or donating powers and/or different metals should be substituted.

The MO diagram for Ru(II)(bpy)₂(bpym) and its bimetallic analog is shown in Figure 5-32. In the case of Ru(bpy)₂(bpym) the ligand field splitting is larger than that of Ru(II)(bpy)₃, but smaller than that of Ru(II)(bpym)₃. This causes the Ru - bpym MLCT to red-shift from 450 nm to 490 nm (1814 cm⁻¹) and blue-shifts Ru - bpy MLCT from 450 nm to 417 nm (1758 cm⁻¹). In the bimetallic complex first notice that the bpym π^* has been stabilized as compared to the monomer. This can be viewed as the second Ru(II) center acting as a Lewis acid. This positive center will stabilize the π^* orbital of bpym. The bridging ligand, bpym, facilitates communication of the two metal centers by d-π^*-d interaction. This type of interaction gives rise to the three MO's of bonding, non-bonding, and anti-bonding nature. The two effects combined to give a low energy Ru(II) - bpym MLCT in the bimetallic complex at 610 nm, which is a ~4000 cm⁻¹ shift from the monomer. Since the bpy-Ru(II) dπ interaction is essentially unaffected, we see that the Ru(II) - bpy MLCT has changed little form the monomer complex. The 417 nm to 410 nm slight shift may be due to the stabilization of dp orbitals by the second Ru(II) center. This effect has been observed in other bimetallics by electrochemical studies.

The MO diagram for mixed ligand bimetallic complexes is shown in Figure 5-33. This MO diagram characterizes all bimetallic complexes of Ru(II), Os(II) with bpy and/or phen ligands. The Os(II) 5d level has been placed higher in energy than the Ru(II) 4d level. Breaking the metal symmetry results in a lower energy MLCT to the bridging bpym ligand. This is because the d-π^*-d interaction results in a transition

from a mainly Os(II) d-orbital to the bpym MLCT, and since Os(II) has a higher lying d-orbital, it consequently red-shifts the transition. The MO diagram also shows that the MLCT from the Ru(II) center will be at higher energy than the Os(II) center regardless of whether the external ligand is phen or bpy.

Fig 5-9
Electronic Absorption Spectrum of
[Ru(II)(bpy)2]bpym[Os(II)(phen)2].

Fig 5-10

Electronic Absorption Spectrum of
[Ru(II)(bpy)₂)bpym[Os(II)(bpy)₂]

Fig 5-11

R.R. of [Ru(II)(phen)₂] bpym [Os(II)(bpy)₂] 514.5 nm exc
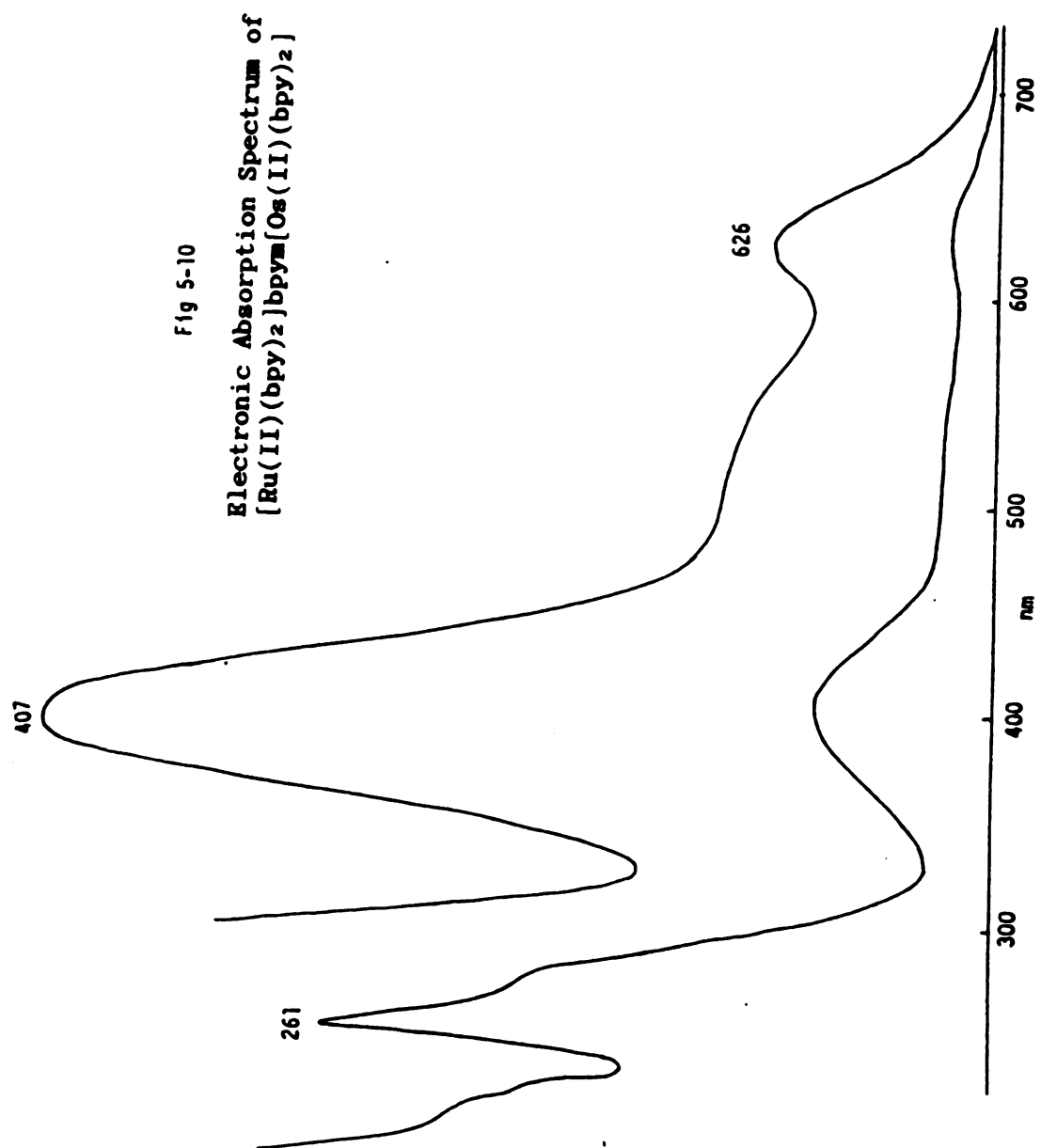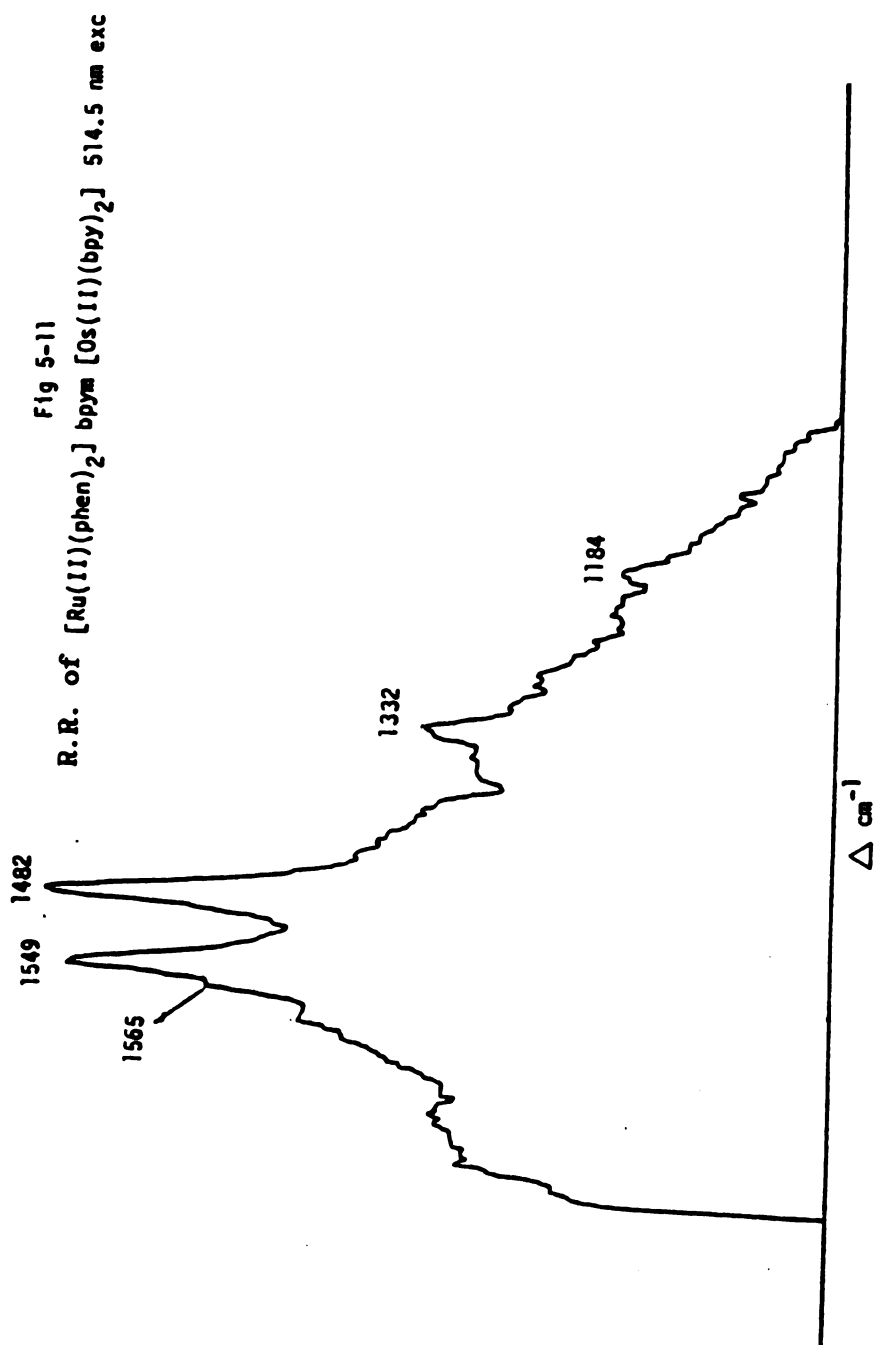
Fig 5-12

R.R. of [Ru(II)(phen)$_2$] bpym [Os(II)(bpy)$_2$]

454.5 nm exc

1541

1478

1459

1330

1305

1212

$\triangle$ cm^{-1}

Fig 5-13

R.R. of [Ru(II)(phen)$_2$] bpym [Os(II)(bpy)$_2$]   441.6 nm exc

Δ cm^{-1}
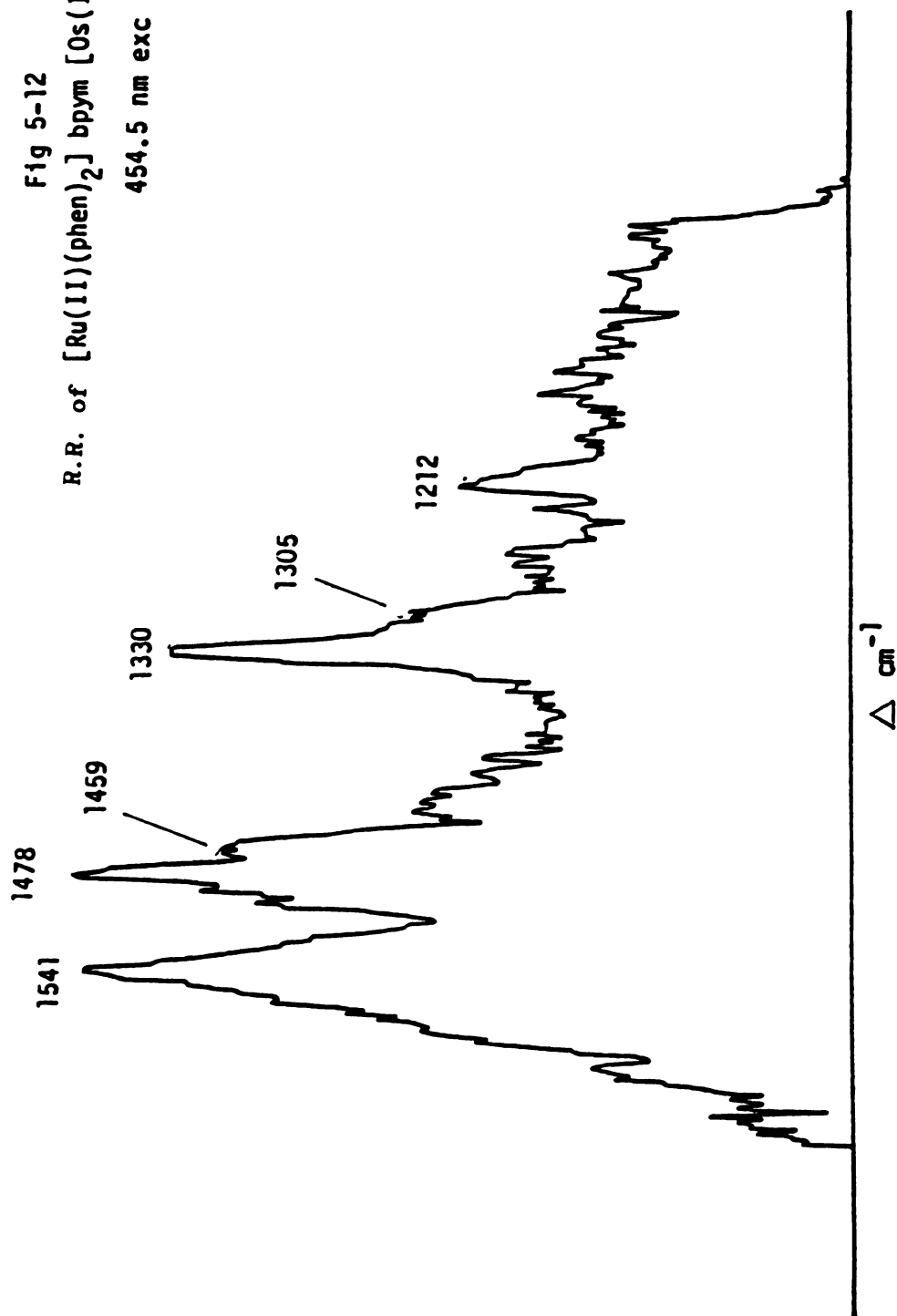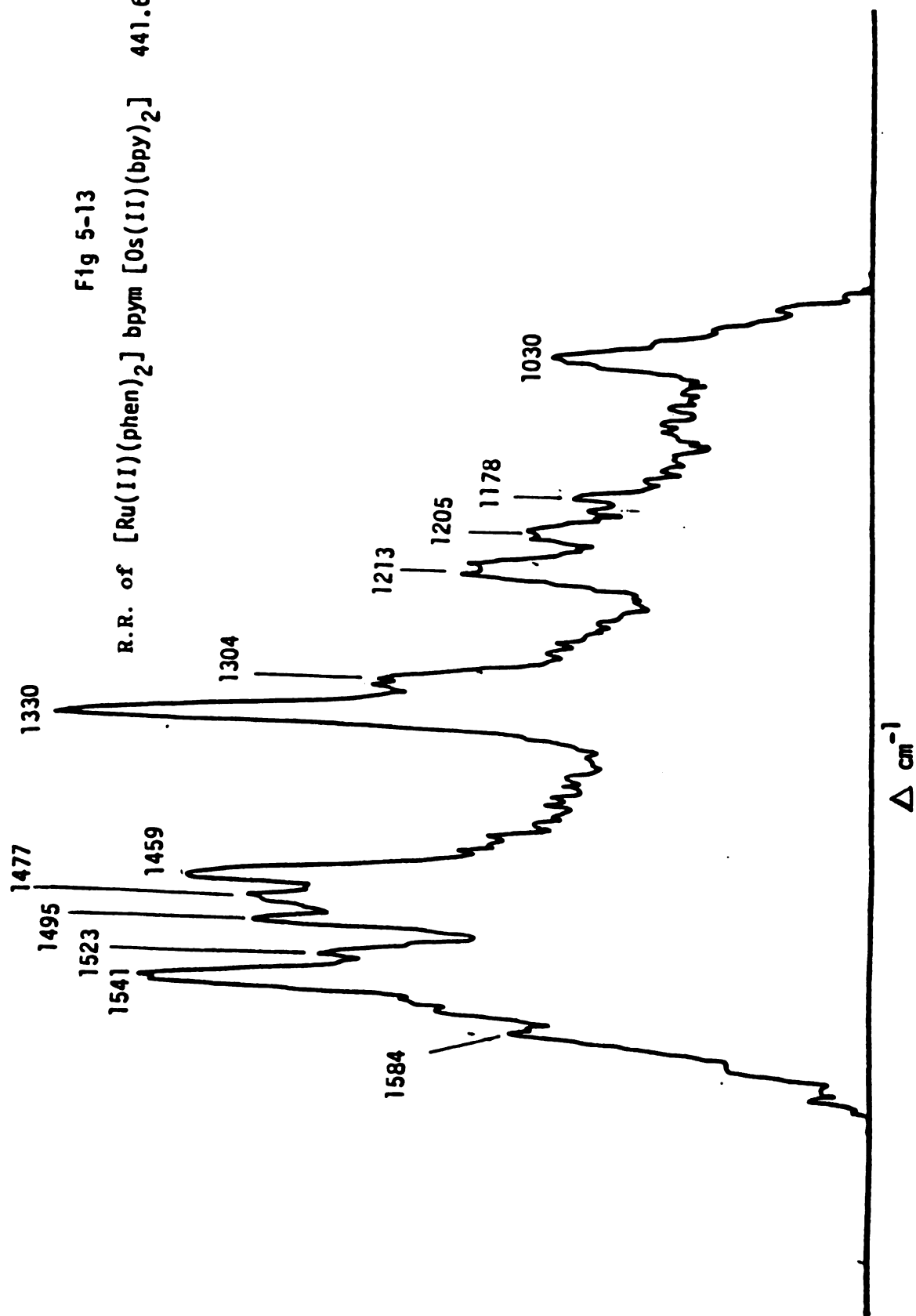
Fig 5-14

R.R. of [Ru(II)(phen)₂] bpym [Os(II)(bpy)₂]

363.8 nm exc

Fig 5-15.

R.R. of [Ru(II)(phen)$_2$] bpym [Os(II)(bpy)$_2$]
430 nm exc

$\triangle$ cm^{-1}

Fig 5-16

R.R. of [Ru(II)(phen)$_2$] bpym [Os(II)(bpy)$_2$]
355 nm exc
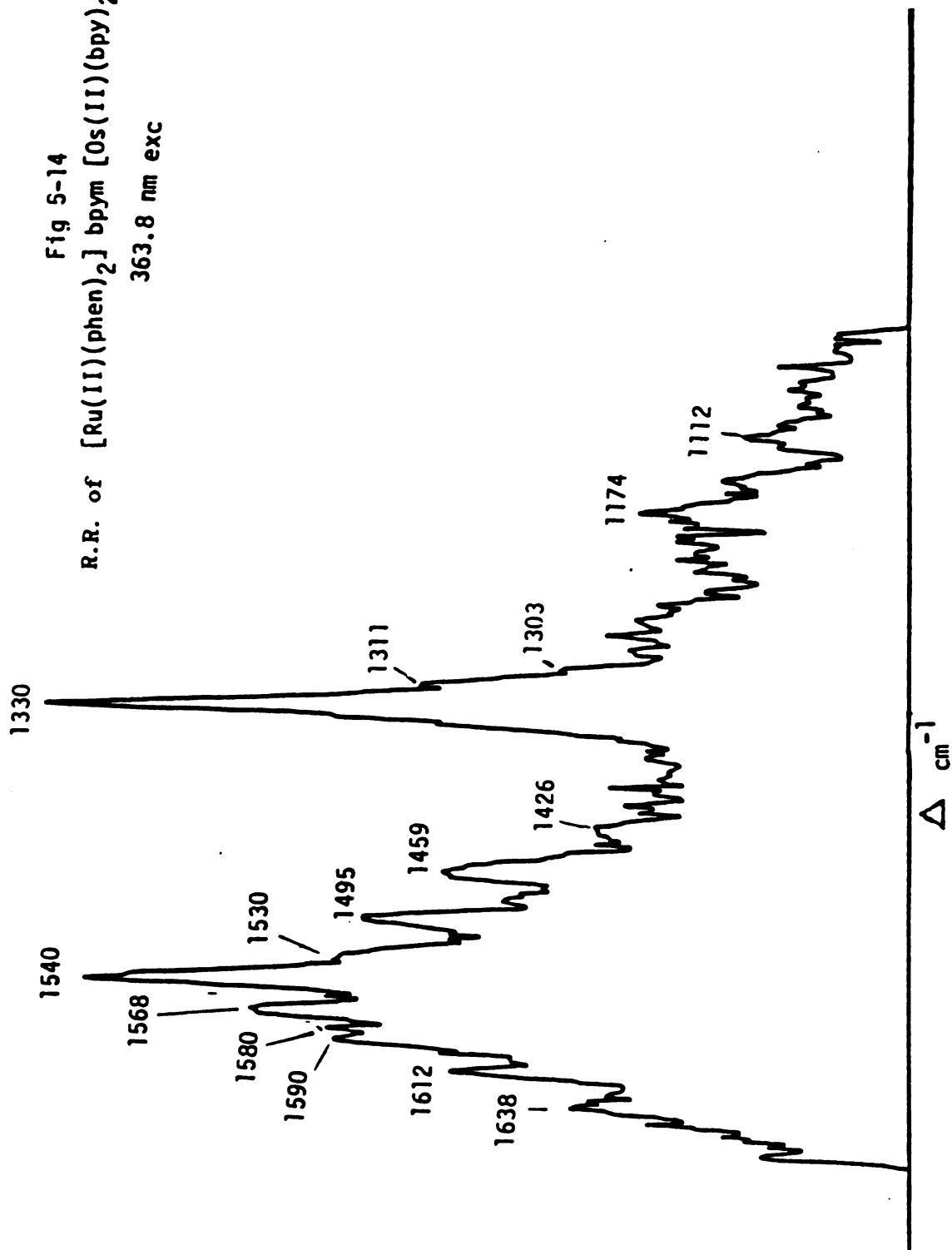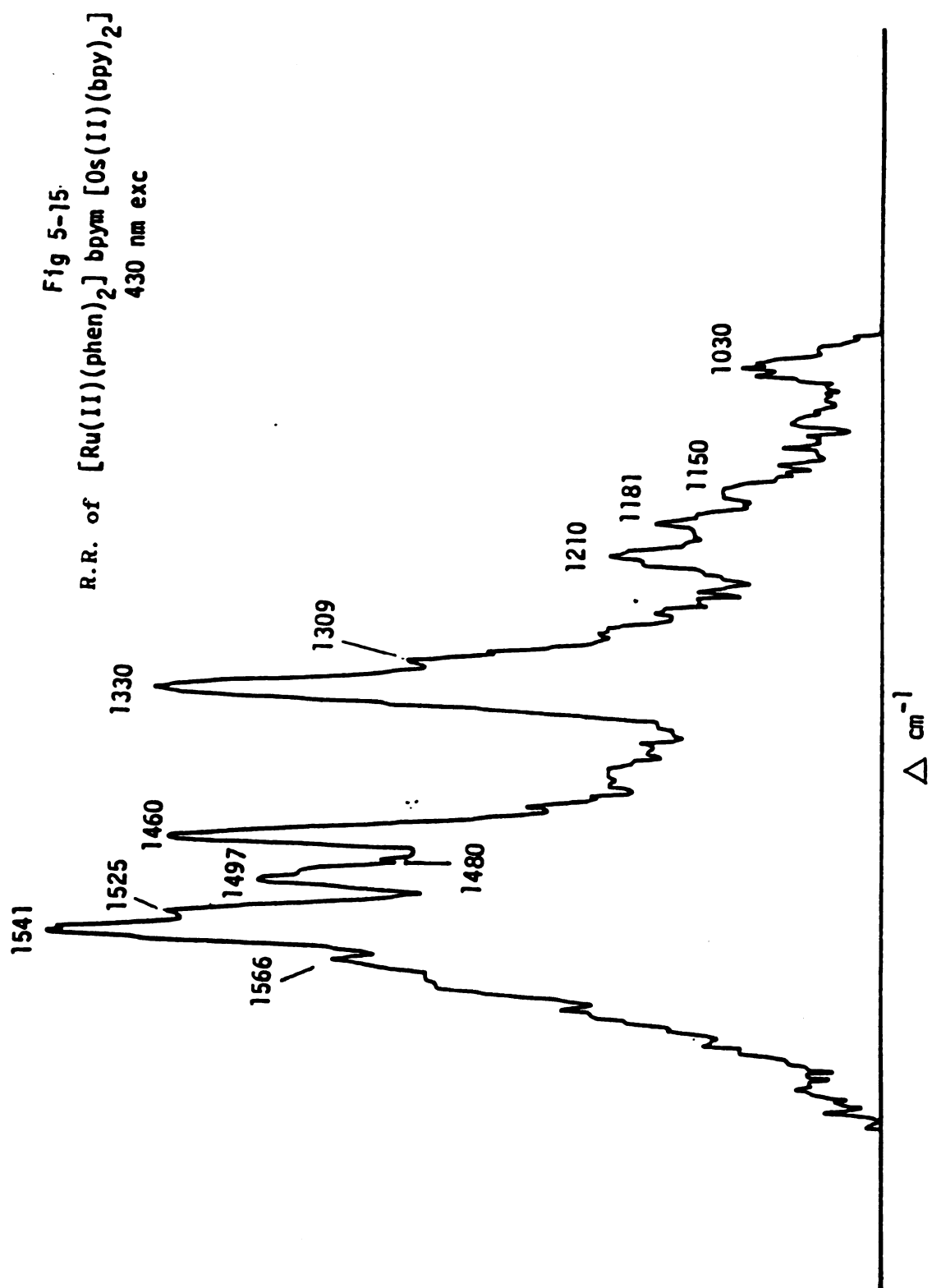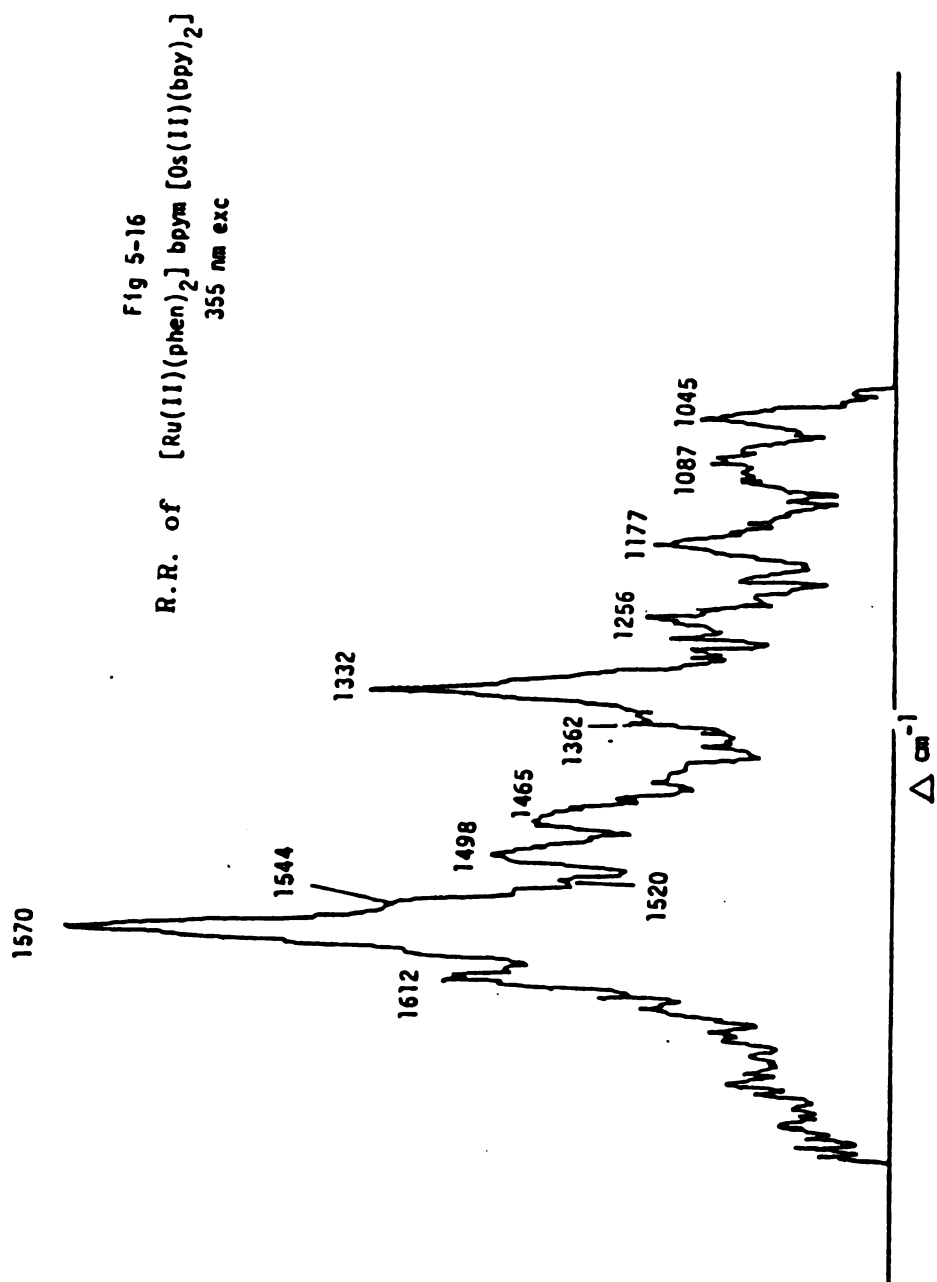
Fig 5-17

R.R. of [Ru(II)(bpy)$_2$] bpym [Os(II)(phen)$_2$]
430 nm exc

1540
1495
1330
1210
1183

$\triangle$ cm^{-1}

Fig 5-18

R.R. of [Ru(II)(bpy)$_2$] bpym [Os(II)(phen)$_2$]
388.5 nm exc

Fig 5-19

R.R. of [Ru(II)(bpy)$_2$] bpym [Os(II)(phen)$_2$]
355 nm exc
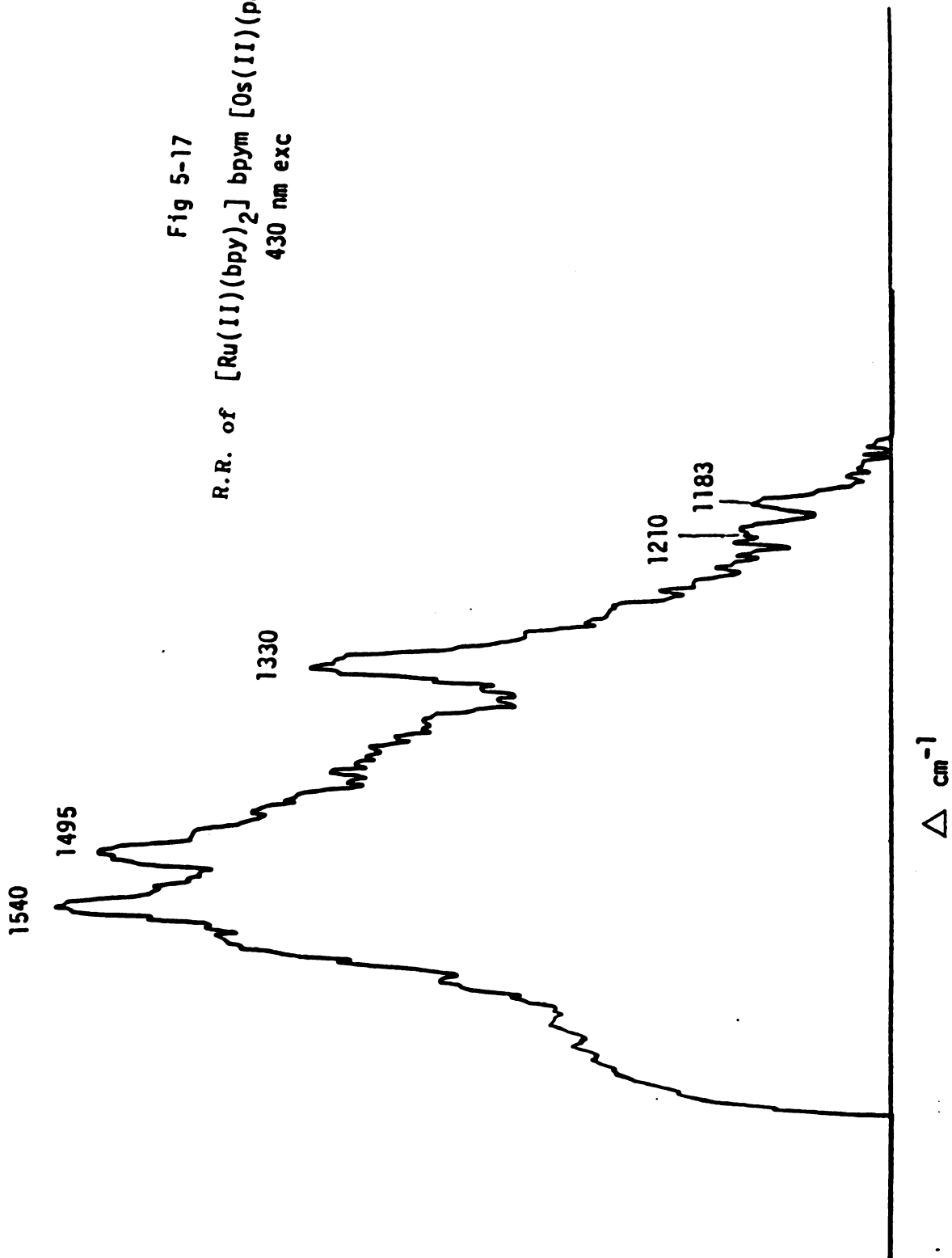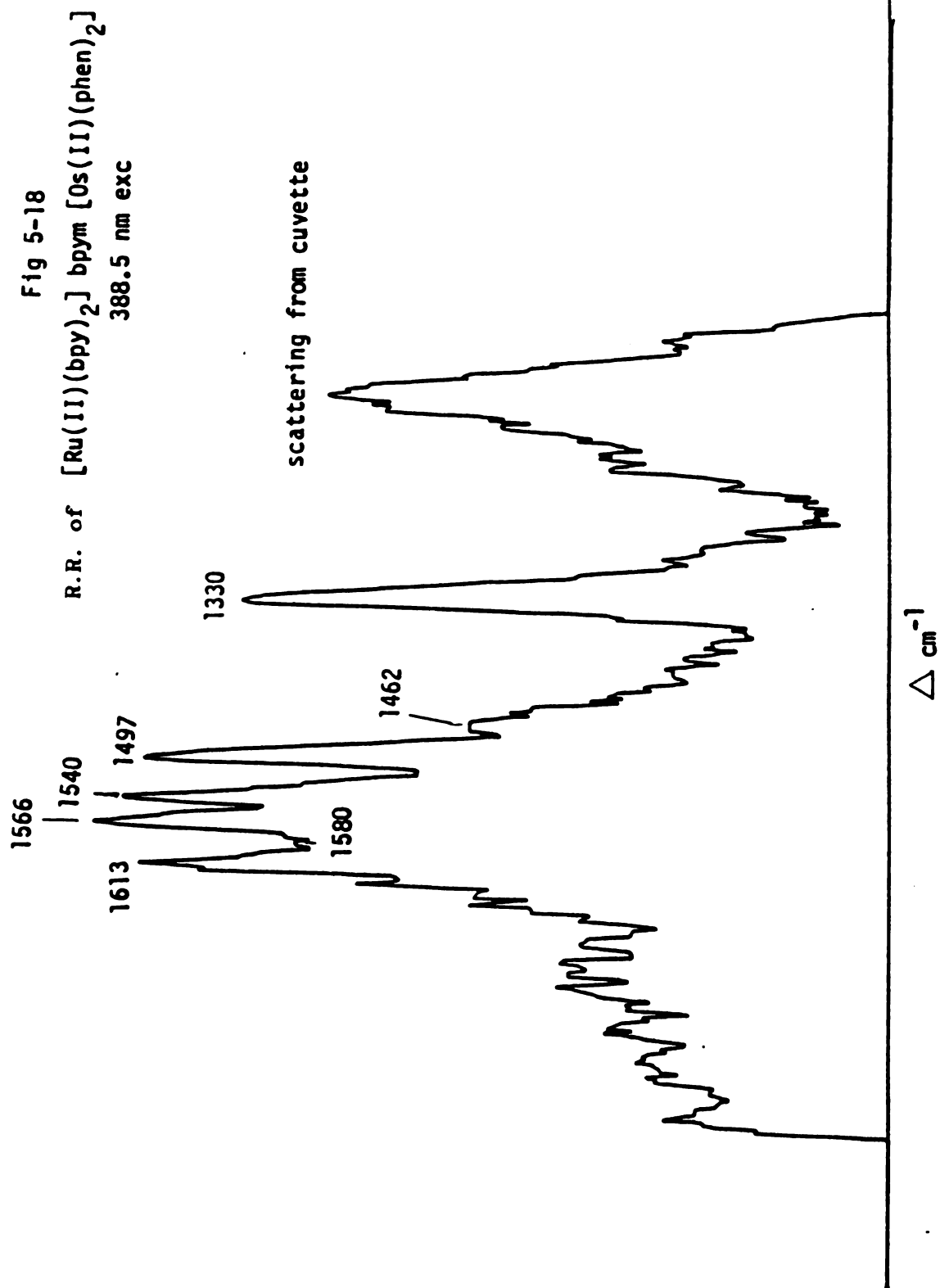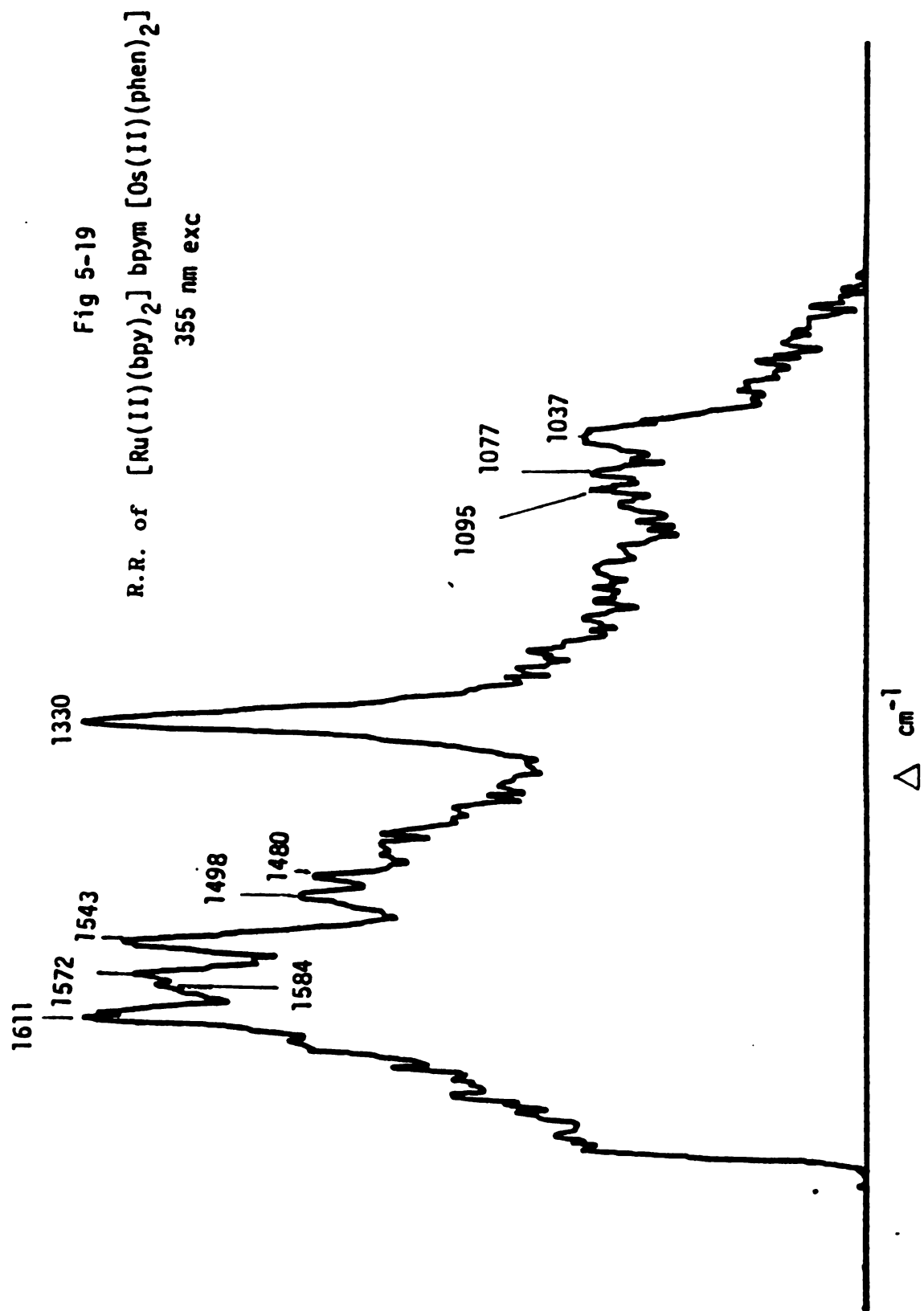
Fig 5-20

Electronic Absorption Spectrum of
[Ru(II)(bpy)₂)bpy≡[Os(II)(bpy)₂]

Fig 5-21

R.R. of [Ru(II)(bpy)$_2$] bpym [Os(II)(bpy)$_2$]
532 nm exc

1539
1480
1611
1327
1187

$\triangle$ cm^{-1}

Fig 5-22

R.R. of [Ru((II)(bpy)₂] bpym [Os(II)(bpy)₂]
441.6 nm exc

Fig 5-23

R.R. of [Ru(II)(bpy)$_2$] bpym [Os(II)(bpy)$_2$]

420 nm exc

Δ cm^{-1}

Fig 5-24

R.R. of [Ru(II)(bpy$_2$)] bpym [Os(II)(bpy)$_2$]

363.8 nm exc

1327

1565

1542

1611

1497

1480

1447

1380

1265

1173

1030

$\triangle$ cm^{-1}

Fig 5-25

R.R. of [Ru(II)(bpy$_2$)] bpym [Os(II)(bpy)$_2$].
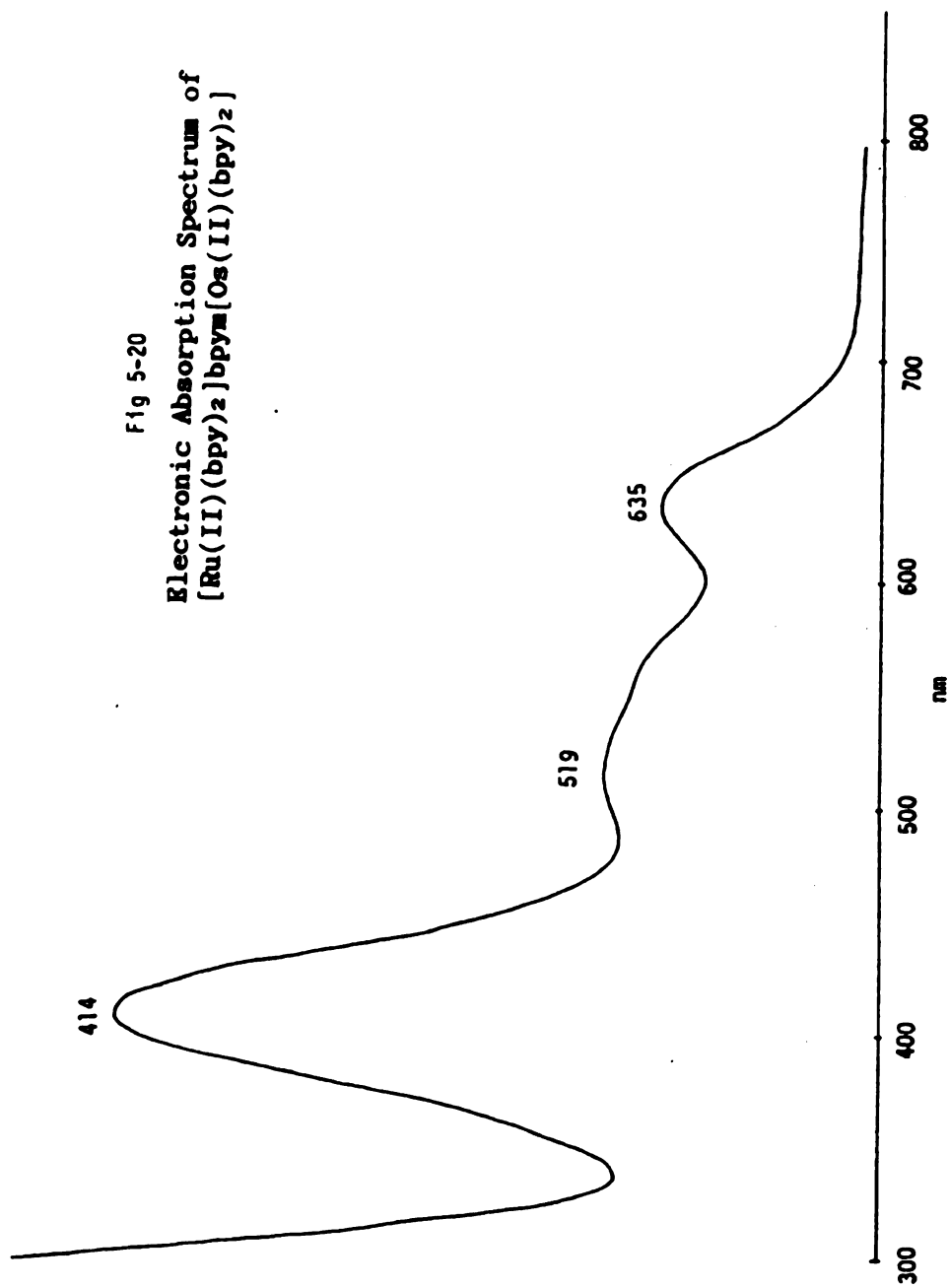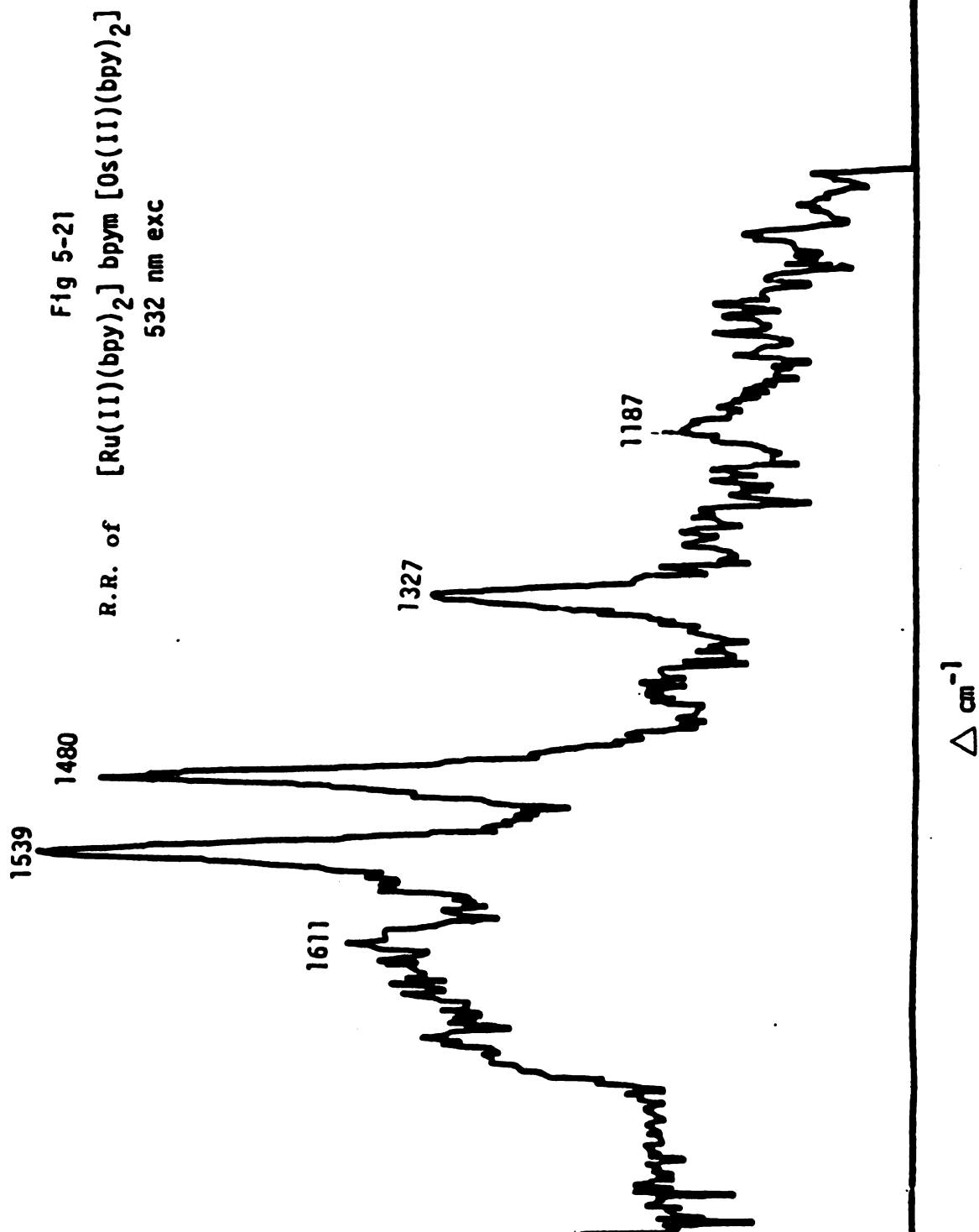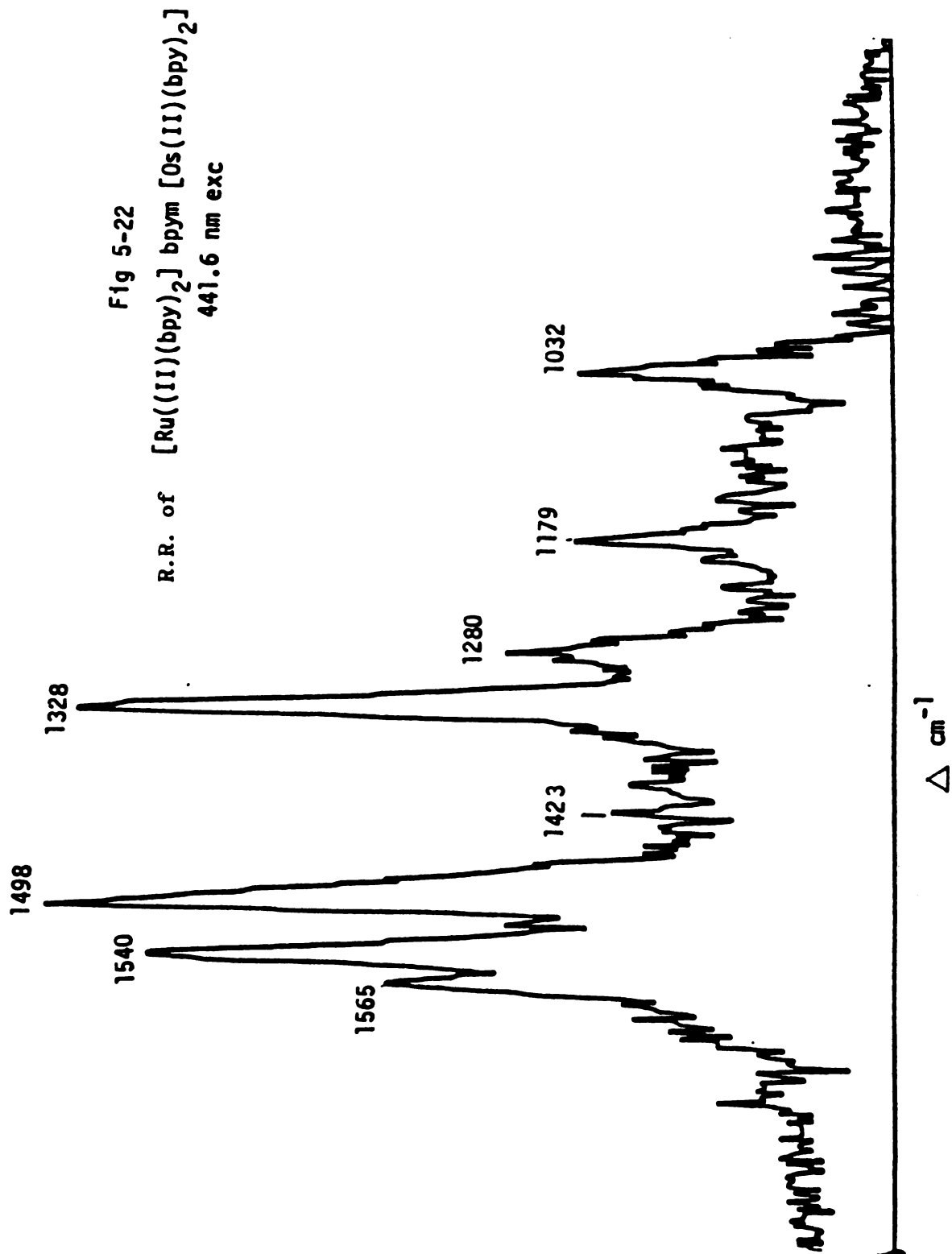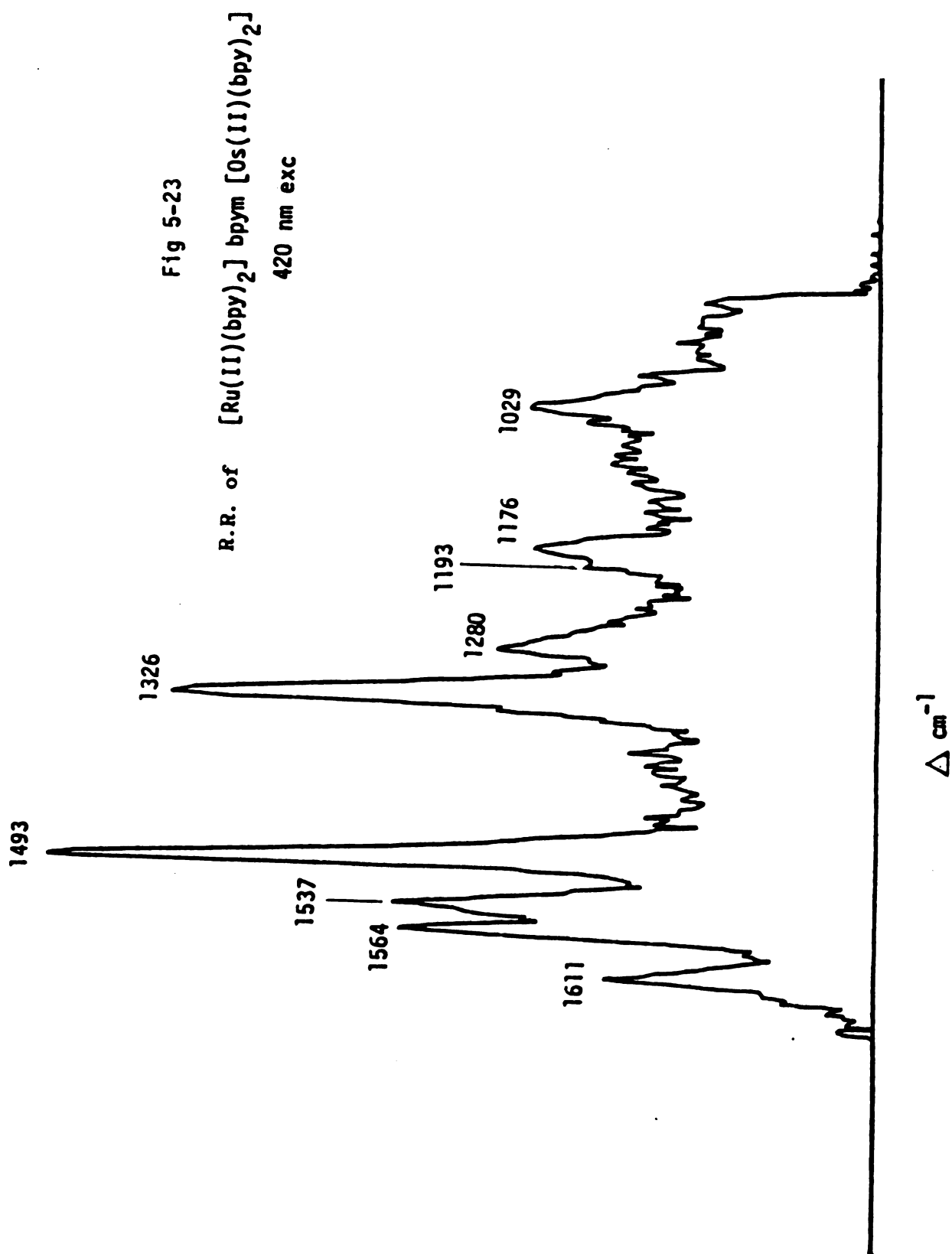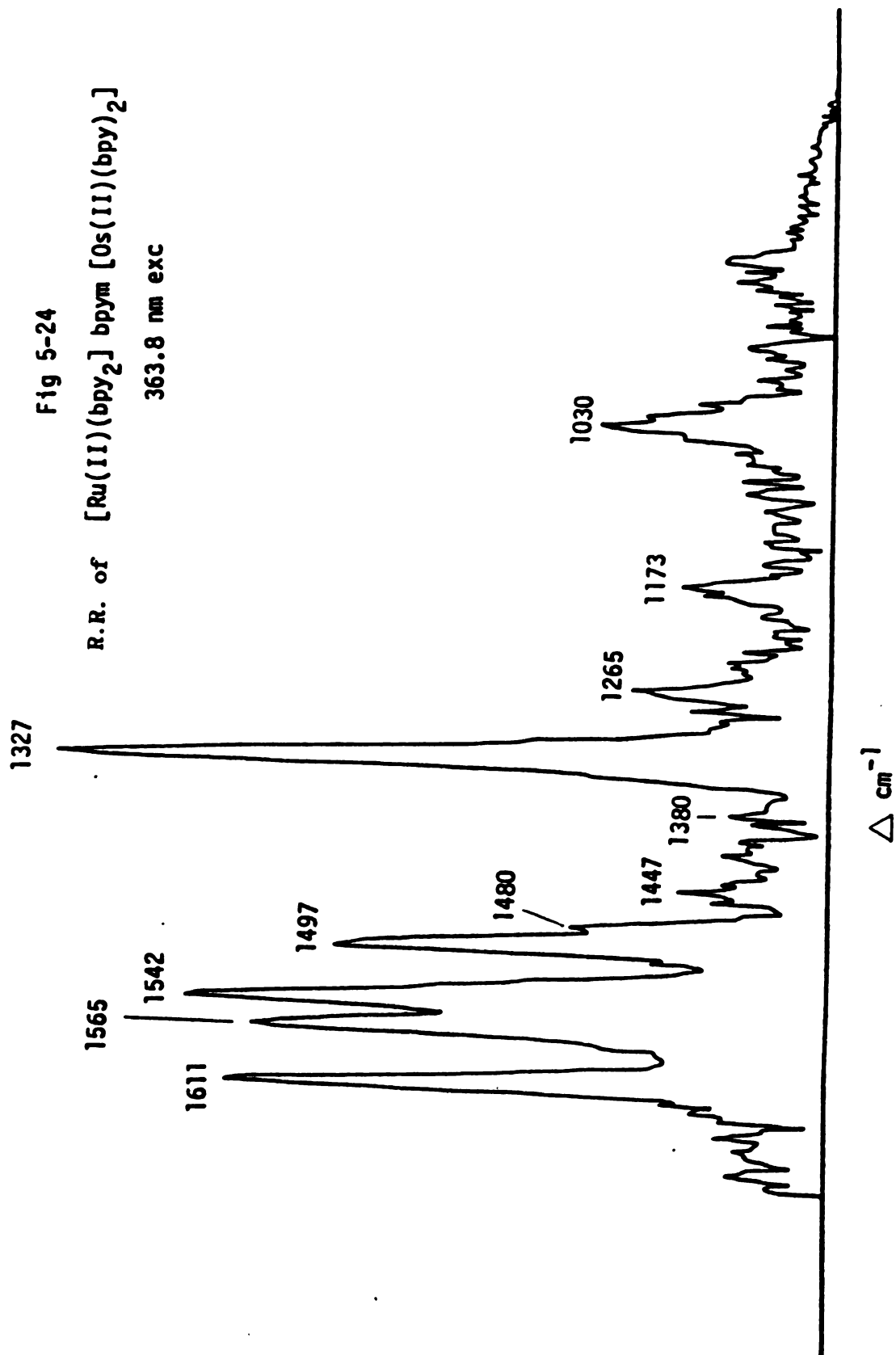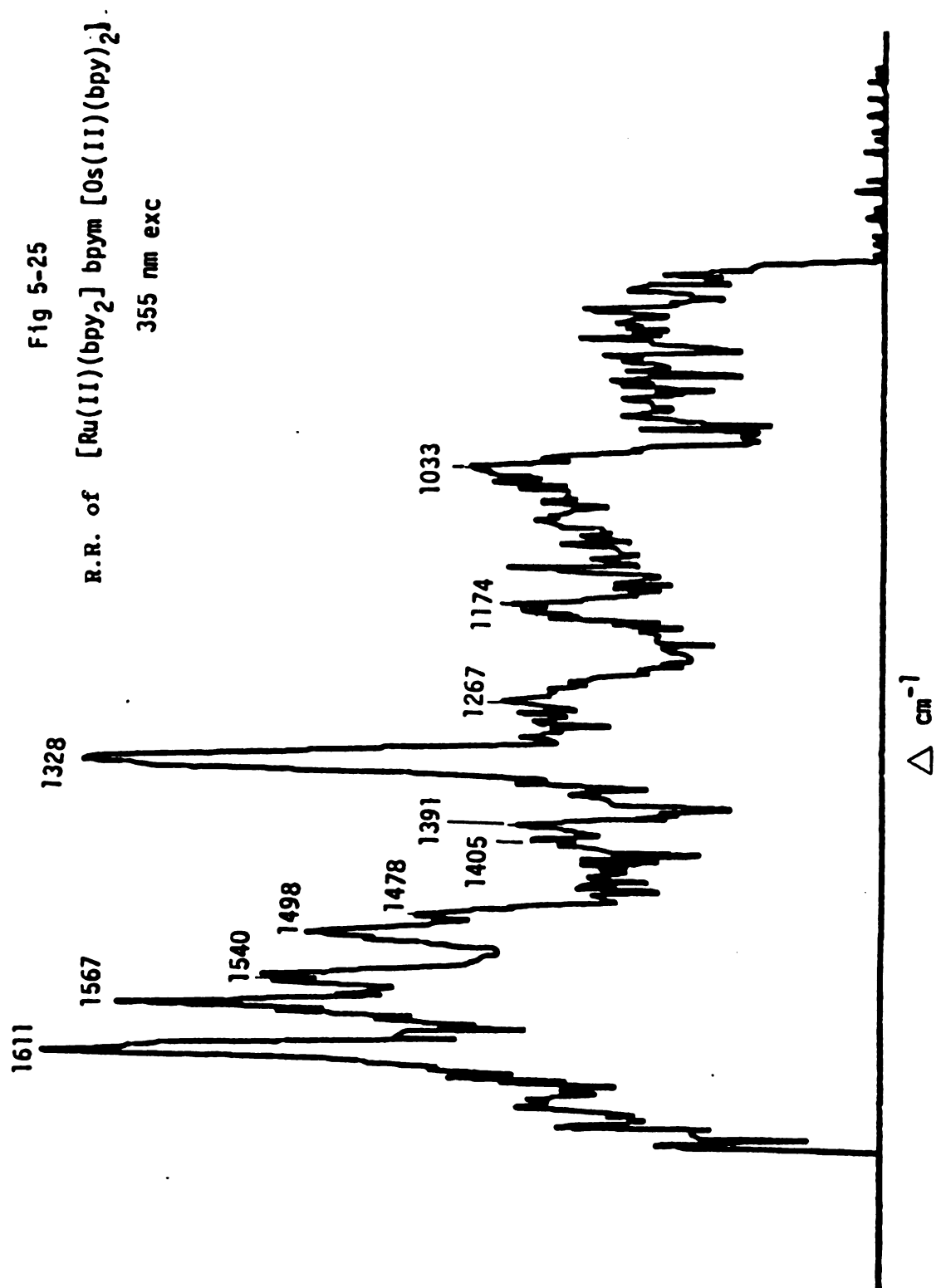
355 nm exc

Fig 5-26

Electronic Absorption Spectrum of
[Ru(II)(phen)₂]₂bpym

Fig 5-27

R.R. of [Ru(II)(phen)$_2$] bpym [Ru(II)(phen)$_2$]
363.8 nm exc

$\triangle$ cm^{-1}

Fig 5-28

R.R. of [Ru(II)(phen)₂]₂ bpym

355 nm exc

Fig 5-29

Electronic Absorption Spectrum of
[Ru(II)(phen)₂]bpym[Os(II)(phen)₂]

Fig 5-30

R.R. of [Ru(II)(phen)$_2$] bpym [Os(II)(phen)$_2$]

363.8 nm exc
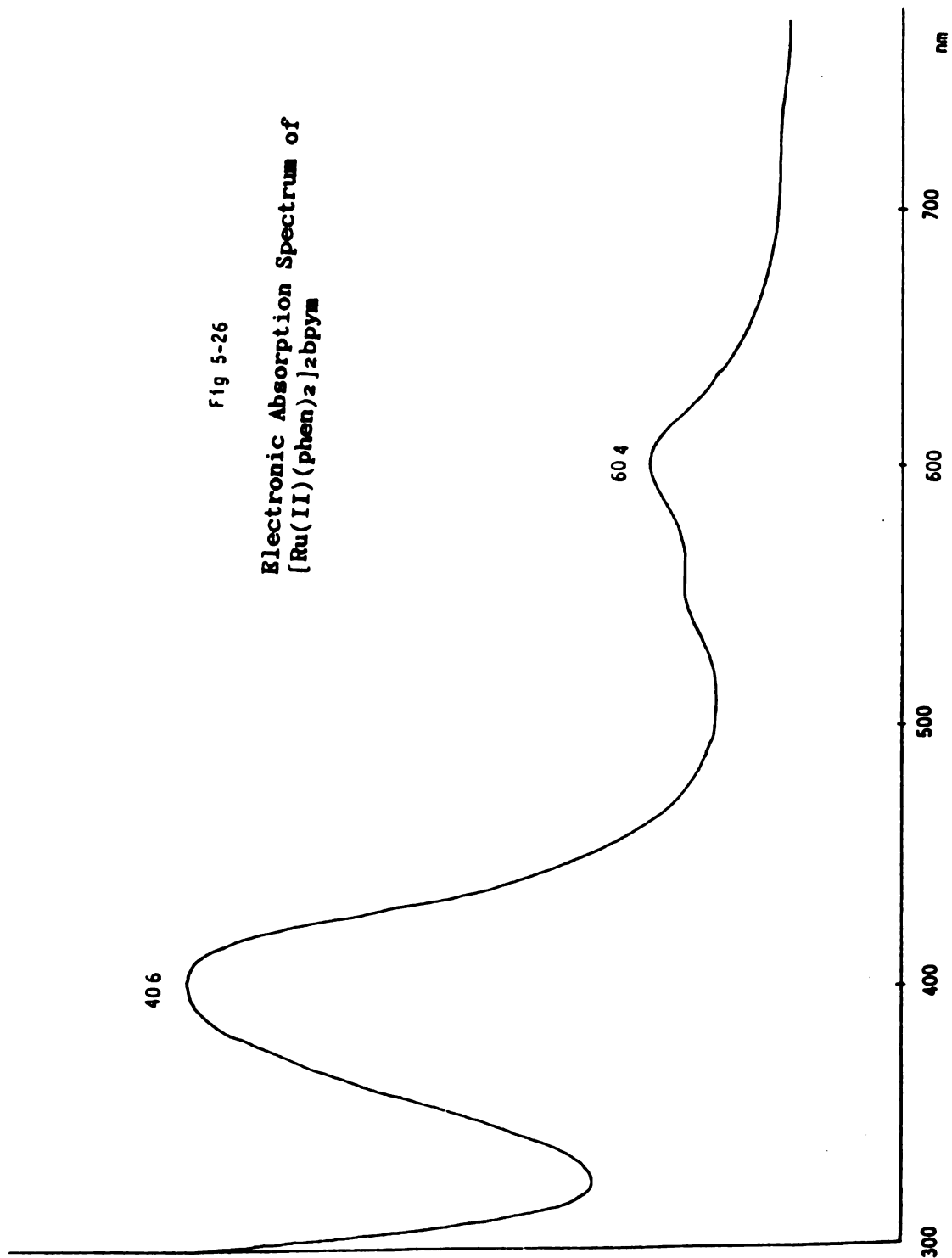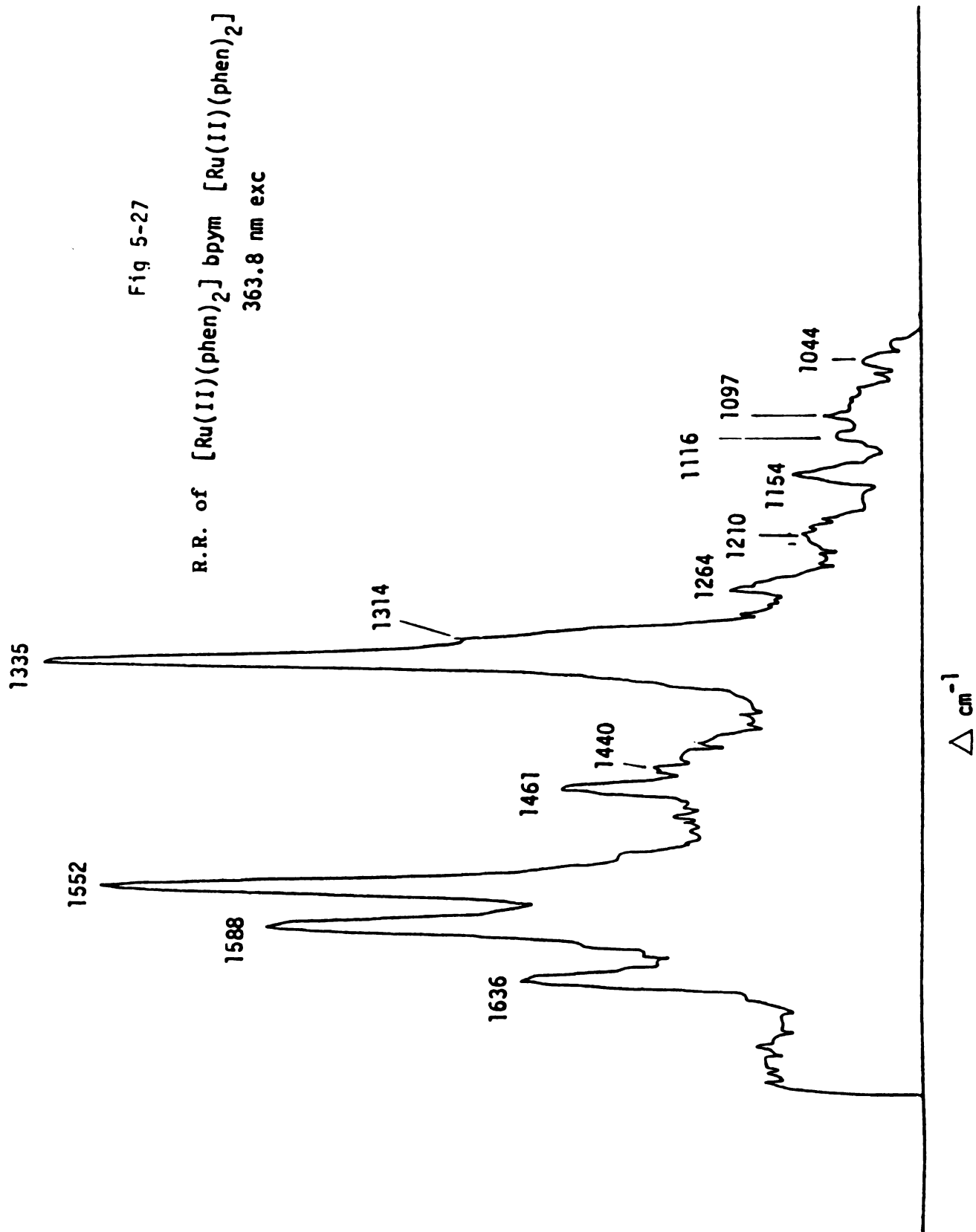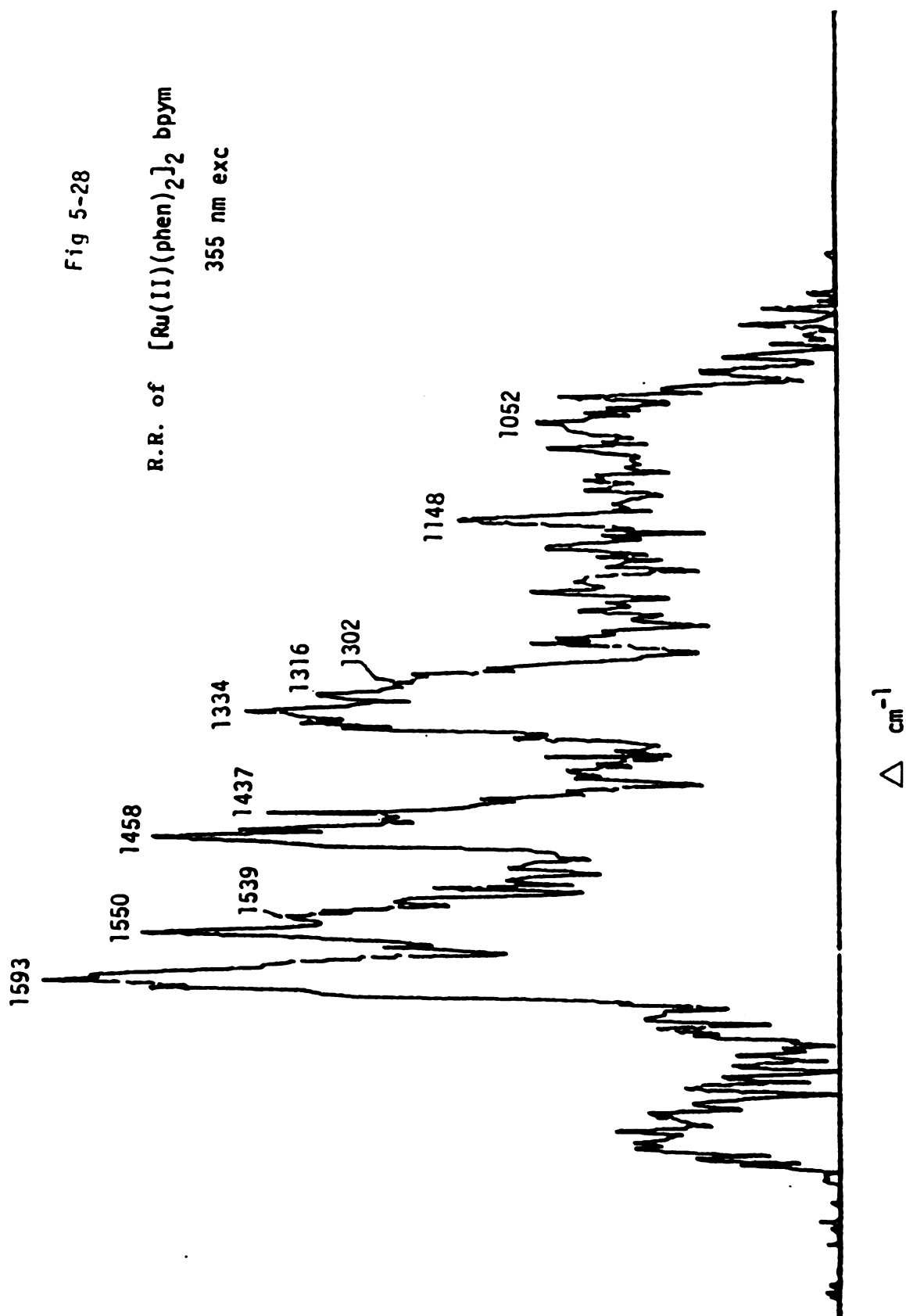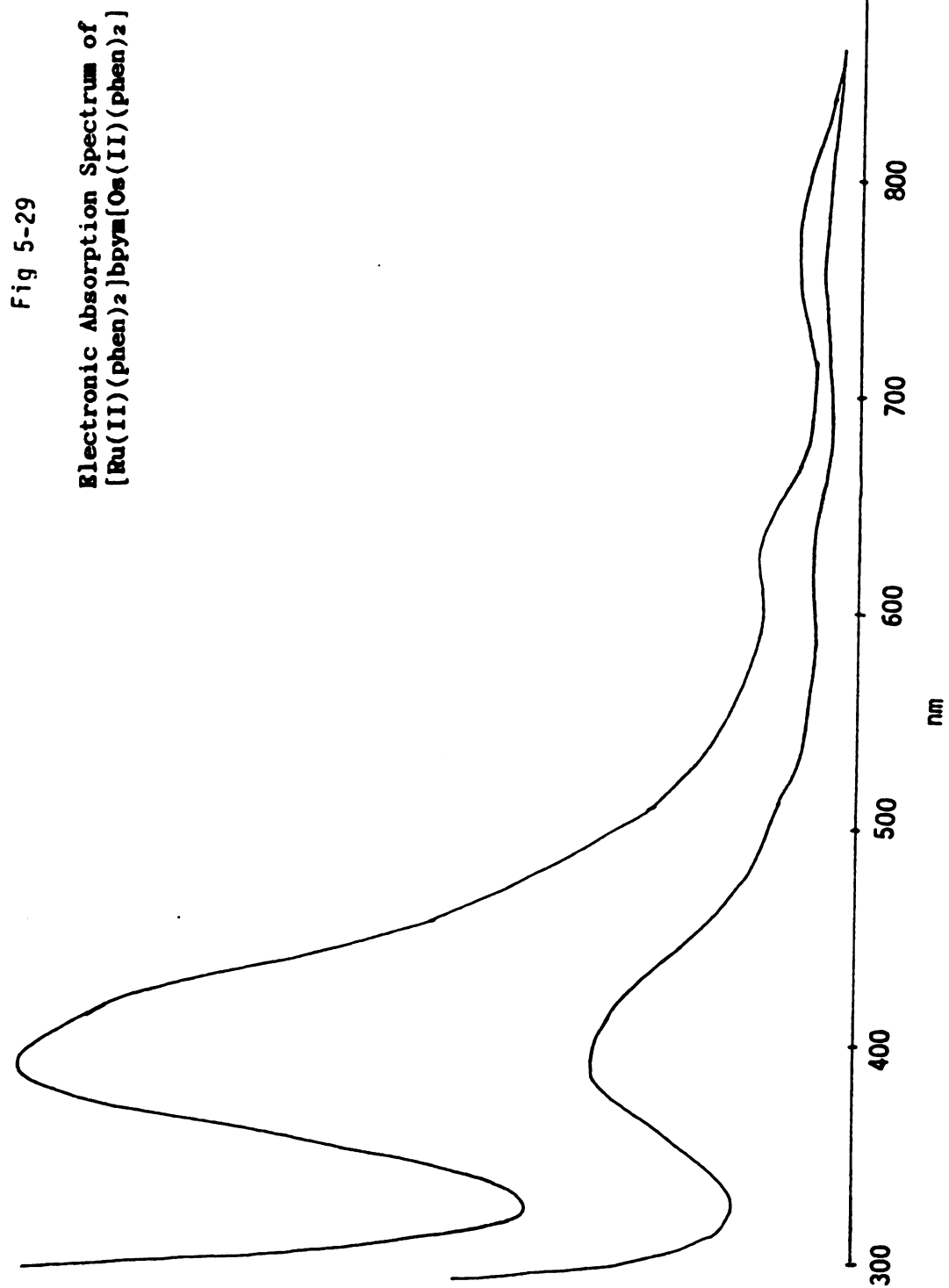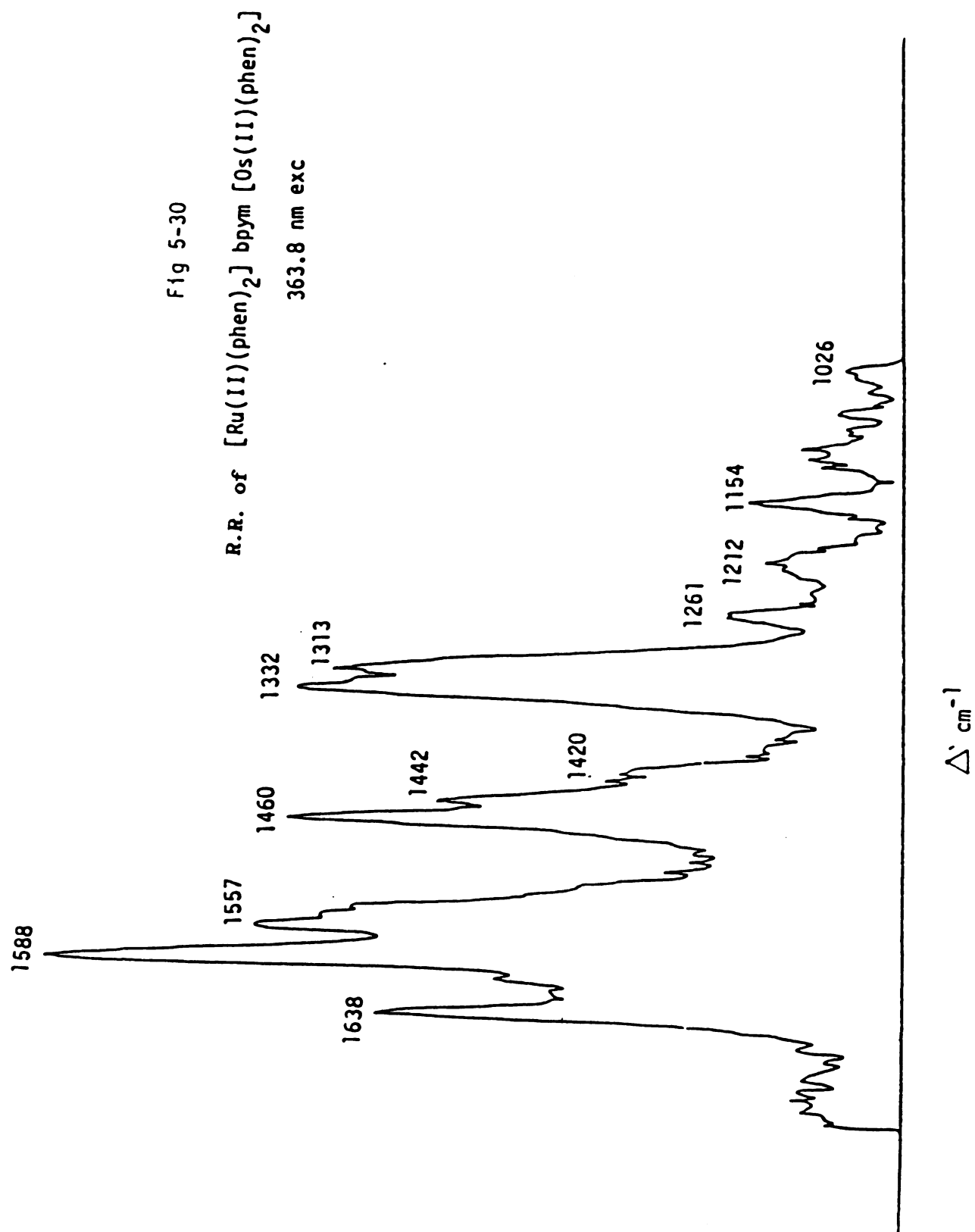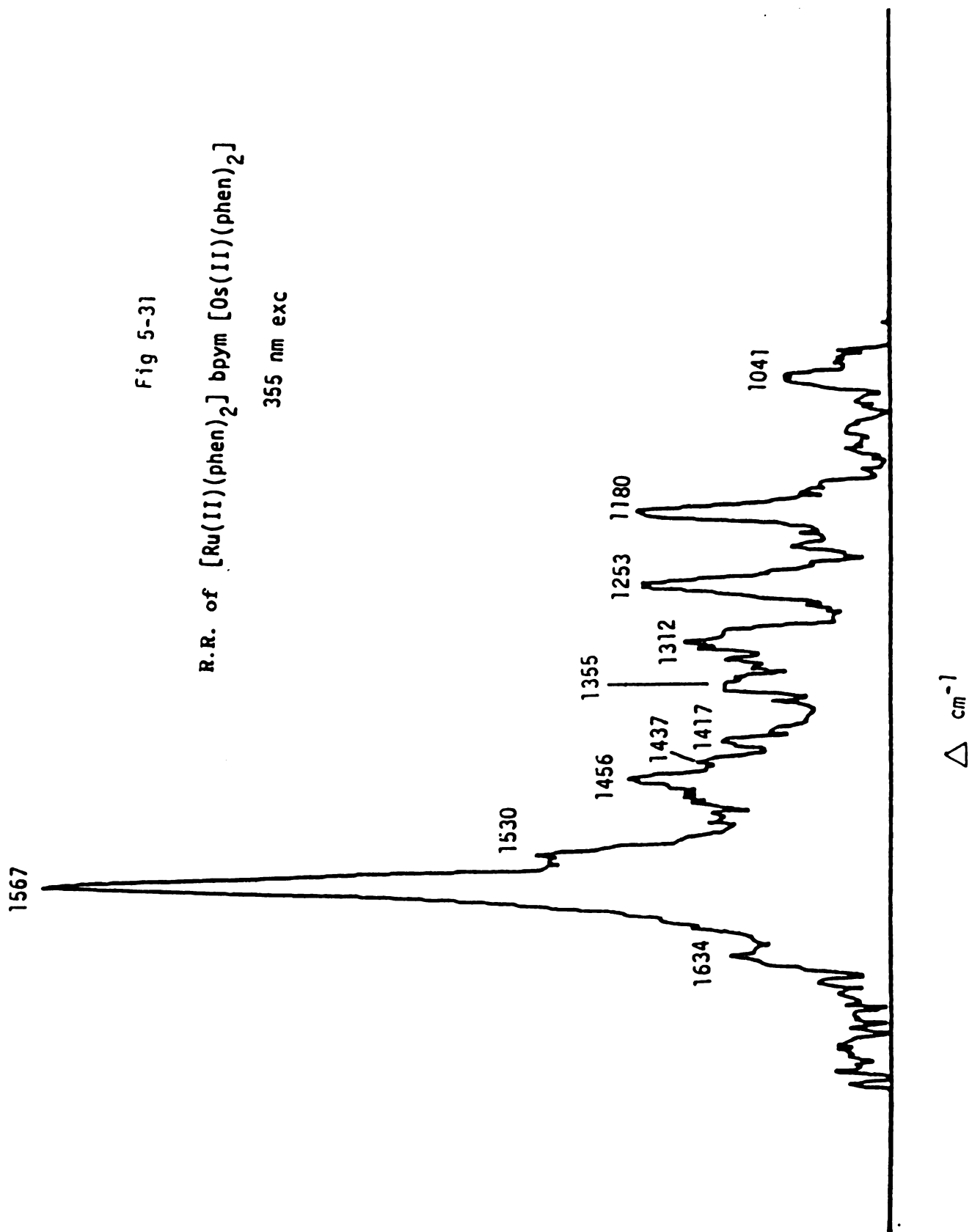
Fig 5-31

R.R. of [Ru(II)(phen)$_2$] bpym [Os(II)(phen)$_2$]

355 nm exc
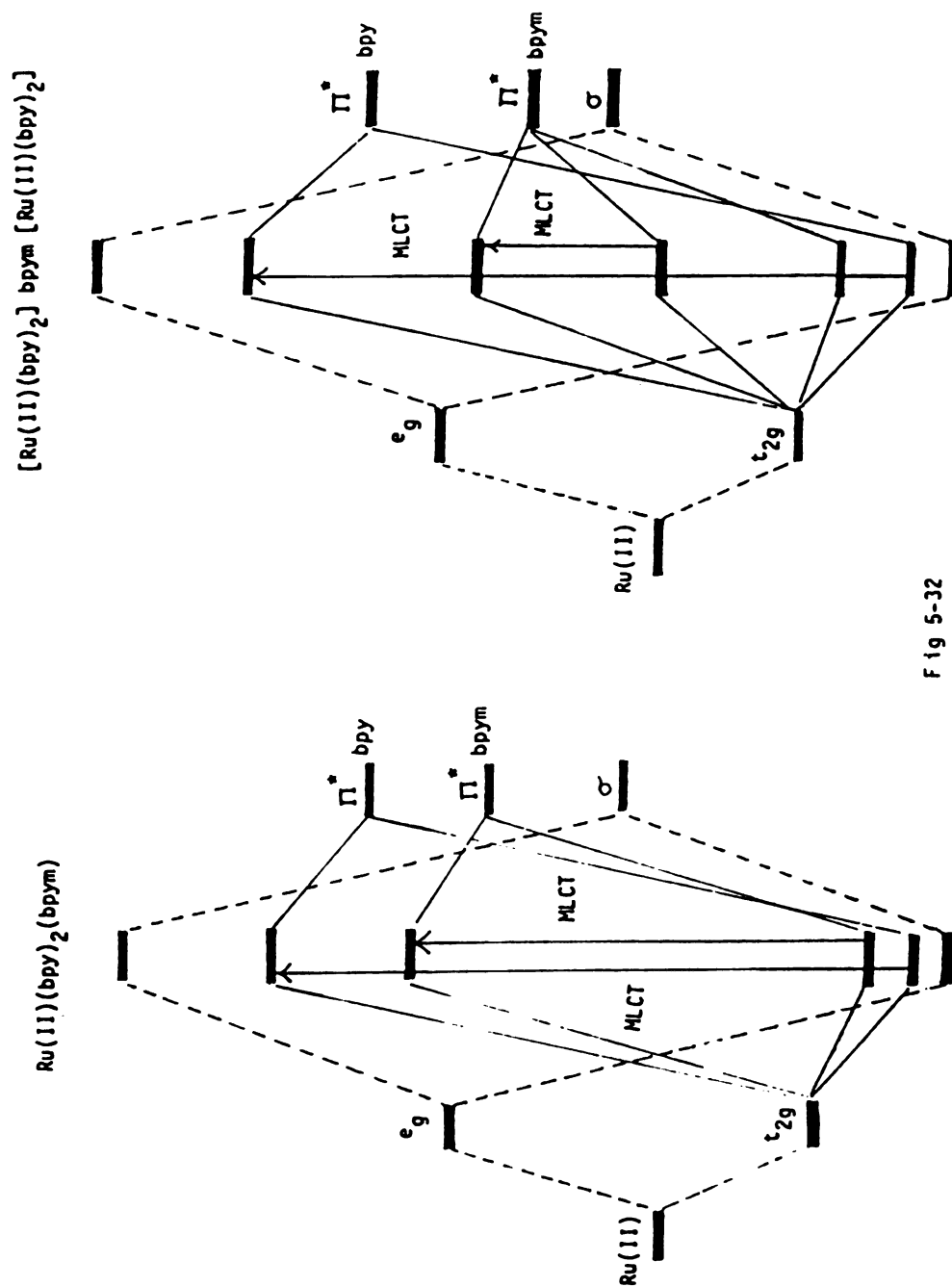
Fig 5-32

MO Diagram of Ru(II)(bpy)2(bpym) and
[Ru(II)(bpy)2]2bpym.

MO Diagram of [M(II)(L)₂]bpym[M'(II)(L')₂]

L=phen and/or bpy
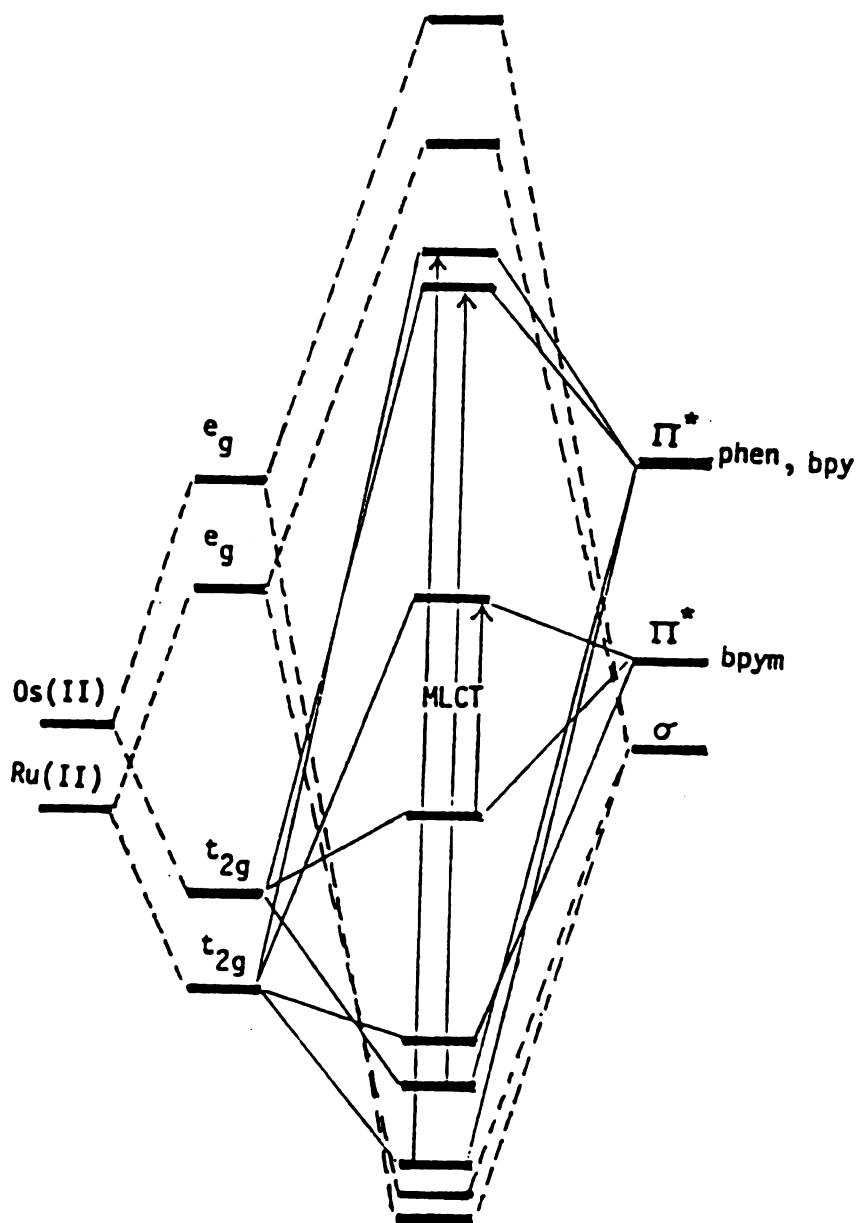
Fig 5-33

CHAPTER 6

Characterization of Multiple Charge Transfer Excited
States of Ru(II)(NH₃)₄(bpy) by Resonance Raman Spectroscopy

Numerous photochemical and photophysical studies[1] have been
performed on low-spin d⁶ octahedral complexes of the type Ru(NH₃)₅L (
where L = unsaturated organic ligand). Most of these complexes exhibit
intense metal-to-ligand charge transfer (MLCT) absorption in the visible
and it is well established that this transition shifts to lower energy as
L increases in electron withdrawing ability. For complexes in which the
lowest excited state is a ligand field (LF) triplet state, efficient
photosubstitution reactions occur. However, when the MLCT excited
state is tuned to energy lower than the LF level the photosubstitution
reaction yield decreases dramatically.

In recent years Ru(II)(NH₃)₄L complexes (where L = bidentate
unsaturated organic ligand) have been studied as possible substitutes
for the better known Ru(II)(bpy)₃ complex. We report here the ground
and excited state Raman spectra of Ru(II)(NH₃)₄(bpy), where bpy = 2,2'-
bipyridine. This complex is of practical interest due to the use of
Ru(II)(bpy)₃ in photosensitization reactions, and therefore comparisons
will be drawn between the two.

Experimental Results

The electronic absorption spectrum of Ru(II)(NH₃)₄(bpy) is shown
in Figure 6-1. In Ru(II)(bpy)₃ there is one absorption in the visible
region, the MLCT transition peaked at 452 nm. In the case of
Ru(II)(NH₃)₄(bpy) there are two peaks in the visible at 520.9 nm and

105

367.2 nm. Are these two peaks due to different electronic transitions or are they components of the same one?

The cw Raman spectrum obtained with excitation at 454.5 nm is shown in Figure 6-2. This spectrum is clearly that of the bpy ligand vibrations and very closely resembles that of $Ru(II)(bpy)_3$ taken with the 363.8 nm line. Spectra obtained at lower excitation energies (e.g., 514.5 nm not shown), resembles that of $Ru(II)(bpy)_3$ taken at 450 nm (i.e., the 1609, 1561, 1488 cm^{-1} peak intensity ratios are 1488>1561>1609). On the other hand, the CW Raman spectrum of $Ru(II)(NH_3)_4(bpy)$ obtained at 363.8 nm which is very close to the second peak in the visible; shows a Raman profile (Figure 6-3) quite different from that of the 454.5 nm spectrum. Notice in particular the low intensity of the 1489 cm^{-1} peak in relation to the bands at 1562 and 1609 cm^{-1}. Note also the presence of new but weak peaks at 1443 and 1417 cm^{-1}. The 1268 cm^{-1} peak has also become more intense than the scattering at 1325 cm^{-1}. These observations clearly show that excitation at 363.8 nm is in resonance with a higher lying π^* MLCT state (call it the second MLCT).

The pulsed excited state Raman spectra shows interesting variation also. The 532 nm pulsed experiment shows (Figure 6-4) only one strong excited state peak, at 1514 cm^{-1}. The corresponding cw spectrum (514 nm not shown) shows an identical pattern except, of course, the 1514 cm^{-1} peak. The excited state Raman spectrum obtained with pulsed 430 nm excitation (Figure 6-5) shows clearly the band at 1514 cm^{-1} as well as new peaks at 1367, 1289, and 1215 cm^{-1}. The spectrum excited by pulsed radiation at 355 nm shows that the 1514 cm^{-1} line has essentially disappeared but now the peaks at 1290 and 1218 cm^{-1} are very strong. (Figure 6-6).

Discussion

First, the cw Raman spectra will be utilized to interpret the absorption spectrum. The 363.8 nm excitation Raman spectrum clearly shows that the absorption peak at 367 nm is due to a transition to a different MLCT state as compared to the absorption at 521 nm. (We rule out an internal ligand transition for the former because it is too low in energy). This result is in contrast to the "parent" complex, Ru(II)(bpy)₃ for which only one MLCT state is seen in the visible. This can be explained as follows: In Ru(II)(NH₃)₄(bpy) four (NH₃) groups replace two (bpy) ligands, which means that the t_{2g} and e_g (in O_h microsymmetry) splitting is reduced. NH₃ is a σ donor, but obviously has no low-lying π^* orbitals to participate in backbonding. This causes small ligand field splitting which means that the MLCT transition should be red-shifted. We can see that the 450 nm peak of Ru(II)(bpy)₃ has indeed red-shifted to 521 nm.

The Raman intensity profile also tells us something about the "parent" complex, Ru(II)(bpy)₃. The two MLCT transitions of Ru(II)(NH₃)₄(bpy) both blue-shifts in Ru(II)(bpy)₃ and only the lowest one at 450 nm can be seen. The higher transition becomes overlapped with a strong internal ligand transition in Ru(II)(bpy)₃. This is strongly suggested by the following correlation of the Raman spectra of the two complexes with the CW excitation wavelength.

Ru(NH₃)₄(bpy)	Ru(bpy)₃
514.5 nm <—>	450. nm
454.5 nm <-->	363.8 nm

Under 363.8 nm excitation of Ru(II)(bpy)₃,[2] the 1489, 1562 and 1612 cm⁻¹ peaks begin to show intensities in the order 1612>1562>1489 cm⁻¹. This intensity pattern holds in the 363.8 nm spectrum of Ru(II)(NH₃)₄(bpy). Of course, if one were to excite Ru(II)(bpy)₃ close to 300 nm the Raman spectrum would reflect the strong overlap between the internal ligand and the second MLCT state.

The 532 nm pulse excited Raman spectrum shows superficial resemblance to the 430 nm pulsed Raman spectrum of Ru(II)(bpy)₃. Of course, the Ru(II)(NH₃)₄(bpy) spectrum shows strong contribution from ground state scattering due to the relatively short lifetime of the tetra ammine complex. The other difference is that the strongest peak in the excited state Raman spectrum of Ru(II)(bpy)₃ under 430 nm illumination lies at 1500 cm⁻¹ which is shifted ~14 cm⁻¹ in Ru(II)(NH₃)₄(bpy). At 430 nm in the pulsed Raman spectrum of Ru(II)(NH₃)₄(bpy) other excited state peaks come into resonance such as 1367, 1289, 1215 cm⁻¹. At 355 nm the two strongest excited state Raman peaks for this complex lie at 1290 and 1218 cm⁻¹ with the 1218 cm⁻¹ band being a little weaker than expected [based on Ru(bpy)₃]. There should also be a relatively strong peak near 1550 cm⁻¹ which cannot be distinguished in our spectrum. (Possibly it is buried under the 1561 cm⁻¹ peak).

In summary resonance Raman spectroscopy can be effectively utilized to assign absorption spectra of transition metal complexes. We have used the technique to identify two distinct MLCT states in Ru(II)(NH₃)₄(bpy); the second MLCT state being observed for the first time. From trends in the Raman peak intensities as a function of wavelength, we conclude, that for Ru(II)(bpy)₃ the second higher energy MLCT is overlapped with the lowest internal ligand transition at 300 nm.

Fig 6-1

Electronic Absorption Spectrum of
Ru(II)(NH₃)₄(bpy)
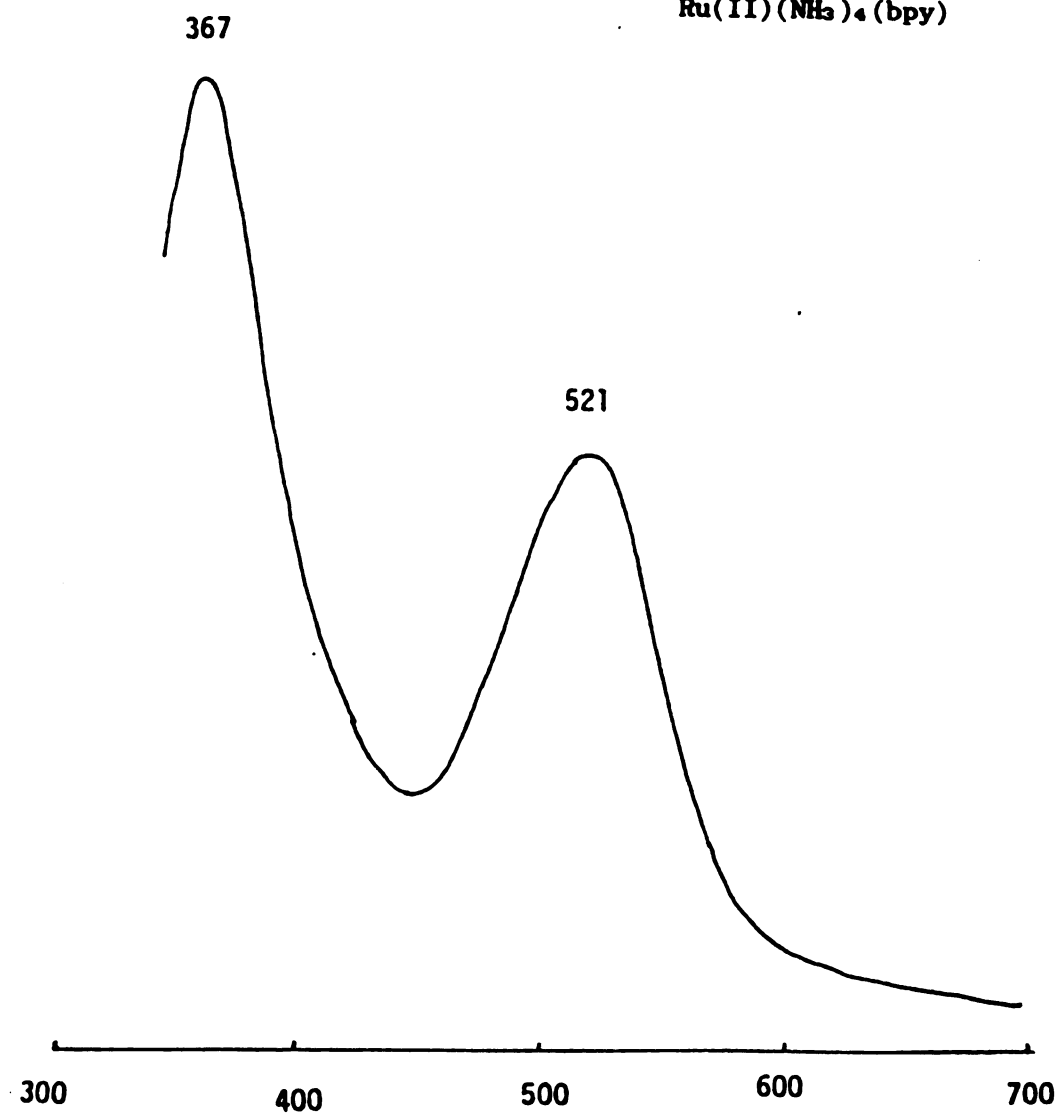
R.R. of Ru(II)(NH₃)₄(bpy), 454.5 nm exc

Fig 6-2

△ cm⁻¹
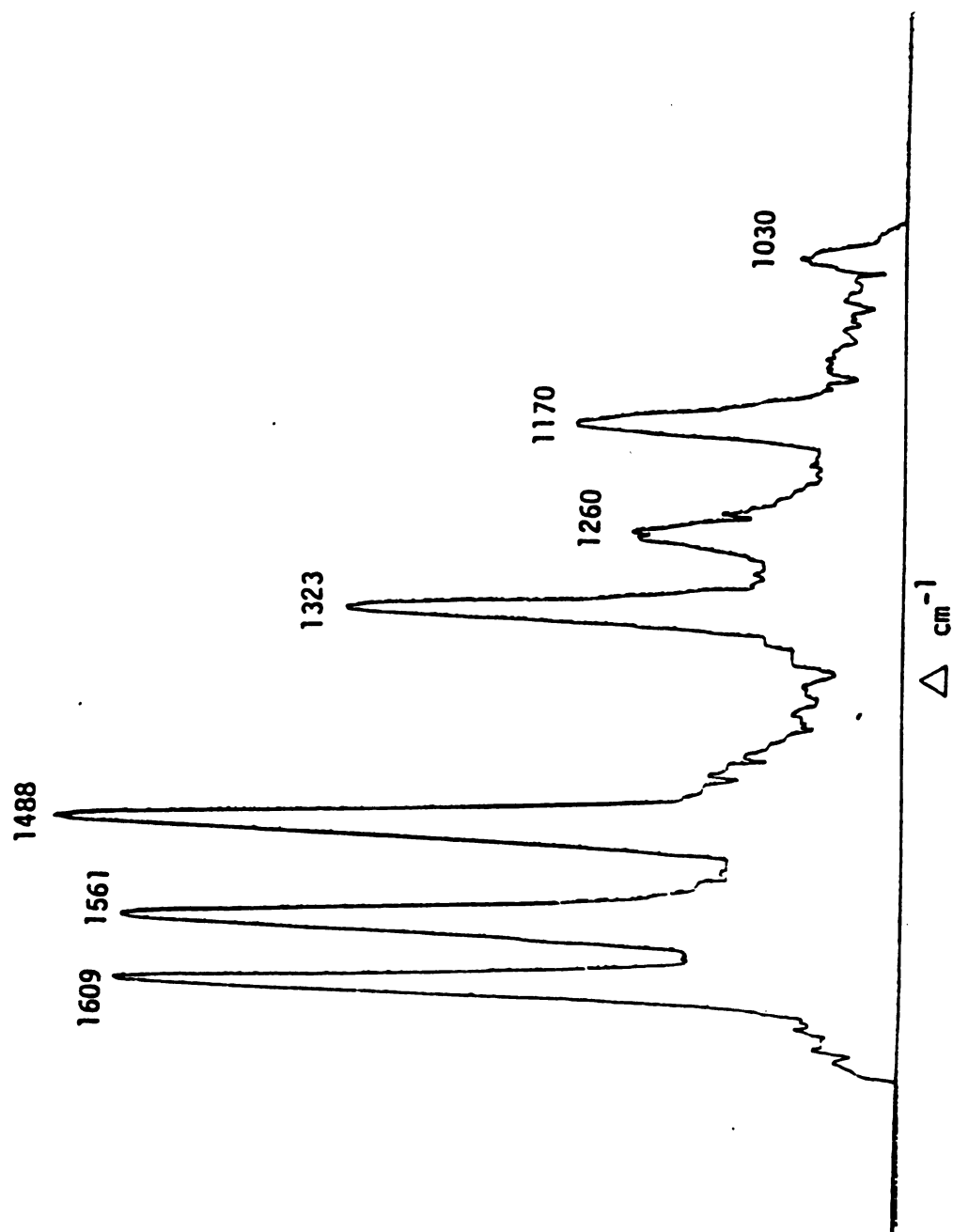
Fig 6-3   363.8 nm exc

R.R. of   Ru(II)(NH$_3$)$_4$(bpy)

1612

1562

1489

1443

1417

1325

1268

1172

1031

$\triangle$ cm^{-1}

Fig 6-4

R.R. of Ru(II)(NH$_3$)$_4$(bpy)

533 nm exc

1489
1514
1558
1606
1321
1260
1220
1173
1032

$\triangle$ cm^{-1}

R.R. of Ru(II)(NH$_3$)$_4$(bpy) Fig 6-5 430 nm exc

1561
1513
1489
1610
1437
1367
1326
1289
1215
1172
1038
1016

$\triangle$ cm^{-1}
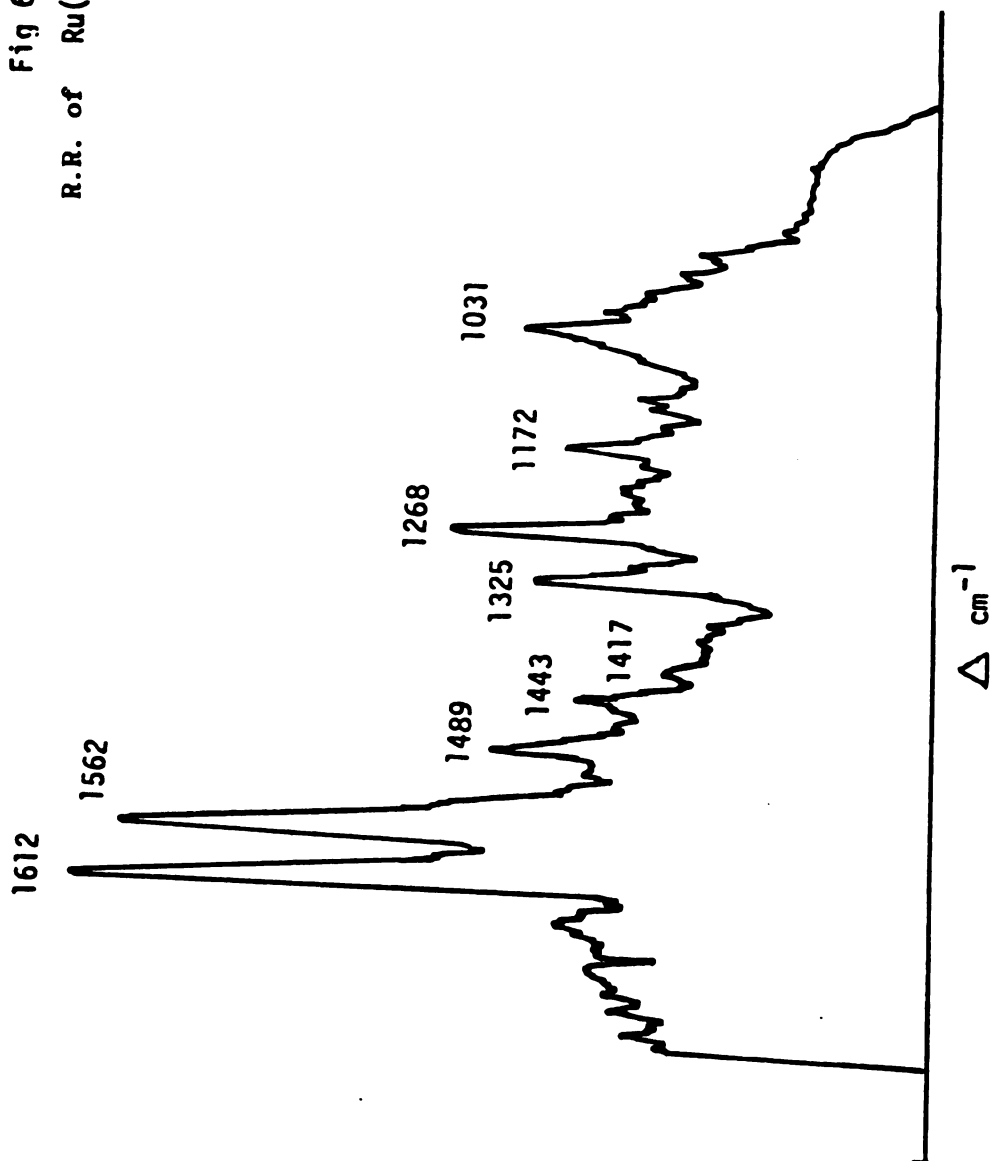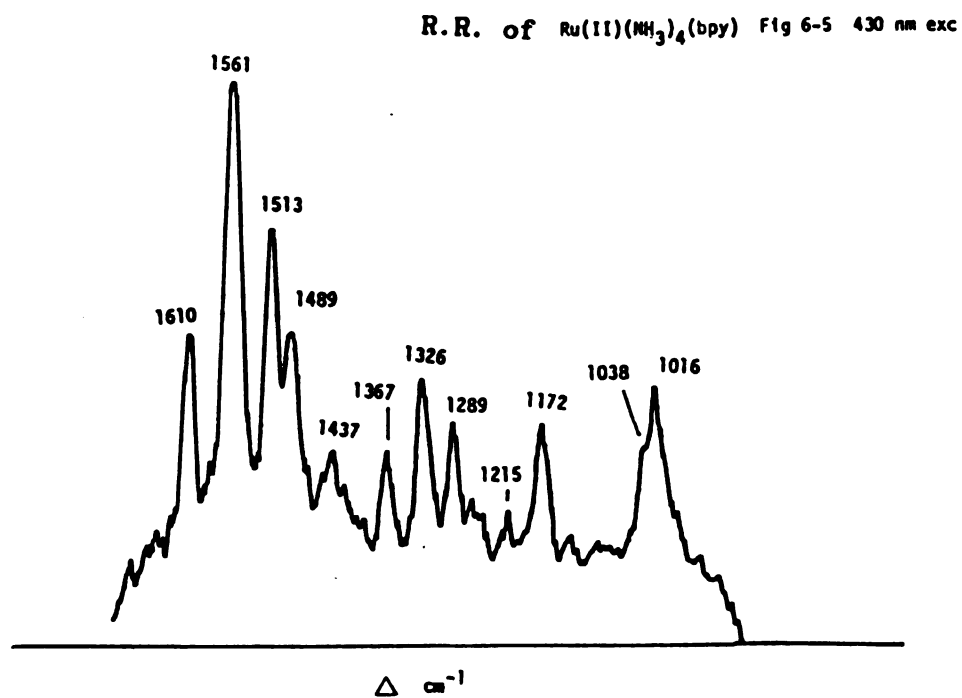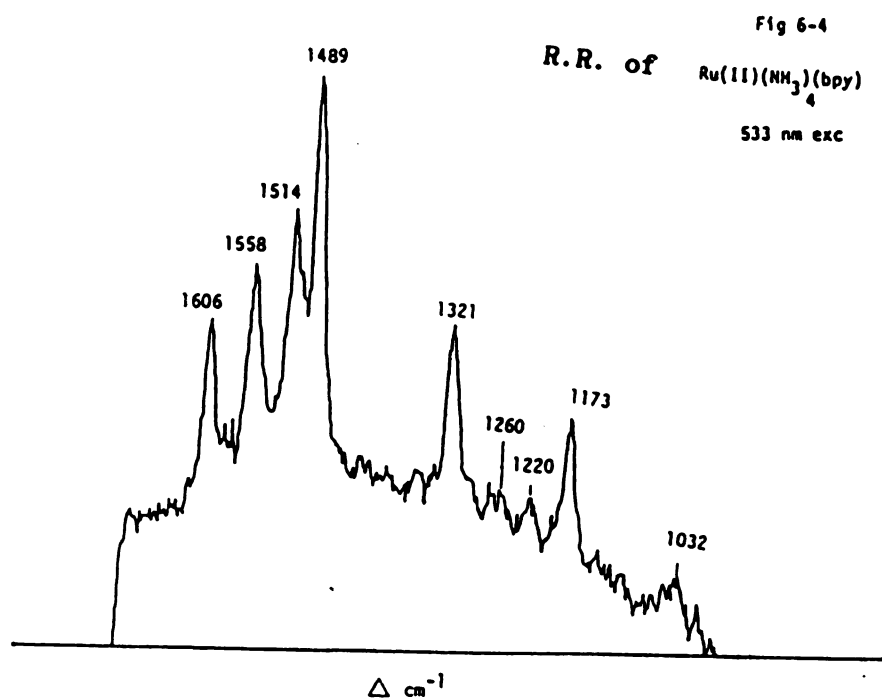
Fig 6-6

R.R. of Ru(II)(NH$_3$)(Bpy)$_4$ 355 nm exc
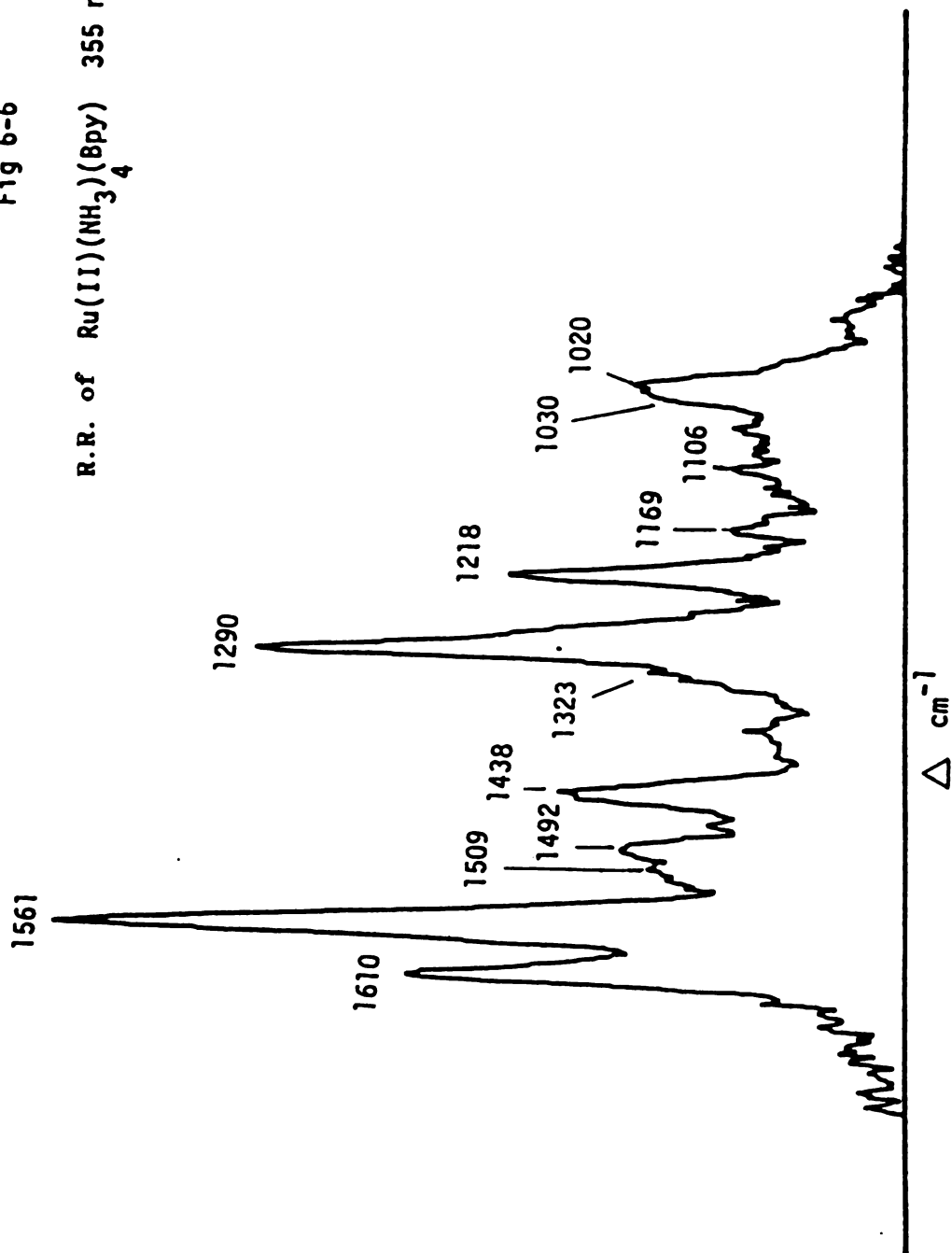
REFERENCES

For examples see:

1.   (a) P. C. Ford, Coord. Chem. Rev. 5, 75 (1970). (b) Y. C. Chung, N. Leventis, P. J. Wagner, G. E. Leroi, J. Am. Chem. Soc. 107, 1414 (1985). (c() G. Malouf, P. C. Ford, J. Am. Chem. Soc. 99, 7213 (1977).

2.   (a) Dallinger, R. F., Woodruff, W. H., J. Am. Chem. Soc. 101, 4391 (1979). (b) M. Forster, R. E. Hester, Chem. Phys. Lett. 81, 42 (1981).

APPENDIX

Complexes of the type Ru(II)(NH₃)₄L (where L = bidentate unsaturated organic ligand) have attracted attention as possible substitutes for the corresponding Ru(II)(L)₃ systems.[1] For example, the Ru(II)(bpy)₃ complex is inefficient as a bimolecular sensitizer for the water splitting process (see Chapter 1). Peterson and other workers have tried to extend these systems to include Ru(II)(NH₃)₄,₅(L) complexes as well as polymetallic structures, so that light absorption and redox reaction can occur in the same molecule.[1c] This is the same general aim as with the [Ru(L)₂]₂bpym system discussed in Chapter 5. As an example of partial success in this direction, Peterson's group reported observation of intramolecular energy transfer in a bimetallic Ru(II)(NH₃)₅L system.[1c] In the complex (NH₃)₅Ru(II)NC-PY-Rh(III)(NH₃)₅, upon irradiation of the Ru(II) to 4-CN-PY band, they observed cleavage of the Rh(III)-4CN-PY bond which is a characteristic of the triplet ligand field excited state associated with Rh(III). The interest here was that known photochemistry could be driven by lower energy irradiation.

As shown in the Ru(II)(NH₃)₄(bpy) chapter, one can also learn something about the Ru(L)₃ complexes by studies on analogous Ru(II)(NH₃)₄L systems. We have obtained resonance Raman spectra of Ru(II)(NH₃)₄(phen) as mentioned in the Ru(II)(phen)₃ chapter. This complex was originally synthesized with the hope of observing the Ru to phen MLCT excited state, but since this was not successful the complex will not be discussed further.

The absorption spectrum of Ru(II)(NH₃)₄(bpym) is shown in Figure 6-7. Ru(II)(NH₃)₄L systems typically display visible absorption red-

shifted in comparison to the Ru(II)(L)₃ parent complex. Two maxima can be distinguished one at 590 nm and the other at 405 nm. These are separated by about 8000 cm⁻¹ whereas in Ru(bpym)₃ the corresponding separation is about 7740 cm⁻¹. In the tetraamine complex the Raman modes under 610 nm excitation (Figure 6-8) appear at similar position (± 10 cm⁻¹) as Ru(II)(bpym)₃ case. With excitation at higher energy, 514.5 nm, Figure 6-9 the second higher-lying MLCT state comes into resonance. Notice the growth of peaks at 1579, 1548 cm⁻¹ and especially 1337 cm⁻¹. Under CW excitation at 363.8 nm, Figure 6-10, we see the dominance of the 1547 and 1337 cm⁻¹ bands which agrees with the generally observed behavior of bpym ligands. In the [Ru(L)₂]₂bpym system, where L is a bidentate ligand, the Raman profile at 363.8 nm displays a stronger resonance to the second MLCT state. Unfortunately, our attempt to synthesize the bimetallic analog [Ru(NH₃)₄]bpym failed. However, the published absorption spectrum (Reference 1b) shows in the bimetallic complex absorption maxima at 424 nm and 697 nm, implying red shifts of the first and second MLCT states by ~2600 cm⁻¹ and 1106 cm⁻¹. That is the lowest MLCT is red-shifted approximately twice as much as the higher one.

Fig 6-7

Electronic Absorption Spectrum of Ru(II)(NH₃)₄(bpym)

300   400   500
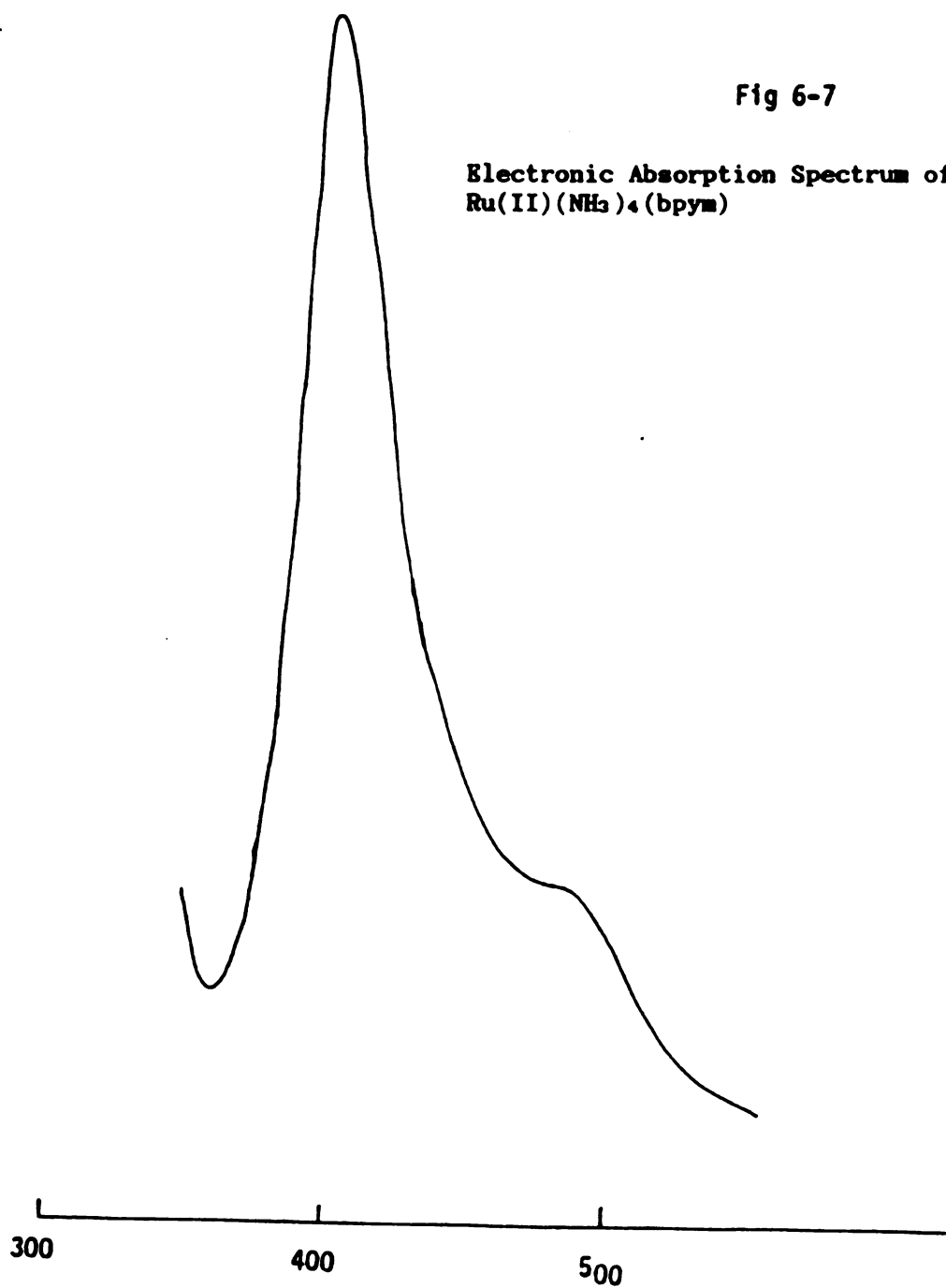
R.R. of

Fig 6-8 Ru(II)(NH$_3$)$_4$(bpym)

610 nm exc

1192

1417

1468

1548

1579

$\triangle$ cm^{-1}
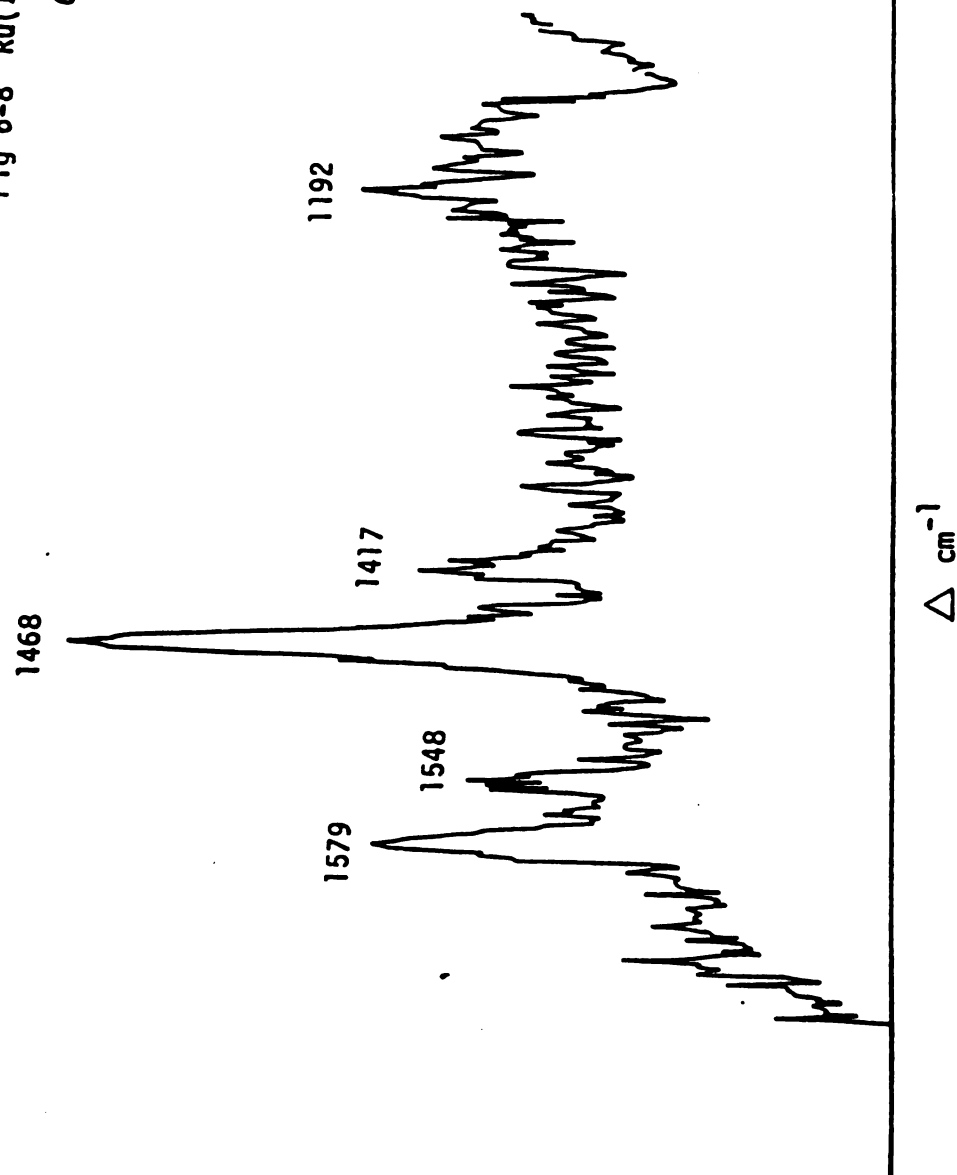
R.R. of

Fig 6-9   Ru(II)(NH$_3$)$_4$(bpym)   514.5 nm exc

1579
1548
1468
1443
1417
1337
1377
1195
1115

$\triangle$ cm^{-1}
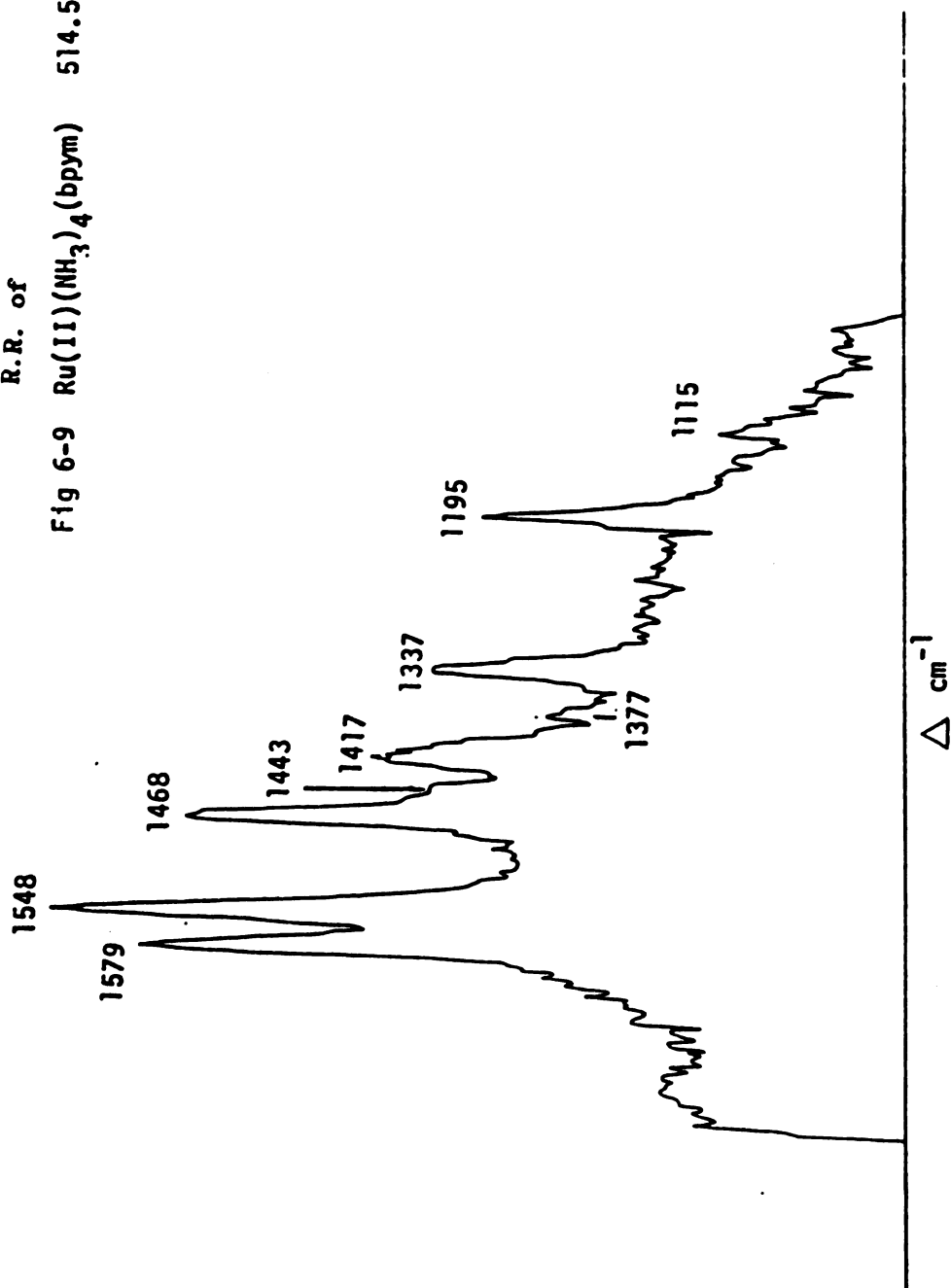
Fig 6-10
R.R. of Ru(II)(NH$_3$)$_4$(bpym)
363.8 nm exc
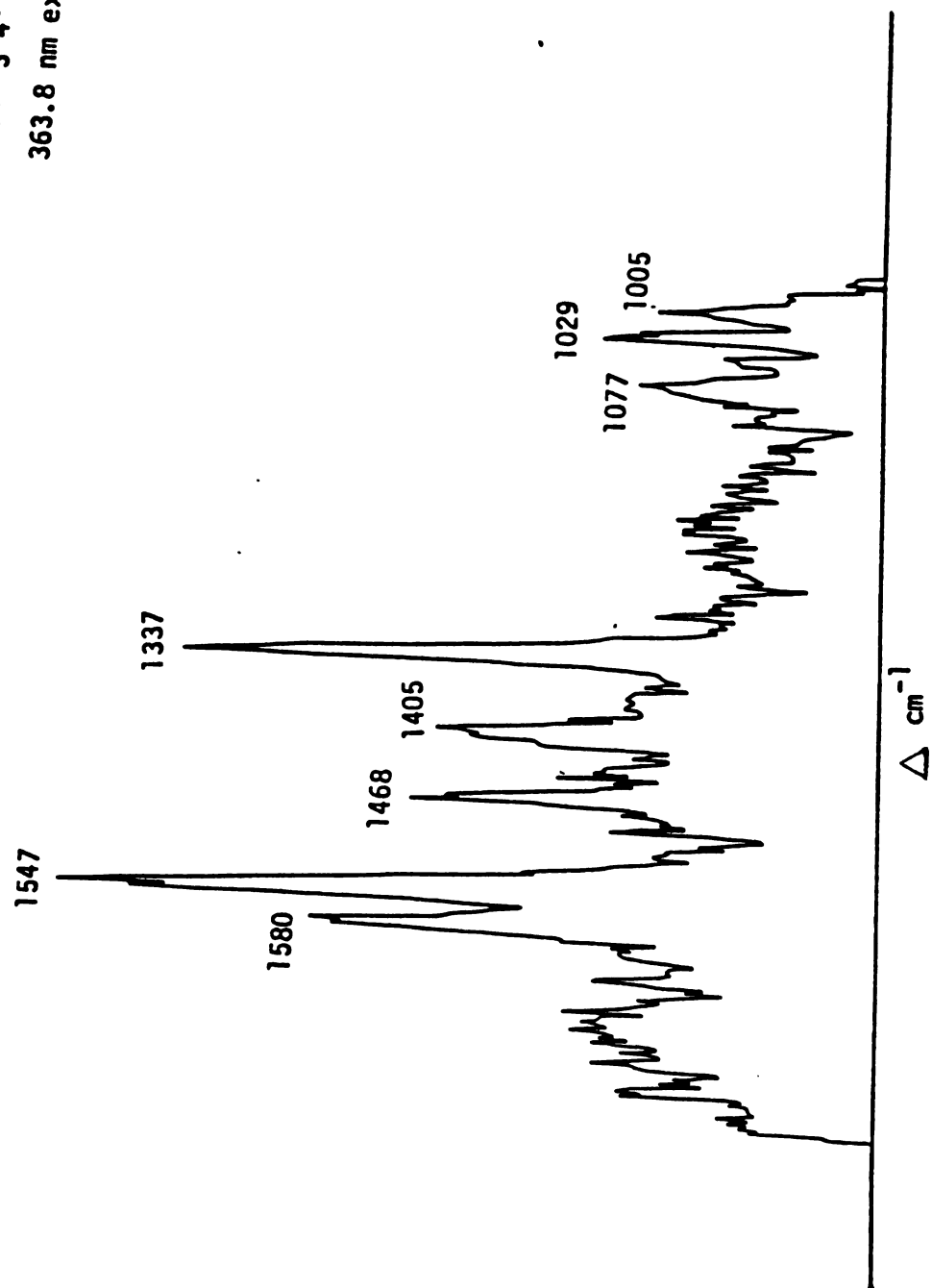
REFERENCES

1. (a) R. Ruminski, J. D. Peterson, Inorg. Chem. 21, 3706 (1982). (b) M. Hunziker, A. Ludi, J. Am. Chem. Soc. 99, 7370 (1977). (c) J. D. Peterson, W. Murphy, R. Sahai, K. Brewer, R. Ruminski, Coord. Chem. Rev. 64, 261 (1985).

CHAPTER 7

Identification of Multiple MLCT States of
Tris-(1,10-phenanthroline) Complexes of Ru(II), Os(II), Fe(II)

Transition metal tris bidendate ligands have been studied extensively because of their interesting spectroscopic properties as well as their potential role as photosensitizers.[1] 1,10-phenanthroline is a well know bidentate ligand and its metal complexes have been the subject of many spectroscopic studies.[2] It has been shown in recent years that the resonance Raman technique can be applied to d6 transition metal polypyridyl complexes to elucidate their various electronic transitions.[3]

The aim of the present study was to apply the resonance Raman method to Ru(II), Os(II) and Fe(II) tris phenanthroline complexes. Many experimental investigations as well as theoretical calculations have suggested the existence of more than one metal-to-ligand charge-transfer transition in the near UV absorption spectra for these complexes. However, the only other resonance Raman application to these complexes has been reported by Clark et al.[4] In that work the authors studied $Fe(II)(phen)_3$ and showed unambigiously that the unresolved structure on the high frequency side of the main absorption band at ~510 nm is due to a vibration in the excited state, i.e., lowest MLCT band. Specifically, it was demonstrated that it was not due to another MLCT state. Unfortunately the authors did not extend their study to higher energies, i.e., the 488.0 nm of the Ar^+ laser line was the highest energy exciting line that was used. They did hint however, that the few depolarized bands observed suggested the presence of another MLCT state.

122

We present the resonance Raman spectra of Ru(II), Fe(II), Os(II) tris-phenanthroline and show unambigiously that at least two MLCT states exist under the broad near UV absorption band envelope.

Figure 7-1 shows the near UV absorption spectra of the three complexes from which the metal dependence of λ_{max} is clear. Notice for example, that the peak of Fe(phen)₃ at 510 nm is far to the red of λ_{max} for Ru(phen)₃. Notice also that Fe(phen)₃ shows a distinct shoulder at ~430 nm.

Figure 7-2 and 7-3 shows the cw resonance Raman spectra of Ru(phen)₃ at the two excitation wavelengths from which dramatic changes in the relative intensities of the major peaks when changing from 441.6 nm to 363.8 nm illumination. The band at 1635 cm⁻¹ shows a dramatic increase while that at 1518 cm⁻¹ decreases in intensity. There are also many new peaks which were not resonantly enhanced at the longer wavelength such as 1608, 1438, 1312, 1113 cm⁻¹. Similar observations hold for the Fe(II) and Os(II) cases. (Figure 7-4 to 7-7.) An interesting comparison can be made between different metal systems excited at the same wavelength. If we compare the three complexes excited in common at 441.6 nm we can see that the Raman profile reveals the different electronic state probed by the same exciting line. The 441.6 nm line probes very close to the λ_{max} (447 nm) of Ru(II)(phen)₃. The same line, however, probes the broad shoulder far to the blue of λ_{max} (510 nm) of Fe(II)(phen)₃.

A similar analysis can be applied to the three spectra excited at 363.8 nm. Notice that many peaks which showed resonance enhancement at 363.8 nm for Ru(II)(phen)₃ show diminished intensity for the Os(II) and Fe(II) complexes. Similarly one would expect that the cluster of

high frequency peaks at 1635, 1608 and 1586 cm^{-1} would greatly decrease in intensity if one were to probe Ru(II)(phen)$_3$ at an excitation lower than 363.8 nm.

The Fe(II)(phen)$_3$ probed at 363.8 nm shows a superficial resemblance to the spectrum obtained at 647.1 nm[4] with the exception of the 1310 cm^{-1} and 1441 cm^{-1} bands in the former case. This arises because neither excitation wavelength is in resonance with the strong, compound MLCT absorption. So the spectra show essentially "normal" Raman scattering from the Fe(II)(phen)$_3$ complex. The two additional bands in the 363.8 nm spectrum may result from pre-resonance with higher energy.

In conclusion, the resonance Raman spectra obtained at several excitation wavelength thus demonstrates that Ru(II), Os(II) and Fe(II) tris-phen series contain multiple charge transfer transition under the one absorption envelope in the near UV. We also see the effective metal-induced tuning of the MLCT levels. Clearly a thorough excitation profile for several of the major peaks would be very helpful in better separating the overlapped MLCT transitions.

Electronic Absorption Spectra of Ru(phen)₃,
Os(phen)₃, Fe(phen)₃.

Fig 7-1

Fe(II)(phen)₃

Os(II)(phen)₃

Ru(II)(phen)₃

300   400   500   600
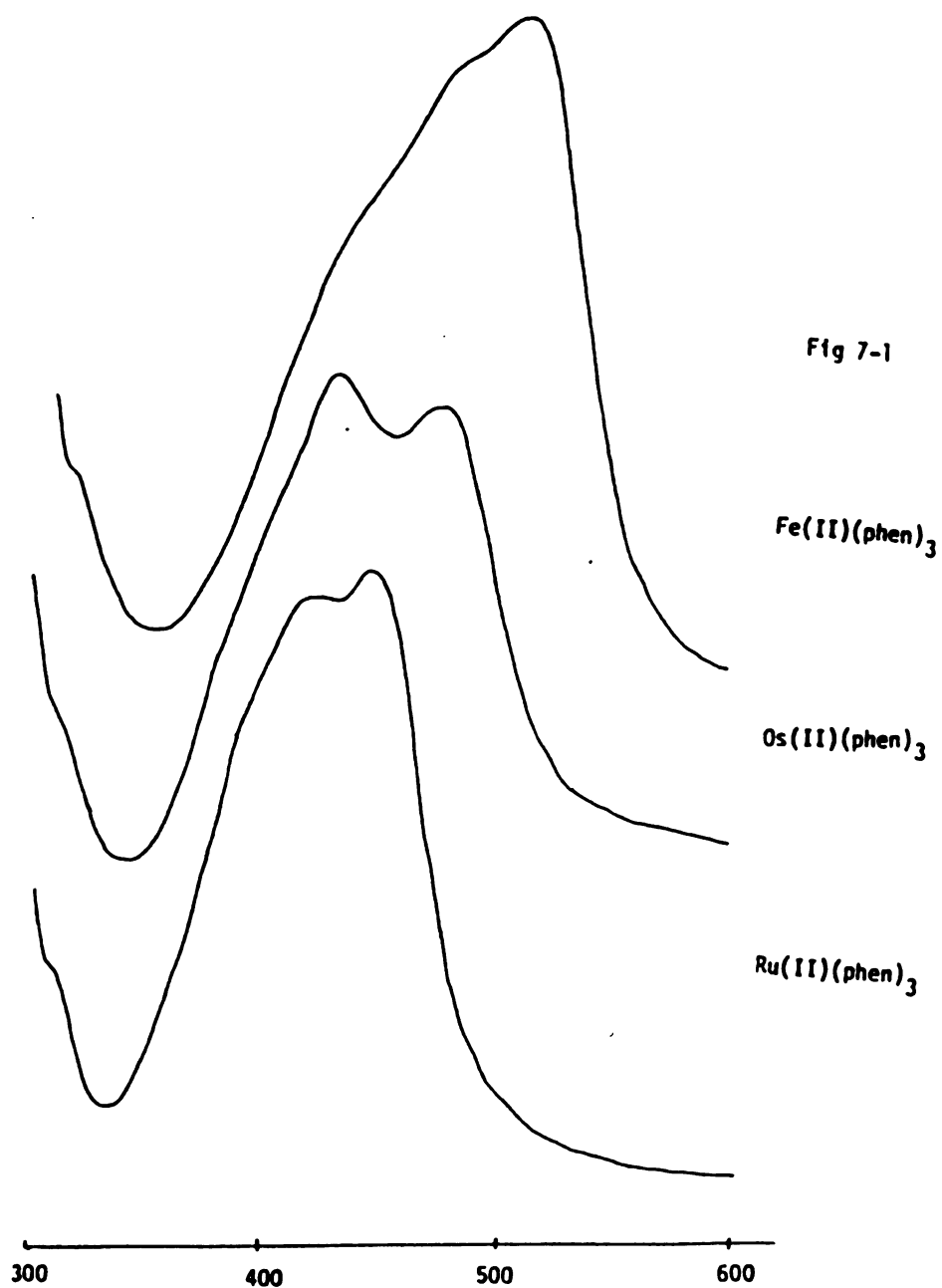
R.R. of

Fig 7-2 Ru(II)(phen)$_3$ 441.6 nm exc

$\triangle$ cm^{-1}

1147

1212

1256

1302

1347

1455

1518

1583

1634
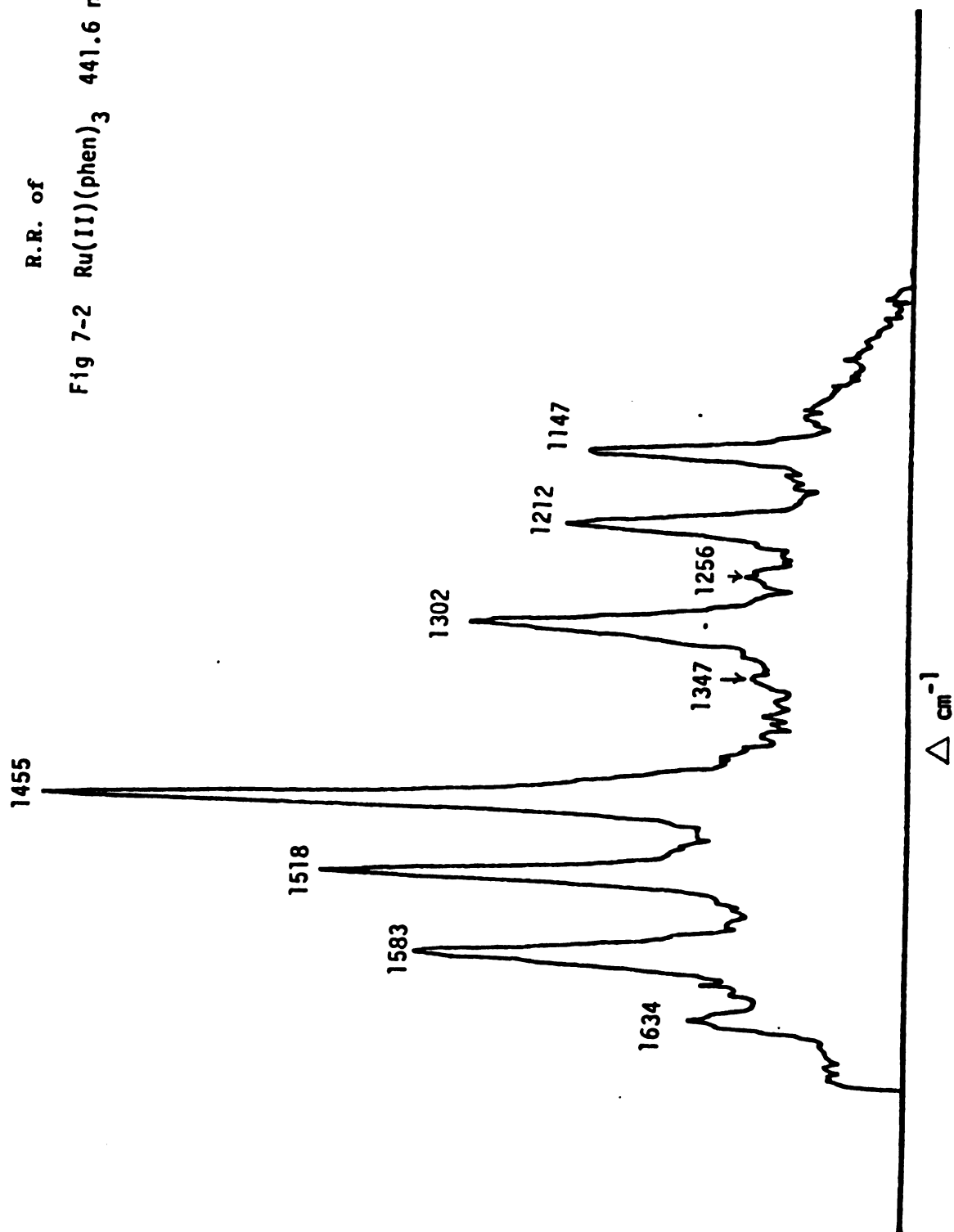
R.R. of

Fig 7-3 Ru(II)(phen)$_3$ 363.8 nm exc
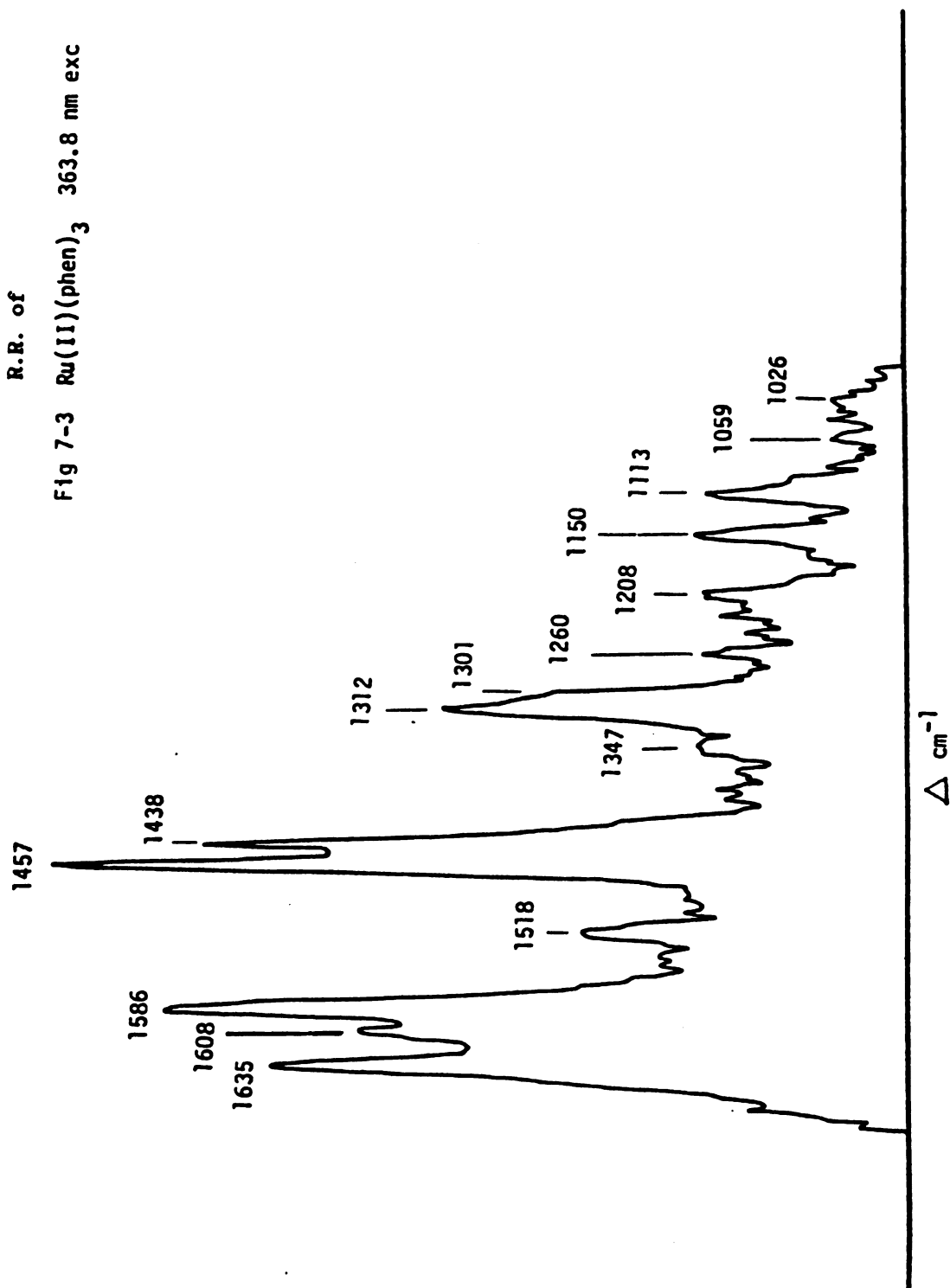
R.R. of

Fig 7-4 Os(II)(phen)$_3$ 441.6 nm
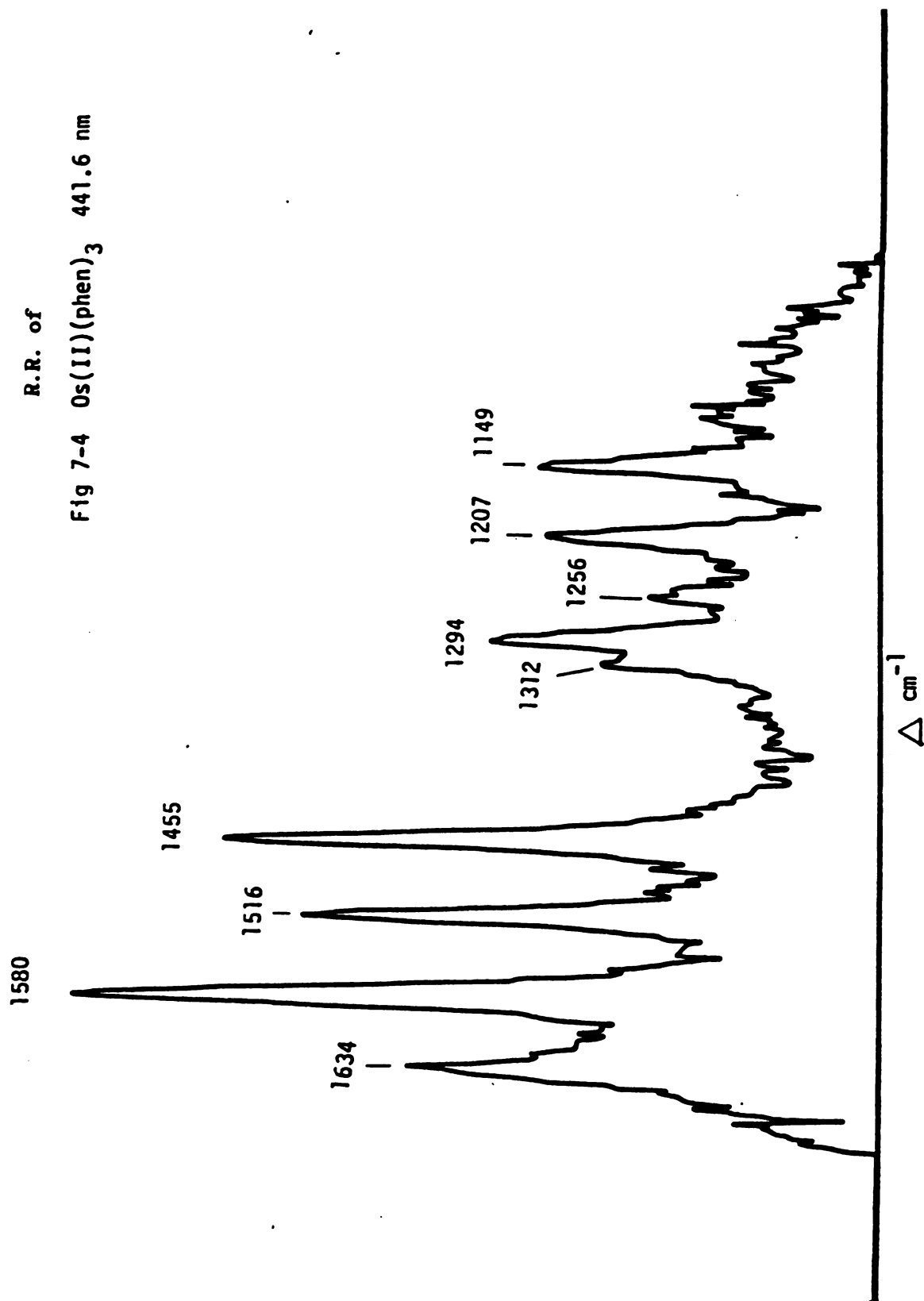
Fig 7-5   Os(II)(phen)$_3$ 363.8 nm

R.R. of

Fig 7-6
R.R. of Fe(II)(phen)$_3$ 441.6 nm exc
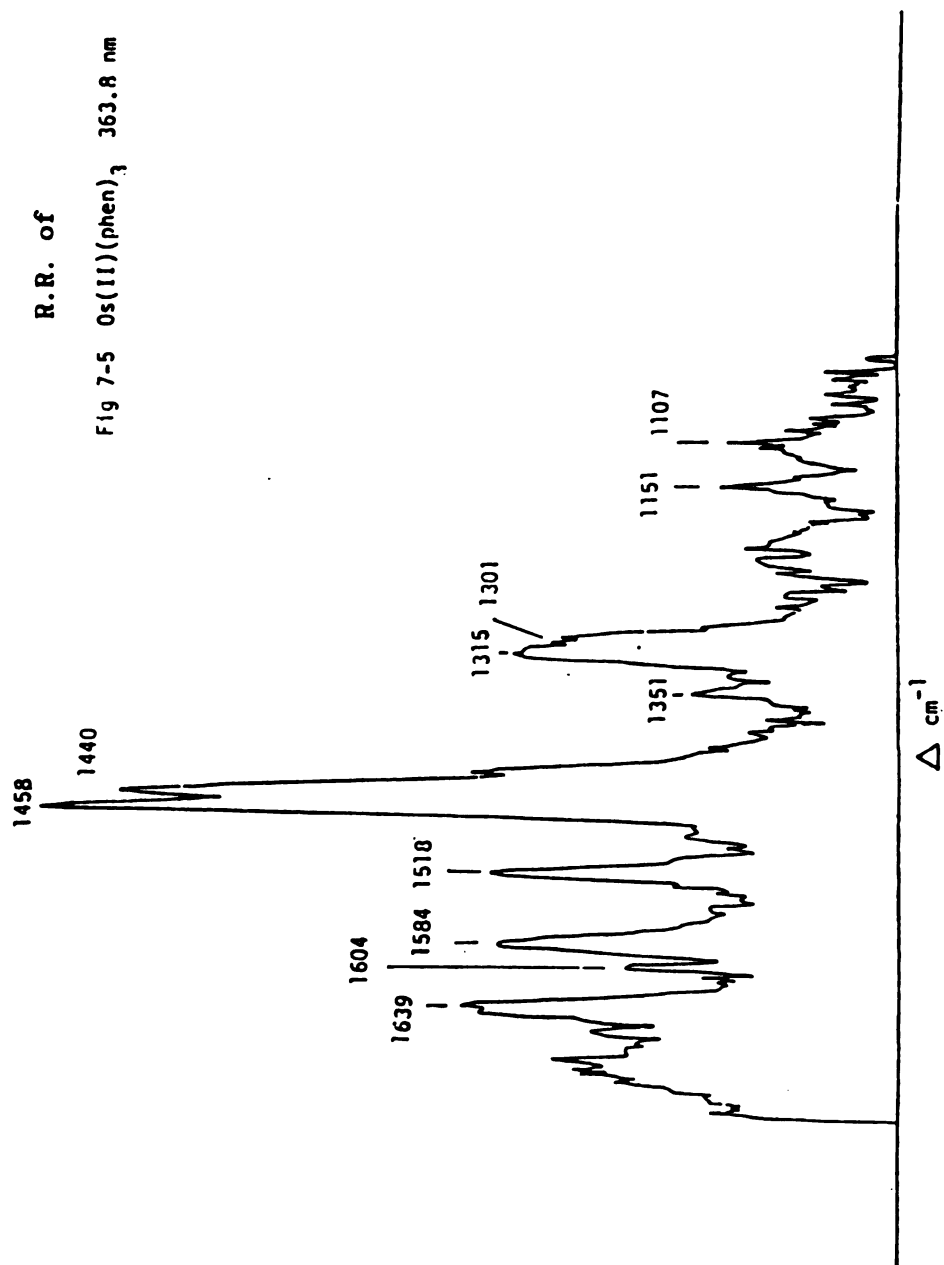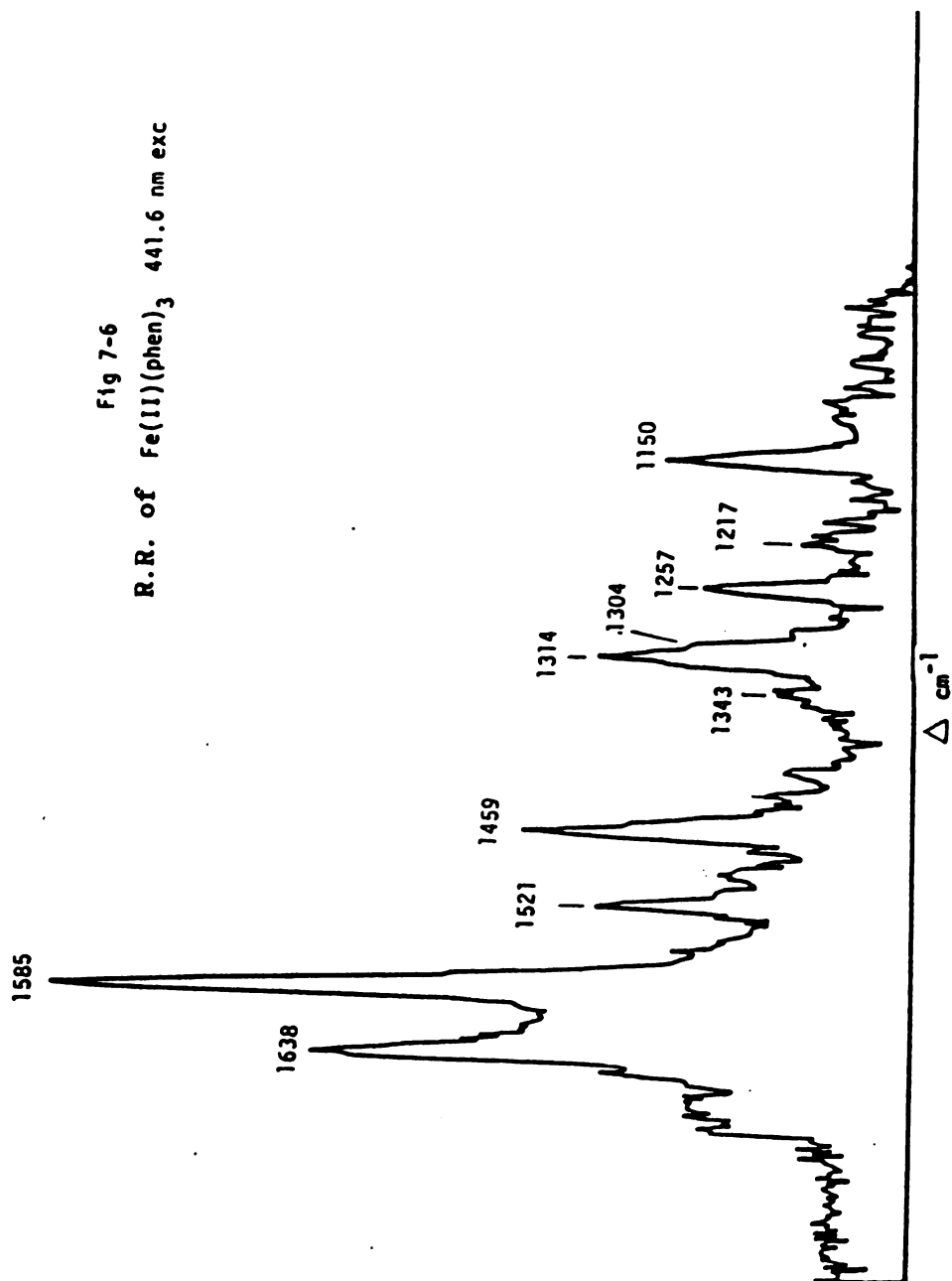
R.R. of

Fig 7-7 Fe(II)(phen)$_3$ 363.8 nm exc
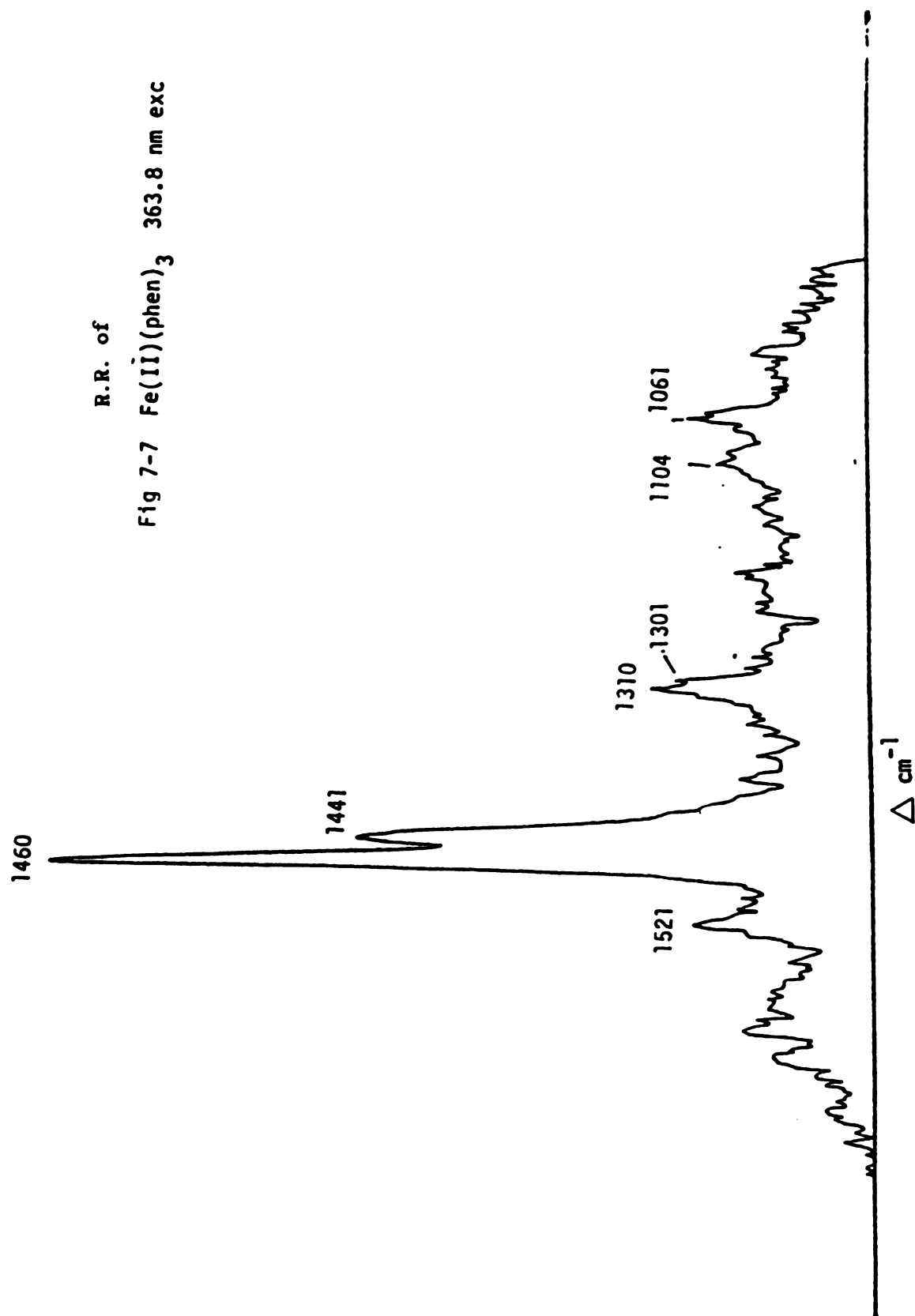
REFERENCES

1. For a representative reviews see "Energy Resources Through Photochemistry and Catalysis" M. Gratzel, Academic Press, New York (1983).

2. (a) J. Hidaka, B. E. Douglas, Inorg. Chem. 3, 1180 (1964). (b) P. Day, N. Sanders, J. Chem. Soc. (A), 1530 (1967). (c) A. J. McCaffrey, S. F. Mason, and B. J. Norman J. Chem. Soc. (A), 1428 (1975). (d) N. Sanders, J. C. S. Dalton 345 (1972). (e) T. Ito, N. Tanaka, I. Hanazaki, S. Nakagura, Bull. Chem. Japan 41, 365 (1968). (f) T. Ho, N. Tanaka,, I Hanazaki, S. Nakagura, Ibid. 42,702 (1969).

3. R. F. Dallinger, W. H. Woodruff, J. Am. Chem. Soc. 101, 4391 (1979).

4. R. J. H. Clark, P. C. Turgle, D. P. Strommen, B. Streusand, J. Kincaid and K. Nakamoto, Inorg. Chem. 16, 84 (1977).

APPENDIX

The one outstanding problem in the M(phen)₃ series is the question of the excited state Raman spectrum. Woodruff, et al, have shown in their Ru(bpy)₃ and Os(bpy)₃ work that the lowest MLCT excited state can be characterized on the Raman time scale as having the transferred electron localized on one ring rather than delocalized over all three. Since phen is quite analogous structurally to bpy we would expect the same or similar phenomena to occur in the phen metal complexes. All attempts to obtain the excited state Raman spectra of Ru(phen)₃ failed. Normally only broad featureless scattering was observed although under high-powered excitation, some ground state peaks could be obtained. The Ru(phen)₃ complex is known to have a long-lived excited state, longer in fact than Ru(bpy)₃. An interesting suggestion has been put forward by E. Krausz (Chem. Phys. Lett. 116, 501 [1985]) that broad Raman scattering observed for Ru(bpy)₃ at low temperature may be due, not to neutral or an averaged $(bpy)^{-1/3}$ species. He showed that at room temperature Ru(bpy)₃ gave the characteristic sharp MLCT excited state Raman spectra observed by Woodruff, et al. However, as the temperature was lowered, the Raman scattering was broadened and became featureless. Krausz suggests that a fast delocalized to localized MLCT transition can occur in Ru(II)(bpy)₃ in room temperature solutions, but that this fast transition cannot occur at low temperature due to the hindered motion of the solvent. In other words, at low temperature it should take a longer time for the promoted electron to localize. If this explanation is correct then it can be inferred that Ru(phen)₃ requires a longer time than Ru(II)(bpy)₃ for the

excited electron to localize at room temperature. Clearly the excited state properties of transition metal complexes are inadequately understood and further studies on perhaps substituted ligands or modified ligands are needed before their varied behavior can be interpreted.

Other related transition metal complexes were studied with the phen ligand in mind. for example, the mixed ligand series of Ru(bpy)$_m$(phen)$_{3-m}$ (m = 0~3) was investigated. The electronic absorption data is shown below. (Figure 7-8.)

Complex	λ_{max}
Ru(bpy)$_3$	452.9 nm
Ru(bpy)$_2$(phen)	450.2 nm
Ru(bpy)(phen)$_2$	450.4 nm
Ru(phen)$_3$	447.7 nm

The ground state absorption of each mixed ligand complex is strongly overlapped as can be seen in the CW Raman spectra taken with 441.6 nm (Figure 7-9, 7-10). The Ru(bpy)$_2$(phen) complex shows a clean separation of the bpy and phen modes with bpy peaks roughly twice as intense as the phen bands. The analogous statement can be made concerning Ru(phen)$_2$(bpy). The excited state spectra were taken with pulsed 355 nm excitation in the hope of observing the phen charge-transfer excited state (Figure 7-11, 7-12).

The Raman spectra of both mixed ligand complexes showed a clean bpy MLCT excited state. As can be seen obtained under these conditions in the Ru(phen)$_2$(bpy) spectra all the peaks due to the bpy excited state can be clearly seen (1550, 1500, 1428, 1284, and 1211 cm^{-1}). The relative intensities of the peaks appear slightly distorted, however,

as compared to Ru(bpy)₃. For example in the Ru(bpy)₃ case the 1500 and 1429 cm⁻¹ bands are roughly similar in intensity (Figure 7-13). In the mixed ligand however, the 1428 cm⁻¹ band is clearly more intense. This is due to the fact that an intense phen ground state mode exists at 1438 cm-1 which contributes to the strength of the 1428 cm⁻¹ peak. Also the bands at 1457 and 1315 cm⁻¹ are due to ground state phen modes (see Ru(phen)₃ Chapter). The assignments are not as clear in the case of Ru(bpy)₂(phen), but in both cases the excited state is localized on the bpy ligand and not on phen. Again, referring to Krausz's paper perhaps phen takes "longer" to localize than bpy at room temperature. In another approach to the phen "problem" other related complexes were investigated. Ru(phen)(NH₃)₄ was studied because it represents a situation where delocalization and localization are clearly irrelevant. The absorption spectrum is typical of Ru(NH₃)₄L complexes but again only a broad featureless scattering was obtained under 355 nm excitation. This seems to imply that at least for phen at room temperature the ostensibly long time scale of localization cannot explain the failure to observe excited state Raman spectra. Another related complex Re(CO)₃(phen)Br was prepared but again, no excited state Raman scattering could be observed. Clearly the phen ligand represents an anomaly in these complexes. The phen ligand has two extra CH fragments compared to bpy which would make the entire ring system more rigid. It is proposed that a thorough truly time resolved experiment be carried out with two independently tunable pulsed lasers. Even though the Ru(phen)₃ MLCT state is known to have a long lifetime, it may take a "long" time to stabilize into a so called localized excited state. This author suggests that some sort of photophysical kinetic barrier may

prevent the lowest MLCT state to be populated on a subpicosecond time scale [such has been measured for Ru(bpy)₃]. Once this barrier is overcome and the MLCT state is populated, it is know to be long-lived (~900 nanoseconds).

Substitution of a similar bidentate ligand such as phen for one of the bpy in Ru(bpy)₃ clearly induces little spectroscopic perturbation as for as bpy is concerned. The spectroscopy is dramatically affected when bpy is substituted by a ligand called 4,5-diazafluorene. (Henceforth abbreviated dzf). The entire series of substituted complex was synthesized and kindly provided to us by W. R. Cherry of Louisiana State University. This ligand differs from bpy by having only one extra CH₂ fragment.
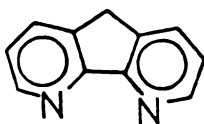
dzf = 4,5-diazafluorene

This CH₂ bridge however, has a drastic effect on the photophysical properties of the metal complexes. The ligand is distorted in such a manner that it reduces the nitrogen-metal overlap. By distorting this ligand "bite" angle dzf becomes much weaker ligand than bpy, i.e., it is lower on the spectrochemical series. This means that the ligand field splitting is reduced and therefore, low energy ligand field transitions should exist. On the other hand, the basic π-conjugated ring system of dzf does not differ significantly from bpy so their electrochemical reduction potentials and hence their charge tranfer energies should be similar. The cw Raman of Ru(dzf)₃ obtained with 363.8 nm is shown in Figure 7-14, 15. Solutions were prepared in two solvents CH₃CN and

CH₃COCH₃. Solvent peaks are marked with capital "S". Four peaks at 1605, 1517, 1186, 1039 cm⁻¹ can be identified. Under high power pulsed excitation at 355 nm in CH₃CN solvent a virtually identical spectrum is obtained. Apparently Ru(dzf)₃ has a ligand field lowest excited state which quickly deactivates to the ground state. The Ru(bpy)₂(dzf) by cw 363.8 shows peaks due to both ligands (Figure 7-16). Clearly 1569, 1497, 1322, 1268 are due to bpy. The pulsed spectrum obtained under 355 nm shows basically the same ground state features (Figure 7-17). There are no indications of bpy excited state scattering. Notice particularly the absence of scattering at 1214, 1287 cm⁻¹ which are the strongest excited state peaks of bpy. Except for expected changes in relative intensities of the ligand peaks, identical spectra were obtained and conclusions drawn from Ru(bpy)(dzf)₂. So the details will not be repeated here. Clearly the geometry of the organic ligand is important in determing the photphysical and hence, photochemical properties of these complexes. [Reference: L. J. Henderson, F. R. Fronczek and W. R. Cherry, J. Am. Chem. Soc. 106, 5876 (1984).]

Electronic Absorption Spectra of
Ru(II)(phen)₃, Ru(II)(bpy)(phen)₂,
Ru(II)(bpy)₂(phen), Ru(II)(bpy)₃ .

Fig 7-8

Ru(II)(phen)$_3$

Ru(II)(bpy)(phen)$_2$

Ru(II)(bpy)$_2$(phen)

Ru(II)(bpy)$_3$

300   400   500   nm

R.R. of

Fig 7-9 Ru(II)(phen)(bpy)$_2$ 441.6 nm exc

Δ cm^{-1}

1493

1566

1583

1610

1634

1518

1456

1320

1302

1279

1213

1176

1148

1033
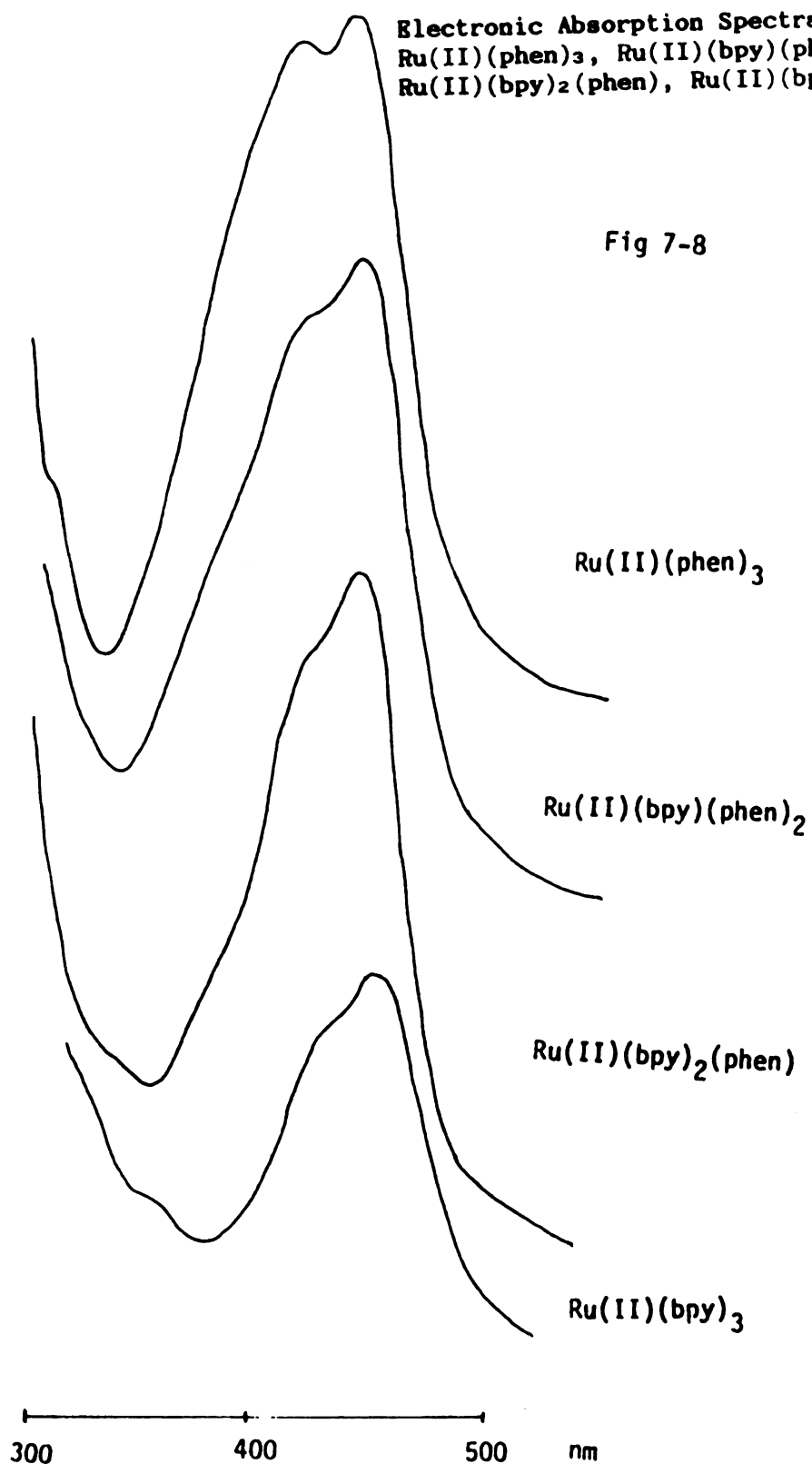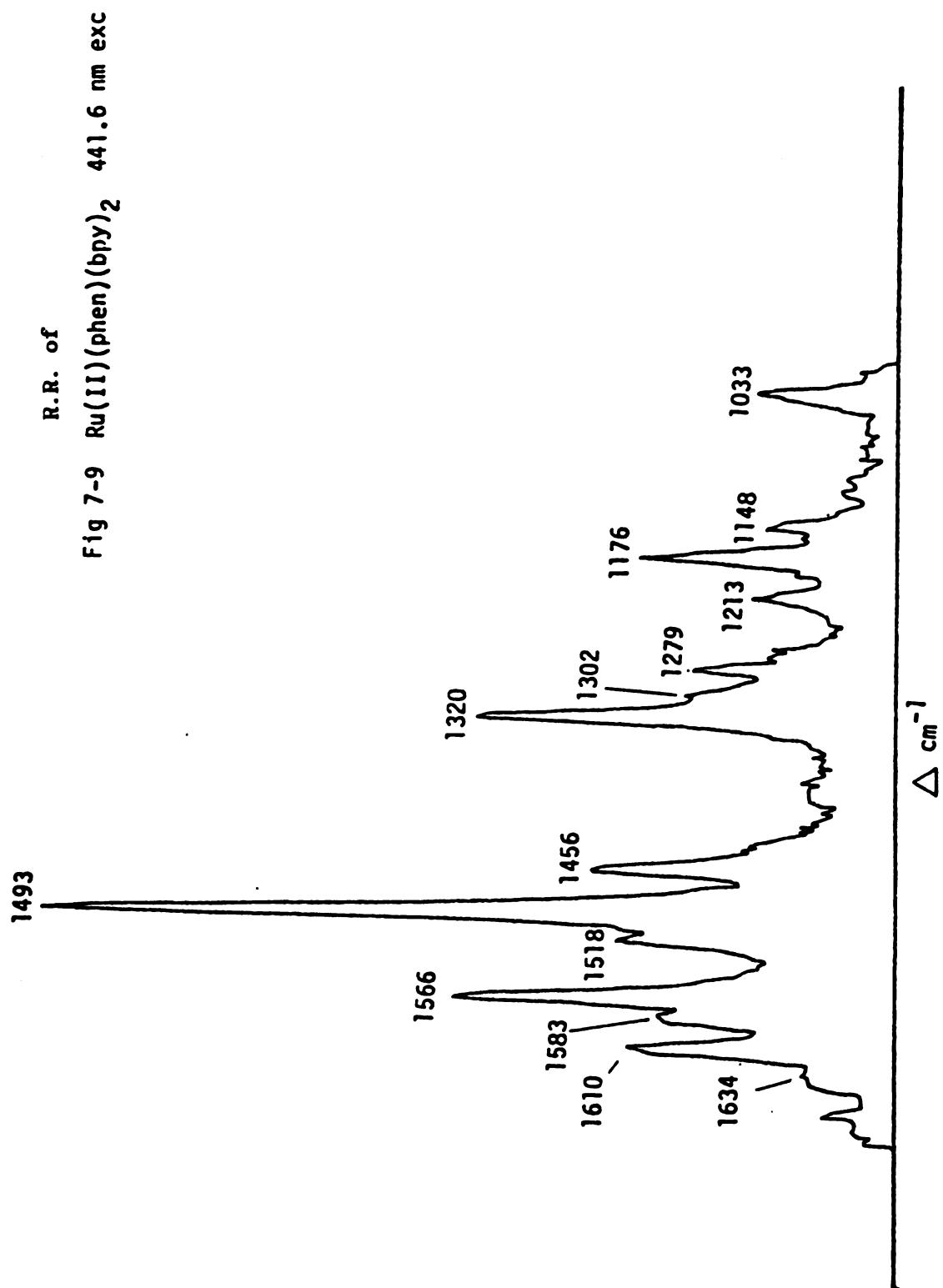
Fig 7-10

R.R. of Ru(II)(bpy)(phen)$_2$

441.6 nm
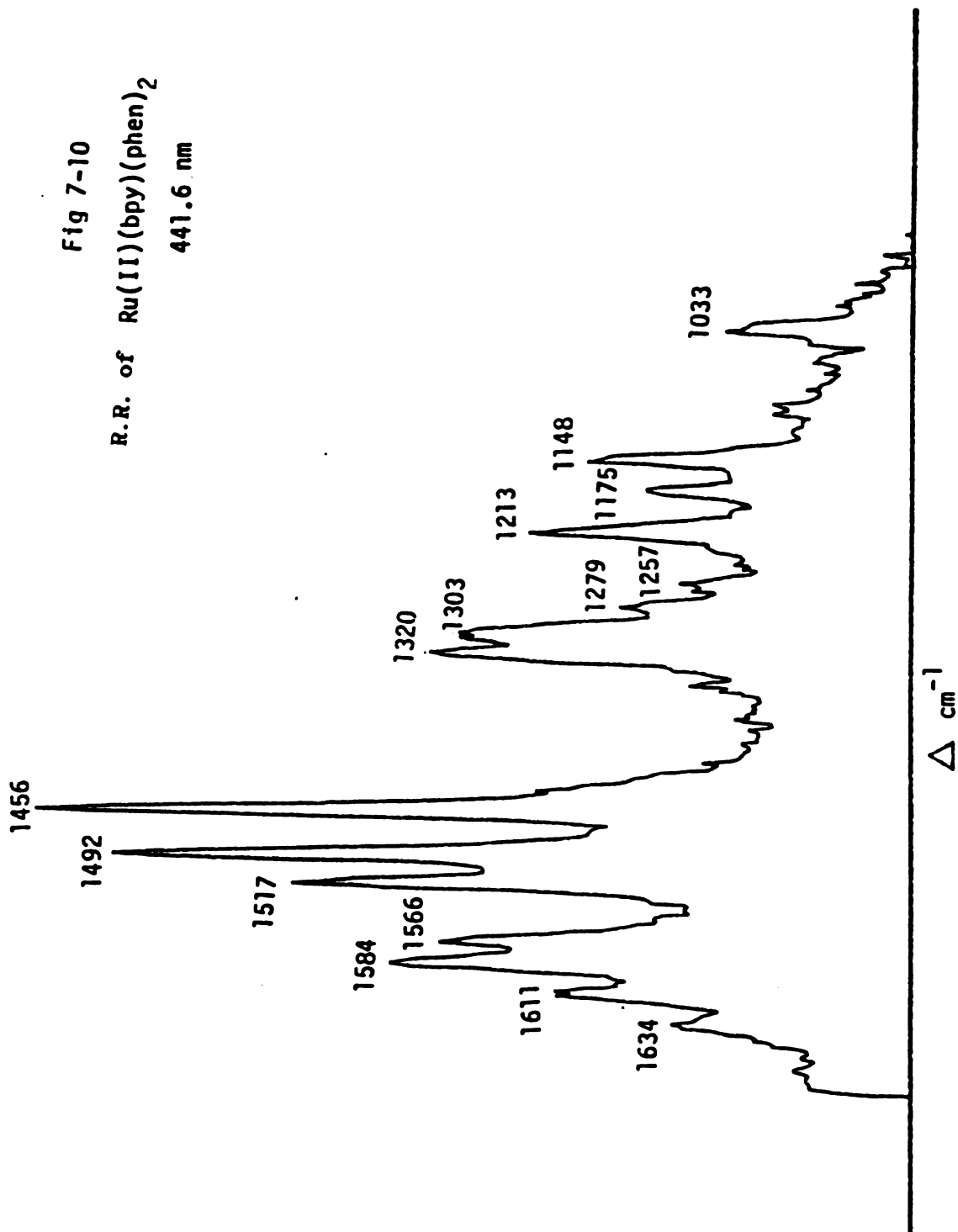
R.R. of

Fig 7-11 Ru(II)(bpy)(phen)$_2$ 355 nm exc

R.R. of

Fig 7-12   Ru(II)(phen)$_2$(bpy)   355 nm exc
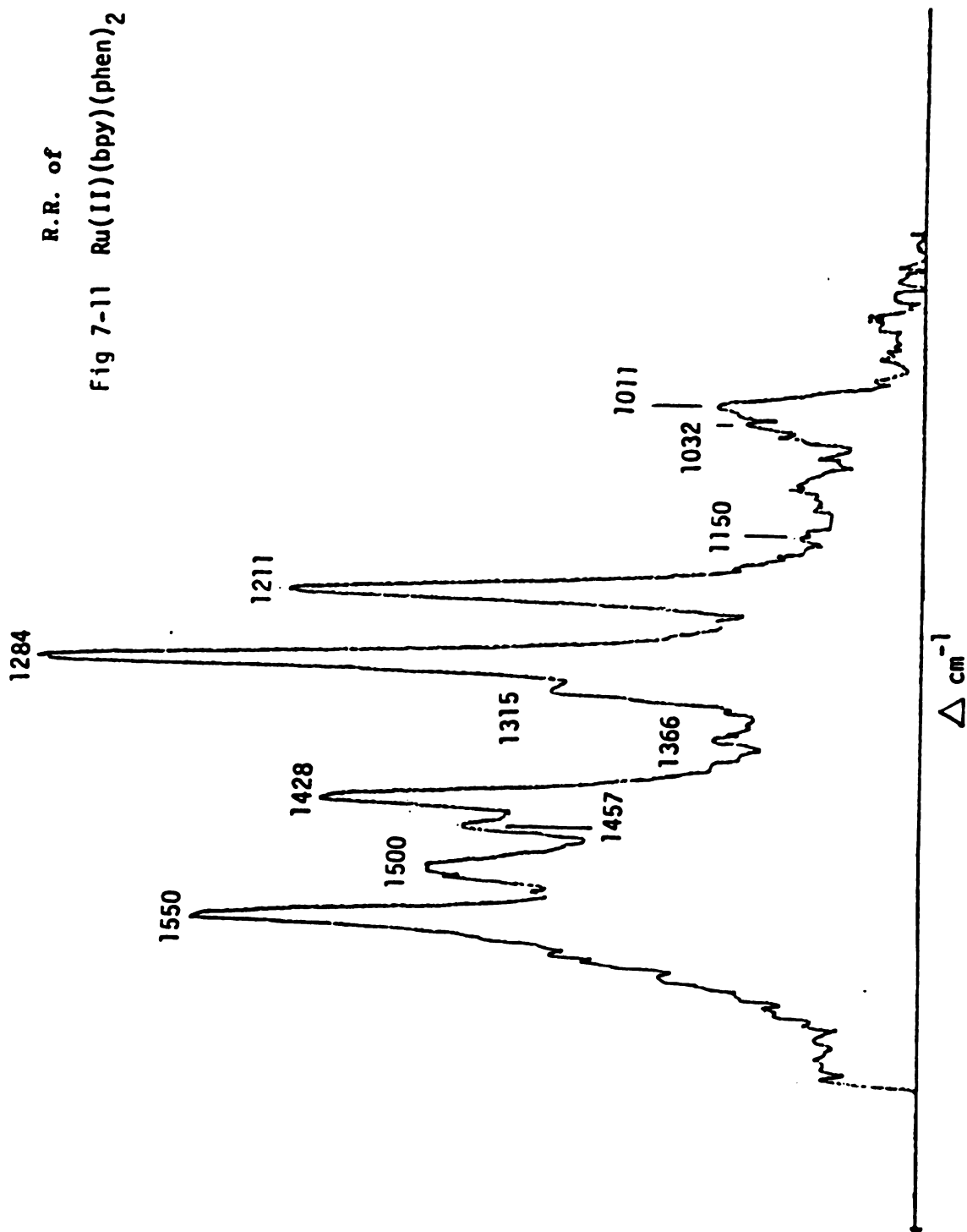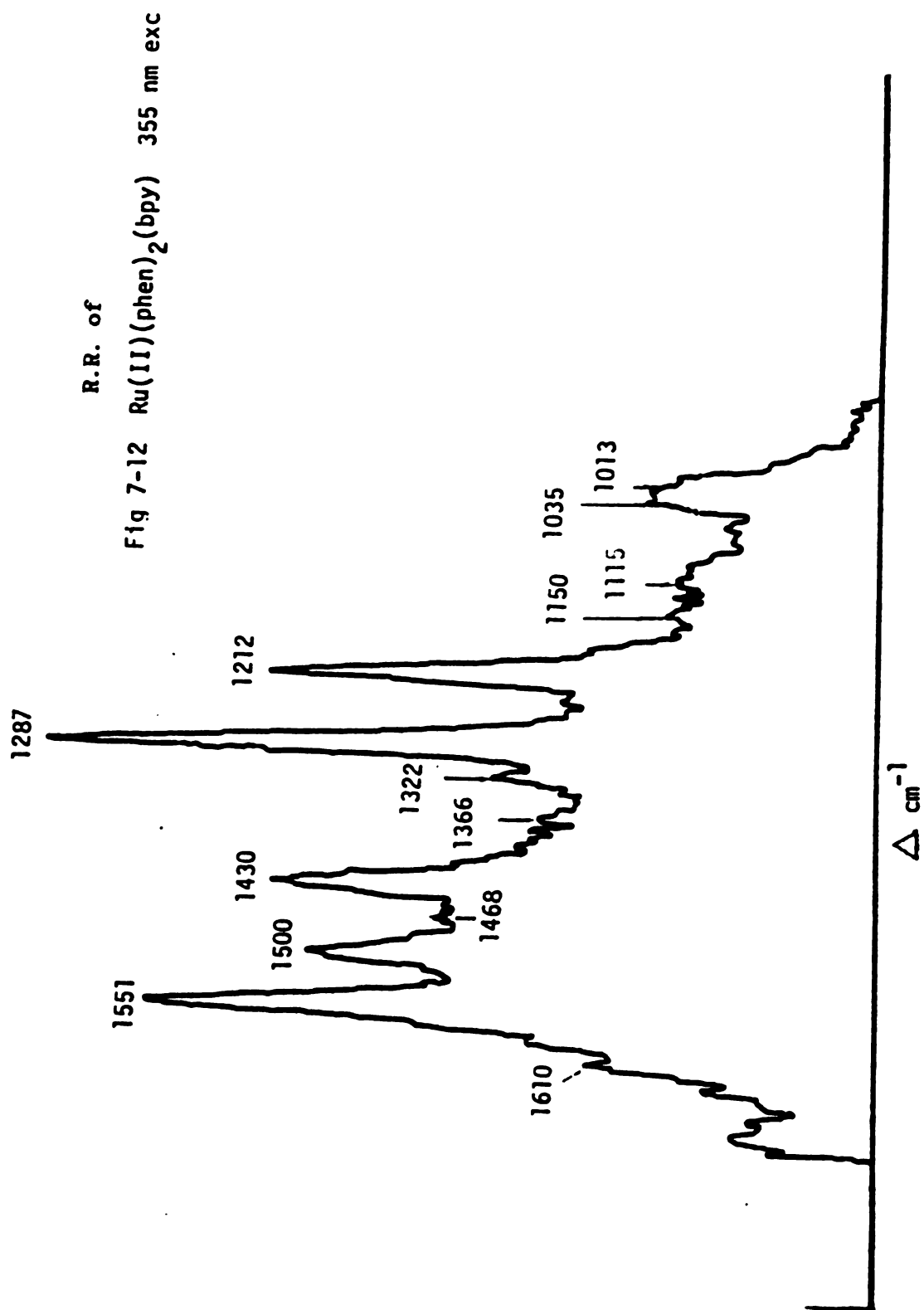
R.R. of

Fig 7-13 Ru(II)(bpy)$_3$ 355 nm exc

1213

1287

1322

1429

1500

1550

1609

$\triangle$ cm^{-1}

Fig 7-14

R.R. of Ru(II)(dzf)$_3$ 363.8 nm exc

CH$_3$CN solv
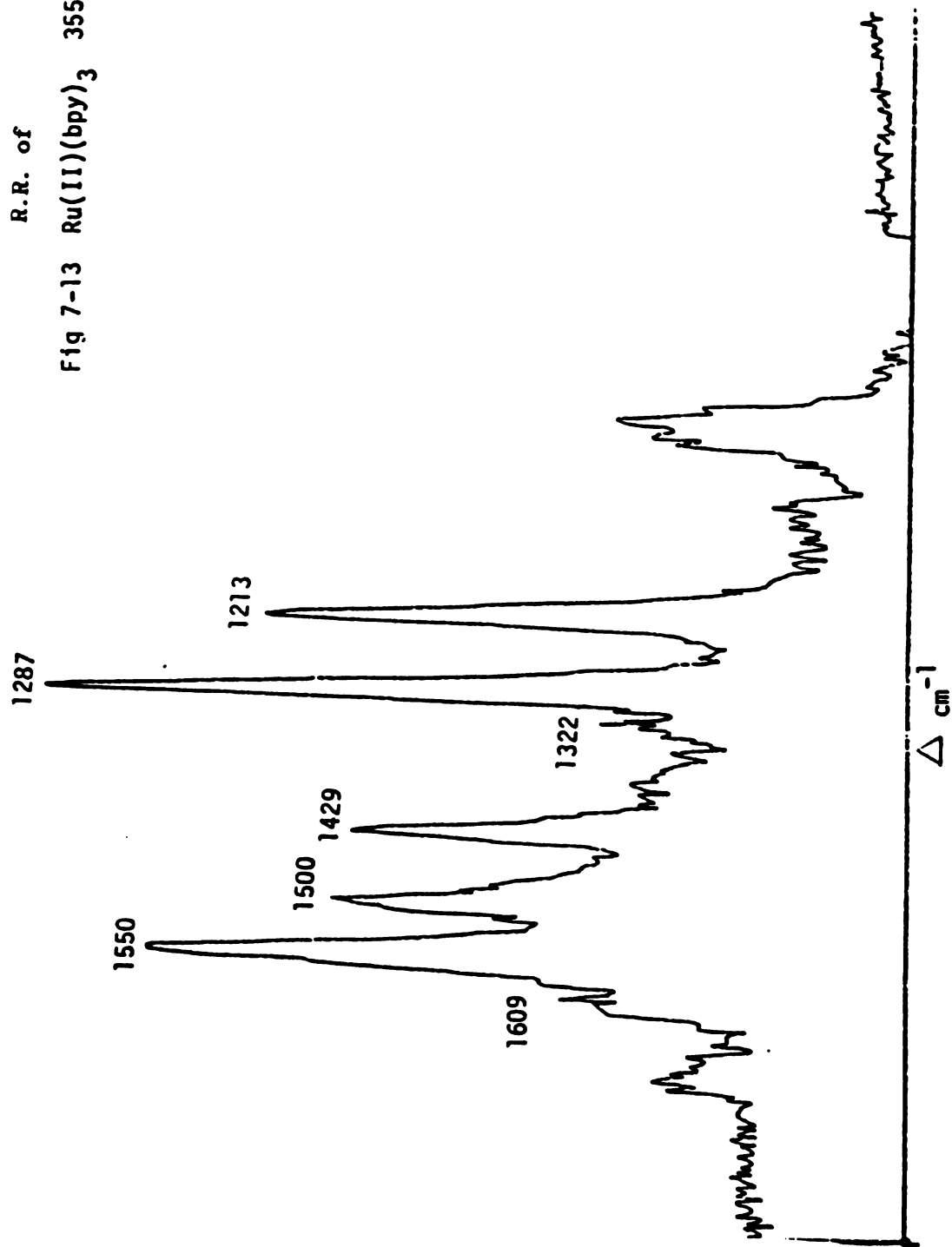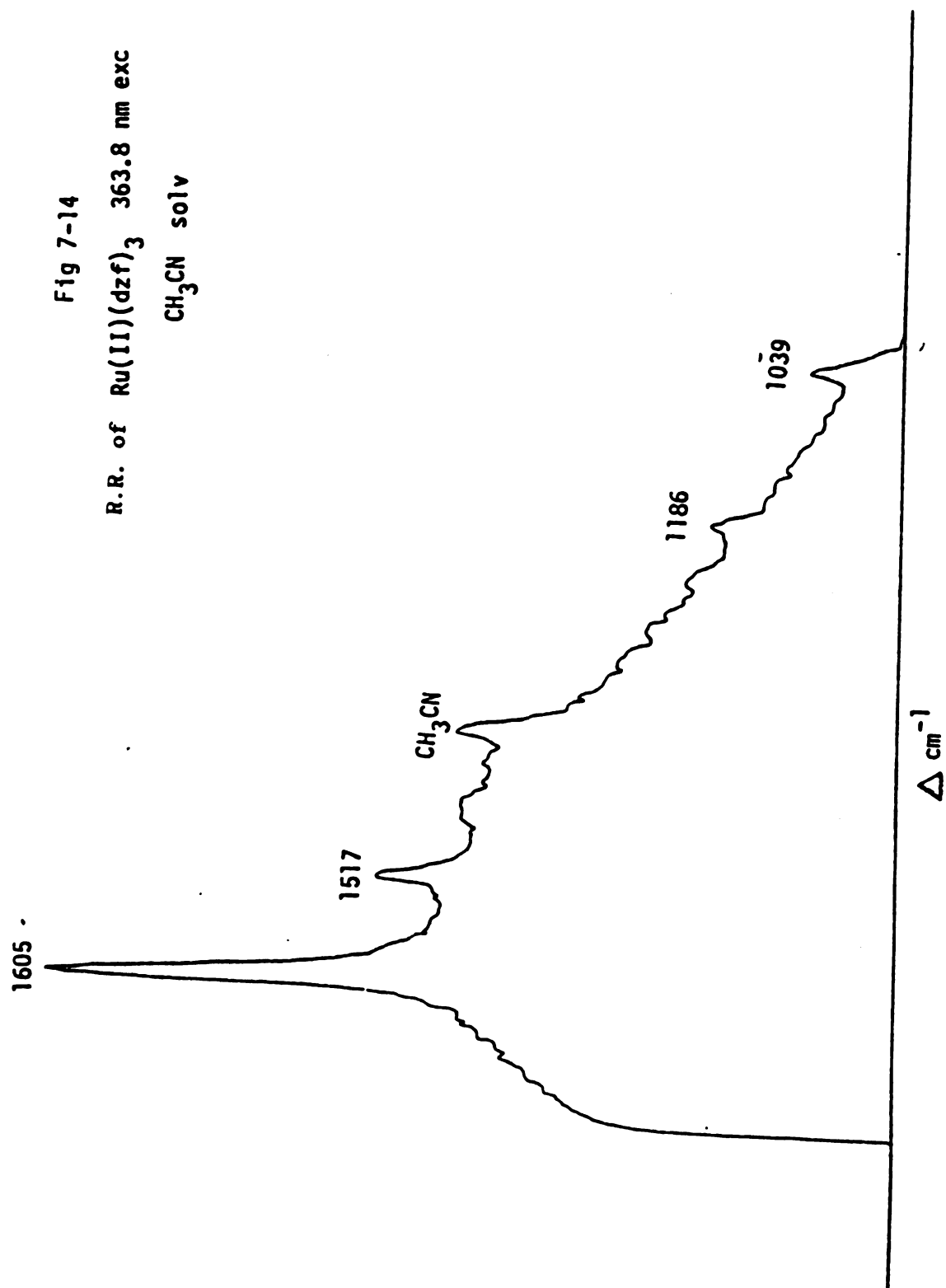
Fig 7-15
R.R. of Ru(II)(dzf)$_3$ 363.8 nm exc

Fig 7-16 R.R. of Ru(II)(bpy)$_2$(dzf) 363.8 nm exc

CH$_3$CN solvent
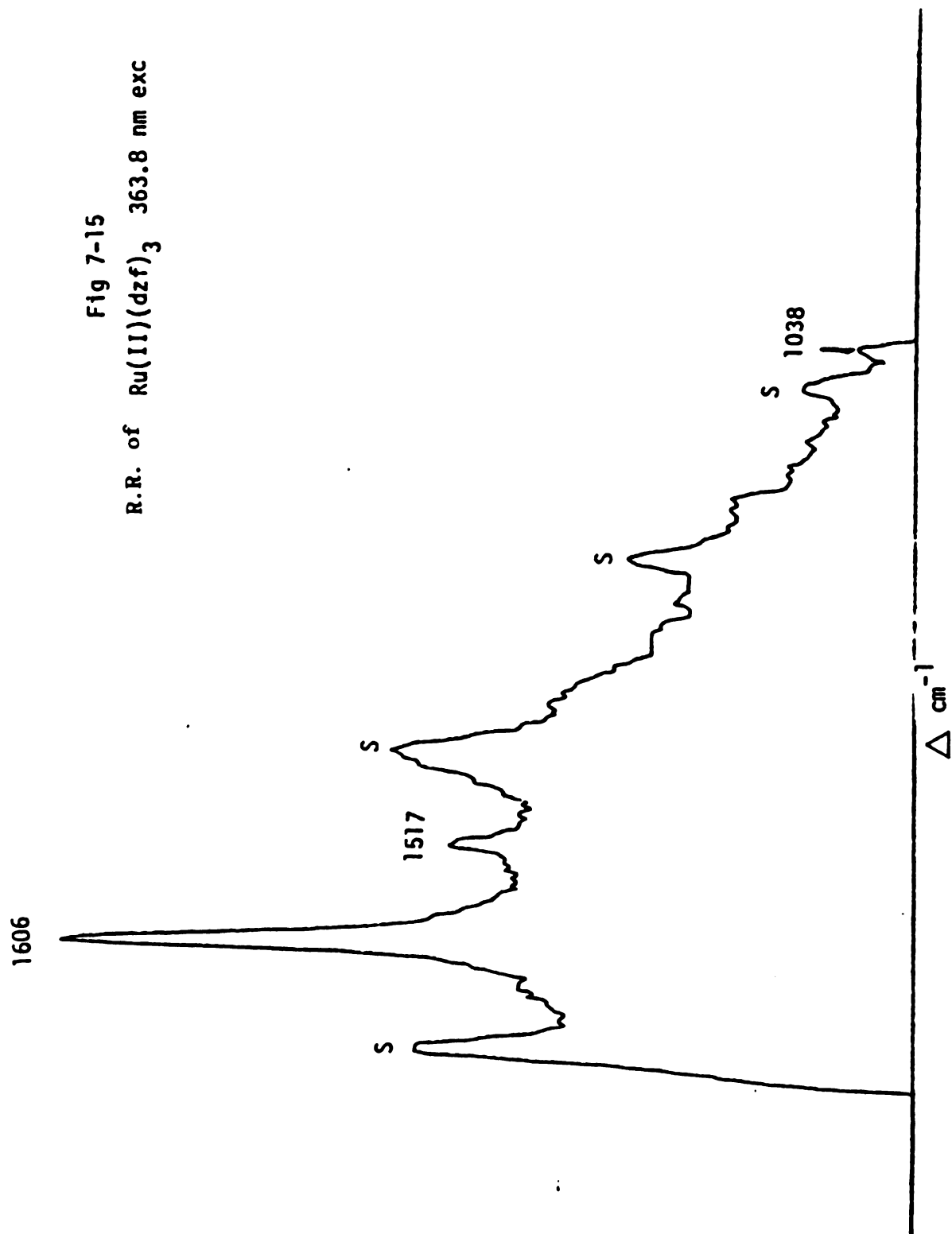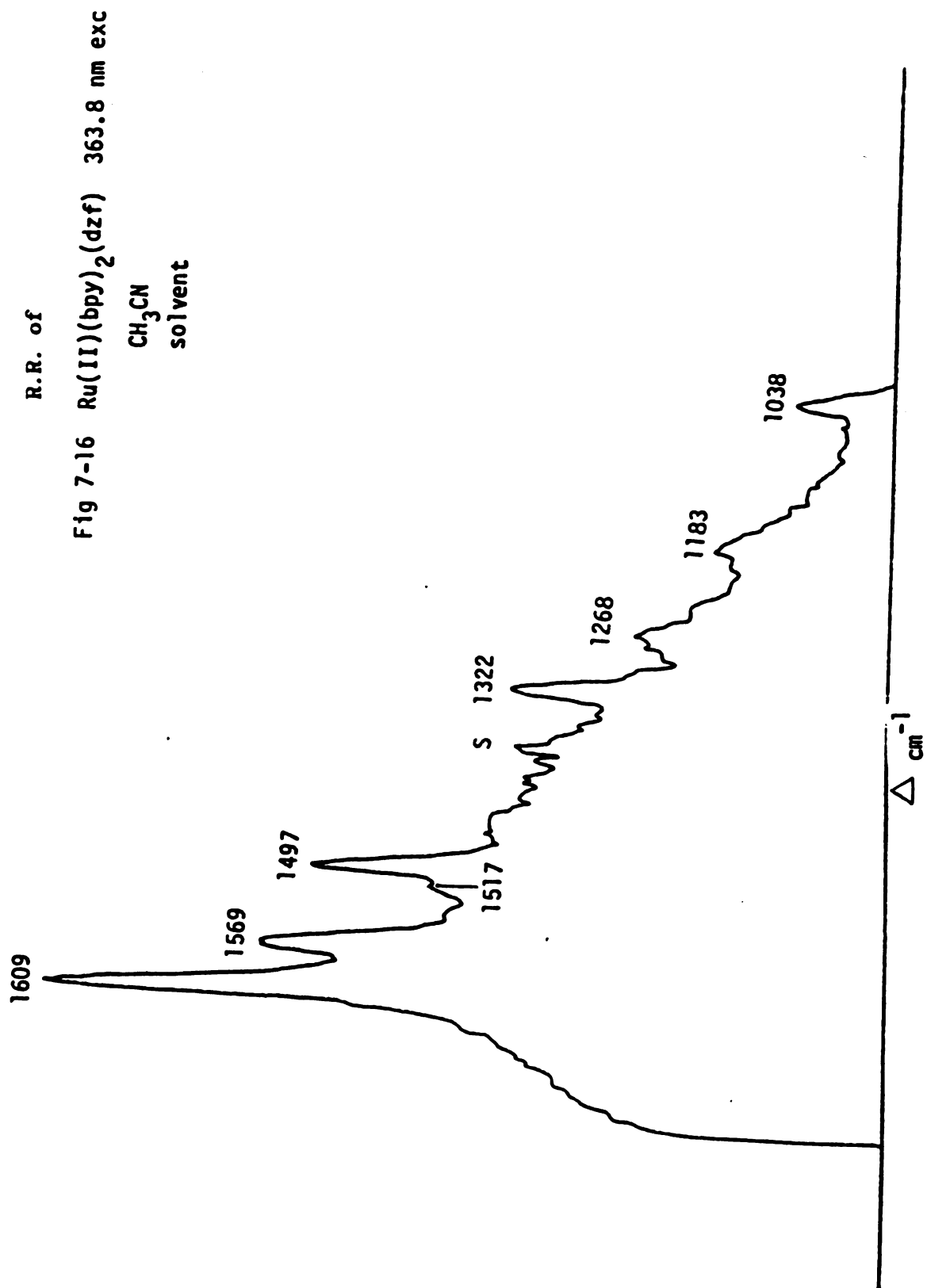
Fig 7-17

R.R. of Ru(II)(bpy)$_2$(dzf)   355 nm exc
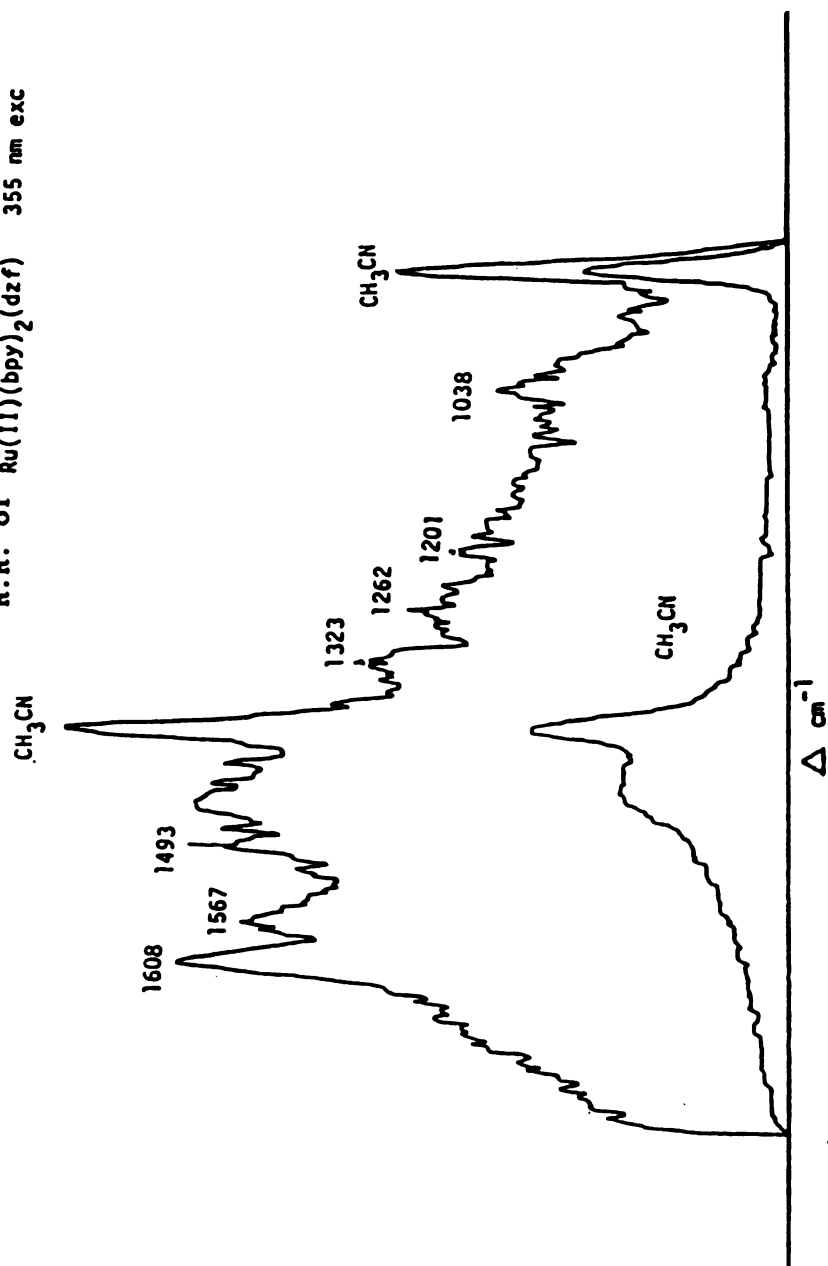
CHAPTER 8

Raman Spectra of Pyridine Resonant to the $S_2(\pi\pi^*)$ State

Absorption spectra of higher excited state of aromatic molecules are often rather diffuse and poorly resolved, thus making vibrational analysis of these states difficult. However, if one obtains resonance Raman spectra through such regions, the intensities of the ground state scattering will reflect the properties of the excited state on a beautifully resolved scale. By analyzing which Raman bands are enhanced in resonance, and by following the enhancement through the absorption region—the excitation profile—the vibrational structure and vibronic coupling in the excited state may be unravelled.[1,2]

Indeed, absorption, emission and Raman scattering can be treated within the same vibronic framework and this has been done by several authors. In Albrecht's treatment of resonance Raman, totally symmetric modes may be directly enhanced by the (dipole-allowed) resonant state provided that the potential curve shifts (Franck-Condon scattering, A-term), as well as by vibronic coupling between (allowed) excited electronic states (Herzberg-Teller coupling B-term). The latter provides the enhancement mechanisms for non-totally symmetric vibrations.

Pyridine, the nitrogen heterocyclic analog of benzene, is an interesting molecule in that excited state luminescence defied observation until recently. The pyridine absorption spectrum has yet to be satisfactorily analyzed.[4] Mochizuki, Kaya and Ito[5] using the techniques of single vibronic level fluorescence (SVL) and pre-resonance Raman spectroscopy have studied the n-π^* state of pyridine in detail. They found strong vibronic coupling between the n-π^* (s_1) and π-π^* (s_2) states, the distortion being along the ν_{6a} mode, and also observed the

Duchinski effect in the n-π^* state. On the other hand information on the S_2 ($\pi-\pi^*$) state of pyridine which lies only ~3600 cm^{-1} above S_1, is extremely sparse because of the diffuseness of the absorption band system. We report here the resonance Raman spectra of pyridine resonant with the S_2 ($\pi-\pi^*$) excited state. The structure of the excited state and the observed vibronic coupling is discussed. The results are compared with resonance Raman scattering from pyrazine and benzene.[7]

Experimental

Fourth harmonic radiation (266 nm) from the Quanta-Ray DCR-1A Nd:YAG laser was used as the excitation source. Pyridine is rather easily decomposed at this wavelength; in order to minimize the fluorescence and scattered light from decomposed molecules, a simple gas flow cell was utilized. The laser output power was kept to a minimum to prevent burning of the sample. The Raman spectra were measured by a Spex model 1400 II double monochromator (300 μm slits) combined with a cooled Hammamatsu R-562 photomultiplier followed by PAR/EGG model 162 boxcar averager. Single beam absorption spectra were obtained with the same monochromator. Comercial samples of pyridine and pyridine-d$_5$ were purified by vacuum distillation.

Results and Discussion

A. Origin of Spectrum

The 266 nm exciting light lies 750 cm^{-1} below the S_2 state and 2825 cm^{-1} above the S_1 state as shown in Figure 8-1.

The π-π^* absorption spectrum of pyridine in this region shows a strong but diffuse absorption band in contrast with a sharp but weak n-π^* band. As noted the 266 nm excitation lies slightly on the red side of the peak in the strong S_2 (π-π^*) band. There exists the possibility that the spectrum obtained is a single vibronic level fluorescence from a higher vibronic band in the n-$\pi^*(S_1)$ excited state. However, we rule out this possibility and conclude that the spectrum is due to Raman scattering in resonant with S_2 for the following reasons: The energy of the excited radiation is 2825 cm^{-1} above the 0-0 band of the n-π^* transition and does not correspond to an overtone or to a combination involving the important, active vibrational modes in the S_1 state. If the spectrum was due to emission from a high vibronic level its features would be accompanied by complex vibronic structure and an intense background. However, the observed spectrum is fairly simple, as can be seen in Figure 8-2. Moreover the spectrum has very different features from that produced by excitation at 514.5 nm. We have also obtained a similar spectrum for pyridine-d$_5$ under 266 nm excitation although fewer bands could be measured accurately due to the weak signal as compared to that of pyridine-h$_5$. The non-totally symmetric vibrational band of pyridine could be enhanced by changing the polarization of the 266 nm excitation beam. Moreover, there is a strong correlation between the vibrational features of the absorption spectrum and the spectrum generated by 266 nm excitation of pyridine. We conclude that the latter is Raman scattering enhanced by coupling with the S_2(π-π^*) state of pyridine.

B.   Characteristics of the Raman Spectra

It can easily be seen in Figure 8-2 that the Raman scattering obtained by 266 nm excitation shows very different features from the Raman spectrum generated by 514.5 nm excitation. The non-resonant Raman spectrum (514.5 nm) reveals strong ν_1 and ν_{12} bands, but in the S_2 resonance-enhanced spectrum (266 nm) the prominent bands are due to ν_1 and ν_{6a}. It is also interesting to note the greatly reduced ν_{12} band under 266 nm excitation. Table 8-1 provides a summary of vibrationally important modes in the electronic transitions and resonance Raman scattering of pyridine. In both absorption and fluorescence spectra involving the $n\pi^*$ state ($S_1 <-> S_0$) the ν_{6a} and ν_1 vibrations are dominant. Unfortunately the breadth of the $\pi-\pi^*$ absorption ($S_2 <-> S_0$) in the vapor phase precluded vibrational resolution. Nonetheless, it is clear that the major features involve vibrations at 550 cm^{-1} (ν_{6a}) and 970 cm^{-1} (ν_1). In this respect the $S_2 <- S_0$ absorption is quite similar to the $\pi-\pi^*$ transition of pyrazine.

The ν_{16a} (b_{1g}, A_2) Raman band of pyrazine[5] and pyridine[4] exhibits a prominent pre-resonance Raman enhancement when the excitation line is close to the $n-\pi^*$ ($S_1 <- S_0$) transition. This enhancement is due to vibronic coupling between the $n-\pi^*(B_{3u}$, $B_1)$ and $\pi-\pi^*(B_{2u},B_2)$ states in pyrazine[5] and pyridine[4], respectively. However, this ν_{16a} mode completely disappears in the Raman spectrum of pyrazine resonant to the S_2 state.[5,10] This agrees with calculations of Hong et al.[11] that the ν_{16a} Raman scattering resonant with S_2 should be about 0.01~0.001 as intense as that resonant to the S_1 region. However, in contrast to pyrazine, the ν_{16a} mode can be easily seen in the S_2 resonance Raman spectrum of pyridine (Figure 8-26). This $S_2(B_2)$ state of pyridine corresponds to the $S_1(B_{2u})$ of benzene. The ν_{16a} (886 cm^{-1}) band of

benzene also exhibits intensity enhancement when the exciting source approaches the S_1 state. it was concluded that this intensity enhancement in benzene is due to vibronic coupling between the lowest B_{2u} state and the $^1A_{2u}$ (σ-π^*) state.[6a-11] This suggests that the ν_{10a} Raman intensity enhancement in pyridine under excitation resonant with S_2 is due to vibronic coupling between the $S_2(B_2)$ and $B_1(\sigma$-$\pi^*)$ states.

The Raman spectrum of pyrazine resonant to $S_2(\pi$-π^*, B_{2u}) shows a long vibronic progression build on the ν_{6a} vibration. The dependence of the ν_{6a} scattering intensity on the excitation wavelength demonstrates the resonance with the S_2 state. It was also concluded from the long vibronic progression that pyrazine experiences a large displacement along the ν_{6a} coordinate in the S_2 excited state.[5] In pyridine, although ν_{6a} is enhanced in the S_2 resonance Raman spectrum, neither overtones nor combination involving ν_{6a} are observed. Moreover, many of the other bands (ν_{6a}, ν_{6b}, ν_{12}, ν_{9b} and ν_{10a}) are present. The general features of the 266 nm excited pyridine Raman spectrum are more similar to those of the pre-resonance Raman spectrum of benzene than to pyrazine resonant to the S_2 state. Studies on the pre-resonance Raman spectrum of benzene showed that the ν_{6a} mode intensity was borrowed from a higher excited state (120 nm region).[6a] The feature of the ν_{6a} mode in the S_2 Raman spectrum of pyridine suggest resonance with higher excited states also. We can concluded, at least, that the distortion along the ν_{6a} coordinate is much smaller in pyridine than in pyrazine.

The results presented here are consistent with the absorption (and fluorescent) properties of pyridine. With the advent of lasers tunable in the UV region, demonstrated in laboratories such as Professor

Asher's group more can be learned by tuning through the S_1 absorption band.

Raman Modes of Pyridine and Benzene.

Table 8-1

Pyridine Raman 5145 Exc. Liquid	2660 Exc. gas	Fluo n-π* 0-0	Abs π-π*	Benzene Raman 3250 Exc
605 a$_1$ (6a)	608 V·S	V·S	S	m
650 b$_2$(6b)	653			
890 a$_2$ (10a)	893 m	m		s
940 b$_2$ (5)				
990 a$_1$ (1)	996 V·S		S	V·S
1030 a$_1$ (12)	1034	V·S		
1218 a$_1$ (9a)				
1583 a$_1$ (8a)	1580 S			S
1593 b$_2$ (8b)	1610			
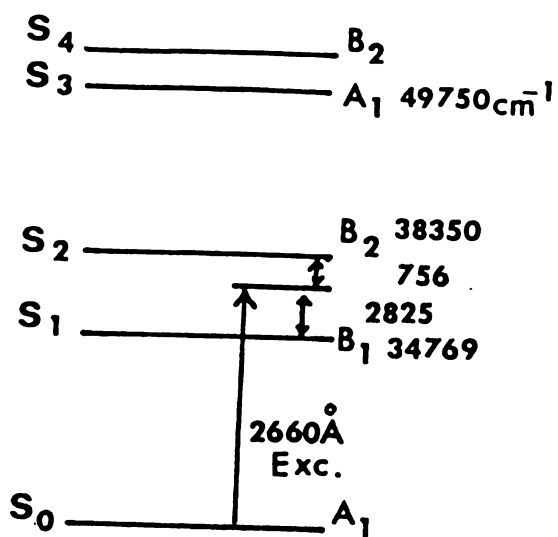
Fig 8 -1

Electronic Energy Levels of Pyridine

8-2 R.R. of Pyridine at 514.5 nm and 266 nm.

514.5 nm exc Liquid

266 nm exc Gas

$\triangle$ cm^{-1}
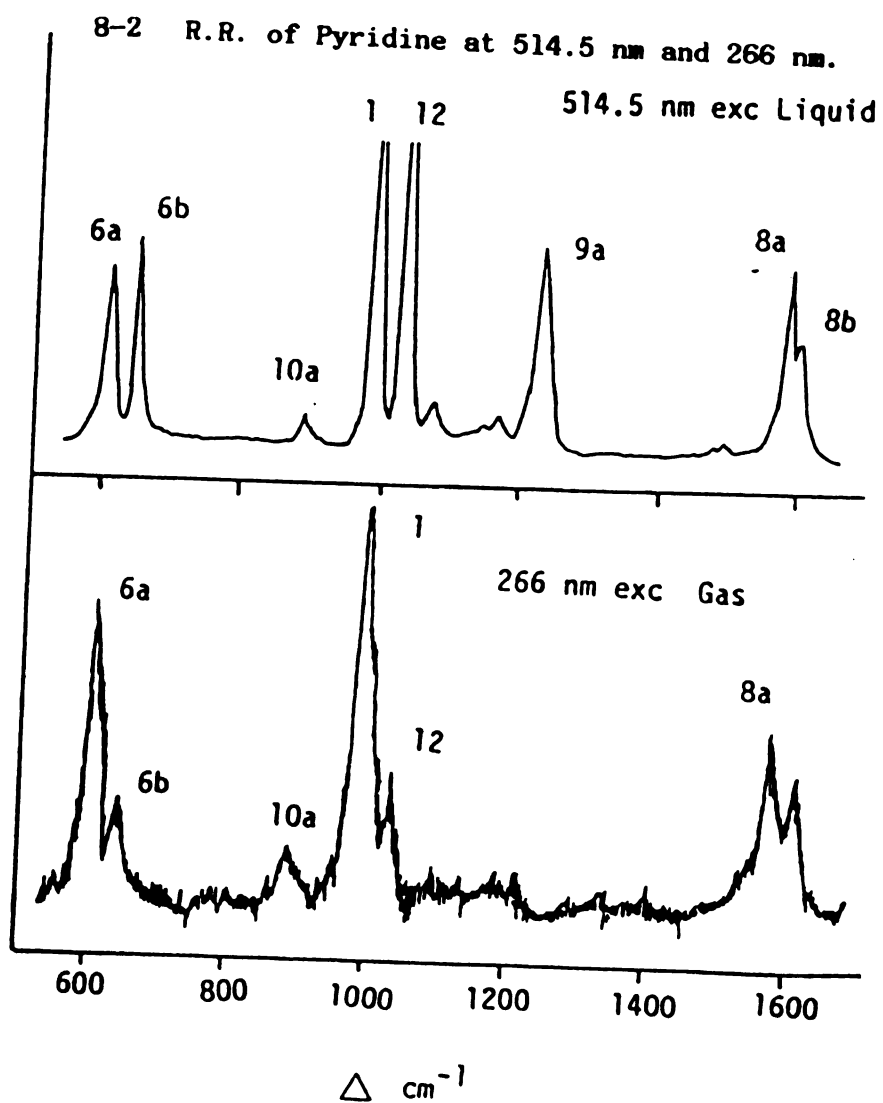
REFERENCES

1. J. Behringer, In Raman Spectroscopy, Vol. 1, p. 168, Ed. H. A. Szymanski, Plenum Press, New YOrk (1967).

2. A. Hirakawa and M. Tsuboi, Science 188, 359 (1975).

3. K. K. Innes, J. P. Byrne and I. G. Ross, J. Mol. Spectry, 22, 125 (1967).

4. Y. Mochizuki, K. Kaya and M. Ito, J. Chem. Phys. 65, 4163 (1976).

5. I. Suzuka, Y. Udagawa and M. Ito, Chem. Phys. Lett. 64, 333 (1979).

6. (a) L. D. Ziegler and A. C. Albredt J. Chem. Phys. 67, 2753 (1977). (b) G. M. Korenowski, L. D. Ziegler and A. C. Albrecht J. Chem. Phys. 68, 1248 (1978). (c) L. D. Ziegler and B. Hudson J. Chem. Phys. 74, 15 (1981).

7. (a) G. Hereberg Molecules Spectra and Molecular Structure (III), p. 664. (b) O. Olsher Spectrochim Acta, B4A, 211 (1978).

8. (a) M. Ito and I. Suzuka. Chem. Phys Lett. 31, 467 (1975).

9. I. Suzuka and Y Udagawa, to be published.

10. M. Ito, H. Ave and J. Murakami J. Chem. Phys. 69, 606 (1978).

11. H. K. Hong and C. W. Jacobsen J. Chem. Phys. 68, 1170 (1978).

CHAPTER 9

Construction of a Tunable Near-IR Dye Laser

There are numerous interesting spectroscopic experiments which can be carried out under the influence of laser radiation in the near infrared region. However, only weak solid state laser sources are availabe in this region, and dye laser emission in this region has been difficult to obtain. Near infrared beams have been generated by pumping organic dyes with ruby, N_2, flashlamps, and Nd:YAG lasers.[1] Ruby and flashlamp-pumped systems have the disadvantage of low repetition rates; N_2 lasers produce high repetition rate pulses, but they have relatively weak output power and thus poor pumping efficiencies. The second harmonic of the Nd:YAG laser (532 nm) is an appropriate pumping source, with its high power and reasonable repetition rate. C. D. Decker obtained broad-band output (15~20 nm) with 11% efficiency by Nd:YAG second harmonic excitation.[2] K. Kato found that infrared dyes pumped by another dye laser produced good results.[3] He obtained 40% conversion efficiency for IR144, when 8.5 MW of 700 nm radiation from Carbazine 720 (carbazine 122) was utilized as the pump beam. However, the spectral width was 12-15A wide.

In this report we describe the generation of narrowly tunable near infrared dye laser beams by using another dye laser as the pump. We have constructed the near IR dye laser optical system, and the performance of the Nd:YAG dye system will be compared with more conventional methods of generating near-IR laser lines.

A schematic diagram of the experimental setup is shown in Figure 9-1. A tandem system comprised of a PDL-1 dye laser pumped by the

second harmonic radiation from a Quanta-Ray DCR-1A Nd:YAG laser served as the pumping source of the near-IR dye laser. The Nd:YAG laser average output power at 532 nm was 900 mW, and the 10Hz pulses were 8ns wide. These pulses pumped the first (commercial) dye laser which contained LD688 or LDS750 dyes (Exciton Chemical Co.); these dyes absorp well at 532 nm and have maximum output in the 700–820 nm range, near the absorption maxima of the near infrared dyes contained in the second (home-build) dye laser. The second dye laser consists of an oscillator and a single side-pumped amplifier with a magnetically stirred dye cell. The output from the first dye laser is divided 1:3 by a beam splitter to pump the second dye laser oscillator and amplifier, respectively. The cavity employs a beam expander with four Littrow prisms, and a 2.7μ blazed grating with sine bar scanning system is used for wavelength tuning. One surface of the Littrow prism combination was multilayer-coated to provide minimum reflection in the 700~1000 nm region. This oscillator cavity design is expected to provide high conversion efficiency, narrow band width and simple alignment. A 10% partially reflecting mirror with antireflection coating on the amplifier side is used as the output mirror.

The near infrared dyes: DOTC, HITC, DTTC, IR144, IR125 and IR140 were tested in the second dye laser. Each dye was obtained from the Excition Chemical Corporation and dissolved (10^{-3} to 10^{-4} M) in spectrophotometric grade DMSO. Output laser powers were measured by a scientech model 362 power meter. Spectral bandwidth and output wavelength were measured by a Spec 1400 II monochromator with Hamamatsu R928 photomultiplier.

The near-infrared dye laser output curves obtained by 70 mW of LDS750 pumping excitation at 735 nm are shown in Figure 9-2 and the relevant data are summarized in Table 9-1. We achieved continuous tunability from about 750 nm to 920 nm using six dyes. Efficiencies as high as 17% to 20% efficiency were obtained in the 817 to 860 nm region. With 60 mW LD688 pumping, we obtained peak output of 3mW (HITC), 3mW (IR125) and 6mW (IR144). These values are lower than those obtained under LDS 750 excitation, and demonstrate the increased efficiency obtained when the pump laser wavelength is closer to the near IR dye absorption maximum. Pierce and Birge have reported near IR dye laser oscillation pumped by N_2 laser excitation (90 mW, 337.1 nm).[4] They were able to obtain output powers of 0.8 mW~2.5 mW in this region. However, they found ~15% decrease in output power from DOTC and HITC dyes after about 30 minutes of operation. We were able to generate ~5 mW output power by directly pumping the dyes IR125 and HITC at 354.7 nm (Nd:YAG, third harmonic), but the output power decreased in a matter of minutes! On the other hand, the near-IR dye laser output power was quite stable for several hours in the LDS750 dye pumped configuration. The worst case was DTTC, which despite stirring of the dye cell, decreased in output power by ~20% after one hour of operation. The spectral bandwidth was about 2A (~2.6 cm^{-1}) at 880 nm using IR140. We plan to install an etalon to obtain narrower output bandwidths.

In the N_2 laser-pumped method[4], 10^{-1}, to 10^{-2} M solutions of the IR dyes were used. In our case much lower concentrations, 10^{-3}M for the oscillator and ~3×10^{-4}M for the amplifier were sufficient to generate near IR laser beams. Thus, the system described in this paper offers several advantages over previous methods of generating near-IR dye

laser radiation: (1) improved efficiency; (2) more stable output power (less photodegradation); (3) narrower spectral width; (4) lower dye concentrations and smaller volumes which lead to lower operating costs.

Near-IR Laser Dye Output

Table 9-1.   LDS 750 Pump Source at 735 nm, 70 mW

Dye	Abs λ_{max}(nm)	Output(mW)	Emission λ_{max}(nm)	Tunable Range(nm)	Approximate Efficiency (at λ_{max})
DOTC[a]	687	12	760	734-778	17%
HITC	751	8	800	780-820	11%
DTTC	763	9[b]	825	817-857	20%[b]
IR144	745	12	850	840-860	17%
IR125	795	9	875	850-920	13%
IR140	823	6	880	870-890	9%

a.   With LD688 pumping; similar efficiency at λ_{max} with LDS 750 excitation.

b.   This value was obtained by 45mW pumping.

Schematic of Homemade Near-IR Dye Laser
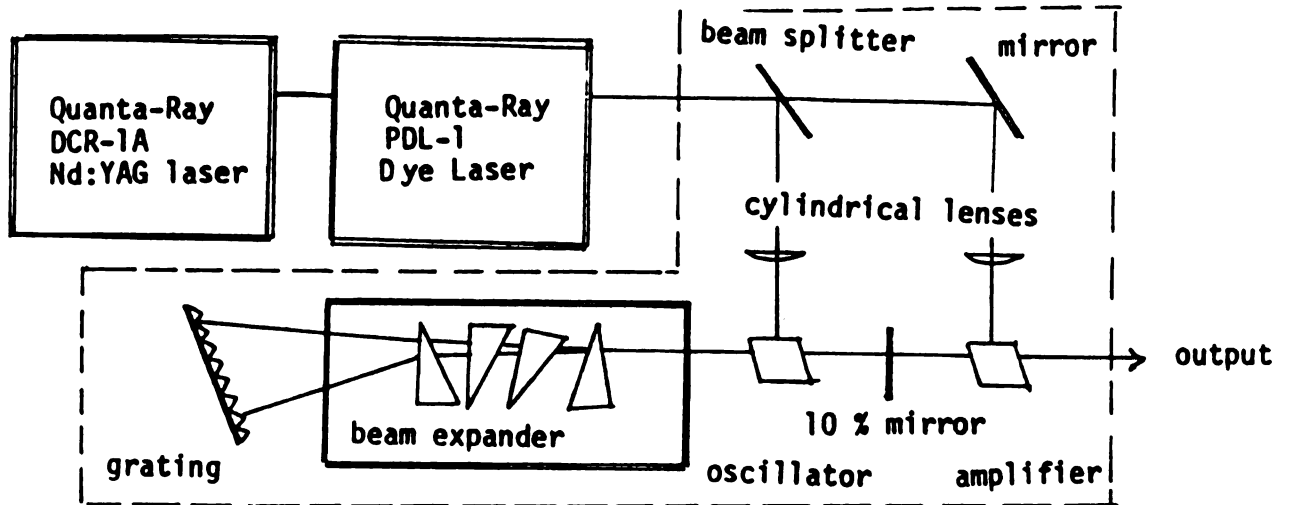
Fig 9-1

Near-IR Dye Laser Output Curves
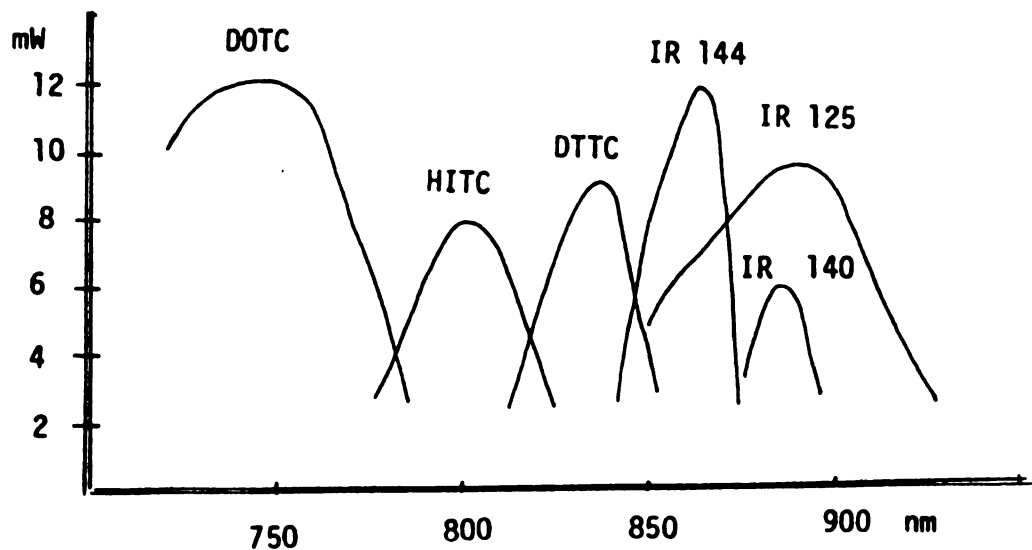
Fig 9-2

REFERENCES

1. (a) Y. Miyazoe, M. Mitsuo, App. Phy. Lett. 12, 206 (1968). (b) P. E. Dettinger, C. F. Dewey, I. E. E. E. J. Quant. Elect. 12, 95 (1976). (c) H. Hildebrand, Opt. Comm. 10, 310 (1974). (d) R. Mahon, T. H. McIlrath and D. W. Koopman. App. Otp. 18, 891 (1979). (e) J. Kuhl, R. Lambrich, D. VonderLinde, App. Phys. Lett. 31(10), 657 (1977). (f) J. P. Webb, F. G. Webster, B. E. Plourde, I.E.E.E. J. Quant. Elect. QE11, 114 (1975).

2. C. D. Decker, App. Phys. Lett. 27, 607 (1975).

3. K. kato, I.E.E.E. J. Quant. Elect. 12, 442 (1976).

4. B. M. Pierce, R. R. Birge, I.E.E.E. J. Quant. Elect. QE18, 1164 (1982).

CHAPTER 10

Two-Photon Spectroscopy of Perylene

Two-photon spectroscopy provides new information about certain molecular eigenstates which cannot be studied by ordinary one-photon spectroscopy. The theory, which was first work out by Goppert-Mayer[1] shows that the parity selection rules for a two-photon transition are complementary to the one-photon case, i.e., $g - g$ and $u - u$ are allowed for two-photon transitions. This makes two photon spectroscopy an ideal method to obtain information about gerade states. This technique also allows the observation of new, gerade vibronic states in a known ungerade electronic excited state since these vibronic states are inaccessible by one-photon transitions. Such vibronically induced transition, where the perturbation is by a nontotally symmetric vibration of ungerade parity in the excited electronic state, provides new insight into the nature of the electronic state and the mechanism of vibronic coupling. A very brief discussion of the symmetry aspect of two-photon spectroscopy is given here as well as some preliminary data obtained for the polyaromatic hydrocarbon, perylene. In one-photon spectroscopy the extinction coefficient ϵ for absorption of a photon of λ polarization is:

$$\epsilon \propto |\lambda M|^2, \text{ where M is transition vector.}$$

In the case of a two-photon transition, the scalar product includes a tensor.[2,3] S_{o-f} is a three-by-three matrix whose elements are basically the products $M^x_{o-i}.M^x_{i-f}$ etc. The extinction coefficient (δ) for photons of polarization λ and μ is: $\delta \propto |\lambda S_{o-f}.\mu|^2$ and S is:

$$S_{0-f} = \sum_{a,b} \sum_{K} \frac{\langle o|\mu_a|k\rangle\langle k|\mu_b|f\rangle}{w_{Ko}-w_1} + \frac{\langle o|\mu_b|k\rangle\langle k|\mu_a|f\rangle}{w_{Kg}-w_2}$$

where:

$|0\rangle$ Initial state.

$|f\rangle$ Final state.

$|k\rangle$ Intermediate states.

a,b   Coordinate axes in the molecular frame.

The effect of the light polarization on the two-photon transition tensor can be more easily visualized when it is written in tensor form.

$$S_{f-f} = \begin{matrix} S_{xx} & S_{xy} & S_{xz} \\ S_{yx} & S_{yy} & S_{yz} \\ S_{zx} & S_{zy} & S_{zz} \end{matrix}$$

The individual tensor elements are numbers which represent the contribution to the strength of the transition from each set of directions, a and b, in the molecule. This tensor is multiplied by both photon polarization vectors to determine absorptivity. The acutal forms that these tensors take are shown in Table 10-1. An extensive list is available in the literature.[4,5]

The expressions for ϵ and δ show that these quantities take variable values depending on the orientation of the molecule relative to λ or to λ and μ. When orientation average is performed one obtains[2,3]

$\langle \epsilon \rangle = 1/3(\lambda \cdot \lambda^*)(M \cdot M^*)$, $\lambda \cdot \lambda^* = 1$ for all polarizations.

Thus, for one-photon absorption the information from polarization dependence is lost. McClain and others[9,10] have shown that in the two-photon case δ it shows a non-zero polarization dependence when the orientation average is carried out.

$\langle \delta \rangle = d_F F + d_G G + d_H H$, where F, G, H are functions of the incident beam polarization.

$$\delta_F = \sum_{i=j=1}^{3} S_{ij}{}^2 \,, \qquad F = -|\lambda.\mu^*|^2 + 4|\lambda.\mu|^2 - 1$$

$$\delta_G = \sum_{j=1}^{3} \sum_{i=1}^{3} |S_{ji}|^2 \,, \qquad G = -|\lambda.\mu^*|^2 - |\lambda.\mu|^2 + 4$$

$$\delta_H = \sum_{j=1}^{3} \sum_{i=1}^{3} S_{ji} S_{ij}^* \,, \qquad H = 4|\lambda.\mu^*| - |\lambda.\mu|^2 - 1$$

Since δ_F is a measure of the diagonal elements it indicates totally symmetric transitions. δ_G is the sum of the squares of all elements in the transition tensor and therefore, does not contain excited state symmetry information

The values for F, G, H under different beam polarization are shown in Table 10-2.

Experimental

There are basically four different methods which can be employed to measure two-photon cross sections:

(1) direct absorption method

(2) indirect excitation method

(3) parametric wave mixing method

(4) thermal lensing method

The details of the experimental aspects of the four methods are reviewed in the literature and will not be repeated here.[11] The method chosen for the two-photon investigation was the indirect fluorescence excitation technique. In this method the sample to be studied is irradiated with one or two laser pulses, of which at least one must be tunable. The two-photon induced fluorescence from the sample is collected at 90° to the incident laser beam, filtered with either an optical filter or a monochromator, and then detected by a photomultiplier. In a one-laser experiment several laser dyes are used to cover the visible region: 450 nm ~ 800 nm (see Figure 12-2). In a two-laser experiment a Raman shifter is used in conjuction with a tunable dye laser. For polarization analysis a soleil-babinet compensator is used to obtain linear or circularly polarized beam without changing the optical path. The fluorescence intensity is gathered under circular polarization laser beam and is compared to the intensity obtained under linear polarization. The ratio then gives the so called polarization ratio, Ω, which is analogous to the depolarization ration ρ of Raman scattering.

The ordinary one-photon absorption spectrum is shown in Figure 10-2. The A_g and B_{3g} states shown are predicted from theory.[12] The two-photon fluorescence excitation spectrum taken in the visible region

is shown in Figure 10-3. Note that there are three strong and two weak peaks. This spectrum was obtained with two photons from the same laser, each with linear polarization, one expects to see two fully-allowed A_g states. It is dangerous, however, to make even preliminary assignments without polarization data, and a complete analysis can be done only after circularly polarized excitation data are available.

After completion of polarization analysis in this liquid phase, ambient temperature experiment, it is proposed that a high resolution experiment with the supersonic free jet apparatus be carried out.

Form of the transition tensor and symmetry of the excited state

$$S_{A_{1g} \rightarrow A_{1g}}(O_h) = \begin{pmatrix} S_1 & 0 & 0 \\ 0 & S_1 & 0 \\ 0 & 0 & S_1 \end{pmatrix} \qquad S_1 = \frac{S_{xx} + S_{yy} + S_{zz}}{3}$$

$$S_{A_{1g} \rightarrow A_{1g}}(D_{4h}) = \begin{pmatrix} S_1 & 0 & 0 \\ 0 & S_1 & 0 \\ 0 & 0 & S_2 \end{pmatrix} \qquad \begin{array}{l} S_1 = \dfrac{S_{xx} + S_{yy}}{2} \\ S_2 = S_{zz} \end{array}$$

$$S_{A_{1g} \rightarrow B_{2g}}(D_{4h}) = \begin{pmatrix} 0 & S_1 & 0 \\ S_1 & 0 & 0 \\ 0 & 0 & 0 \end{pmatrix} \qquad S_o = \frac{S_{yx} + S_{xy}}{2}$$

$$S_{A_{1g} \rightarrow B_{1g}}(D_{2h}) = \begin{pmatrix} 0 & S_1 & 0 \\ S_2 & 0 & 0 \\ 0 & 0 & 0 \end{pmatrix}$$

Classification

(a) Zero trace symmetric

(b) Zero trace antisymmetric

(c) Zero trace nonsymmetric

$$S_{A_{1g} \rightarrow A_{2g}}(D_{4h}) = \begin{pmatrix} 0 & S_1 & 0 \\ -S_1 & 0 & 0 \\ 0 & 0 & 0 \end{pmatrix}$$

(d) totally symmetric

Table 10-1

Two-Photon Transition Tensor

Values of the Polarization Variables *F*, *G*, and *H*, for Eight Two-Photon Transitions

Polarization variable	Case[b]							
	1	2	3	4	5	6	7	8
F	2	-1	-1	$-\frac{1}{4}$	$-\frac{1}{2}$	$-\frac{1}{2}$	-2	3
G	2	4	4	$\frac{7}{2}$	3	3	3	3
H	2	-1	-1	$-\frac{1}{4}$	$-\frac{1}{2}$	$-\frac{1}{2}$	3	-2

Table 10-2

DYES   (nm)

Coumarine 540A   530 ~ 585

Rhodamine 590   550 ~ 580

Rhodamine 610   570 ~ 610

Rhodamine 640   600 ~ 620

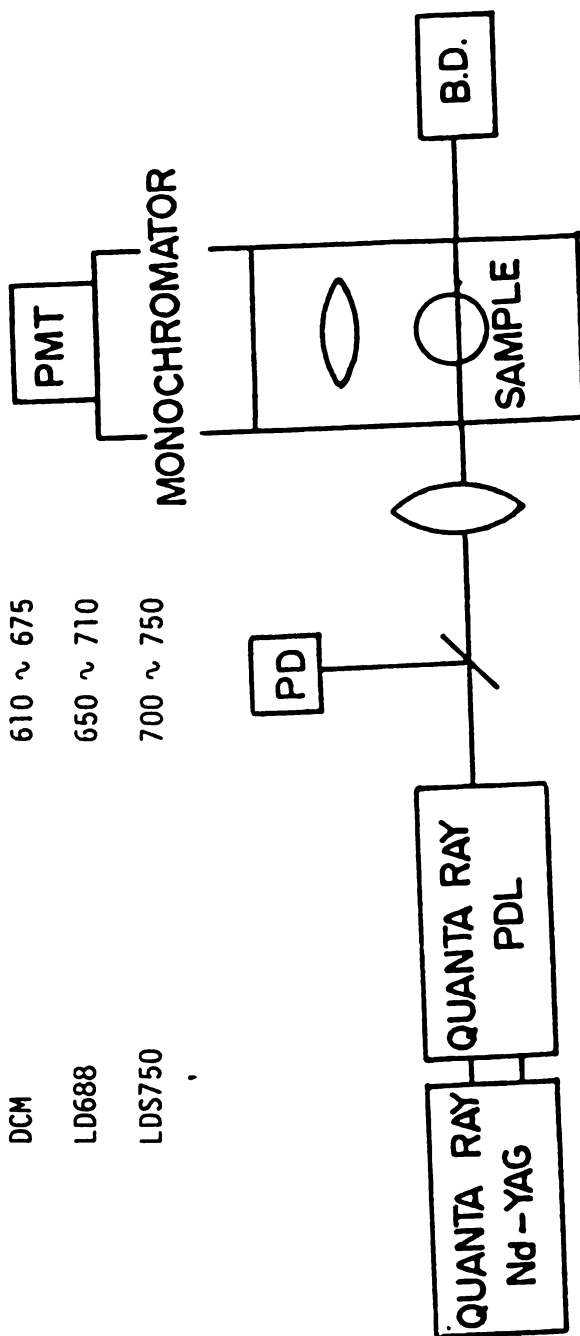DCM   610 ~ 675

LD688   650 ~ 710

LDS750   700 ~ 750
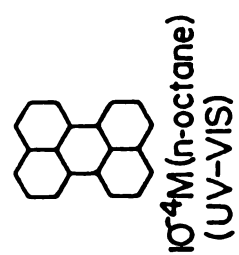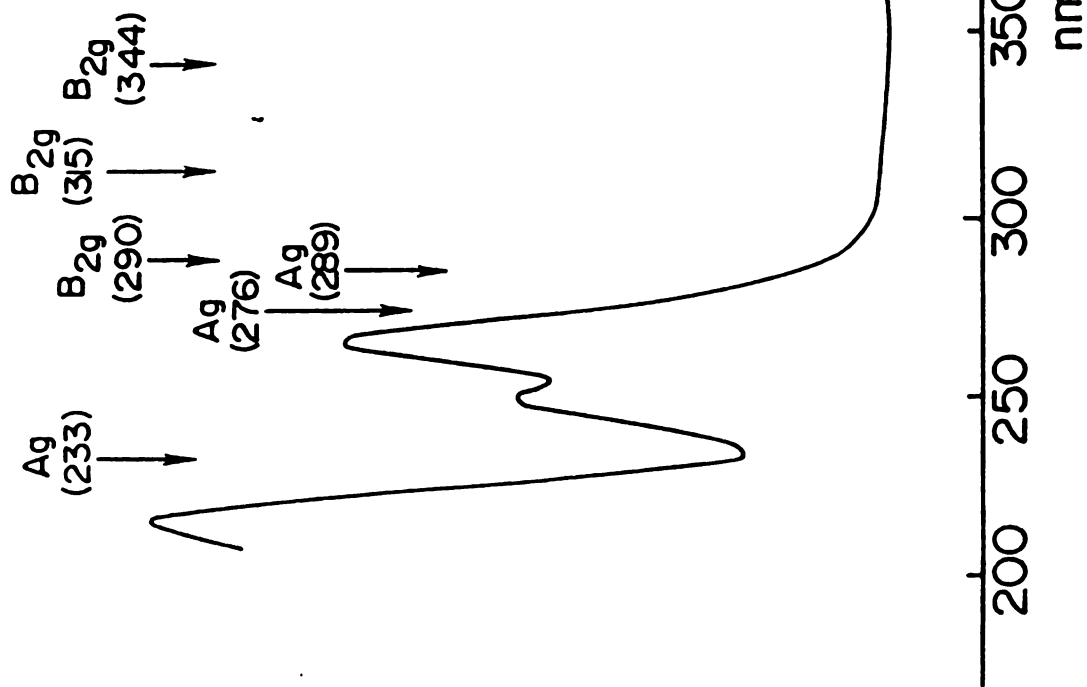
Fig 10-1

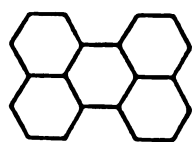**Experimental Setup of Two-Photon**
Electronic Excitation

Electronic Absorption Spectrum of Perylene

Fig 10-2

10^{-4}M(n-octane)
(UV-VIS)

Ag
(233)

B$_{2g}$
(315)

B$_{2g}$
(344)

B$_{2g}$
(290)

Ag
(276)

Ag
(289)

nm

10^{-4}M(n-octane)
(TPE)

Fig 10-3

Two-Photon Excitation Spectrum of Perylene

nm
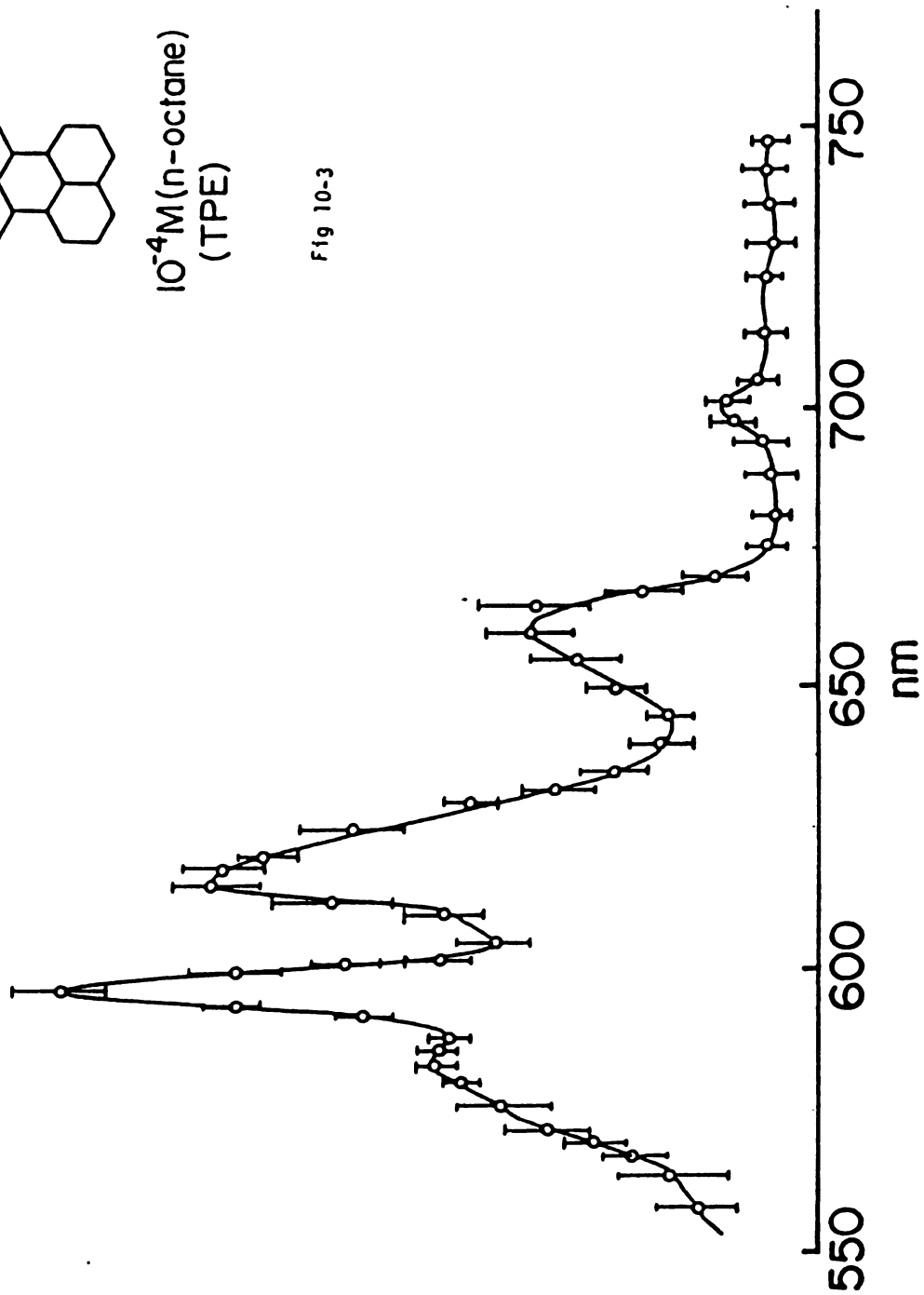
REFERENCES

1. M. Goeppert-Mayer, Ann. Physik. 9, 273 (1931).

2. W. M. McClain, J. Chem. Phys. 53, 29 (1970).

3. P. R. Monson, W. M. McClain J. Chem. Phys. 56, 4817 (1972).

4. L. N. Ovander, Opt. Spect. 9, 302 (1960).

5. M. Inoue, Y. Toyozawa, J. Phys. Soc. Jap. 20, 363 (1965).

6. R. Bader, A. Gold, Phys. Rev. 171, 997 (1968).

7. W. M. McClain, J. Chem. Phys. 55, 2789 (1971).

8. D. Frohlich, B. Staginnus, Phys. Rev. Lett. 19, 1032 (1967).

9. W. M. McClain, J. Chem. Phys. 57, 2264 (1972).

10. W. M. McClain, R. P. Drucker, Chem. Phys. Lett. 28, 255 (1974).

11. H. L.-B. Fang, Ph.D. Dissertation, Michigan State University (1977).

12. Y. Tanizaki, T. Yoshiaga, Spectrochemica. Acta. 34A, 206 (1978).